# Organo-Polyoxometalates for acid catalysis : a combined experimental/modeling study

Debora Vilona

▶ **To cite this version:**

Debora Vilona. Organo-Polyoxometalates for acid catalysis : a combined experimental/modeling study. Catalysis. Université de Lyon, 2017. English. NNT : 2017LYSE1190 . tel-01678068

HAL Id: tel-01678068

https://theses.hal.science/tel-01678068

Submitted on 8 Jan 2018

N°d'ordre NNT: 2017LYSE1190

# THESE de DOCTORAT DE L'UNIVERSITE DE LYON

opérée au sein de

## l'Université Claude Bernard Lyon 1

### Ecole Doctorale de Chimie N° 206

**Spécialité de doctorat**: Chimie

Soutenue publiquement le 28/09/2017, par:

## Debora VILONA

# Organo-Polyoxometalates for acid catalysis: a combined experimental/modeling study

Devant le jury composé de:

| | | | |
|---|---|---|---|
| MARTIN-VACA, Blanca | Professeur | Univ. Toulouse | Rapporteure |
| MIALANE, Pierre | Professeur | Univ. Versailles | Rapporteur |
| BO, Carles | Professeur | ICIQ Tarragona | Examinateur |
| DARWICH, Chaza | Maitre de Conférence | Univ. Lyon 1 | Examinatrice |
| DUMONT, Elise | Professeur | ENS de Lyon | Co-directrice de thése |
| LACÔTE, Emmanuel | Directeur de recherche | Univ. Lyon 1 | Directeur de thése |
| BUCHER, Christophe | Directeur de recherche | ENS de Lyon | Invité |
| LELLI, Moreno | Professeur associè | Univ. Florence | Invité |

Science is a discipline in which the fool of this generation can go beyond the point reached by the genius of the last generation.

(Max Gluckman)

# UNIVERSITE CLAUDE BERNARD - LYON 1

# Acknowledgements

First of all I would like to thank my thesis supervisor Emmanuel LACÔTE for letting me enjoy the research world during these three beautiful years. Your faith in me encouraged me everyday to continue my research and stimulated me to do my best. Thanks a lot for your precious scientific advices and also for succeeding to motivate me after each meeting.

Many thanks also to my thesis co-supervisor Elise DUMONT for the kindness and patience that she put to teach me MDs and DFT calculations. I know that it was challenging, many thanks for the time that you gave me to learn and for your kind words which helped me to believe in myself.

I am also grateful to our collaborator Moreno LELLI who tought me the powerfull of NMR tools and made me independent in using them. I really appreciated the NMR time and the scientific discussion with you that enriched me after each session.

I would like to thank Prof. Blanca MARTIN-VACA and Prof. Pierre MIALANE which accepted to read and judge my thesis and for their important remarks. Many thanks also to Prof. Carles BO and Dr. Chaza DARWICH which accepted to come to my defense, to examinate my thesis and for their insightful comments which enriched me and my work. I am sincerely gratefull also to Dr. Christophe BUCHER which followed my work along these three years, showing a great interest: his argute advices were important in the development of this job. Many thanks to all of you for making scientifically great my defense!

Thanks to the C2P2 laboratory, the "laboratoire de chimie" of ENS and the CRMN of Lyon which hosted me along these three years and many thanks to all the permanent and non-permanent staff which enriched scientifically and emotionally each day of this experience. In particular, I would like to thank Jessica, Enza, Emanuele, Pooja, Tapish, Giuliana, Benjamin and Cherif for their important friendship in the lab.

# The project

The aim of this project is to develop new bio-inspired catalysts able to perform asymmetric acid catalysis, exploiting non-noble and easily recyclable metals.

Indeed, accessing enantiopure compounds is an important challenge for pharmaceutical industry (as in some cases one mirror image of a molecule has a beneficial effect, while the other is a poison). Normal synthesis delivers a mixture of both mirror images, and one has to physically separate the enantiomers and discard the wrong one, generating waste. On the other hand, regular asymmetric synthesis requires chiral reagents that are expensive.

The use of a chiral catalyst, that can transfer its chiral information with high turnover, avoids the general synthetic asymmetric pathway. Its ecological footprint is extremely good, as the reactions lead directly and selectively to the desired enantiomers starting from achiral substrates. It is therefore a crucial tool for the sustainable production of active ingredients and essential contributor to the green chemistry.

With this idea in mind, mimicking nature seems to be the best way!

Enzymes are macromolecular biological catalysts that have evolved over eons to be able to catalyze chemoselective, regioselective and stereospecific reactions. All enzymes have a chiral pocket that surrounds a catalytically active site, where the reaction takes place and where the chiral information is transmitted to the substrates.

In view of the above, we decided to focus our attention on hybrid catalytic systems (organic/inorganic) based on Polyoxometalates (POMs) to create an artificial enzyme. Polyoxometalates (POMs) are nanometric polyanionic clusters, made from highly oxidized early transition metals, typically W(VI), V(V), or Mo(VI), connected by oxo-bridges. The possibility to tune their structures and properties, changing synthetic conditions, make them widely used in a score of applications. Combining these inorganic clusters with organic moieties expands their properties and consequently the applications of these interesting molecules.

Our general idea is to create a chiral pocket around a catalytically active site of the POM that is itself generated by the specific combination of an organic group with the inorganic surface.

The project therefore seeks to understand how the organic pocket arranges itself around the active site and it is divided into two main parts:

- The synthesis of targeted hybrid-POMs, where the inorganic cluster is functionalized with designed organic moieties, to fully study how the POM can generate a catalytic property and thus create an active site;

- The synthesis of POMs functionalized with polypeptides arms to understand through High-field NMR and Molecular Modeling how the POM can interact intramolecularly with a peptide chain and thus rationally figure out how the chiral pocket can be formed.

# Résumé

**Contexte**

Le but de cette thèse est de développer des nouveaux catalyseurs bio-inspirés capables d'exécuter la catalyse acide asymétrique, exploitant des métaux non-nobles et facilement recyclables.

Avoir accès à des composés enantiopures est un défi important pour l'industrie pharmaceutique. La synthèse non-asymétrique livre un mélange des deux énantiomères qui doivent être séparées, mais ce processus est difficile et onéreux. D'autre part, la synthèse asymétrique exige des réactifs chiraux qui coutent chers. L'utilisation d'un catalyseur chiral permet de transférer les informations chirales et évite l'utilisation des réactifs chiraux onéreux. La catalyse chiral permet d'obtenir directement et sélectivement l'énantiomère désiré en commençant d'un substrat achiral, et par conséquence son empreinte écologique est extrêmement bonne. C'est donc un outil crucial pour la production durable de principes actifs et le collaborateur essentiel à la chimie verte.

Dans ce contexte, imiter la nature semble être le meilleur chemin ! Les enzymes sont les catalyseurs biologiques macromoléculaires qui se sont développés pour pouvoir catalyser chimio-sélectivement, régio-sélectivement et stéréospécifiquement des réactions chimiques. Toutes les enzymes ont une poche chirale qui entoure le site actif où la réaction a lieu et où les informations chirales sont transmises aux substrats.

Ainsi, nous avons décidé de concentrer notre attention sur des systèmes catalytiques hybrides (organique/inorganique) basés sur les Polyoxométallates (POMs), pour créer une enzyme artificielle. Les POMs sont des complexes poly anioniques nanométriques, faits par les premiers métaux de transition fortement oxydés, typiquement $W^{VI}$, $V^V$, ou $Mo^{VI}$ connectés par des ponts oxo. La possibilité de contrôler finement leurs structures et propriétés, en changeant les conditions de synthèse, rend les POMs largement utilisés dans un large champ d'applications. L'union de ces groupes inorganiques avec des fragments organiques étend leurs propriétés et par conséquent leurs applications.

**Le projet**

Notre idée générale est de créer une poche chirale autour d'un site actif du POM qui est lui-même produit par la combinaison spécifique d'un groupe organique avec la structure inorganique. Il faut du coup comprendre comment la poche organique s'arrange autour du site actif. Le travail a été divisé en deux parties principales:

- La synthèse de POMs hybrides, où le complexe inorganique est fonctionnalisé par des ligands organiques. Ces complexes hybrides sont conçus entièrement pour étudier comment le POM peut influencer les propriétés catalytiques du ligand organique et créer ainsi un site actif;

- La synthèse des POMs hybrides fonctionnalisés avec des bras polypeptidiques. Ces systèmes ont été étudiés par RMN à très haut champ et par Modélisation Moléculaire pour comprendre comment le POM peut interagir avec une chaîne de peptides par interactions supramoléculaire et ainsi comment créer une poche chirale.

**POM hybrides pour la catalyse acide**

Des hybrides moléculaires ont alors été synthétisés et testés comme catalyseurs acides. En particulier, nous avons commencé notre étude avec la fonctionnalisation d'un POM, le Dawson $[P_2W_{15}V_3O_{61}]^{9-}$, avec des ligands phényle diolamides, en couvrant toute la gamme des propriétés électroniques sur l'anneau phénylique. Ces hybrides déjà testés en catalyse acide, comme acides de Brønsted pour la réduction des quinoléines, ont été caractérisés par RMN et DFT pour bien comprendre où se trouve le site catalytique. En fait, les tests catalytiques ont montré que les POMs hybrides sont très actifs pour la réduction des quinoléines, au contraire du ligand libre qui est inactif pour cette réaction. Cette activité est probablement due au caractère électro-attracteur du POM, qui permet de stabiliser

la charge négative générée quand le proton amidique est transféré au substrat quinoléique. La RMN du proton nous montre un grand déblindage du proton amidique lorsque le ligand est greffé dans la structure du polyoxométallate ce qui entraîne une plus forte acidité du proton. Pour être sûr que le site catalytique soit bien placé sur l'azote amidique et non autour du POM, ou sur un autre site basique de la molécule, des spectres de RMN bidimensionnelles ont été réalisés. Les spectres du $^1$H-$^{13}$C HSQC et $^1$H-$^{13}$C HMBC nous ont confirmés la présence d'un proton lié à l'azote amidique et les études de DFT effectuées après l'optimisation des structures nous montrent que l'affinité protonique de l'azote est supérieure à celle des atomes d'oxygène du POM. Les calculs DFT ont aussi permis de simuler la RMN des protons amidiques des hybrides, confirmant ainsi un bon accord entre les valeurs expérimentales et simulées. La structure des complexes est bien stable: le site catalytique est bien confiné sur l'azote amidique.
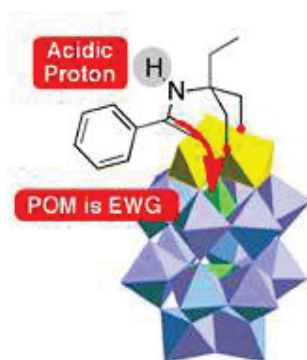


**Figure 1-** diolamides@ POM etudièes.

De la même façon, le POM Dawson, $[P_2V_3W_{15}O_{61}]^{9-}$ a été fonctionnalisé par des ligands uréiques. En fait, les urées, comme les diolamides, sont capables d'effectuer la catalyse acide de Brønsted par interaction hydrogène avec le substrat, mais sans un transfert protonique effectif. Toute la gamme des propriétés électroniques a été couverte sur le ligand uréique et l'activité catalytique a été testée sur la réaction d'alkylation de Friedel-Crafts des indoles par le trans-β-nitro styrène (TBNS). En général, la RMN du proton indique un déblindage des signaux uréiques lorsque le ligand est greffé dans la structure inorganique traduisant

l'augmentation de l'acidité grâce à l'effet électro-attracteur du POM. Tous nos catalyseurs ont montrés une bonne activité catalytique, au contraire du ligand libre. En particulier, les hybrides, contenant des groupes électro-attracteurs sur l'anneau phénylique, montrent une meilleur cinétique pour la réaction d'alkylation de l'indole.

Des études sur le processus catalytique ont été faites. Nous avons suivi par RMN [1]H l'éventuelle interaction entre les protons uréiques et le groupe nitro du substrat par ajout de substrat (le trans-β-nitro styrène), sur certains catalyseurs. En fait, le processus catalytique général prévoit une interaction entre les deux protons uréiques et les deux oxygènes du groupe nitro du TBNS: la RMN du proton peut nous montrer cette éventuelle interaction, car un déplacement du signal du proton est enregistré s'il y a cette interaction.

Les titrages RMN montrent qu'une interaction apparaît entre les protons uréiques et le groupe nitro du TBNS, si des groupes électro-attracteurs sont présents sur l'anneau phénylique. Les constantes d'interaction ont été calculées quand cela a été possible.

Des études de DFT ont été faites pour optimiser les structures des hybrides et les simulations RMN du proton ont montré un bon accord entre les valeurs expérimentales et calculées.

Des calculs de DFT statique sont en cours pour voir l'éventuel transfert de charge entre le catalyseur et le TBNS pendant le processus catalytique. Enfin, le recyclage de notre catalyseur a été effectué, montrant que l'activité catalytique est encore maintenue après le troisième cycle.
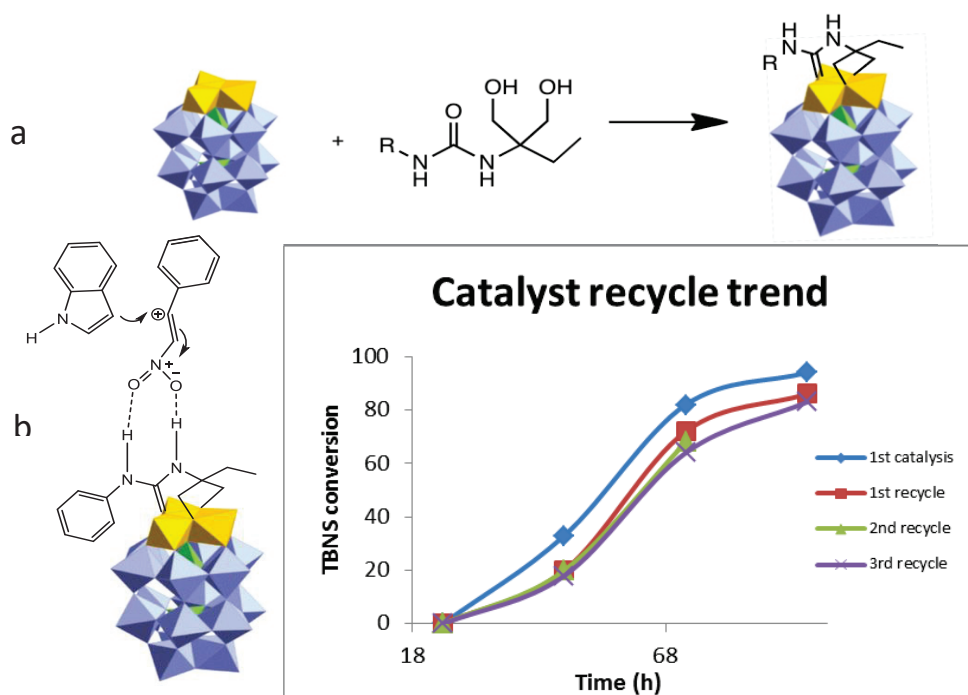
**Figure 2-** a) Synthèse des POM@ureas; b) Mécanisme catalytique par l'alkylation de l'indole par le TBNS; c) Recyclage du catalyseur.

## POM peptides pour les études de conformation en solution

La deuxième partie du projet de recherche prévoit l'étude des interactions supramoléculaires entre le POM et des substrats d'intérêt biologique. Pour comprendre comme construire une poche chiral autour du site catalytique, nous avons fonctionnalisé un Dawson polyoxotungstate lacunaire, le $[P_2W_{17}O_{61}]^{10-}$ avec des ligands polyglyciniques et étudié comment les ligands de différente longueur interagissent avec les charges négatives présentes sur la surface du POM. Après la synthèse des hybrides $[P_2W_{17}O_{61}SnCH_2CH_2CO(Gly)_nNH_2]^{7-}$ (avec n=1-6), l'RMN à très haut champ (1 GHz) à été utilisé pour suivre les signaux des protons amidiques des glycines. En fait, si les glycines n'interagissent pas avec le POM, un seul signal du proton sera enregistré au RMN par tous les protons amidiques, car la chaine polyglycinique se trouve dans un arrangement à *random coil*. Dans notre cas, les signaux des protons amidiques de la chaine latérale sont bien différenciés les uns des autres, signe d'un environnement magnétique différent, dû a

l'interaction des protons avec les oxygénés du POM. La dynamique moléculaire nous a confirmé l'interaction et a montré que la chaine polyglycinique s'enroule autour du POM avec un mécanisme à éclair (*zip-like*). Le comportement de repliement de la chaine peptidique autour du POM est différent selon la position de la lacune sur le POM et de la longueur de la chaine latérale et ainsi de l'effective position du proton sur la chaine peptidique. Les liaisons hydrogène entre la chaine organique et le POM ont été mappés.
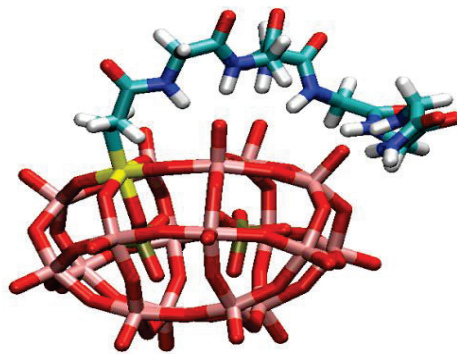


**Figure 3-** Schéma représentant l'enroulement de la chaine glycinique autour de la surface du POM par le α1-POM@Gly$_5$.

# Table of content

# CHAPTER 1: HYBRID POLYOXOMETALATES

## 1.1    Polyoxometalates: a general introduction

Polyoxometalates (POMs) discovery dates back to the last third of the XIX century, when early transition metals of groups V and VI, such as Nb, V, Ta, Mo, and W in their highest oxidation states (configuration $d^0$ or $d^1$) were found to form polynuclear oxoanions in aqueous solution at acidic pH.[1–6] The dimensions of these inorganic molecules can range from a few Angstrom[7,8] to several nanometers.[9] POMs can be classified into two big families depending on the chemical composition:

a) Isopolyanions, with general formula $[M_mO_y]_p$, that are made by only one metal and oxygen;

b) Heteropolyanions, with general formula $[X_xM_mO_y]_q$

where M is the main transition metal constituent of the polyoxometalate, O is the oxygen atom and X can be a non-metal atom, such as P, Si, As, Sb, or a different transition metal.

The main characteristics that a metal has to possess to lead to polyoxometalate complexes are:[2]

1)    Cationic radius compatible with octahedral coordination;
2)    Empty d orbitals to allow the formation of terminal metal-oxygen double bonds.

This second property is essential to get discrete molecular structures rather than common extended metal-oxide. Indeed, terminal oxygens are less basic than bridging ones and consequently they are not suitable for condensation with other monomeric units, thus avoiding the polymerization of the single molecular metal-oxide.[2]

The main feature of these discrete polyanions, that has made them widely studied in the last decades, is the possibility to easily master their structural diversity

through synthesis and consequently their properties. Indeed, different polyoxometallic structures are obtainable, such as for example the Keggin, Well-Dawson, Lindqvist, Anderson-Evans in Figure 1.1, by carefully tuning the synthetic reaction parameters: stoichiometric ratio, concentration, pH and temperature.[10–15]
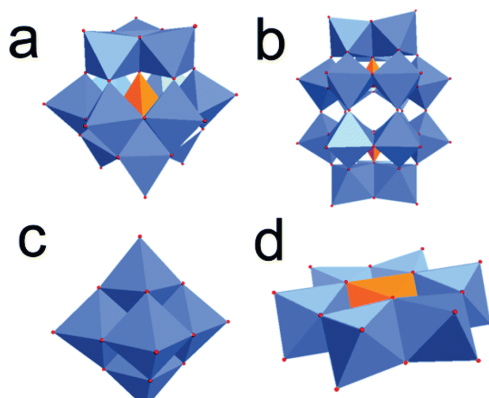


**Figure 1. 1**- Polyhedral illustration of archetypal POM anions, highlighting their structural diversity. (a) Keggin anion $[XM_{12}O_{40}]^{n-}$; (b) Dawson anion $[X_2M_{18}O_{62}]^{n-}$; (c) Lindqvist anion $[Mo_6O_{19}]^{2-}$; (d) Anderson anion $[XM_6O_{24}]^{n-}$.

Their general structures are based upon $\{MO_6\}$ (in blue) and $\{XO_4\}$ (in orange) polyhedra sharing vertices [one $\mu_2$ oxygen], edges [two $\mu_2$ oxygens] or, more rarely, faces [three $\mu_2$ oxygens]. The tridimensional structure is defined by the number of oxygen bridges ($\mu_2$-oxo) between the metal atoms (Figure 1.2).
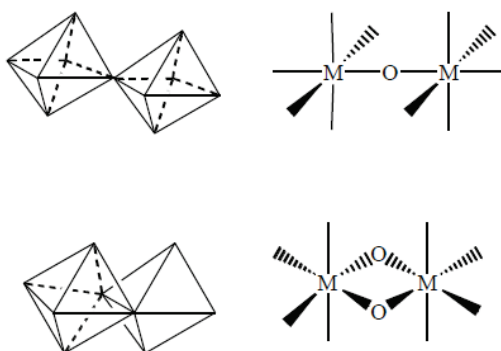


**Figure 1. 2-** Representation of most common $\mu_2$ oxygen bridges in POM structures.

The possibility to easily access this structural diversity leads to a wide range of tunable properties, such as shape, size, solubility, acidity, or redox potential of the

cluster. It is possible to tune the solubility of the cluster by changing the counterion, or master the redox potential or the acidity changing the nature of the heteroatom.[16] This confers to POMs an essential role in various area ranging from catalysis,[17,18] medicine,[19,20] electrochemistry,[21] photocromism,[22] magnetism, etc.[23]

In particular, in catalysis they have been used as oxidants since the '80. Indeed POM can easily exchange electrons with other substrates and suffer only marginal structural rearrangement.[24-26] Moreover, polyoxometalates are more stable towards the oxidative degradation than generic organic molecules, since they are made of metals in their highest oxidation state.[27] The protonated form have been used as Brønsted acids since '70s.[28] In this case they are called Heteropolyacids (HPAs), and they approach the superacidic behavior, being more acidic than classic inorganic acids, such as $H_2SO_4$ or $H_3PO_4$.

To install new properties or tune existing ones and consequently widens the applications of these interesting molecules, the anchoring of organic substituents on the POM surface has taken hold. Indeed, hybrids efficiently mix the properties of the inorganic nanoclusters with that of the organic moieties.[29] Moreover, while simple polyoxometalates are crystalline solids very hard to manipulate in organic solvents, the creation of hybrid-species provides different ways to process them, for example integrating them into functional architectures.[30]

The POMs can have multiple roles in the hybrid systems such as oxygen-enriched ligands, inorganic templates or structural nodes.

*Next paragraphs will be devoted first to the different methodologies employed, up to now, to get hybrid systems based on POMs. Successively, an overview on the supramolecular interactions between inorganic POMs and organic moieties will be addressed, to better understand how the POM presence can influence the organic moiety conformation in solution and vice versa.*

## 1.2  Hybrid-Polyoxometalates

The POM functionalization with organic substituents offers the possibility to deeply tune the properties of the hybrid resulting system. Indeed, depending on the nature of the organic moiety, it is possible to master the solubility, or the reactivity and hydrolytic stability of the resulting molecules.[28,29,31–34] Considering the anionic nature of polyoxometalates often the interaction with the organic molecule depends only on the nature of the organic part. Hybrid-POMs are classified into two main classes according to the nature of the interaction between the two domains:

- Hybrids *I class*: where only non-covalent interactions are present between the two domains (such as H-bonding, electrostatic interactions and/or Van der Waals contacts);
- Hybrids *II class*: where the organic moiety is covalently anchored to the POM surface.

Inorganic-Organic Hybrids

class I
Electronic, hydrogen bonds or van der Waals interactions

class II
Covalent or iono-covalent bonds
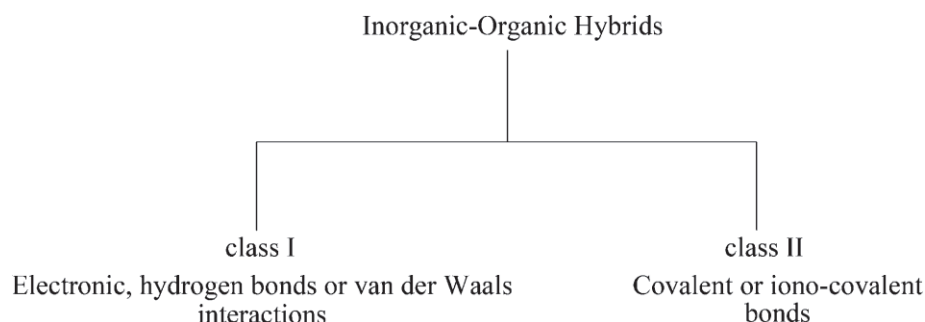
**Scheme 1. 1**- Classification of organic-inorganic hybrids based on POMs.

### 1.2.1 Hybrids *I class*

As described in the previous paragraph, the *I class* hybrids are obtained when only non-covalent interactions happen between the inorganic cluster and the organic molecule. Three different types of communication are taken into account:

a)  Electrostatic interactions;

b)    Hydrogen-bonds;

c)    Van der Waals contacts


## A. *Electrostatic interactions*

*Organic-cations*

Considering the polyanionic nature of the cluster, in presence of organic-cations the ionic interaction is generally exploited to modulate the solubility of the inorganic scaffold in organic solvents, or to generate new functional highly stable nano-architectures. Indeed, by tuning the solubility of the cluster in organic solvents, it is possible to experience the catalytic activity of polyoxometalates, such as oxidant or Brønsted acid, with organic substrates unable to interact with the inorganic catalyst in aqueous solution.

As an example of this important achievement, in 2003 the Neumann group used a perfluorinated quaternary ammonium counterion, as the $[CF_3(CF_2)_7(CH_2)_3]_3CH_3N^+$, to solubilize the sandwich-type Keggin $[WZnM_2(H_2O)_2(ZnW_9O_{34})_2]^{12-}$ in organic solvents. Indeed, despite the polyanionic character of the polyoxometalate, it became freely soluble in perfluorohydrocarbons solvents at room temperature and in ethyl acetate or toluene at 60-80°C. This soluble hybrid-POM was then exploited to perform the catalytic oxidation of aliphatic alcohols or the epoxidation of alkenes in biphasic environment.[35]

Another strategy to improve the solubility of polyoxometalates in organic solvents is widely employed by Nlate group. They focus their attention in the synthesis of different families of DENDRI-POMs, where electrostatic assembly between negatively charged POMs and cationic dendrons is exploited to create catalytic systems easily recyclable. These hybrid compounds were prepared by the reaction of various $BF_4^-$ dendritic salts with the heteropolyacid $H_3PW_{12}O_{40}$ in the presence of $H_2O_2$. Three different families of DENDRI-POMs were developed: (A) POM units located at the dendrimer periphery, (B) POM encapsulated within the cavities of the dendrimer, (C) POM-cored dendrimers: the catalytic activity is

affected by the DENDRI-POM structure.[36] As an example of DENDRI-POMs with POM units encapsulated within the dendrimer cavities, they prepared a family of 36-armed dendrimers [Methylphenyl-terminated dendrimer] containing 6 internal amino groups and used them to incorporate two $[PO_4\{WO(O_2)_2\}_4]^{3-}$ units into their structures by ionic interaction, under acidic conditions.
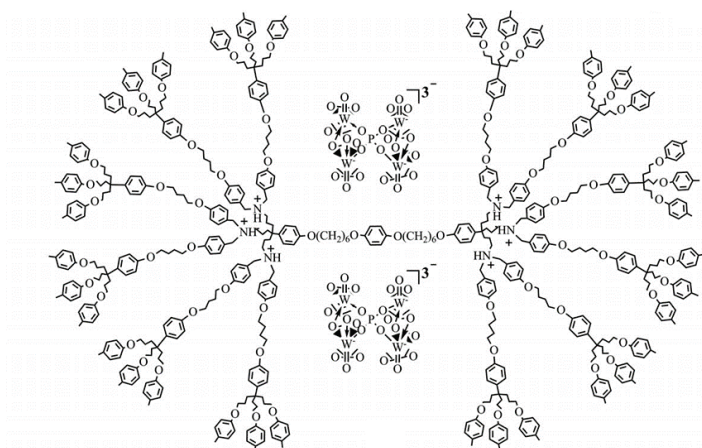


**Figure 1. 3-** Structure of the encapsulated-POM into polycationic dendritic units

The system was efficiently employed for the epoxidation of cyclooctene in aqueous/CDCl$_3$ biphasic mixture (total conversion of the substrate after 3h) and the dendritic structure allowed to enhance the stability, the recovery, and the recyclability of the catalyst, without affecting significantly their catalytic properties.[37]

More recently Hakouk and coworkers synthesized seven new photochromic hybrid organic-inorganic supramolecular assemblies combining a photoswitchable cationic spiropyran with different polyoxometalates [such as $[Mo_8O_{26}]^{4-}$, $[M(OH)_6Mo_6O_{18}]^{3-}$ (M=Al, Fe), and $[Mo_6O_{19}]^{2-}$]. Different hybrids were obtained varying the POM topology, the SP/POM ratio, and the nature of the crystallized solvent molecules. Through the ionic interaction with the inorganic cluster, a charge transfer occurs between the donor spiropyran and the acceptor POM, improving the photochromic performances in the assembled system.[38]
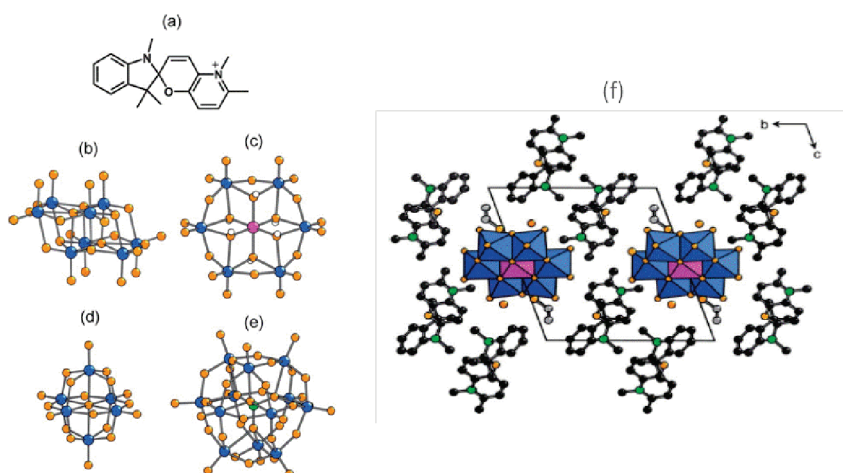
**Figure 1. 4-** Representation of: (a) cationic spiropyran (SP), (b) β-$[Mo_8O_{26}]^{4-}$, (c) the $[Mo_6(OH)_6O_{18}]^{3-}$, (d) the $[Mo_6O_{19}]^{2-}$, (e) the $[PMo_{12}O_{40}]^{3-}$, (f) example of the supramolecular organic framework formed by the SP cations and the Anderson $[Al(OH)_6Mo_6O_{18}]^{3-}$ anion.

The ionic interaction is also exploited to transfer chirality to the POM surface.[39-43] For example, Wu and coworkers employed, in 2012, a chiral amphiphilic cation with two stereocenters to encapsulate a catalytically activated sandwich-type polyoxometalate, $Na_{12}[WZn_3(H_2O)_2(ZnW_9O_{34})_2]$, through electrostatic interactions. The prepared chiral organic cation-encapsulated polyoxometalate complexes were found to self-aggregate into spherical supramolecular assemblies with a diameter of ca. 100 nm in the reaction solution and it exhibits an efficient asymmetric catalytic activity for the oxidation of sulfide with up to 72% enantiomeric excess.[44]
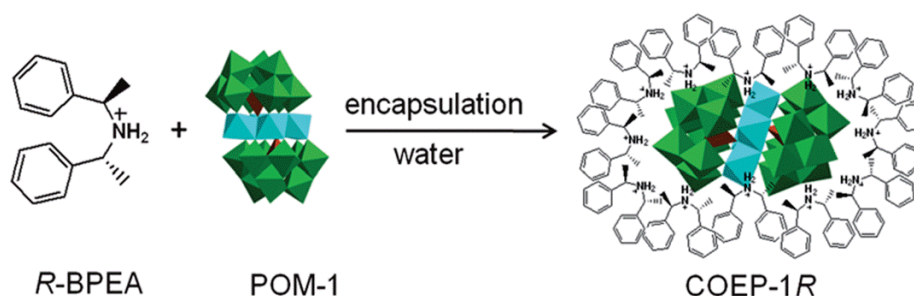


**Figure 1. 5-** A schematic illustration of the preparation procedure of the encapsulated-POM assembly.

Chiral organo-amines were also used as POM-counterion to get hybrid catalytic systems. The two moieties were combined by Luo et al. to give highly efficient,

stereoselective and recoverable enamine-based catalysts. In this case different Keggin POMs, [such as $PW_{12}O_{40}$, $PMo_{12}O_{40}$, $SiW_{12}O_{40}$, $SiMo_{12}O_{40}$ and $Cs_{2.5}PW_{12}O_{40}$] act only as inorganic scaffold for the easy recovery of the enamine-based catalyst. All the hybrid catalysts were efficiently examined for the direct asymmetric aldol reaction of acetone and p-nitrobenzaldehyde.[45]
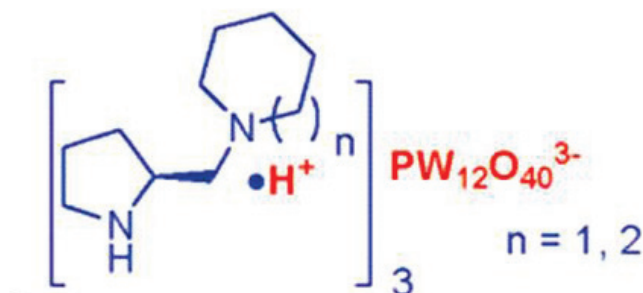


**Figure 1. 6**- Example of chiral amine-based hybrid POM developed by Luo et al.

*Cationic Polymers*

A similar strategy was exploited to create new functional materials with polycharged polymer species. The polyoxometalate/polymer hybrid materials concurrently possess the unique optical, electrical or catalytic properties of polyoxometalates and the favorable processability and stability of polymer matrices.[46]

As an example, Haimov and Neumann have used this pathway to develop a new type of catalyst composed of polyelectrolytes and POMs that exhibit excellent performance in the oxidation of hydrophobic 2-alkanols. A cross-linked polyethyleneimine polymer containing the $[ZnWZn_2(H_2O)_2(ZnW_9O_{34})_2]^{12-}$ polyoxometalate was prepared from branched polyethyleneimine (Mw=600), the polyoxometalate, and a n-octylamine-epichlorohydrin cross-linking reagent. This catalytic assembly was active for the selective oxidation of 2-alkanols to 2-alkanones with aqueous $H_2O_2$: the catalytic reaction presumably occurs at the hydrophobic domain. The synergy between the properties of POMs and of the polymer enables the hybrid materials to perform efficiently in the catalytic oxidation of 2-alkanols to the corresponding ketones.[47]
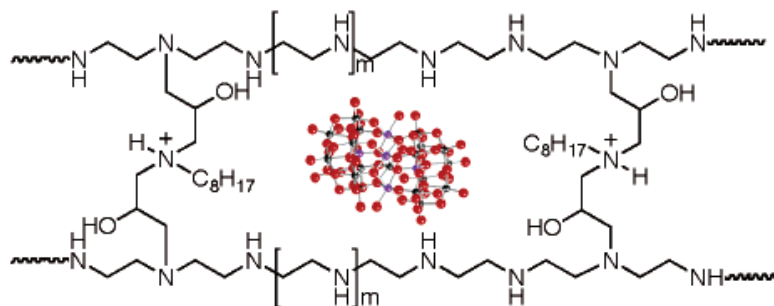
**Figure 1. 7-** 1.1Cross-Linked Polyethyleneimine Containing $[ZnWZn_2(H_2O)_2(ZnW_9O_{34})_2]^{12-}$

Following the same idea, electrostatic interactions with alkyl ammonium polycations were used to create heterogeneous catalyst for industrial applications, considering that in this manner the catalyst can be easily recycled, reducing the environmental impact and providing better thermal stability.[32] As an example, in 2007 Richards, Kortz and co-workers immobilized different tetrairon(III)-substituted polytungstates $[Fe_4(H_2O)_{10}(\alpha-XW_9O_{33})_2]^{n-}$ (n=6, if X=As$^{III}$, Sb$^{III}$; n=4, if X=Se$^{IV}$, Te$^{IV}$) on modified SBA-15. In particular, they modified the oxide surface with (3-aminopropyl)triethoxysilane, giving a positive charge to the surface, that interacts efficiently with the negative POM, generating an heterogeneous catalyst, able to perform the solvent-free aerobic oxidation of long-chain n-alkanes using air as oxidant.[48]
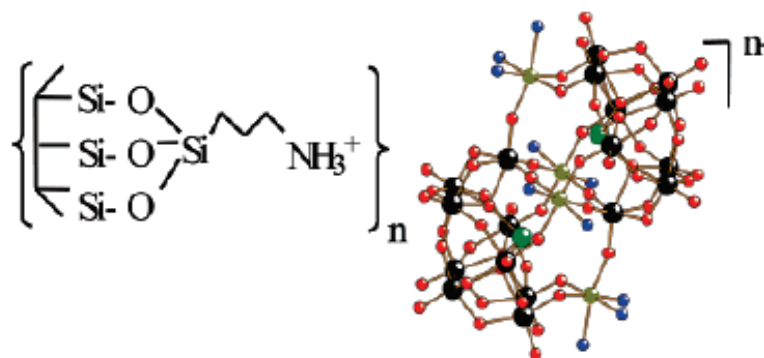


**Figure 1. 8-** SBA-15-apts-Fe$_4$X$_2$W$_{18}$ (n=6, if X=As$^{III}$, Sb$^{III}$; n=4, if X=Se$^{IV}$, Te$^{IV}$)

*Cationic surfactants*

A similar electrostatic approach was used between hydrophilic POMs of different sizes and shapes and hydrophobic cationic surfactants.[49] Indeed, to improve the

processability of the inorganic cluster several strategies have been adopted to prepare POM-based nanostructured thin films, including (i) POMs entrapped in polymer matrices; (ii) self-organized hybrids based on POMs and cationic surfactants; (iii) Langmuir—Blodgett techniques; (iv) layer-by-layer self-assembly methods and (v) other approaches. As an example, in 2000 Kurth and co-workers produced core–shell like assemblies, called surfactant-encapsulated clusters (SEPs), thanks to a cationic-ligand exchange process in the second coordination sphere of the POM. The countercations from the hydration sphere of the POM anions were replaced by the cationic amphiphiles and resulted in discrete core-shell type assemblies, in which a hydrophilic POM core was surrounded by a hydrophobic shell with outward alkyl chains.[50]

Different Surfactant-encapsulated clusters were also developed by the Wu group to get new functionalized materials.[51-54] For example, the terbium-substituted Keggin heteropolyoxotungstate complex [L1]$_{13}$[Tb(SiW$_{11}$O$_{39}$)$_2$]*30H$_2$O bearing mesomorphous groups (L1=azobenzene-containing surfactant) was prepared by the ionic self-assembling route, exhibiting characteristic thermotropic liquid-crystalline behavior, because of the presence of the organic surfactant. Moreover the obtained complex is immiscible in water but readily dissolved in organic media.[54]
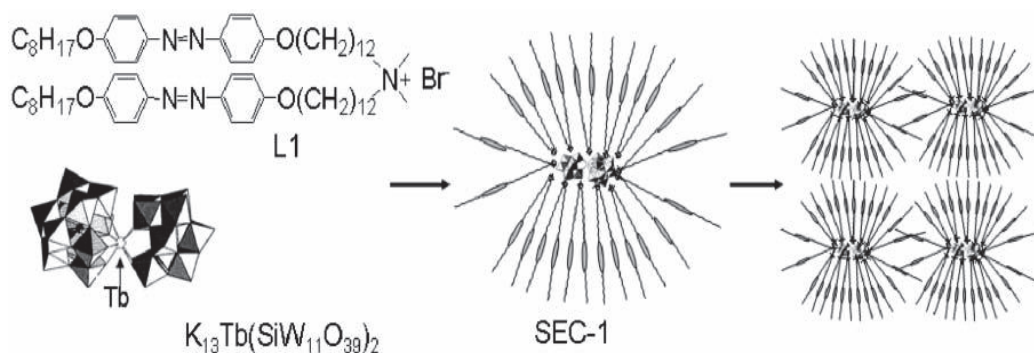


**Figure 1. 9-** Surfactant-encapsulated cluster exhibiting thermotropic liquid-crystalline behavior, developed by the Wu group.

*Ionic liquids*

Furthermore, electrostatic interactions were used to create hybrid-POM based on ionic liquids (IL), to exploit the interesting properties of IL[55] to improve the catalytic activity of the inorganic complex.[56,57]

Cuan and Yan developed a multicomponent hybrid-POM based on silica support modified with ionic liquids. In particular they developed a new photofunctional hybrid material based on the photoactive Keggin POM $Na_9EuW_{10}O_{36} \cdot 32H_2O$, and benzoate (4-aminobenzoate, 4-hydroxybenzoate, 4-mercaptobenzoate) modified mesoporous silica through imidazolium ionic liquid (IL, 1-methyl-3-(trimethoxysilylpropyl). Here IL behaved as double linkage, which interacted with POM through electrostatic force and form covalent bond to the functionalized SBA-15 mesoporous silica thanks to its alkoxy group. The new photoactive system possessed high chemical and thermal stabilities (decomposition temperature can reach more than 400 °C) and highly uniform ordered 2-dimensional structure. Furthermore it exhibits strong characteristic $Eu^{3+}$ luminescence with long decay time (to millisecond scale) and large radiative transition areas to contribute high quantum efficiency.[58]

A few months ago, the Yu group developed a pH-responsive POM based supramolecular hybrid, exploiting ionic interaction between a COOH-functionalized ionic liquid, such as the N-decyl-N'-carboxymethyl imidazolium bromide, and the Keggin type polyoxometalate $H_3PW_{12}O_{40}$. The prepared material possesses multiple properties, including reversible pH-response and renewable catalyst for dye degradation. Indeed the degradation of methyl orange (MO) in aqueous solution was selected as a standard reaction to examine the catalytic activity of the hybrid system. In general, POM can activate $H_2O_2$ for the oxidation of organic compounds only under strong light irradiation (<400 nm), while in this system they succeed to efficiently degrade the MO without light irradiation in presence of $H_2O_2$. More interestingly they saw that the hybrid catalyst material became yellow, aggregated and lost activity after conducting catalysis reaction for

11

6–8 times, probably because some residual organic molecules have been absorbed on the catalyst surface and blocked the access to catalytic POM interface.

When the pH of the aqueous solution was adjusted to 6.5, the yellow aggregates in solution reduced gradually and the hybrid catalyst dissociated due to the electrostatic repulsions between negatively charged POM and the deprotonated ionic liquid. After adjusting the pH to 3.0, the nanosphere were reformed and the catalytic activity regenerated.[59]
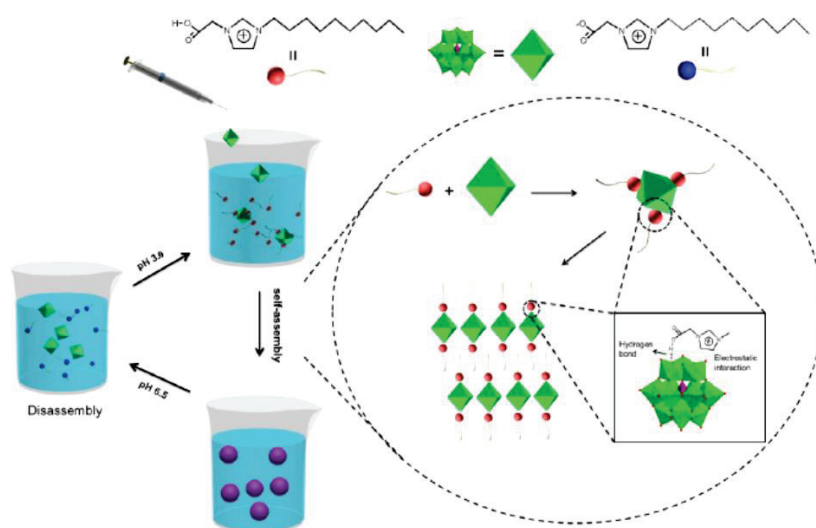


**Figure 1. 10-** Schematic illustration of the formation mechanism of POM/[N-C10, N'-COOH-Im]Br hybrid materials and the reversible disassembly and assembly processes induced by changing pH in the aqueous solution.

## B.    *Hydrogen-bonding*

Another way to get type I POM-based hybrids is to rely an H-bonding between an organic H-donor and the POM, whose metal-oxide is the H-acceptor.[60] The ability of large POM anions to act as templating agents, thanks to hydrogen bonds, has been clearly demonstrated by Fang and co-workers in 2013, with the formation of {Mo24Fe12} macrocycles.

They discovered that the Keggin $[SiMo_{12}O_{40}]^{4-}$ and Dawson $[P_2W_{18}O_{62}]^{6-}$ POMs act as hydrogen bonds acceptor toward the organic Fe-EDTA ligand. Indeed, considering that both moieties are negatively charged, a columbic repulsion was expected. Instead, the organic moiety arranges itself around the belt of the two

POMs in a macrocyclic pathway, thanks to multiple weak supramolecular hydrogen bonds that, despite being individually weak, collectively drive and stabilize this giant assembly.
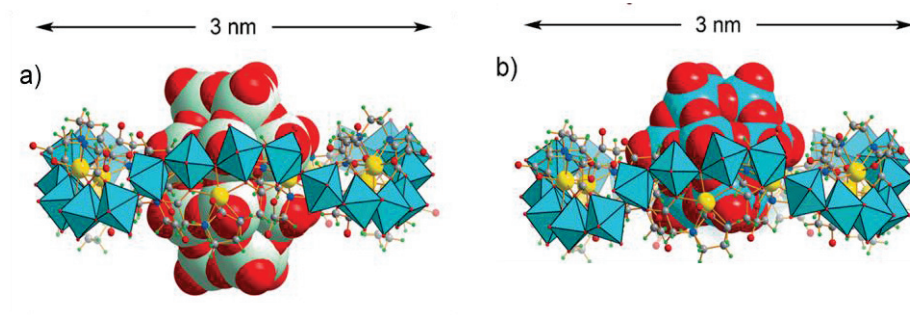


**Figure 1. 11-** a) Well-Dawson Hybrid $[(P_2W_{18}O_{62})Mo_{24}(Fe\text{-}edta)_{12}O_{72}]^{18-}$; and b) Keggin hybrid $[(SiMo_{12}O_{40})Mo_{24}(Fe\text{-}edta)_{12}O_{72}]^{16-}$.

In particular exterior oxygen atoms of the Keggin guest, terminal and bridging ones, are the recipients of hydrogen bonds originating from $CH_2$ groups of the inward-pointing EDTA ligands. All hydrogen bonding interactions were found to be fairly weak, as expected from C-H donors, with donor(C)–acceptor(O) distances longer than 3.2 Å. Same arrangement of the organic ligand was found for Dawson POM. Indeed, the belt layer has more oxygen acceptors than a polar layer, particularly terminal ones that are easily accessible to donor groups. Hydrogen-bonding interactions occurring at belt layers of the guest are thus more robust, imparting additional stability to the host–guest assembly. The authors performed also some studies in solution seeing that the host–guest complexes maintain their solid-state structure in solution, and no free {$Mo_{24}Fe_{12}$} macrocycle could be isolated or detected without an encapsulated guest. Moreover no exchange with external POM anions was observed even at elevated temperature (80°C), by adding an excess amount of $[SiMo_{12}O_{40}]^{4-}$ to a solution of encapsulated Dawson anion. [61]

Another example of hydrogen-bond interactions between polyoxometalates and organic molecules was given by Shi et coworkers in 2009.[62] In that case, two new

hybrid polyoxometalates $[HN(C_2H_5)_3]_3[PMo_{12}O_{40}]$ and $NH_2(C_2H_4NH_3)_2]_2[Mo_5P_2O_{23}]$ were synthesized and the crystal structure analyses reveal complex 3D-supramolecular networks given by multiple hydrogen bonds, in both hybrid species, between the organic ligand and the inorganic scaffold. However, no evidence of the maintained hydrogen bonds network in solution was presented.

The Wu group carried out a series of studies on the Anderson $MnMo_6$-containing main chain Cluster Supramolecular Polymers (CSPs) driven by hydrogen bonding interactions.[63–66] For example, they synthesized an azobenzene (Azo) grafted $MnMo_6$ cluster with dimethyldioctadecylammonium (DODA) as counterion. It was found that the novel surfactant-encapsulated Azo-grafted POM complex exhibits a fiber-like morphology in its *trans* state, while upon UV irradiation it displays a spherical structure. C–H--O hydrogen bonds existed between the terminal oxygen atoms of $MnMo_6$ and hydrogen atoms of the phenyl ring of the Azo groups in the trans-form, which drove Azo-$MnMo_6$ to self-assemble in fibers. The reversibility of the *trans–cis* isomerization of the Azo group induced the association and dissociation of the hydrogen bonds. As a result, a photoresponsive morphological transformation of Azo-$MnMo_6$ from fibers to spheres was achieved by the authors.[63]
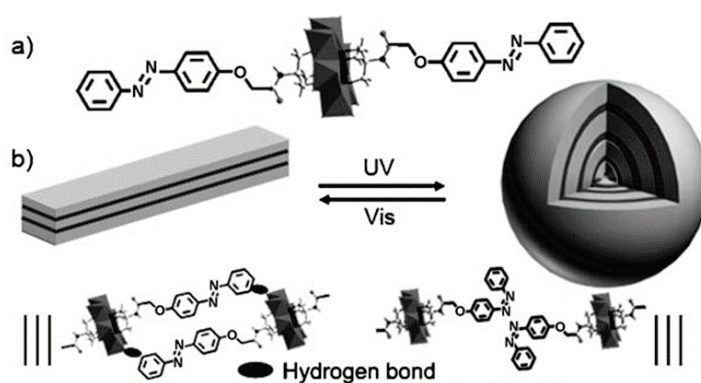


**Figure 1. 12-** a) Structure of anionic grafted azo-POM. b) Reversible morphology change of the surfactant-encapsulated organically grafted polyoxometalate between fibrous and spherical structures upon stimulation by light.

*No more examples about the existence of H-bonds in solution at molecular level are present in literature.*

## C. *Supramolecular Host-Guest interactions*

Beyond the self-assembly process which has much uncertainty, the synthesis of rational organic–inorganic hybrid POM compounds by incorporating POMs into prefabricated MOFs (Metal-Organic frameworks) is also an interesting method to get *type I* hybrid POMs.[67] One of the representative compounds is a Keggin-type polyoxoanion incorporated in HKUST-1 reported by Yamase in 2003. In this case, the Keggin-type polyoxoanion is entrapped into the HKUST-1 pores due to the perfect matching in size and symmetry between the two domains. The high loading of the POM in the porous structure facilitates the catalytic reactions.[68]

In 2009, Liu and co-workers reported a serie of organic–inorganic hybrid POM compounds by the one-pot hydrothermal reaction of Cu ions, BTC (1,3,5-benzencarbonxylate) and Keggin-type polyoxoanions ($H_4SiW_{12}O_{40}$ $nH_2O$, $H_4SiMo_{12}O_{40}$ $nH_2O$, $H_4GeW_{12}O_{40}$ $nH_2O$, $H_3AsMo_{12}O_{40}$ $nH_2O$, $H_3PW_{12}O_{40}$ $nH_2O$, or $H_3PMo_{12}O_{40}$ $nH_2O$). Indeed, the MOF presents two different cavities type with diameters of 13 Å and 11 Å and sizes of accessible windows of 11 Å and 9.3 Å, respectively. As shown in the Figure 1.13, cavity A is occupied by Keggin polyoxoanions and cavity B is occupied by $(CH_3)_4N^+$ cations and water molecules. They chose the hydrolysis of ester in water to test the acid catalytic properties of the compounds finding that, while HKUST-1 showed no catalytic activity and the simple mixture of HKUST-1 and $H_3PW_{12}O_{40}$ gave low conversion in the same reaction, the POM-MOF presents a big activity toward the hydrolysis of ethyl acetate in excess of water.[69]
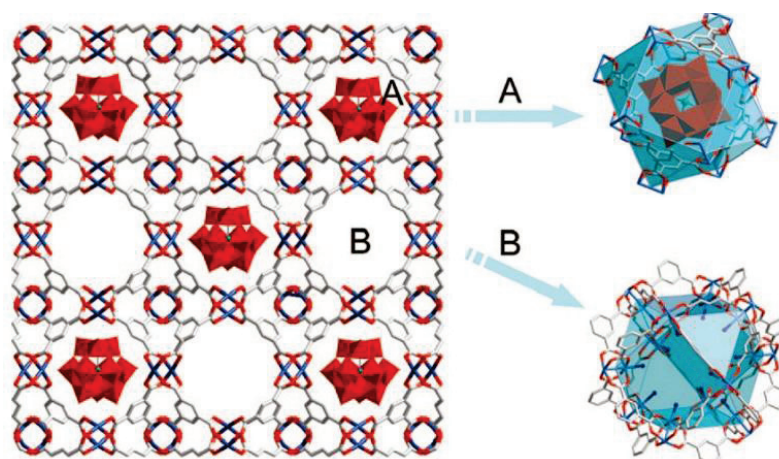
**Figure 1. 13-** Polyhedral and ball-and-stick representation of a representative POM-MOF hybrid: Color code: Blue, Cu; red, O; grey, C.

More recently, Tong and coworkers encapsulates two different POMs, such as the $H_4PMo_{11}VO_{40}$ and $H_5PMo_{10}V_2O_{40}$, in a metal-organic framework (MIL-100) using a direct hydrothermal method. The catalytic performances of the new material were experienced toward the allylic oxidation of the cyclohexene with $H_2O_2$ as green oxidant and, the catalyst could be recycled at least five times without no loss of activity.[70]

Dolbecq and collaborators developed a big family of zeolitic Polyoxometalate-Based Metal-Organic Frameworks (Z-POMOFs), changing the linker grafted in the POM surface.[71-73] As an example, in 2011 they developed, in situ under hydrothermal conditions, a POMOF system based on tetrahedral ε-Keggin polyoxometalates capped by Zn(II) ions, functionalized with triangular 1,3,5-benzene tricarboxylate linkers $(TBA)_3[PMo^V_8Mo^{VI}_4O_{36}(OH)_4Zn_4][C_6H_3(COO)_3]_{4/3}$ *6H_2O. A 3D open-framework was obtained, where the molecular Keggin units were connected by tricarboxylate linkers with channels occupied by tetrabutylammonium (TBA) counterions. The new highly stable POMOF system was employed to modify electrodes by direct adsorption of the POMOFs on glassy carbon or entrapment in carbon paste (CPE) and a good electrocatalytic hydrogen evolution reaction was detected with a yield greater than 95%, and a turnover number as high as 1.2* $10^5$ was obtained after 5 h.[71]
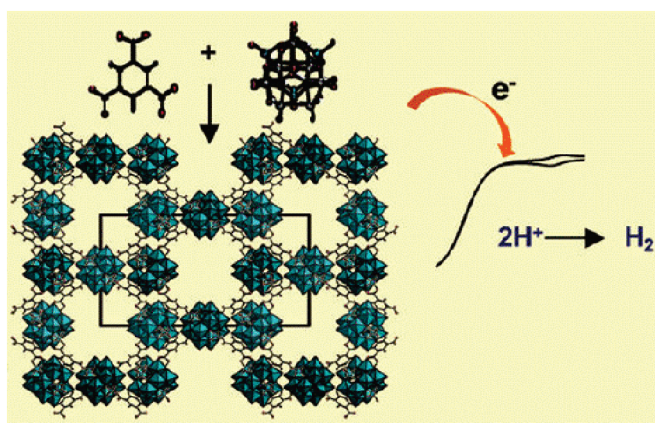
**Figure 1. 14-** Illustration of a POMOF system obtained by Dolbecq and collaborators (ref. 71) and its employ as electrocatalyst toward the hydrogen evolution reaction.

Besides the POM-MOF materials, the host-guest interaction was used also to promote the assembly between POMs and Cyclodextrines (CDs). For example, Wu and co-workers in 2015, discovered that a supramolecular association happens between CDs (α and β- CDs) and a POM $[PMo_{12}O_{40}]^{3-}$ in aqueous solution, as well as in the solid state. Structural analyses of these unprecedented hybrid complexes have revealed the partial encapsulation of the anionic POMs in the inner cavities of CDs, in contradiction to the well-recognized belief that only hydrophobic compounds undergo association with CDs in aqueous solutions.[74]

Before them, the host-guest interaction between a POM and cyclodextrine was studied by Izzet et al. In that case, the Dawson polyoxometalate was already hybridized with an aromatic moiety $K_7[α_2-P_2W_{17}O_{61}\{Sn(C_6H_{4I})\}]$. The organic moiety was the CD-cavity guest, driving the interaction with the α-CD and β- CD. In particular, the authors investigated the host-guest interaction in solution through ${}^1$H-NMR, finding binding constants of 780±50 M$^{-1}$ for the α-CD and 1020±50 M$^{-1}$ for the β-CD. Moreover, they evidenced that only a partial inclusion of the POM aromatic part happens with the secondary face of the α-CDs; while a deep inclusion of the aromatic substituent takes place in the cavity of the β-CD. Finally, they demonstrated that the inclusion complexes allow the restoration of the anchored organic moiety after a basic stress, a process otherwise not fully

reversible. The full recovery of the original material after four successive basic degradations was demonstrated. [75]
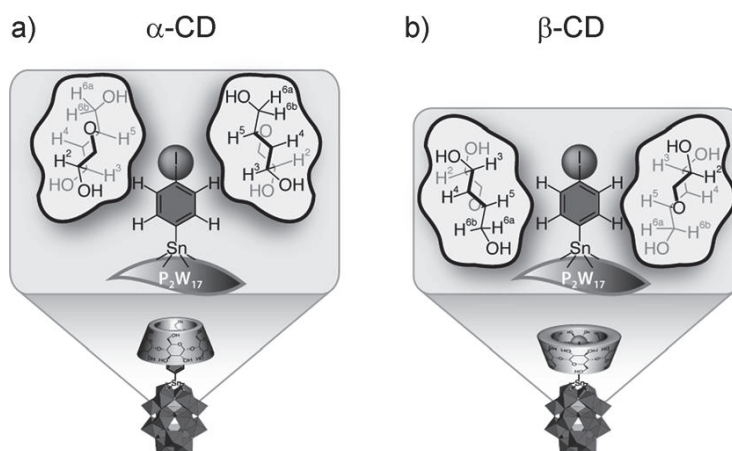


**Figure 1. 15-** Ilustration of the two POM adducts with a) α-CD and b) β-CD

## 1.2.2    **Hybrids *II* class**

Although such electrostatically immobilized POM-based materials often display appreciable stability, catalyst leaching may remain a problem. The *type II* hybrid polyoxometalates are obtained through covalent functionalization of the inorganic scaffold with organic moieties. Two main strategies are known to modify the POM structure:

a)    Creation of lacunary POMs, followed by coordination of such metals or organo-metallic groups, from the nucleophilic vacant oxygen atoms exposed on the POM surface, giving *Transition Metals-Substituted Polyoxometalates* (TMSPs) complexes.

b)    Grafting of organic moiety into the POM structure, thanks to the substitution of the oxo-ligands of the POM by the oxygen atoms of the organic part.

## A.    *Lacunary species functionalization*

Plenary POMs usually are weakly basic and nucleophilic, except when the surface charge is increased either by substitution of metals from groups 4 or 5 or by reduction. Lacunary POMs have higher charges, hence increased basicity and nucleophilicity compared to their parent complete species. Thus they react quite easily with a variety of electrophilic groups in water or in non-aqueous solvents. Since POMs are hydrolytically unstable in alkaline media, it is possible to exploit this behavior to promote in a controlled way the selective formation of structural defects.[76,77] The resulting vacant or "lacunary" POM complexes derive from the saturated precursors through the formal loss of one or more $MO_6$ octahedral unit and can be used as ligands for electrophilic species, as well as transition metals and organometallic groups, such as organophosponates, organoarsenates, organotin, etc.[31,33,34,78–82]



pH = 4 ~ 5

-MO

$[XM_{12}O_{40}]^{n-}$
**Parent POM**

$[XM_{11}O_{39}]^{(n-m)-}$
**Mono Lacunary POM**
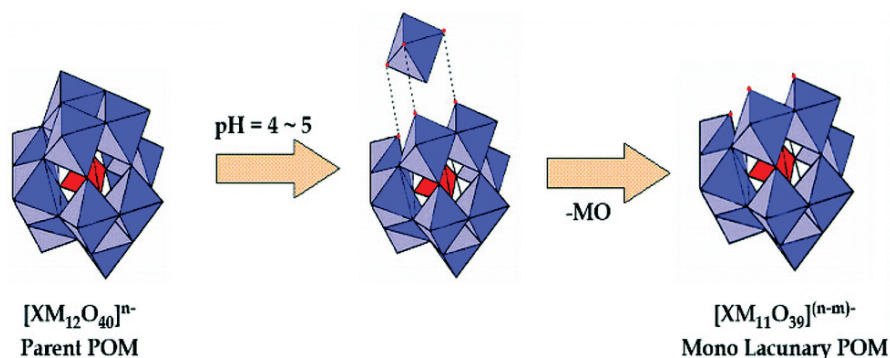
**Figure 1. 16-** Formation scheme of a mono-lacunary POM.

Siloxane- or stannane-based class II hybrids can be easily synthesized because Si-$C_{sp}^3$ and Sn-$C_{sp}^3$ bonds are resonably stable toward attack by nucleophilic species such as water, alcohols, hydroxylated ligands, etc. The precursors of these compounds are organo-substituted silicic acid esters of general formula $R'_nSi(OR)^{4-n}$, bridged precursors of silesquioxanes $X_3Si-R'-SiX_3$ (X=Cl, Br, OR) or organostannanes, $R'_nSn(X)^{4-n}$ (X=OR, Cl, or C≡CH), where R' can be any organo-functional group and $n$ is usually 1 or 2.

Klemperer was the first, in 1978, to have the idea to synthesize a functionalized polyoxometalate from a lacunary structure: $[PW_{11}O_{39}]^{7-}$ reacted with $CpTiCl_3$ in $CH_2Cl_2$ to give $[PW_{11}O_{39} (TiCp)]$.[83]

After the use of Titanium atom as coordinating metal, different other metals were used from other groups to functionalize the lacunary POMs: Silicium,[31,84–88] Germanium[89,89] and Tin atoms.[90–95]

Depending on the radius dimension of the metal, the exposed oxygen atoms of the POM could coordinate one or two metals at the same time, open also the possibility of the bis-functionalization. This is the case for Germanium and Silicium substituted polyoxometalates, where two atoms are necessary to fill the lacuna on the POM because of the small dimension of the radius metal (r=54 pm and r=67 pm, for $Si^{4+}$ and $Ge^{4+}$ respectively). Differently, the $Sn^{4+}$ and $Ti^{3+}$ cations have the good radius dimension to fill entirely the POM vacancy (r=83 pm and r=81 pm, for $Sn^{4+}$ and $Ti^{3+}$ respectively).
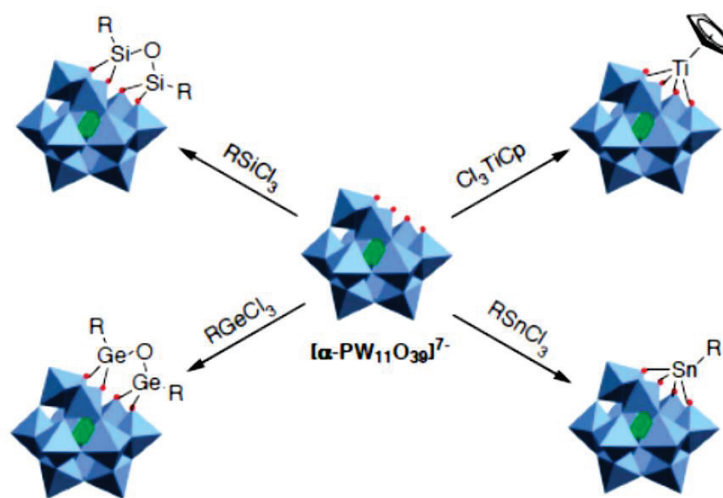


**Figure 1. 17-** Examples of lacunary POMs functionalization (the monolacunary Keggin $[\alpha\text{-}PW_{11}O_{39}]^{7-}$) with organic ligands.

Concerning organogermyl,-arsenyl and-stibyl functionalized POMs only few examples can be found in the literature.[92,96] More interesting are the cases of organo-tin, organo-silyl and organo-phosphonate derivatives.

*A brief highlight of these hybrids will be given below.*

*Organo-tin*

Organo-tin derivatives are a quite interesting family because of the relatively high stability of the Sn-C bond toward hydrolysis, the similar size of $Sn^{IV}$ and $W^{VI}$, the facile inclusion of organotin fragments in lacunary polyoxotungstates, and the ability to characterize the species in solution using multinuclear NMR spectroscopy, such as ^{119}Sn-NMR. Different groups contributed to the development of the chemistry of organo-tin lacunary polyoxometalates.[29] Starting with Liu et co-worker in 1998, they studied the reactivity of mono-organotin moieties with mono-, di-, and trivacant Keggin or monovacant Dawson heteropolyoxotungstates, using four different organotin fragments, $\{SnPh\}^{3+}$, $\{Sn(CH_2)_2CN\}^{3+}$, $\{Sn(CH_2)_2C(O)OCH_3\}^{3+}$, and $\{CH_2-CH(CH_3)C(O)OCH_3\}^{3+}$ and, then they studied the antitumoral activity of these hybrids to Hela and SSMC-7721 tumor cells.[97–100]

Another interesting example was given by Pope et co-workers that synthesized the dimer of the trivacant tungstoantimoniate $\alpha$-SbW$_9$O$_{33}$ thanks to three phenyltin fragments that stabilize the dimeric structure.
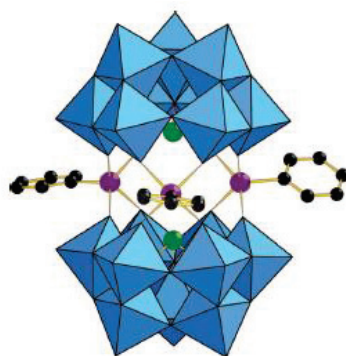


**Figure 1. 18-** Structure of organo-tin derivative [(PhSn)$_3$-Na$_3$($\gamma$-SbW$_9$O$_{33}$)$_2$]$^{6-}$ synthesized by Pope.

Lacôte, Thorimbert and Hasenknopf decided to attach a mono-organotin trichloride group to the lacunary Dawson polyoxotungstate [$\alpha$-P$_2$W$_{17}$O$_{61}$]$^{10-}$, in manner to retain a reactive group on the organo chain (such as carboxylic acid, azide, alkyne), easily post-functionalizable: an extended family of hybrids was generated.[80,81,95,101,102]
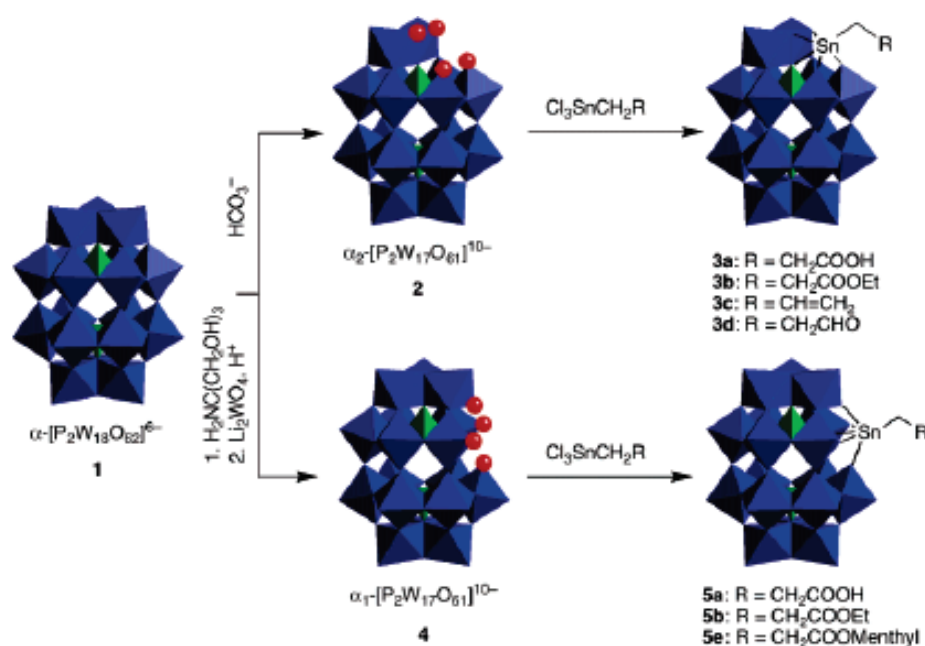
**Figure 1. 19-** Scheme of functionalization reaction of lacunary Dawson polyoxotungstates with reactive organo-tin groups.

Moreover, coordination or coupling of chiral amines or aminoacids has allowed to differentiate between the enantiomers of $[\alpha_1\text{-}P_2W_{17}O_{61}Ln(H_2O)_x]^{7-}$ and those of $[\alpha_1\text{-}P_2W_{17}O_{61}SnCH_2CH_2CO_2H]^{7-}$. These results opened the way to the resolution of the chiral $[\alpha_1\text{-}P_2W_{17}O_{61}]^{10-}$ polyoxoanion.

*Organo-silyl*

Also organo-silyl and-phosphoryl groups have attracted great interest.

Organosilyl derivatives are in general obtained from reactions between lacunary heteropolyoxometalates (Keggin or Dawson lacunary structures) and the appropriate organosilane ($RSi^{3+}$). The first organosilyl hybrid-POM was described by Knoth in 1979. The reaction between the organotrichlorosilanes and the Keggin $[\alpha\text{-}SiW_{11}O_{39}]^{8-}$ afforded the anions $[\alpha\text{-}SiW_{11}O_{39}\{O(SiR)_2\}]^{4-}$ (with R $=C_2H_5$, $C_6H_5$, $NC(CH_2)_3$, $C_3H_5$).[103] Starting from 2004 this functionalization strategy with organo-silyl moieties had been extended also to monovacant Dawson heteropolyoxometalates $[P_2W_{17}O_{61}]^{10-}$ [85–88,104–106] and in parallel to the divacant [γ-

$SiW_{10}O_{36}]^{8-}$ and $[\gamma\text{-}PW_{10}O_{36}]^{7-[31,84,107–109]}$ or the trivacant Keggin $[PW_9O_{34}]^{9-}$ polyanion.[110]

Bonchio and co-workers described the synthesis and photocatalytic activity of POM–fullerene hybrids resulting from the direct functionalization of $[\gamma\text{-}SiW_{10}O_{36}]^{8-}$ with organosilyl fulleropyrrolidines. The resulting hybrids were found to be active in catalytic photo-oxygenation of phenol and L-methionine ester in water, in heterogeneous conditions, using visible light irradiation for waste-water treatment applications.[31]
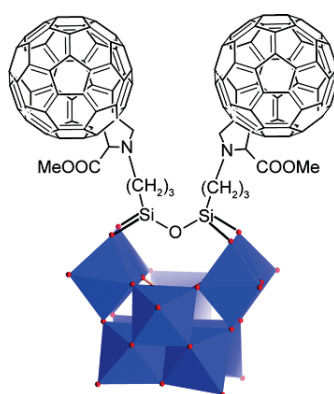


**Figure 1. 20-** Organosilyl fulleropyrrolidines derivative based on lacunary keggin POM synthesized by Bonchio and coworkers.

*Organo-phosphonate*

The functionalization of mono-, di- and trilacunary Keggin-type phospho- or silicotungstates with organo-phosphonate moieties has been thoroughly explored as well. Organophosphonic acids $RPO(OH)_2$ and organophosphonic dichlorides $RPOCl_2$ react with lacunary heteropolytungstates in homogeneous solution or under phase transfer conditions. By contrast to organosilyl groups, only two $RPO^{2+}$ electrophilic groups are grafted even when multivacant Keggin tungstates are used. The group of Hill was the first to report the synthesis of $[\alpha\text{-}XW_{11}O_{39}(PhPO)_2]^{(8-n)-}$ by reaction of $[\alpha\text{-}XW_{11}O_{39}]^{(12-n)-}$ with $PhPOCl_2$ in acetonitrile.[111]

Some reports on the reactivity of Wells–Dawson, $[P_2W_{17}O_{61}]^{10-}$ and Keggin-type $[XW_{11}O_{39}]^{n-}$ (X =B, Ga, Ge) monovacant frameworks can be found in the

literature.[112] As an example, Bonchio et al. reported the decoration of divacant Keggin-type polyoxotungstate $[\gamma\text{-}SiW_{10}O_{36}]^{8-}$ with chiral phosphonic groups, yielding the bis-functionalized hybrid $[\gamma\text{-}SiW_{10}O_{36}(R^*PO)_2]^{4-}$ with R*=N-protected aminoalkyl groups or O-protected amino acid derivatives. Through Circular dichroism analysis, they showed a chirality transfer between the organic ligand and the inorganic complex.[113]
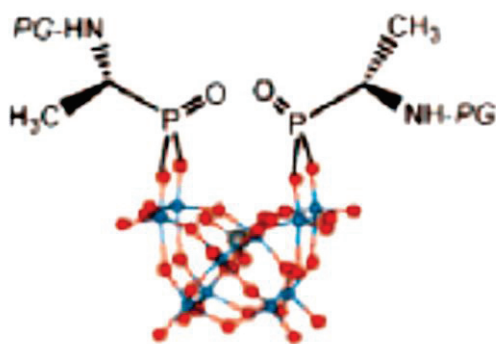


**Figure 1. 21-** Grafting of N-protected aminoethyl phosphonic acids into the divacant $(\gamma\text{-}SiW_{10}O_{36})^{8-}$ Keggin type POM.

These chiral organo-POMs were used as asymmetric catalysts toward the oxidation of sulfides in sulfoxides, with hydrogen peroxide under microwave irradiation *(more details about the catalytic activity will be given in the next chapter)*.

## B.   *Grafting of organic molecules*

The second synthetic pathway to hybridize the inorganic oxocluster provides the substitution of some oxo-ligands on the POM surface with the organic molecule.

First examples of Organoimido and nitrido POMs were reported by Kang and Zubieta, who designed the Lindqvist-type derivatives $[Mo_6O_{18}(NTol)]^{2-}$ and $[Mo_6O_{18}(N)]^{3-}$, obtained by condensation of $[Mo_2O_7]^{2-}$ with $[Mo(NTol)Cl_4(thf)]$ and $[MoNCl_4]^{-}$, respectively.[114]

Maatta reported the first example of well characterized di-[115,116] and poly-[117] organoimido derivatives on the same hexamolybdate.
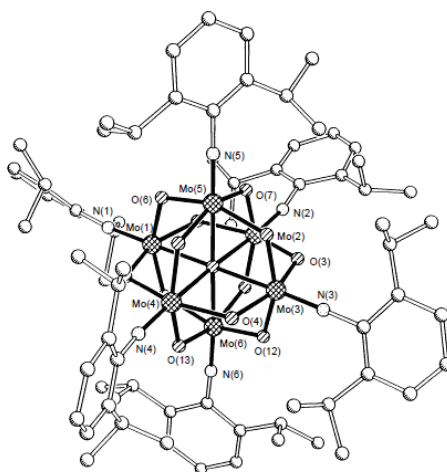
**Figure 1. 22-** Structure of the $[Mo_6(NAr)_6O_{13}H]_2$ anion synthesized by Maata et co-worker.

The only successful two cases in the synthesis of Keggin-type imido derivatives were reported by Proust and Duncan in 2004 and 2007, respectively.[118,119]

In the same manner, monodentate alkoxo ligands has been used to functionalize POM structures,[120–122] but the main strategy to easily functionalize these inorganic structures is using trialkoxo ligands. Indeed, trialkoxo-POMs are obtained by treatment of $\alpha$-$[Mo_8O_{26}]^{4-}$ with the appropriate metal precursor and the designed trisalkoxo ligand in refluxing acetonitrile.[123–129]
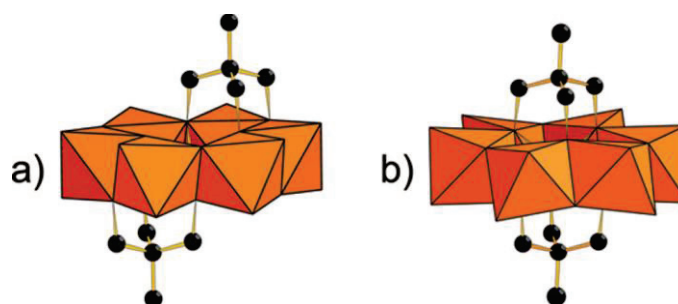


**Figure 1. 23-** Examples of bis-functionalized Anderson-type polyoxometalates with trisalkoxo ligand: (a) $\chi$ isomer and (b) $\delta$ isomer

Hill and Cronin focused their attention on the functionalization of a Dawson tungstovanadate, such as $[H_4P_2V_3W_{15}O_{62}]^{5-}$, with trialkoxo ligands.[130,131] In particular, Hill was the first that used tris(hydroxymethyl) groups in dry polar aprotic organic solvents, to generate tetra(polyoxometalate) terminated dendrimers.

Cronin, later, synthesized and characterized a series of trisalkoxopolyoxometalates, such as $[(RC(CH_2O)_3)\text{-} P_2V_3W_{15}O_{59}]^{6-}$, with R =CH$_3$, NH$_2$, NO$_2$.
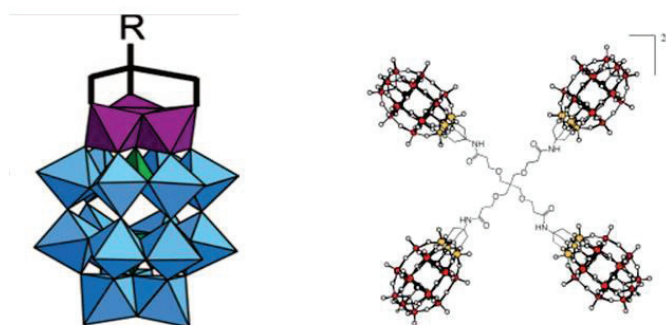


**Figure 1. 24-** Polyhedral representation of $[(RC(CH_2O)_3)\text{-} P_2V_3W_{15}O_{59}]^{6-}$ (R =CH$_3$, NH$_2$, NO$_2$) on the left, and representation of the tetra-polyoxometalate dendrimer synthesized by Hill and co-workers, on the right.

Finally, Lacôte, Hasenknopf, Thorimbert and collaborators used the same Dawson polyoxotungstovanadate to graft a series of diols,[132,133] substituting one sp$^3$ oxygen of the general trialkoxy organic ligand with an sp$^2$ one, such as diolamides, diolureas, diolcarbammates ligands, which generates an electronic conjugation between the inorganic scaffold and the organic ligand.
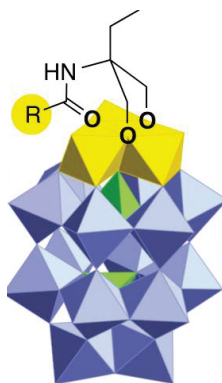


**Figure 1. 25-** Insertion of a diolamide ligand into a Dawson $[P_2V_3W_{15}O_{62}]^{9-}$

Because of this electronic interaction between the organic ligand and the inorganic scaffold, the nature of the substituent on the phenyl ring can affect the redox potential of the polyoxometalate, also leading to more chemoselectivity *(More details about the catalytic activity will be given in the next chapter).*

### C.    *Post-functionalization of organo-polyoxometalates*

In some cases the organic part of a POM hybrid can be modified through common organic reactions, so that the original hybrid behaves as a platform from which further derivatives are conveniently prepared. The method offers greater simplicity than direct functionalization, although the reactivity of the incorporated organic group is sometimes altered with respect to the ''free'' group.

Keana and co-workers were the first, in 1985, to go along this direction. They studied the reactivity of an organic function supported by a POM, a Dawson- and Keggin-type anion monofunctionalized by a Ti$^{IV}$ ion bearing a substituted cyclopentadienyl group (Cp), and further exploited the chemistry of the organic ligand attached to the Cp group.[134,135] In particular, they used the N-phenylmaleimides as versatile group for the post-attachment of a variety of protein-reactive groups to the polyanions.

Starting from there, in the last decade the synthesis of organo-POM suitable for successive post-functionalization reactions has taken hold.[29] Different methodologies have been exploited to easily post-functionalize organo-POMs: click-chemistry approach, carbon-carbon cross couplings, metal coordination pathway, peptide bonds formation and, very recently, nucleophilic substitutions.

*Click Chemistry*

Hasenknopf, Lacôte and Thorimbert were the first in 2007 to exploit the potential of 1,3 dipolar cycloaddition between azides and alkynes catalyzed by CuSO$_4$, to post-functionalize an organotin-polyoxotungstate. In particular they bound a great variety of lipophilic and hydrophilic ligands to the $[\alpha_1/\alpha_2\text{-}P_2W_7O_{61}SnR]^{7-}$ and $[PW_{11}O_{39}SnR]^{4-}$, in a mixed solvent CH$_3$CN/H$_2$O (1:2) which allows the solubilization of the tetrabutylammonium salt of the inorganic cluster.[101]
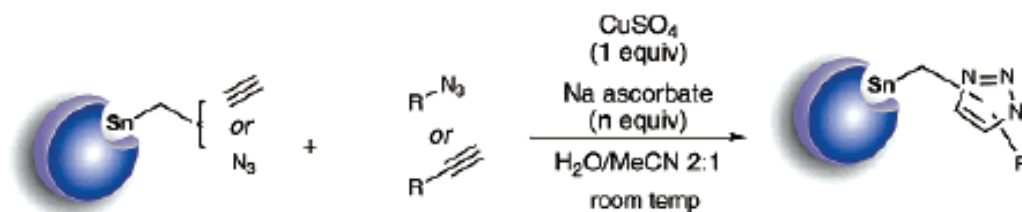
**Figure 1. 26-** Grafting of Organic Molecules to organotin-Polyoxotungstates through Copper-Catalyzed Dipolar Cycloaddition.

The same procedure was applied by Mayer, Odobel and co-workers to couple bis(azidoethyl-phosphonate) or bis(azidoethyl-silyl) derivatives of the Wells-Dawson anion $[P_2W_{17}O_{61}]^{10-}$ with perylene moniimide[105] or metalloporphyrins[106,136] bearing an alkyne residue. Indeed, with the aim to design new photochemical devices to achieve photo-accumulative electron transfer, which is an important function for mimicking artificial photosynthesis, they covalently coupled the POM with the light-harvesting antenna systems. The copper-catalyzed Huisgen reaction was exploited between the azido and alkyne residues to get the hybrid products in high yields.
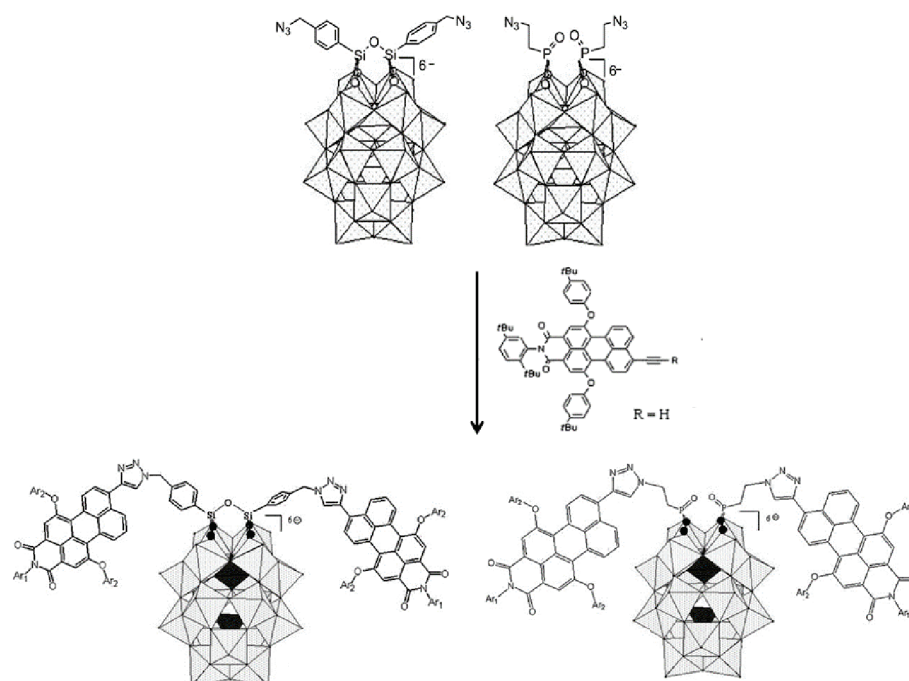


**Scheme 1. 2-** Copper-catalyzed Huisgen reaction employed by Mayer and coworkers between perylenes and organo-POMs to post-functionalize it (ref.105). Reaction conditions: DMF, $CuSO_4 \cdot 5H_2O$, ascorbic acid, 50°C, 16 h, Y=100%.

*C-C cross couplings*

Peng and co-workers were the first performing a Sonogashira cross-coupling on the hexamolybdate $[Mo_6O_{18}(NArX)]^{2-}$ (X=I or CCH) with 1-ethynyl-3,5-di(tert-butyl)benzene or 1-ethyn- yl-4-methylbenzene. The reaction was carried out in acetonitrile at room temperature under the protection of nitrogen.[137,138]

Then the same reaction was exploited in a variety of Lindqvist hexamolybdates to introduce enantiopure compounds[139] or coordinative ligands (such as terpyridine)[140,141] or polymers[142–144] or to directly attach the organo POM on silica.[145]

Concerning the Pd-catalyzed Heck cross-coupling reaction, only one example involving a hybrid Lindqvist POM platform is reported in the literature, by Wei and co-workers. They started from the bromo- or iodo- functionalized aryl derivative of hexamolybdates $[Mo_6O_{18}(NArX)]^{2-}$ (X =Br, I) to add remote olefin units.[146]

More recently, in 2013, Lorioni et al. extended the list of cross-coupling Pd-catalyzed reactions on organo-POMs to Keggin and Dawson platforms, exploiting the Mizoroki–Heck olefin coupling, the Suzuki and the Hiyama cross-couplings, as well as the Miyaura borylation, to introduce a variety of organic ligands on the iodophenyltin derivative of lacunary Keggin-type $[PW_{11}O_{39}]^{7-}$ and Dawson-type $[P_2W_{17}O_{61}]^{10-}$.[147]
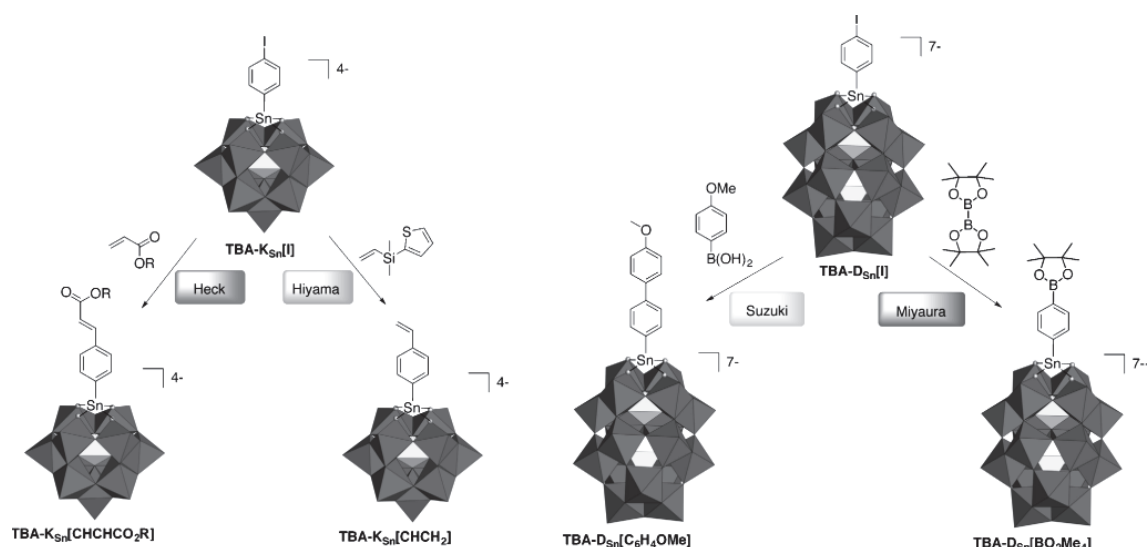
**Scheme 1. 3-** Pd-catalyzed post-functionalization reactions exploited by Lorioni and coworkers on Keggin-type organo-POM (on the left) and Dawson type organo-POM (on the right).

*Metal coordination*

As mentioned in the previous paragraph Sonogashira cross-coupling was exploited by Peng and co-workers to introduce terpyridine ligands on the Lindqvist hexamolybdate. The terpyridine ligand was then used to coordinate transition-metals, such as $Fe^{2+}$, that allows the development of molecular hybrid containing POM clusters and transition metal complexes connected through an extended π-conjugated bridge.[148]

The same coordinative strategy was used by Hasenknopf and co-workers on the trisalkoxo-derivatives of Dawson, Lindqvist and Anderson platforms functionalized with terpyridine ligands, to coordinate Ru and Pd metal ions respectively.[149]

More recently, the same group demonstrated that the combination of the concepts of metallo-supramolecular chemistry with the synthesis of organic– inorganic POM hybrids gives access to predictable architectures. Indeed the organo Lindqvist POM $TBA_2[V_6O_{13}\{(OCH_2)_3CNHC(O)-3-C_5H_4N\}_2]$, functionalized with pyridine ligands forms a trimeric complex in the presence of $[PdCl_2(CH_3CN)_2]$ in N,N' –dimethylacetamide, thanks to the complexation of the Pd.
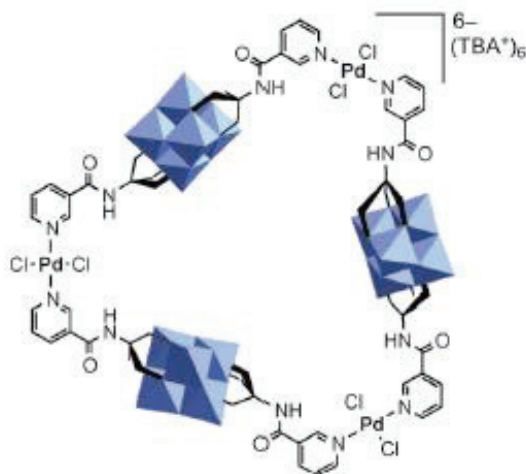
**Figure 1. 27-** Triangle structures obtained from functionalized Lindqvist POM derivative and PdCl$_2$(CH$_3$CN)$_2$.

Coordination also drives the assembly of POMs and porphyrins, starting from bis(pyridine-trisalkoxo)-Anderson-type POMs and metallic porphyrins (M =Zn, Ru).[129]

*Peptide bonds formation*

Lacôte and co-workers investigated deeply this type of post-functionalization reaction, that depends on the nature of the coupling agent. In particular they saw that the best results in the coupling of the tin derivatives $\alpha_1$- and $\alpha_2$-[P$_2$W$_{17}$O$_{61}$(SnCH$_2$CH$_2$COOH)]$^{7-}$ or [PW$_{11}$O$_{39}$(SnCH$_2$CH$_2$-COOH)]$^{4-}$, as tetrabutylammonium salts in MeCN, with various amines or thiols is given with isobutylchloroformiate in the presence of a base (tBuOK or NEt$_3$), while dicyclohexyl urea was preferred as coupling agent when reactions with alcohols are considered.[81,95] A mixed anhydride intermediate was isolated and involved in further reactions, notably with peptides. It led also to chiral recognition and kinetic resolution of the starting material.[150]
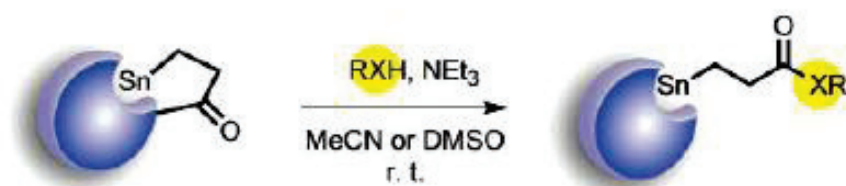
**Scheme 1. 4-** General scheme for the peptidic bond formation described by Lacôte and co-workers.

In the same manner Cronin and co-workers described a full family of amphiphilic Anderson-type POMs, obtained by post-functionalization of the initial hybrid Anderson platform $[MnMo_6O_{18}\{(OCH_2)_3CNH_2\}_2]^{3-}$ with acyl chloride in presence of $NEt_3$.[151,152] With the same strategy, surfactant-encapsulated photoresponsive POM assemblies[153] were obtained by Yan and co-workers. Finally, Bonchio's group described a fluorescent chemosensor obtained by the reaction between an organo-Keggin type POM, $[\gamma\text{-}SiW_{10}O_{36}\text{-}\{O(SiC_3H_6NH_2)_2\}]^{4-}$, and a sulfonyl chloride (dansyl chloride).[154]
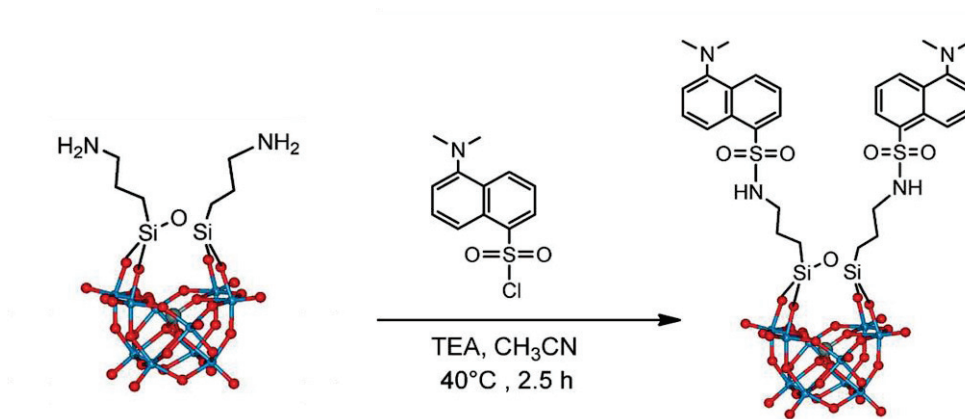


**Scheme 1. 5-** Reaction pathway to get the Dansyl derivative of the Keggin polyoxosilicotungstate, proposed by Bonchio et al.

*Nucleophilic substitution*

Only a few months ago the first post-functionalization pathway exploiting simple nucleophilic substitution was reported by the Parac-Vogt group. They used the

functionalized Anderson-type POM ($(C_{16}H_{36}N)_3$-[$MnMo_6O_{18}$- (($OCH_2$)$_3$C-NH-CO-$CH_2$-Cl)$_2$, with chloroacetamide as the precursor group, to exploit the higher electrophilic character of this particular sp$^3$ hybridized carbon. Using this method, several types of different nucleophiles including primary and secondary amines, carboxylates, and thiolates were efficiently coupled to a chloride-functionalized Anderson-type POM in high yields and purity.[155]
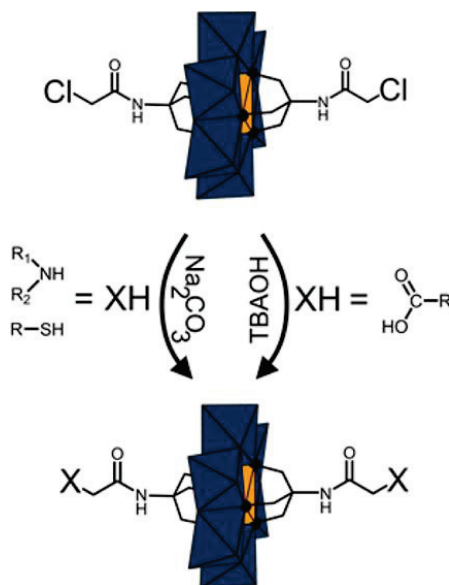


**Figure 1. 28-** First example of nucleophilic substitution as post-functionalizing method on organo-polyoxometalates.

## 1.3    Organic/Inorganic interaction in POMs

Previous studies on their applications in medicine have demonstrated that POMs are important drug candidates with remarkable antiviral, antibacterial and antitumoral activities.[156–160] The unique advantage of POMs as drug candidates lies in the fact that it is possible to tune molecular properties that impact the recognition and reactivity of POMs with targeted biological macromolecules. As an example, a significant antitumoral effect of $[NH_3Pr^i]_6[Mo_7O_{24}]*3H_2O$ (PM-8) was found against the MX-1 murine mammary cancer cell line, Meth A sarcoma, and MM46 adeno-carcinoma.[161] The antitumor mechanism of POMs involves the induction of cell apoptosis, nonspecific weak interactions with DNA, and the inhibition of ATP generation and angiogenesis-promoting factors.[158,160,162,163] Unfortunately, no POM product can be really exploited yet for clinical trials, mainly because of their toxic side effect on normal cells, which may be addressed by either increasing the cell specificity or targeted delivery. Moreover, because of the excess of oxo ligands over metallic ions, POMs are usually highly negatively charged: a characteristic unfavorable for penetration of POMs into cells.

Yet some studies report that under certain circumstances, POMs might cross the barrier and enter into the cells.[164]

As mentioned before, the mechanism of antiviral, antitumoral, and antibiotic activities is supposed to involve some kind of interaction of the POMs with the viral cell membrane.[165] Specific POM-protein interaction studies include POM inhibition of HIV reverse transcriptase activity,[166] POM inhibition of HIV protease[167] and chemotherapeutic activity.[160] POMs may open the way toward new, innovative, and cheap therapeutic strategies for various human diseases. However, the mechanisms of these potential therapeutic effects remain to be described at a molecular level. Understanding the physicochemical foundations of the interactions between POMs and biomolecules might have important implications for medical and biochemical applications of POMs beyond selective peptide hydrolysis.

In this context, the study of the interactions between polyoxometalates and molecules of biological interest appears as one of the necessary steps toward a fundamental understanding of the biological activity at molecular level of these interesting chemicals.

*In this paragraph we will describe first the supramolecular interactions that occur between POM and neutral molecules of biological interest. Successively a detailed paragraph will be devoted to the interactions between POM and biomolecules, followed by a paragraph explaining how Molecular Dynamics Simulation tools are nowadays exploited to better understand the POM behavior in solution and there, its interaction with other organo-molecules.*

### 1.3.1 H-bonding interactions POM@biomolecules

Hydrogen bonding is essential in biological structures. H-bond donor (HBD) groups in some enzyme can serve as active sites and promote the reactivity of electrophilic substrates and thus participate in conceptually parallel processes. This could be translated to POMs, whose metal-oxide surface could be a H-bond acceptor.

Not a lot of studies have been carried out about POM-neutral biomolecules interactions.

Debbi Crans et coworkers in 1994 were the first to structurally characterize a POM-peptide system in solid state. They demonstrated that in presence of diglycine compound, the decavanadate $V_{10}O_{28}*4H_2O$ interacts through hydrogen bonds with the dipeptide, probably involving the most basic site on the anion. Moreover, they saw that modification of the dipeptide affects the polyoxoanion-dipeptide interaction, since a related complex between the decavanadate anion and glycylhistidine (Gly-His) has a different stoichiometry.[168]
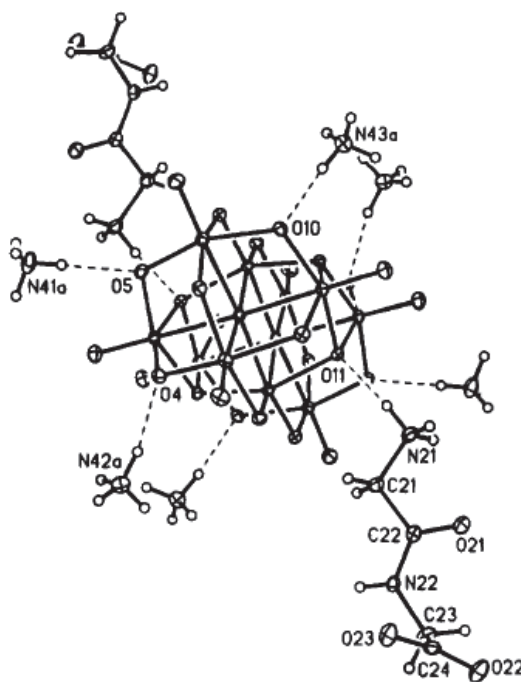
**Figure 1. 29-** Representation of the hydrogen-bond interactions between the polyoxovanadate anion, the cations, and the Gly-Gly zwitterions in the hybrid system $(NH_4)_6(Gly-Gly)-V_{10}O_{28}*4H_2O$

More recently, Eshtiagh-Hosseini and Mirzaei synthesized two novel chiral hybrids based on Preyssler and Dawson anions crystallized in presence of Valine, Glycine and Proline as aminoacids, $(Hval)_2(Hgly)(H_3O)_6K_5[Na(H_2O)P_5W_{30}O_{110}]*19.5H_2O$ and $(Hpro)_6[P_2W_{18}O_{62}]*8H_2O$. They showed that all kinds of oxygen atoms in the structure of the heteropolyanions interact with the hydrogen atoms in amino acids and water molecules. In these compounds, the amino acids presence led to pseudo organic–inorganic hybrid materials since the system was stable also in solution.[169]

With the aim to improve the chiral sensing of a chiral Dawson POM, such as $\alpha_1$-$P_2W_{17}O_{61}$, Micoine et al. functionalized it with different tripeptides chains. Indeed, they hypothesized that a strong bond to the organic ligand, coupled to additional hydrogen bonds, allowed better chiral sensing of the chiral $[\alpha_1-P_2W_{17}O_{61}]^{7-}$. They saw that variation of the amino acid residue resulted in slight modifications in the selectivity, validating the initial hypothesis that extended chains should better wrap around the nanosized POM, and that this predominantly takes place via

hydrogen bonding of the peptide to the negatively charged cluster. Yet no mapping of the interaction was provided and this aspect remains under studied.[80]

## 1.3.2     Electrostatic interactions POM@biomolecules

Due to their negative charges, POMs are expected to bind to any proteins containing positively charged patches on their surfaces. Such kind of electrostatic binding may induce secondary (or even tertiary) structural changes in the protein. The physico-chemical properties of the protein may thus be affected, in particular its aggregation.

A lot of insights at the molecular level have been gained, in which several factors such as the size, shape, and nature of the embedded metal ion in the architecture of POM are demonstrated to be crucial in governing the interactions. [170–173]

### A.     Human Serum Albumine (HSA)

One of the first detailed studies about the interaction POM-biomolecules was done by Zhang and co-workers in 2007. They organized the interaction between human serum albumin (HSA) and a Keggin-type POM, $[H_2W_{12}O_{40}]^{6-}$ as well as a wheel shaped $[(NaP_5W_{30}O_{110}]^{14-}]$ where the binding was mainly attributed to the electrostatic interaction between them.[174–176] Moreover both size and charges of the polyoxometalates play key roles in the molecular interaction process. At neutral pH, the Keggin type polyoxometalate $[H_2W_{12}O_{40}]^{6-}$ specifically binds on one site of the protein and forms a 1:1 protein-POM complex, whereas the wheel shaped $[NaP_5W_{30}O_{110}]^{14-}$ binds to more than five sites of the protein and forms a complicated complex with the protein.

The binding of $[H_2W_{12}O_{40}]^{6-}$ has almost no effect on the protein structure, in contrast with the binding of $[NaP_5W_{30}O_{110}]^{14-}$ which destabilizes the protein structure.

In addition, Zheng et al. reported the interaction of Eu containing decatungstate $[EuW_{10}O_{36}]^{9-}$ and another Gd containing polyoxometalate with HSA, and found enhanced emission during binding. In particular the interaction between the Gd-containing tungstosilicate $[Gd(\beta_2\text{-}SiW_{11}O_{39})_2]^{13-}$ and HSA showed that the POM forms a 1:1 complex with HSA and the binding of the POM significantly alters the secondary structure of the protein.[177]

The same group extend its attention to Dawson polyoxometalates interacting with HSA. They found that for the lacunary Dawson POMs, there are two main binding sites on HSA. For the Ni-substituted POM, there are at least three binding sites on the protein. There is only one main binding site on the protein for Cu-substituted POM. Because the three compounds virtually have the same structure, the marked differences in the binding behaviors can be attributed to their compositions, but how the composition affects the binding is still unknown. Moreover the nominal negative charge of the POMs does not appear as a single parameter governing the binding process and its consequences.[176]

A further step toward the understanding of the parameters responsible for the interaction between hydrolytically active polyoxometalate analogues and albumin proteins on a molecular level was done by the Parac-Vogt group.

Through the interaction study between $H_3PW_{12}O_{40}$, lacunary Keggin $K_7PW_{11}O_{39}$ and the Eu(III)-substituted Keggin $K_4EuPW_{11}O_{39}$ (Eu-Keggin) type polyoxometalates (POMs), and the proteins human and bovine serum albumin (HSA and BSA) they succeeded to localize the binding position on the surface of the protein. The positive charge on the protein surface is mainly caused by the high number of lysine and arginine residues in close proximity of the cavity whose size is able to fit Keggin type POMs.[178]
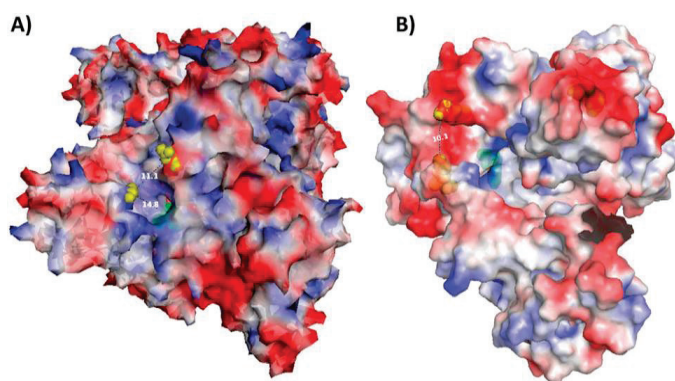
**Figure 1. 30-** Surface potential of HSA (A) and BSA (B) (blue for positively and red for negatively charged areas). Tryptophan residues are indicated with green spheres, while the boundaries of the cavity are depicted with yellow spheres

## B. *Bovine Serum Albumin*

Similar to HSA, Bovine Serum Albumin (BSA) also possesses typical biological functions and plays a key role in biochemical experiments, such as cell culture protocols, stabilization of some enzymes and so on.[178,179]

Few years ago Wu's group has focused its attention on the interaction between an Europium Keggin POM, such as $K_{13}[Eu\text{-}(SiW_9Mo_2O_{39})_2]$, and the BSA. They followed mainly through fluorescence the interaction between the two domains, discovering a two-step binding process and especially a large luminescence enhancement of the inorganic cluster, of about 13-fold larger than the initial one. The electrostatic interaction of POMs with the positively charged surface areas of the protein plays an important role on the multistep bindings. Indeed, under low protein concentration (<3.0 μM), its binding with POMs promoted EuSiWMo aggregation at the protein surface; while at high protein concentration (>8.0 μM), the aggregated POMs would be dispersed owing to a competitive interaction by the large amount of BSA.[180]
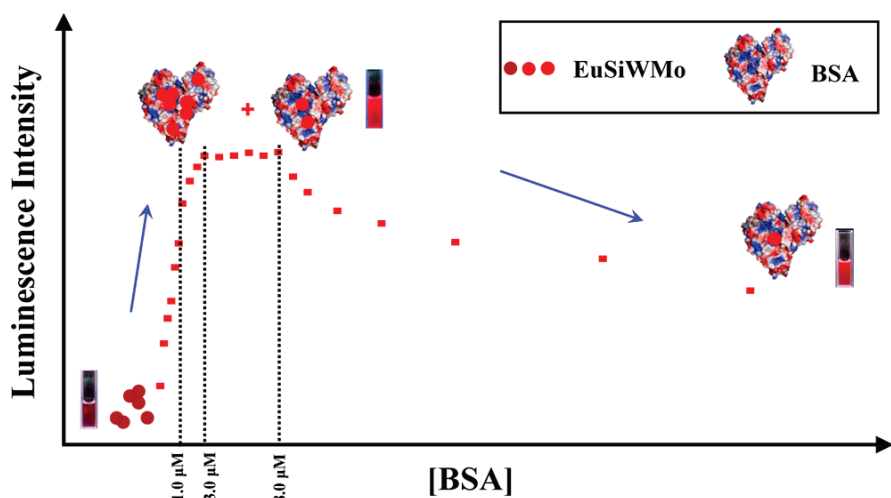
**Figure 1. 31-** Diagram showing the binding model between EuSiWMo and BSA in the different titration stages

In the same manner Hungerford et al. reported that the interaction between europium decatungstate ($[EuW_{10}O_{36}]^{9-}$) and bovine serum albumin (BSA) has only a moderate association constant. They found that the larger Eu-containing structure of the selected POM had a significantly higher affinity to the proteins than the smaller decatungstate parent.[170,171]

## C.    Lysozyme

Following the same strategy, Parac-Vogt performed interesting experiments to investigate the electrostatic interaction between some Keggin POMs, such as $K_7PW_{11}O_{39}$, $K_4EuPW_{11}O_{39}$ and $[Me_2NH_2]_{10}[Ce(PW_{11}O_{39})_2]$, and two proteins, such as the positively charged hen egg white lysozyme (HEWL) and the structurally homologous negative charged α-lactalbumin (α-LA). In particular, with the lacunary and Eu(III)-substituted Keggin POM, a 1:1 POM:HEWL complex was formed, which can be attributed to the binding of the POM near the Trp28–Val29 cleavage site. These experiments were also carried out with Ce-Keggin, which exhibited stronger interaction as a result of the increased Lewis acidity of Ce(IV) as compared to Eu(III). In particular, the number of bound POM molecules to HEWL was found to be 1.04 for the lacunary Keggin POM, and 1.0 for Eu-Keggin,

indicating the formation of a 1:1 POM/HEWL complex, while it was 1.38 for Ce-Keggin derivative, probably indicating a transition from 1:1 to 1:2 complex.

In contrast, in presence of the negative charged α-LA, a protein which is structurally highly homologous to HEWL, no fluorescence intensity increase was observed: indicating that no interaction occurs because of the electrostatic repulsion.[181,182]

### D. Amyloids

Another example of interesting POM@proteins interaction via ionic binding is given by Zhou et coworkers that studied how two representative POMs, the wheel-shaped Preyssler anion $[NaP_5W_{30}O_{110}]^{14-}$ and the Keggin-type anion $[H_2W_{12}O_{40}]^{6-}$, interact with amyloid Aβ1-40, a protein associated with Alzheimer's disease.

Thanks to the electrostatic interaction with the cationic residues of the protein, Arg5, His6, His13, His14, and Lys16, POMs succeed to inhibit its fibrillization, thus altering the Aβ aggregation behavior that lead to a β-sheet conformation. Also the dimension of the POM plays a key role in the interaction and inhibition mechanism.[183]
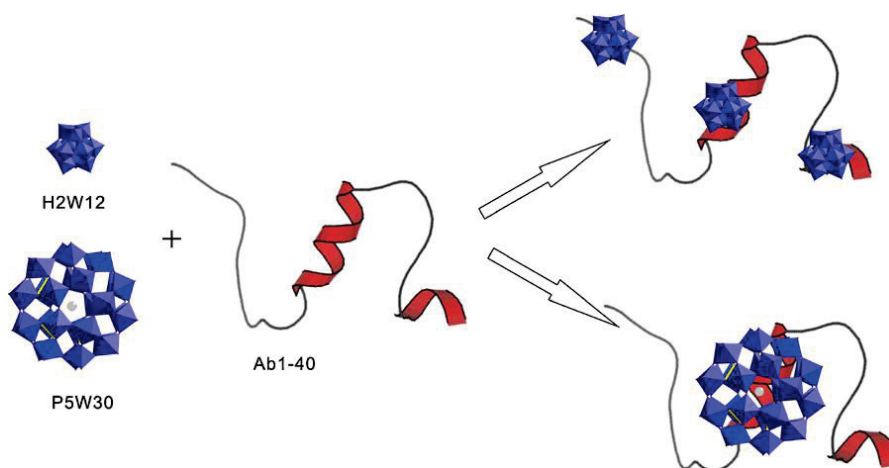


**Figure 1. 32-**The different binding patterns for the two POMs, depending on its dimension.

Similarly Qu et al. proposed that POMs, such as the Dawson $K_8[P_2CoW_{17}O_{61}]$, the Keggin α-$Na_9H[SiW_9O_{34}]$ and the smaller Anderson $Na_5[IMo_6O_{24}]$, are bound to

the positively charged His13-Lys16 cluster region of the amyloid β–peptides. The authors found an apparent trend related to POM composition: the larger the negative charge, the higher the binding affinity, and the stronger the inhibitory effect.[184]

### 1.3.3 Molecular dynamics simulations to investigate POM interactions in solution

Molecular dynamics simulations (MDs) is an interesting theoretical tool to investigate the POM behavior in solutions, since experimental characterization techniques often are not able to completely describe the system in solution. Firstly, MDs have been exploited to understand the behavior of simple polyoxometalates in solution and how POMs interact with inorganic molecules ($H_2O$, metal ions etc…). More recently MDs have been employed to investigate the interaction between POMs and biological molecules.

*An outlook about what has been done with MDs concerning POM interactions in solution will be given below.*

### A. *POMs in solution*

Starting with the general POM behavior in solution, Lopez and coworkers were the first in 2005 to investigate via MDs the hydration and dynamic properties of Keggin POM, such as $\alpha$-$PW_{12}O_{40}^{3-}$ with $Na^+$ counterions. Their results showed that the terminal oxygens of the cluster are invariably more effectively solvated by water because of their prominent position within the framework, while the bridging ones, which are confined in more internal positions, contribute a smaller portion of the whole solvation. Then they investigated the hydrogen bonds existing between water and the cluster, confirming that the terminal positions form more contacts with $H_2O$ than any other site of the cluster, but the lifetime of such contacts is longer with bridging oxygens, presumably due to the higher charge densities of these sites.[185]

Leroy et al. focused their attention on the impact of the charge of three Keggin $[XW_{12}O_{40}]^{n-}$ anions (X =P/Si/W), and of varied inorganic counterions (Li+ /Na+ /K+) on ion pairing and dynamics in water. They concluded that a competition in the electrostatic interactions between the ions and the stability of the solvation shell was established.[186]
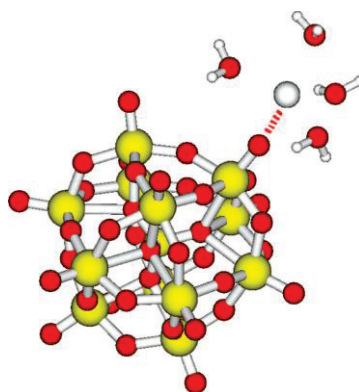


**Figure 1. 33-**Illustration of a direct contact between a sodium cation and one $O_{term}$ of the $PW_{12}$ anion. Water molecules of the solvatation shell are explicited.

Similarly, Chaumont and Wipff investigated through MDs aqueous solutions of α-$[PW_{12}O_{40}]^{3-}$ $M^{n+}$ salts at two concentrations (0.06 and ca. 0.15 mol/l$^{-1}$), comparing cations of different charges and hydrophilic character, such as $NBu_4^+$, $Cs^+$, $H_3O^+$, $H_5O_2^+$, $UO_2^{2+}$ and $Eu^{3+}$. There, in spite of their mutual repulsions, PW3 anions can make short contact in water (at P...P distances of ca. 11 Å). The amount and lifetime of the $(PW3)_n$ dimers and oligomers are modulated by the nature of the Mn+ counterions.[187,188]
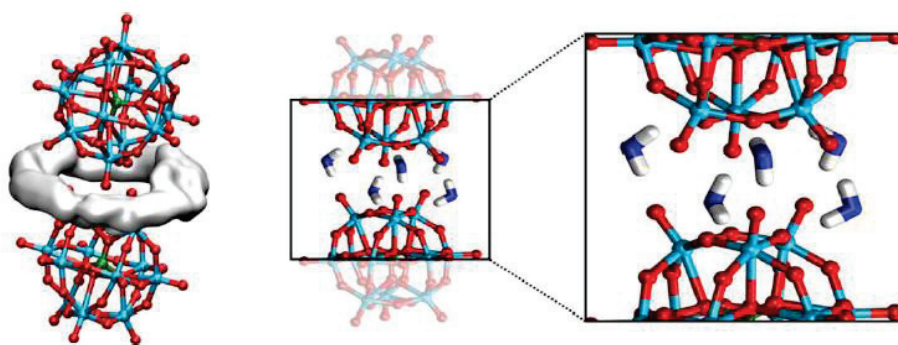


**Figure 1. 34-** PW$^{3-}$...PW$^{3-}$ dimer in water: $H_2O$ density between two PW's (averaged over 500 ps; left) and snapshot of bridging water molecules (middle and right)

Lozano et al. instead focused their attention on Zr-substituted Lindvist and Keggin anions to study the influence of pH in aqueous solution. Both DFT and Car−Parrinello MD methods suggested that the Zr center tends to have a coordination number higher than 6 and can bind up to 3 water molecules. The MDs also show that the Zr atom fluctuates within the oxide POM framework, providing a flexible coordination environment.
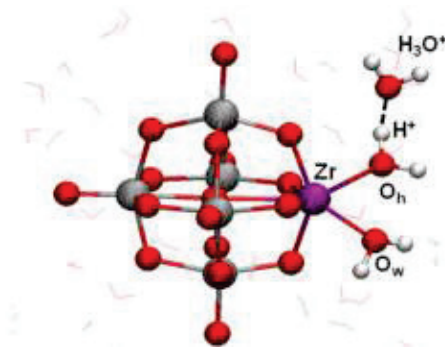


**Figure 1. 35-** Car−Parrinello MD simulation at acidic conditions starting from Zr-hydroxo $[W_5O_{18}Zr(OH)]^{3-}$ anion, finally forming the seven-coordinated Zr species.

Moreover, they confirmed that an increased acidity favors the formation of Zr-water species, explaining why dimer dissociation is promoted at low pH. At basic conditions Zr-hydroxo species are generated, providing the reactive groups to form Zr···Zr linkages.[189]

A similar study was previously done on the lacunary Dawson $[P_2W_{17}O_{61}]^{10-}$ by Duprè et al.[190] and on the Keggin $\{\varepsilon\text{-}PMo_{12}O_{40}\}$ by el Moll et al.[191] Indeed they coordinated different lanthanides (such as Ln, Zr, Sc, Y, Hf, Ce, etc) to the lacunary inorganic scaffolds, demonstrating the increment on the Lewis acidity of the metal-substituted inorganic system, with respect to the free metals. Evidences that the metal center enhances the acidity of the water molecules were given.

Based on the same approach, very recently the same group investigated the mechanism by which Zr-substituted and other metal-substituted POMs assembled covalently into dimeric clusters. Dimerization occurs through the stepwise

formation of two covalent Zr−μO(H)−Zr linkages, for which the computed overall free energy barrier is low.[192]

The structure and dynamics of water encapsulated in porous POM- based nano capsules has also been simulated by MD.[193,194]

### B.          *Organic/Inorganic interactions in solution*

The first real study through MDs on the interaction between a POM and an organo moiety, can be attributed to Brodbeck and co-workers in 2008.

Dendrimer encapsulated PW3 anions have been simulated by MD in trichloromethane solution to model dendrizyme. These dendrizyme model compounds are non-charged ionic clusters composed of a central POM (the core), an α-Keggin ion $[(XO_4)W_{12}O_{36}]^{n-}$ (if X =P, n =3; if X=Zn, n =6), and surrounding dendritic ammonium or pyridinium ions. They concluded that substrate selectivity is influenced by the size exclusion effect of the dendrizyme shell, depending primarily on the permeability of the dendrizyme shell and on the unshielded part of the surface of the dendrizyme core.[195]



$(C_{74}H_{96}N)_6[ZnW_{12}O_{40}]$       $(C_{116}H_{124}NO_{28})_6[ZnW_{12}O_{40}]$
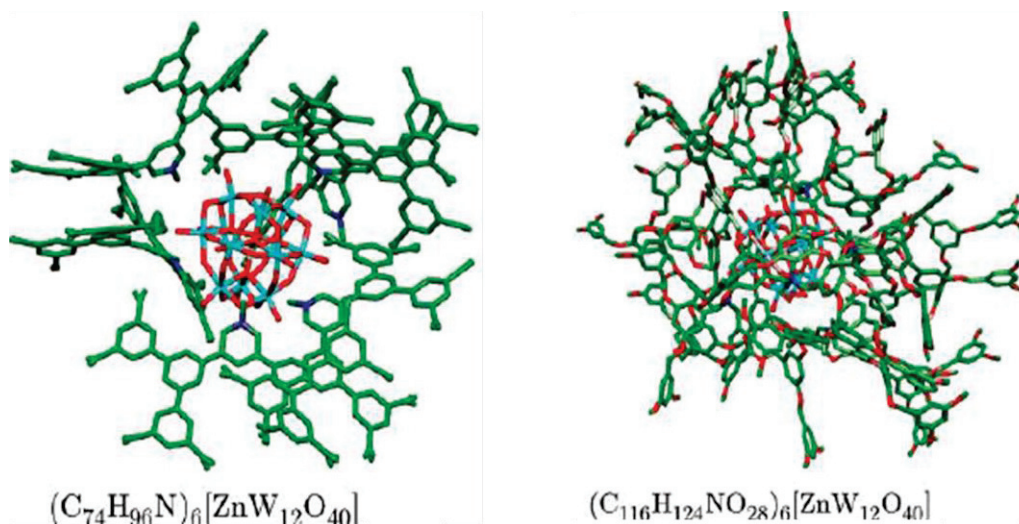
**Figure 1. 36-** Dendrizyme model compounds with pyridinium dendrimers on the left and ammonium dendrimers on the right.

In light of these interesting models in solution, computational simulations could facilitate the understanding of the molecular properties that govern the POM--

protein interaction to further develop metal-substituted POMs with specific interaction properties, but up to now, only one very recent example is present in literature.

Last year, the Carbò group simulated for the first time the interaction between three different POM structures and a protein, which is HEWL in aqueous solution. The three POMs are Ce-substituted Keggin-type anion $[PW_{11}O_{39}Ce(OH_2)_4]^{3-}$ (CeK), the corresponding 1:2 dimer $[Ce(PW_{11}O_{39})_2]^{10-}$ (CeK2) and the Zr-substituted Lindqvist-type anion $[W_5O_{18}Zr(OH_2)(OH)]^{3-}$ (ZrL)], which differ in the overall charge, the size, the shape and the type of substituted metal. Thanks to MDs they identified two sites of the protein with which the POM interacts strongly by complexation. This interaction behavior can be related to the observed selectivity in hydrolytic activity of Ce[IV]- and Zr[IV]-substituted POMs towards the Trp28-VaL29 (site I) and Asn44–Arg45 (site II) bonds. They concluded that the interaction of POMs with HEWL involves charge attraction and hydrogen bonding of the basic oxygen atoms of POM framework with the side chains of positively charged amino acids (arginine and lysine) and of polar uncharged amino acids (tyrosine, serine and asparagine).
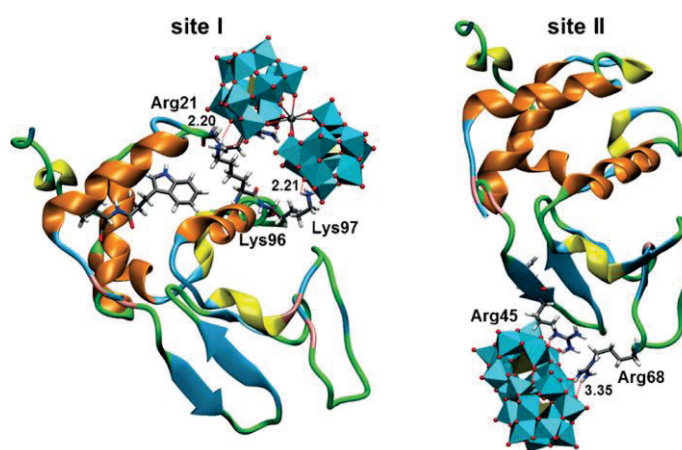


**Figure 1. 37-** Illustrative snapshots of CeK2···HEWL interaction at sites I and II presented by Carbo and Parac-Vogt's group. Left: the most strongly interacting amino acids for simulation at site I: Arg21, Lys96, and Lys97. Right: those for simulation at site II: Arg45 and Arg68.

Moreover, the formation of hydrogen bonding with the N-H amide group of the main protein chain is also plausible, although its extent is less important.[196]

*Not much is therefore known about organics/POM interaction in solution and even less for organo-POMs.*

## 1.4   Conclusions

*In this chapter the POM hybridization methods have been described, allowing to give an overview on the different families of hybrid-POMs present in literature. Successively the supramolecular interaction behavior in solution, between the inorganic POM and organo biomolecules, have been highlighted.*

*In the next chapter we will investigate more deeply the catalytic activity of these hybrid systems, to understand how the interplay between the organic and inorganic part has influenced the properties of the inorganic scaffold and vice versa.*

## 1.5 Bibliography

[1] *The Early Transition Metals*, Academic Press, London, **1972**.

[2] M. T. Pope, Y. Jeannin, M. Fournier, *Heteropoly and Isopoly Oxometalates: With 40 Tables*, Springer, Berlin, **1983**.

[3] M. T. Pope, A. Müller, *Angew. Chem. Int. Ed. Engl.* **1991**, *30*, 34–48.

[4] A. Hiskia, A. Mylonas, E. Papaconstantinou, *Chem. Soc. Rev.* **2001**, *30*, 62–69.

[5] C. L. Hill, *Chem. Rev.* **1998**, *98*, 1–2.

[6] Y. P. Jeannin, *Chem. Rev.* **1998**, *98*, 51–76.

[7] H. R. Allcock, E. C. Bissell, E. T. Shawl, *Inorg. Chem.* **1973**, *12*, 2963–2968.

[8] H. R. Allcock, E. C. Bissell, E. T. Shawl, *J. Am. Chem. Soc.* **1972**, *94*, 8603–8604.

[9] A. Müller, E. Beckmann, H. Bögge, M. Schmidtmann, A. Dress, *Angew. Chem. Int. Ed.* **2002**, *41*, 1162–1167.

[10] I. Lindqvist, *Ark Kemi* **1952**, 247.

[11] J. F. Keggin, *Nature* **1933**, 908.

[12] B. Dawson, *Acta Crystallogr.* **1953**, *6*, 113–126.

[13] J. S. Anderson, *Nature* **1937**, 850.

[14] H. T. Evans, *J. Am. Chem. Soc.* **1948**, *70*, 1291–1292.

[15] D. D. Dexter, J. V. Silverton, *J. Am. Chem. Soc.* **1968**, *90*, 3589–3590.

[16] M. T. Pope, A. Müller, in *Polyoxometalate Chem. Topol. Self-Assem. Appl.* (Eds.: M.T. Pope, A. Müller), Springer Netherlands, **2001**, pp. 1–6.

[17] C. L. Hill, *J. Mol. Catal. Chem.* **2007**, *262*, 1.

[18] N. Mizuno, K. Yamaguchi, K. Kamata, *Coord. Chem. Rev.* **2005**, *249*, 1944–1956.

[19] B. Hasenknopf, *Front Biosci* **2005**, 275.

[20] J. T. Rhule, C. L. Hill, D. A. Judd, R. F. Schinazi, *Chem. Rev.* **1998**, *98*, 327–358.

[21] B. Keita, L. Nadjo, in *Encycl. Electrochem.*, Wiley-VCH Verlag GmbH & Co. KGaA, **2007**.

[22] T. He, J. Yao, *Prog. Mater. Sci.* **2006**, *51*, 810–879.

[23] J. M. Clemente-Juan, E. Coronado, *Coord. Chem. Rev.* **1999**, *193–195*, 361–394.

[24] C. M. Flynn, M. T. Pope, *Inorg. Chem.* **1972**, *11*, 1950–1952.

[25] M. Sadakane, E. Steckhan, *Chem. Rev.* **1998**, *98*, 219–238.

[26] I. A. Weinstock, *Chem. Rev.* **1998**, *98*, 113–170.

[27] C. L. Hill, C. M. Prosser-McCartha, *Coord. Chem. Rev.* **1995**, *143*, 407–455.

[28] P. Gouzerh, A. Proust, *Chem. Rev.* **1998**, *98*, 77–111.

[29] A. Dolbecq, E. Dumas, C. R. Mayer, P. Mialane, *Chem. Rev.* **2010**, *110*, 6009–6048.

[30] Y. Ren, M. Wang, X. Chen, B. Yue, H. He, *Materials* **2015**, *8*, 1545–1567.

[31] M. Bonchio, M. Carraro, G. Scorrano, A. Bagno, *Adv. Synth. Catal.* **2004**, *346*, 648–654.

[32]   A. Proust, B. Matt, R. Villanneau, G. Guillemot, P. Gouzerh, G. Izzet, *Chem. Soc. Rev.* **2012**, *41*, 7605–7622.

[33]   S. Berardi, M. Bonchio, M. Carraro, V. Conte, A. Sartorel, G. Scorrano, *J. Org. Chem.* **2007**, *72*, 8954–8957.

[34]   M. Carraro, L. Sandei, A. Sartorel, G. Scorrano, M. Bonchio, *Org. Lett.* **2006**, *8*, 3671–3674.

[35]   G. Maayan, R. H. Fish, R. Neumann, *Org. Lett.* **2003**, *5*, 3547–3550.

[36]   S. Nlate, C. Jahier, *Eur. J. Inorg. Chem.* **2013**, *2013*, 1606–1619.

[37]   C. Jahier, L. Plault, S. Nlate, *Isr. J. Chem.* **2009**, *49*, 109–118.

[38]   K. Hakouk, O. Oms, A. Dolbecq, J. Marrot, A. Saad, P. Mialane, H. El Bekkachi, S. Jobic, P. Deniard, R. Dessapt, *J. Mater. Chem. C* **2014**, *2*, 1628.

[39]   C. Jahier, F.-X. Felpin, C. Méliet, F. Agbossou-Niedercorn, J.-C. Hierso, S. Nlate, *Eur. J. Inorg. Chem.* **2009**, *2009*, 5148–5155.

[40]   C. Jahier, S. S. Mal, U. Kortz, S. Nlate, *Eur. J. Inorg. Chem.* **2010**, *2010*, 1559–1566.

[41]   C. Jahier, L. Plault, S. Nlate, *Isr. J. Chem.* **2009**, *49*, 109–118.

[42]   S. Nlate, C. Jahier, *Eur. J. Inorg. Chem.* **2013**, *2013*, 1606–1619.

[43]   X. Fang, T. M. Anderson, C. L. Hill, *Angew. Chem. Int. Ed.* **2005**, *44*, 3540–3544.

[44]   Y. Wang, H. Li, W. Qi, Y. Yang, Y. Yan, B. Li, L. Wu, *J. Mater. Chem.* **2012**, *22*, 9181.

[45]   S. Luo, J. Li, H. Xu, L. Zhang, J.-P. Cheng, *Org. Lett.* **2007**, *9*, 3675–3678.

[46]   W. Qi, L. Wu, *Polym. Int.* **2009**, *58*, 1217–1225.

[47]   A. Haimov, R. Neumann, *J. Am. Chem. Soc.* **2006**, *128*, 15697–15700.

[48]   L. Chen, K. Zhu, L.-H. Bi, A. Suchopar, M. Reicke, G. Mathys, H. Jaensch, U. Kortz, R. M. Richards, *Inorg. Chem.* **2007**, *46*, 8457–8459.

[49]   S. Liu, Z. Tang, *Nano Today* **2010**, *5*, 267–281.

[50]   D. G. Kurth, P. Lehmann, D. Volkmer, H. Cölfen, M. J. Koop, A. Müller, A. Du Chesne, *Chem. – Eur. J.* **2000**, *6*, 385–393.

[51]   W. Bu, L. Wu, X. Zhang, A.-C. Tang, *J. Phys. Chem. B* **2003**, *107*, 13425–13431.

[52]   W. Bu, H. Li, W. Li, L. Wu, C. Zhai, Y. Wu, *J. Phys. Chem. B* **2004**, *108*, 12776–12782.

[53]   W. Bu, H. Fan, L. Wu, X. Hou, C. Hu, G. Zhang, X. Zhang, *Langmuir* **2002**, *18*, 6398–6403.

[54]   W. Li, W. Bu, H. Li, L. Wu, M. Li, *Chem. Commun.* **2005**, 3785–3787.

[55]   M. J. Earle, K. R. Seddon, *Pure Appl. Chem.* **2000**, *72*, 1391–1398.

[56]   X. Cai, Q. Wang, Y. Liu, J. Xie, Z. Long, Y. Zhou, J. Wang, *ACS Sustain. Chem. Eng.* **2016**, *4*, 4986–4996.

[57]   S. Ivanova, *ISRN Chem. Eng.* **2014**, *2014*, 1–13.

[58]   J. Cuan and B. Yan, *Microporous Mesoporous Mater.* **2014**, 9.

[59]  Y. Gong, Y. Guo, Q. Hu, C. Wang, L. Zang, L. Yu, *ACS Sustain. Chem. Eng.* **2017**, DOI 10.1021/acssuschemeng.6b02791.

[60]  Q.-G. Zhai, X.-Y. Wu, S.-M. Chen, Z.-G. Zhao, C.-Z. Lu, *Inorg. Chem.* **2007**, *46*, 5046–5058.

[61]  X. Fang, L. Hansen, F. Haso, P. Yin, A. Pandey, L. Engelhardt, I. Slowing, T. Li, T. Liu, M. Luban, et al., *Angew. Chem. Int. Ed.* **2013**, *52*, 10500–10504.

[62]  S.-Y. Shi, J.-N. Xu, W.-Y. MA, X.-B. Cui, Y. Wang, G.-W. Wang, J.-Q. Xu, *J. Coord. Chem.* **2009**, *62*, 3885–3894.

[63]  Y. Yan, H. Wang, B. Li, G. Hou, Z. Yin, L. Wu, V. W. W. Yam, *Angew. Chem. Int. Ed.* **2010**, *49*, 9233–9236.

[64]  Z. He, Y. Yan, B. Li, H. Ai, H. Wang, H. Li, L. Wu, *Dalton Trans.* **2012**, *41*, 10043–10051.

[65]  Z. He, H. Wang, Y. Wang, Y. Wu, H. Li, L. Bi, L. Wu, *Soft Matter* **2012**, *8*, 3315–3321.

[66]  H. Li, L. Wu, *Soft Matter* **2014**, *10*, 9038–9053.

[67]  D.-Y. Du, J.-S. Qin, S.-L. Li, Z.-M. Su, Y.-Q. Lan, *Chem. Soc. Rev.* **2014**, *43*, 4615–4632.

[68]  L. Yang, H. Naruke, T. Yamase, *Inorg. Chem. Commun.* **2003**, *8*, 1020–1024.

[69]  C.-Y. Sun, S.-X. Liu, D.-D. Liang, K.-Z. Shao, Y.-H. Ren, Z.-M. Su, *J. Am. Chem. Soc.* **2009**, *131*, 1883–1888.

[70]  J. Tong, W. Wang, L. Su, Q. Li, F. Liu, W. Ma, Z. Lei, L. Bo, *Catal Sci Technol* **2017**, *7*, 222–230.

[71]  B. Nohra, H. El Moll, L. M. Rodriguez Albelo, P. Mialane, J. Marrot, C. Mellot-Draznieks, M. O'Keeffe, R. Ngo Biboum, J. Lemaire, B. Keita, et al., *J. Am. Chem. Soc.* **2011**, *133*, 13363–13374.

[72]  L. Marleny Rodriguez-Albelo, A. R. Ruiz-Salvador, A. Sampieri, D. W. Lewis, A. Gómez, B. Nohra, P. Mialane, J. Marrot, F. Sécheresse, C. Mellot-Draznieks, et al., *J. Am. Chem. Soc.* **2009**, *131*, 16078–16087.

[73]  L. M. R. Albelo, A. R. Ruiz-Salvador, D. W. Lewis, A. Gómez, P. Mialane, J. Marrot, A. Dolbecq, A. Sampieri, C. Mellot-Draznieks, *Phys. Chem. Chem. Phys.* **2010**, *12*, 8632–8639.

[74]  Y. Wu, R. Shi, Y.-L. Wu, J. M. Holcroft, Z. Liu, M. Frasconi, M. R. Wasielewski, H. Li, J. F. Stoddart, *J. Am. Chem. Soc.* **2015**, *137*, 4111–4118.

[75]  G. Izzet, M. Ménand, B. Matt, S. Renaudineau, L.-M. Chamoreau, M. Sollogoub, A. Proust, *Angew. Chem. Int. Ed.* **2012**, *51*, 487–490.

[76]  Pope, M.T., Müller, A., *Eds Kluwer Acad. Publ. Alphen Aan Den Rijn Neth.* **1993**.

[77]  J. Canny, A. Teze, R. Thouvenot, G. Herve, *Inorg. Chem.* **1986**, *25*, 2114–2119.

[78]  M. Bonchio, M. Carraro, G. Scorrano, E. Fontananova, E. Drioli, *Adv. Synth. Catal.* **2003**, *345*, 1119–1126.

[79]  A. Müller, P. Kögerler, *Coord. Chem. Rev.* **1999**, *182*, 3–17.

[80] K. Micoine, B. Hasenknopf, S. Thorimbert, E. Lacôte, M. Malacria, *Angew. Chem. Int. Ed.* **2009**, *48*, 3466–3468.

[81] C. Boglio, K. Micoine, É. Derat, R. Thouvenot, B. Hasenknopf, S. Thorimbert, E. Lacôte, M. Malacria, *J. Am. Chem. Soc.* **2008**, *130*, 4553–4561.

[82] B. Riflade, D. Lachkar, J. Oble, J. Li, S. Thorimbert, B. Hasenknopf, E. Lacôte, *Org. Lett.* **2014**, *16*, 3860–3863.

[83] R. K. C. Ho, W. G. Klemperer, *J. Am. Chem. Soc.* **1978**, *100*, 6772–6774.

[84] C. R. Mayer, S. Neveu, V. Cabuil, *Angew. Chem. Int. Ed.* **2002**, *41*, 501–503.

[85] C. R. Mayer, C. Roch-Marchal, H. Lavanant, R. Thouvenot, N. Sellier, J.-C. Blais, F. Sécheresse, *Chem. – Eur. J.* **2004**, *10*, 5517–5523.

[86] C. Cannizzo, C. R. Mayer, F. Sécheresse, C. Larpent, *Adv. Mater.* **2005**, *17*, 2888–2892.

[87] C. N. Kato, Y. Kasahara, K. Hayashi, A. Yamaguchi, T. Hasegawa, K. Nomiya, *Eur. J. Inorg. Chem.* **2006**, *2006*, 4834–4842.

[88] T. Hasegawa, K. Shimizu, H. Seki, H. Murakami, S. Yoshida, K. Yoza, K. Nomiya, *Inorg. Chem. Commun.* **2007**, *10*, 1140–1144.

[89] G. Sazani, M. T. Pope, *Dalton Trans.* **2004**, 1989–1994.

[90] F. Hussain, U. Kortz, *Chem. Commun.* **2005**, 1191–1193.

[91] S. Reinoso, M. H. Dickman, A. Praetorius, L. F. Piedra-Garza, U. Kortz, *Inorg. Chem.* **2008**, *47*, 8798–8806.

[92] L. F. Piedra-Garza, S. Reinoso, M. H. Dickman, M. M. Sanguineti, U. Kortz, *Dalton Trans.* **2009**, 6231–6234.

[93] I. Bar-Nahum, J. Ettedgui, L. Konstantinovski, V. Kogan, R. Neumann, *Inorg. Chem.* **2007**, *46*, 5798–5804.

[94] S.-L. Li, Y.-M. Zhang, J.-F. Ma, Y.-Q. Lan, J. Yang, *Dalton Trans.* **2008**, 1000–1002.

[95] S. Bareyt, S. Piligkos, B. Hasenknopf, P. Gouzerh, E. Lacôte, S. Thorimbert, M. Malacria, *J. Am. Chem. Soc.* **2005**, *127*, 6788–6794.

[96] K. Nomiya, Y. Togashi, Y. Kasahara, S. Aoki, H. Seki, M. Noguchi, S. Yoshida, *Inorg. Chem.* **2011**, *50*, 9606–9619.

[97] Wang, X.-H.; Dai, H.-C.; Liu, J.-F., *Transit. Met Chem* **1999**, 600.

[98] Wang, X. H.; Liu, J. F., *J Coord Chem* **2000**, 73.

[99] Yang, Q. H.; Dai, H. C.; Liu, J. F., *Transit. Met Chem* **1998**, 93.

[100] X. H. Wang, H. C. Dai, J. F. Liu, *Polyhedron* **1999**, *18*, 2293–2300.

[101] K. Micoine, B. Hasenknopf, S. Thorimbert, E. Lacôte, M. Malacria, *Org. Lett.* **2007**, *9*, 3981–3984.

[102] S. Bareyt, S. Piligkos, B. Hasenknopf, P. Gouzerh, E. Lacôte, S. Thorimbert, M. Malacria, *Angew. Chem. Int. Ed.* **2003**, *42*, 3404–3406.

[103] W. H. Knoth, *J. Am. Chem. Soc.* **1979**, *101*, 759–760.

[104] M. Boujtita, J. Boixel, E. Blart, C. R. Mayer, F. Odobel, *Polyhedron* **2008**, *27*, 688–692.

[105] F. Odobel, M. Séverac, Y. Pellegrin, E. Blart, C. Fosse, C. Cannizzo, C. R. Mayer, K. J. Elliott, A. Harriman, *Chem. – Eur. J.* **2009**, *15*, 3130–3138.

[106] A. Harriman, K. J. Elliott, M. A. H. Alamiry, L. L. Pleux, M. Séverac, Y. Pellegrin, E. Blart, C. Fosse, C. Cannizzo, C. R. Mayer, et al., *J. Phys. Chem. C* **2009**, *113*, 5834–5842.

[107] C. R. Mayer, I. Fournier, R. Thouvenot, *Chem. – Eur. J.* **2000**, *6*, 105–110.

[108] C. R. Mayer, R. Thouvenot, T. Lalot, *Chem. Mater.* **2000**, *12*, 257–260.

[109] H. Chen, L. Xie, H. Lu, Y. Yang, *J. Mater. Chem.* **2007**, *17*, 1258–1261.

[110] D. Agustin, C. Coelho, A. Mazeaud, P. Herson, A. Proust, **2004**, 2049.

[111] G. S. Kim, K. S. Hagen, C. L. Hill, *Inorg. Chem.* **1992**, *31*, 5316–5324.

[112] C. R. Mayer, P. Herson, R. Thouvenot, *Inorg. Chem.* **1999**, *38*, 6152–6158.

[113] M. Carraro, G. Modugno, A. Sartorel, G. Scorrano, M. Bonchio, *Eur. J. Inorg. Chem.* **2009**, *2009*, 5164–5174.

[114] H. Kang, J. Zubieta, *J. Chem. Soc., Chem. Commun.* **1988**, 1192–1193.

[115] J. B. Strong, R. Ostrander, A. L. Rheingold, E. A. Maatta, *J. Am. Chem. Soc.* **1994**, *116*, 3601–3602.

[116] J. B. Strong, G. P. A. Yap, R. Ostrander, L. M. Liable-Sands, A. L. Rheingold, R. Thouvenot, P. Gouzerh, E. A. Maatta, *J. Am. Chem. Soc.* **2000**, *122*, 639–649.

[117] J. B. Strong, B. S. Haggerty, A. L. Rheingold, E. A. Maatta, *Chem. Commun.* **1997**, 1137–1138.

[118] C. Dablemont, A. Proust, R. Thouvenot, C. Afonso, F. Fournier, J.-C. Tabet, *Inorg. Chem.* **2004**, *43*, 3514–3520.

[119] J. C. Duhacek, D. C. Duncan, *Inorg. Chem.* **2007**, *46*, 7253–7255.

[120] S. Liu, S. N. Shaikh, J. Zubieta, *Inorg. Chem.* **1987**, *26*, 4303–4305.

[121] D. Honda, T. Ozeki, A. Yagasaki, *Inorg. Chem.* **2005**, *44*, 9616–9618.

[122] W. H. Knoth, R. L. Harlow, *J. Am. Chem. Soc.* **1981**, *103*, 4265–4266.

[123] B. Hasenknopf, R. Delmont, P. Herson, P. Gouzerh, *Eur. J. Inorg. Chem.* **2002**, *2002*, 1081–1087.

[124] P. R. Marcoux, B. Hasenknopf, J. Vaissermann, P. Gouzerh, *Eur. J. Inorg. Chem.* **2003**, *2003*, 2406–2412.

[125] S. Favette, B. Hasenknopf, J. Vaissermann, P. Gouzerh, C. Roux, *Chem. Commun.* **2003**, 2664–2665.

[126] Y.-F. Song, D.-L. Long, L. Cronin, *Angew. Chem. Int. Ed.* **2007**, *46*, 3900–3904.

[127] Y.-F. Song, N. McMillan, D.-L. Long, J. Thiel, Y. Ding, H. Chen, N. Gadegaard, L. Cronin, *Chem. – Eur. J.* **2008**, *14*, 2349–2354.

[128] Y.-F. Song, N. McMillan, D.-L. Long, S. Kane, J. Malm, M. O. Riehle, C. P. Pradeep, N. Gadegaard, L. Cronin, *J. Am. Chem. Soc.* **2009**, *131*, 1340–1341.

[129] C. Allain, S. Favette, L.-M. Chamoreau, J. Vaissermann, L. Ruhlmann, B. Hasenknopf, *Eur. J. Inorg. Chem.* **2008**, *2008*, 3433–3441.

[130] H. Zeng, G. R. Newkome, C. L. Hill, *Angew. Chem. Int. Ed.* **2000**, *39*, 1771–1774.

[131] C. P. Pradeep, D.-L. Long, G. N. Newton, Y.-F. Song, L. Cronin, *Angew. Chem. Int. Ed.* **2008**, *47*, 4388–4391.

[132] J. Li, I. Huth, L.-M. Chamoreau, B. Hasenknopf, E. Lacôte, S. Thorimbert, M. Malacria, *Angew. Chem. Int. Ed.* **2009**, *48*, 2035–2038.

[133] J. Oble, B. Riflade, A. Noël, M. Malacria, S. Thorimbert, B. Hasenknopf, E. Lacôte, *Org. Lett.* **2011**, *13*, 5990–5993.

[134] J. F. W. Keana, M. D. Ogan, Y. Lu, M. Beer, J. Varkey, *J. Am. Chem. Soc.* **1985**, *107*, 6714–6715.

[135] J. F. W. Keana, M. D. Ogan, *J. Am. Chem. Soc.* **1986**, *108*, 7951–7957.

[136] K. J. Elliott, A. Harriman, L. L. Pleux, Y. Pellegrin, E. Blart, C. R. Mayer, F. Odobel, *Phys. Chem. Chem. Phys.* **2009**, *11*, 8767–8773.

[137] B. Xu, Y. Wei, C. L. Barnes, Z. Peng, *Angew. Chem. Int. Ed.* **2001**, *40*, 2290–2292.

[138] Y. Wei, B. Xu, C. L. Barnes, Z. Peng, *J. Am. Chem. Soc.* **2001**, *123*, 4083–4084.

[139] M. Lu, J. Kang, D. Wang, Z. Peng, *Inorg. Chem.* **2005**, *44*, 9977–9977.

[140] J. Kang, B. Xu, Z. Peng, X. Zhu, Y. Wei, D. R. Powell, *Angew. Chem. Int. Ed.* **2005**, *44*, 6902–6905.

[141] B. Xu, Z. Peng, Y. Wei, D. R. Powell, *Chem. Commun.* **2003**, 2562–2563.

[142] B. Xu, M. Lu, J. Kang, D. Wang, J. Brown, Z. Peng, *Chem. Mater.* **2005**, *17*, 2841–2851.

[143] L. Xu, M. Lu, B. Xu, Y. Wei, Z. Peng, D. R. Powell, *Angew. Chem. Int. Ed.* **2002**, *41*, 4129–4132.

[144] M. Lu, B. Xie, J. Kang, F.-C. Chen, Yang, Z. Peng, *Chem. Mater.* **2005**, *17*, 402–408.

[145] M. Lu, W. M. Nolte, T. He, D. A. Corley, J. M. Tour, *Chem. Mater.* **2009**, *21*, 442–446.

[146] Y. Zhu, L. Wang, J. Hao, P. Yin, J. Zhang, Q. Li, L. Zhu, Y. Wei, *Chem. – Eur. J.* **2009**, *15*, 3076–3080.

[147] M. M. Lorion, B. Matt, S. Alves, A. Proust, G. Poli, J. Oble, G. Izzet, *Chem.-Eur. J.* **2013**, *19*, 12607–12612.

[148] J. Kang, B. Xu, Z. Peng, X. Zhu, Y. Wei, D. R. Powell, *Angew. Chem. Int. Ed.* **2005**, *44*, 6902–6905.

[149] M.-P. Santoni, A. K. Pal, G. S. Hanan, A. Proust, B. Hasenknopf, *Inorg. Chem.* **2011**, *50*, 6737–6745.

[150] K. Micoine, B. Hasenknopf, S. Thorimbert, E. Lacôte, M. Malacria, *Angew. Chem. Int. Ed.* **2009**, *48*, 3466–3468.

[151] J. Zhang, Y.-F. Song, L. Cronin, T. Liu, *Chem. – Eur. J.* **2010**, *16*, 11320–11324.

[152] C. P. Pradeep, M. F. Misdrahi, F.-Y. Li, J. Zhang, L. Xu, D.-L. Long, T. Liu, L. Cronin, *Angew. Chem. Int. Ed.* **2009**, *48*, 8309–8313.

[153] Y. Yan, H. Wang, B. Li, G. Hou, Z. Yin, L. Wu, V. W. W. Yam, *Angew. Chem. Int. Ed.* **2010**, *49*, 9233–9236.

[154] M. Carraro, G. Modugno, G. Fiorani, C. Maccato, A. Sartorel, M. Bonchio, *Eur. J. Org. Chem.* **2012**, *2012*, 281–289.

[155] S. Vanhaecht, T. Quanten, T. N. Parac-Vogt, *Inorg. Chem.* **2017**, *56*, 3095–3101.

[156] J. T. Rhule, C. L. Hill, D. A. Judd, R. F. Schinazi, *Chem. Rev.* **1998**, *98*, 327–358.

[157] B. Hasenknopf, *Front. Biosci. J. Virtual Libr.* **2005**, *10*, 275–287.

[158] H. Yanagie, A. Ogata, S. Mitsui, T. Hisa, T. Yamase, M. Eriguchi, *Biomed. Pharmacother. Biomedecine Pharmacother.* **2006**, *60*, 349–352.

[159] Z. Dong, R. Tan, J. Cao, Y. Yang, C. Kong, J. Du, S. Zhu, Y. Zhang, J. Lu, B. Huang, et al., *Eur. J. Med. Chem.* **2011**, *46*, 2477–2484.

[160] T. Yamase, *J. Mater. Chem.* **2005**, *15*, 4773–4782.

[161] T. Yamase, H. Fujita, K. Fukushima, *Inorganica Chim. Acta* **1988**, *151*, 15–18.

[162] A. Ogata, H. Yanagie, E. Ishikawa, Y. Morishita, S. Mitsui, A. Yamashita, K. Hasumi, S. Takamoto, T. Yamase, M. Eriguchi, *Br. J. Cancer* **2008**, *98*, 399–409.

[163] Q. Wu, J. Wang, L. Zhang, A. Hong, J. Ren, *Angew. Chem. Int. Ed.* **2005**, *44*, 4048–4052.

[164] N. Fukuda, T. Yamase, Y. Tajima, *Biol. Pharm. Bull.* **1999**, *22*, 463–470.

[165] Crans, D. C., *Comments Inorg Chem* **1994**, 35–76.

[166] S. G. Sarafianos, U. Kortz, M. T. Pope, M. J. Modak, *Biochem. J.* **1996**, *319*, 619–626.

[167] D. A. Judd, J. H. Nettles, N. Nevins, J. P. Snyder, D. C. Liotta, J. Tang, J. Ermolieff, R. F. Schinazi, C. L. Hill, *J. Am. Chem. Soc.* **2001**, *123*, 886–897.

[168] D. C. Crans, M. Mahroof-Tahir, O. P. Anderson, M. M. Miller, *Inorg. Chem.* **1994**, *33*, 5586–5590.

[169] H. Eshtiagh-Hosseini, M. Mirzaei, *J. Clust. Sci.* **2012**, *23*, 345–355.

[170] G. Hungerford, K. Suhling, M. Green, *Photochem. Photobiol. Sci.* **2008**, *7*, 734–737.

[171] G. Hungerford, F. Hussain, G. R. Patzke, M. Green, *Phys. Chem. Chem. Phys.* **2010**, *12*, 7266–7275.

[172] H. Stephan, M. Kubeil, F. Emmerling, C. E. Müller, *Eur. J. Inorg. Chem.* **2013**, *2013*, 1585–1594.

[173] K. Stroobants, E. Moelants, H. G. T. Ly, P. Proost, K. Bartik, T. N. Parac-Vogt, *Chem. – Eur. J.* **2013**, *19*, 2848–2858.

[174] G. Zhang, B. Keita, J.-C. Brochon, P. de Oliveira, L. Nadjo, C. T. Craescu, S. Miron, *J. Phys. Chem. B* **2007**, *111*, 1809–1814.

[175] G. Zhang, B. Keita, C. T. Craescu, S. Miron, P. de Oliveira, L. Nadjo, *J. Phys. Chem. B* **2007**, *111*, 11253–11259.

[176] G. Zhang, B. Keita, C. T. Craescu, S. Miron, P. de Oliveira, L. Nadjo, *Biomacromolecules* **2008**, *9*, 812–817.

[177] L. Zheng, Y. Ma, G. Zhang, J. Yao, B. S. Bassil, U. Kortz, B. Keita, P. de Oliveira, L. Nadjo, C. T. Craescu, et al., *Eur. J. Inorg. Chem.* **2009**, *2009*, 5189–5193.

[178] V. Goovaerts, K. Stroobants, G. Absillis, T. N. Parac-Vogt, *Phys. Chem. Chem. Phys.* **2013**, *15*, 18378–18387.

[179] P. Bourassa, I. Hasni, H. A. Tajmir-Riahi, *Food Chem.* **2011**, *129*, 1148–1155.

[180] P.-F. Gao, S. Zhang, H.-W. Li, T. Zhang, Y. Wu, L. Wu, *Langmuir* **2015**, *31*, 10888–10896.

[181] A. Sap, E. De Zitter, L. Van Meervelt, T. N. Parac-Vogt, *Chem. – Eur. J.* **2015**, *21*, 11692–11695.

[182] V. Goovaerts, K. Stroobants, G. Absillis, T. N. Parac-Vogt, *J. Inorg. Biochem.* **2015**, *150*, 72–80.

[183] Y. Zhou, L. Zheng, F. Han, G. Zhang, Y. Ma, J. Yao, B. Keita, P. de Oliveira, L. Nadjo, *Colloids Surf. Physicochem. Eng. Asp.* **2011**, *375*, 97–101.

[184] J. Geng, M. Li, J. Ren, E. Wang, X. Qu, *Angew. Chem. Int. Ed.* **2011**, *50*, 4184–4188.

[185] X. López, C. Nieto-Draghi, C. Bo, J. B. Avalos, J. M. Poblet, *J. Phys. Chem. A* **2005**, *109*, 1216–1222.

[186] F. Leroy, P. Miró, J. M. Poblet, C. Bo, J. Bonet Ávalos, *J. Phys. Chem. B* **2008**, *112*, 8591–8599.

[187] A. Chaumont, G. Wipff, *Phys. Chem. Chem. Phys.* **2008**, *10*, 6940–6953.

[188] A. Chaumont, G. Wipff, *Comptes Rendus Chim.* **2012**, *15*, 107–117.

[189] P. Jiménez-Lozano, J. J. Carbó, A. Chaumont, J. M. Poblet, A. Rodríguez-Fortea, G. Wipff, *Inorg. Chem.* **2014**, *53*, 778–786.

[190] N. Dupré, P. Rémy, K. Micoine, C. Boglio, S. Thorimbert, E. Lacôte, B. Hasenknopf, M. Malacria, *Chem. – Eur. J.* **2010**, *16*, 7256–7264.

[191] H. El Moll, B. Nohra, P. Mialane, J. Marrot, N. Dupré, B. Riflade, M. Malacria, S. Thorimbert, B. Hasenknopf, E. Lacôte, et al., *Chem. – Eur. J.* **2011**, *17*, 14129–14138.

[192] P. Jiménez-Lozano, A. Solé-Daura, G. Wipff, J. M. Poblet, A. Chaumont, J. J. Carbó, *Inorg. Chem.* **2017**, DOI 10.1021/acs.inorgchem.7b00096.

[193] T. Mitra, P. Miró, A.-R. Tomsa, A. Merca, H. Bögge, J. B. Ávalos, J. M. Poblet, C. Bo, A. Müller, *Chem. – Eur. J.* **2009**, *15*, 1844–1852.

[194] M. Garcia-Ratés, P. Miró, J. M. Poblet, C. Bo, J. B. Avalos, *J. Phys. Chem. B* **2011**, *115*, 5980–5992.

[195] R. Brodbeck, T. Tönsing, D. Andrae, D. Volkmer, *J. Phys. Chem. B* **2008**, *112*, 5153–5162.

[196] A. Solé-Daura, V. Goovaerts, K. Stroobants, G. Absillis, P. Jiménez-Lozano, J. M. Poblet, J. D. Hirst, T. N. Parac-Vogt, J. J. Carbó, *Chem.- Eur. J.* **2016**, *22*, 15280–15289.

# CHAPTER 2: HYBRID POLYOXOMETALATES IN CATALYSIS

## 2.1     Introduction

Polyoxometalates have been extensively applied in homogeneous or heterogeneous catalysis, as Brønsted or Lewis acid catalysts[1,2] or as oxidants, and more recently as basic catalysts.[3,4]

The derivatization of the inorganic scaffold with different organic moieties has been well exploited for creating new functional nanoscaled materials, easily recyclable. The functionalization with organo-ligands, indeed, allows one to better exploit the main properties of POMs also in the organic synthesis field (in organic media), generally for oxidation reactions.[5–9]

Moreover, as introduced in the previous chapter, the insertion of organic ligands has led to improve, through synergistic effects, the reactivity of the inorganic scaffold and/or of the organic ligand.

*In this chapter an outlook on class I and class II POM-hybrids, will be given in order to present how the hybridization makes it possible to improve some catalytic performances of the inorganic scaffold and vice versa. Both experiments and theoretical characterizations of the hybrids properties will be taken into account.*

## 2.2     Hybrid POMs toward catalytic oxidation reactions

### 2.2.1     Type I hybrid-POM catalysts

One of the most important advancement in this class of compounds is the introduction by Nlate group of the DENDRI-POMs. The most common methodology to prepare DENDRI-POM hybrids involves the electrostatic assembly of ammonium dendrimers with polyanionic POM species. The advantage of these interesting systems concerns the possibility to experience them toward different oxidation reactions in organic media and, after that, to easily recycle them.[10]
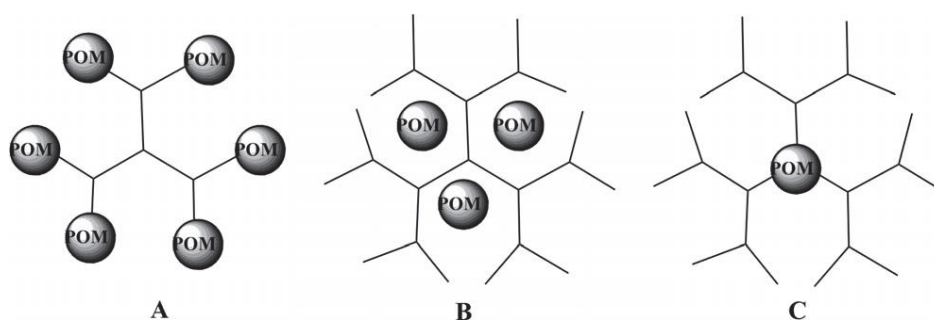
**Figure 2. 1-** Three families of DENDRI-POM hybrids: (A) POM units located at the dendrimer periphery, (B) POM encapsulated within the cavities of the dendrimer, (C) POM-cored dendrimers,; developed by Nlate's group for oxidative catalysis.

As an interesting example of these DENDRI-POM systems the zirconium-based DENDRI-POM obtained by coupling the peroxotungstosilicate polyanion $[Zr_2(O_2)_2(SiW_{11}O_{39})_2]^{12-}$ with various benzyl ammonium dendrons. These DENDRI-POMs were found to be stable, efficient, recoverable, and reusable catalysts for the oxidation of sulfides in an aqueous/$CDCl_3$ biphasic medium with $H_2O_2$ as the oxidant. Two cycles of catalytic reactions could be performed without any appreciable loss of activity.[11]
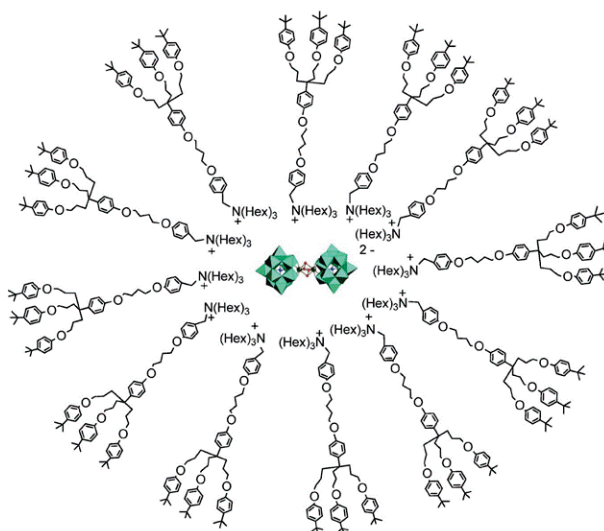


**Figure 2. 2**- Structure of 36-(4-tert-butylphenyl) DENDRI-POM based on the Zr-substituted peroxotungstosilicate anion.

59

Poly(ionic liquid)s (PIL), namely poly-[1-vinyl,3-alkylimidazolium] bromine (PVABr), with different lengths of monomer carbon chains have been synthesized and assembled also with $[\beta\text{-}Mo_8O_{26}]^{4-}$ into novel interlinked thin-layer nano-wire mesoporous materials. The resulting POM/PIL hybrids were employed to catalyze the oxidative desulfurization (ODS) of thiophenic compounds with $H_2O_2$ as oxidant. The catalyst could at least be reused six times without noticeable changes in catalytic performance.

In the ODS of real diesel, the PIL/POM catalyst exhibited excellent desulfurization efficiency under mild conditions without the need of reaction medium. Indeed the steric effect of long carbon chains between polymeric cations, brings them to be crosslinked in a two-dimensional direction, and thus to form thin-layer skeletons.[12]
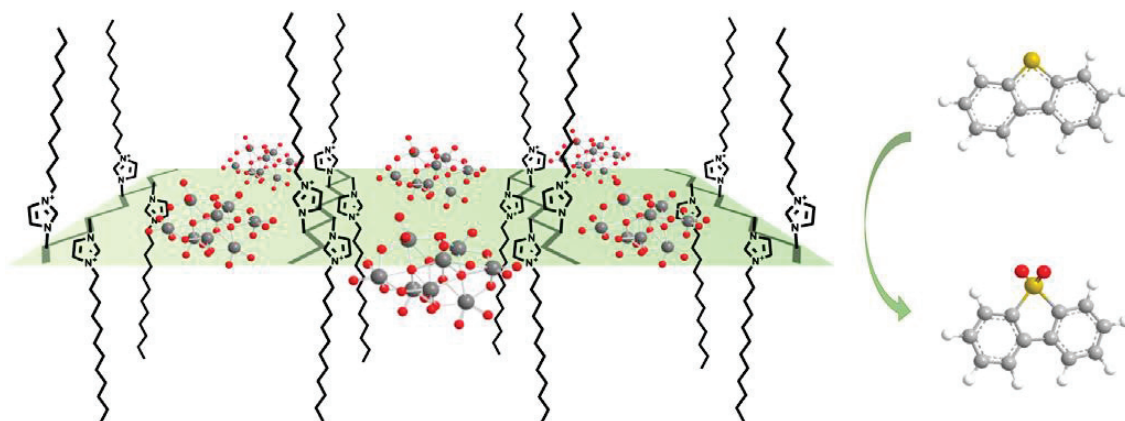


**Figure 2. 3-** Mesoporous PIL/POM catalysts recently presented by Yang et al. for the oxidative desulfurization of thiophenic compounds.

A series of POM-supported organometallic complexes has been developed by Finke and coworkers as precatalysts for the oxygenation of norbornene and cyclohexene using $(PhIO)_n$ as oxidant. Eleven new polyoxoanion-supported transition metal acetonitrile complexes have been prepared in 1:1, 1:2, and even 1:3 Mn+ to polyoxoanion compositions, with general formula $\{m(CH_3CN)_xM^{n+}/P_2W_{15}Nb_3O_{62}{}^{9-}\}$ ($M^{n+}=Mn^{2+}$, $Fe^{2+}$, $Co^{2+}$, $m=1, 2$; $Mn^+=Cu^{2+}$, $m=2, 3$; $M^{n+}=Ni^{2+}$, $Zn^{2+}$, $Cu^+$, $m=2$). The results show a ca. 14-fold rate increase for $\{(CH_3CN)_xMn^{2+}/P_2W_{15}Nb_3O_{62}{}^{9-}\}$ and $\{2(CH_3CN)_xMn^{2+}/P_2W_{15}Nb_3O_{62}{}^{9-}\}$ in

norbornene and cyclohexene epoxidation compared to the polyoxoanion-free $[Mn^{II}(CH_3CN)_4]^-(BF_4)_2]$-solvate.[13]
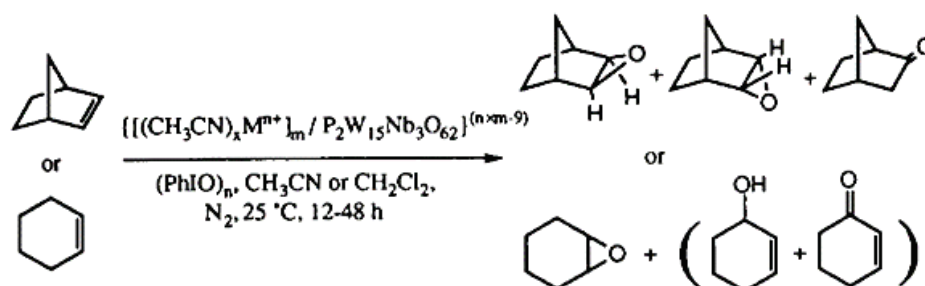


**Figure 2. 4-** General procedure for Dawson-Type Polyoxoanion-Supported Transition Metal Precatalysts catalyzed reactions.

Another organometallic-polyoxometalate complex, based on the redox active $H_5PV_2Mo_{10}O_{40}$ polyoxometalate, was prepared in 2009 by Ettedgui and Neumann. They synthesized a $Pd^{II}$(15-crown-5-phen)$Cl_2$-$H_5PV_2Mo_{10}O_{40}$ catalyst, exploiting the induced dipole interactions between the crown ether and the hydronium cation of the polyoxometalates. Then, the hybrid complex was employed in the oxidation of different alkenes in presence of molecular oxygen, finding that the hybrid system was more active and selective than $Pd^{II}$(phen)$Cl_2$ or $Pd^{II}$(phen)$Cl_2$ plus $H_5PV_2Mo_{10}O_{40}$. Moreover, more interestingly, they tested the catalytic activity of this hybrid complex toward the Wacker oxidation of terminal alkenes, such as 1-octene, in the presence of the more environmentally benign $N_2O$ as oxidant. Both higher selectivities and yields versus the corresponding 2-octanone were observed, while the use of a simple mixture of $Pd_{II}$(phen)$Cl_2$ and $H_5PV_2Mo_{10}O_{40}$ yielded significantly lower yields and also reduced reaction selectivities.[14]

Assembled catalyst
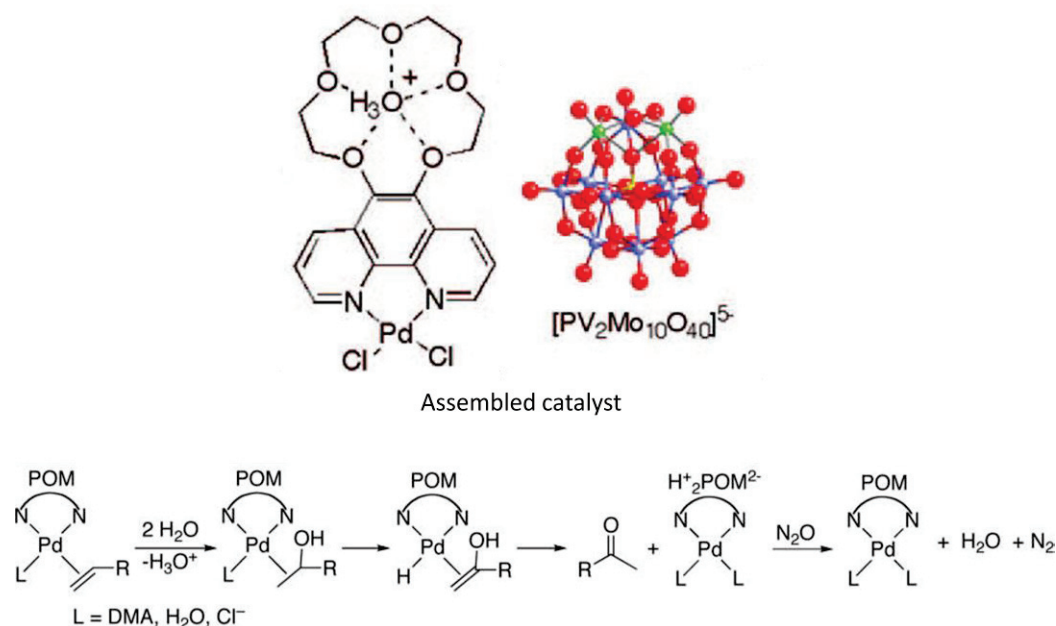
**Figure 2. 5-** Structure of the two component of the hybrid catalytic system (on the top) and proposed catalytic mechanism for the Wacker reaction in presence of $N_2O$.

An important type I hybridized POM system with interesting catalytic properties was introduced by Prato, Bonchio and coworkers. They succeeded in functionalizing a Multi Walled Carbon Nanotubes (MWCN) with polycationic dendrons, in order to exploit the electrostatic interaction between the positively charged conductive bed of MWCN and the highly negatively charged ruthenium-based Keggin POM, $M_{10}[Ru_4(H_2O)_4(\mu-O)_4(\mu-OH)_2(\gamma-SiW_{10}O_{36})_2]$. An oxygen evolving anode was then developed, since the polyoxometalate is known to achieve the water oxidation.[15] They yielded TOF values in the range 36-306 h$^{-1}$, depending on the applied overpotential: at pH 7.0, an appreciable catalytic current with a TOF of 36 h$^{-1}$ was observed when the overpotential was η=0.35 V and a peak performance of 306 h$^{-1}$ when η=0.60 V.[16] In any case, the TOF efficiency was slightly inferior with respect to homogeneous conditions that employed Ce(IV) as the bulk oxidant (TOF > 450 h$^{-1}$), but it was justified as a reasonable compromise because of the different experimental conditions and the transfer on a heterogeneous surface.
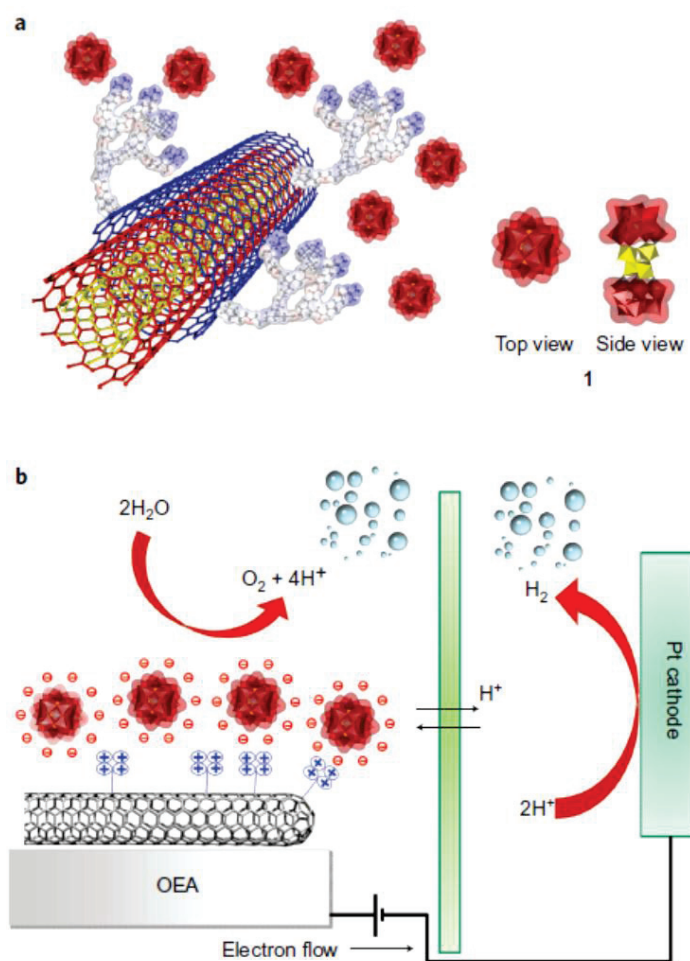
**Figure 2. 6-** General scheme for a water-splitting electrocatalytic cell (b) with the integrated nanostructured Oxygen Evolving Anode explicated in (a).

Some polyoxometalates were also electrostatically functionalized with calix[4]arene ligands for the sulfoxidation of thioethers to sulfoxides and to sulfones,[17] or as heterogeneous catalysts toward the catalytic oxidative desulfurization.[18] The attractive features of these easily recyclable systems are the high catalytic activity at a low catalyst loading, mild reaction conditions and wide substrate scope, with a strictly stoichiometric amount of $H_2O_2$.

The presence of calix[4]arene tetra-ammonium units, indeed, enhanced the catalytic activity of the hybrid when compared to the conversion observed when using a $(Ph_4P)_2Na_2[Mo_8O_{25}]$ derivative. This result might be rationalized by invoking favourable homophilic interactions displayed by the large calix[4]arene tetra-ammonium portion of the hybrid with the organic sulfide and thus

improving the mass transfer between the inorganic POM and the organic substrate.[17]
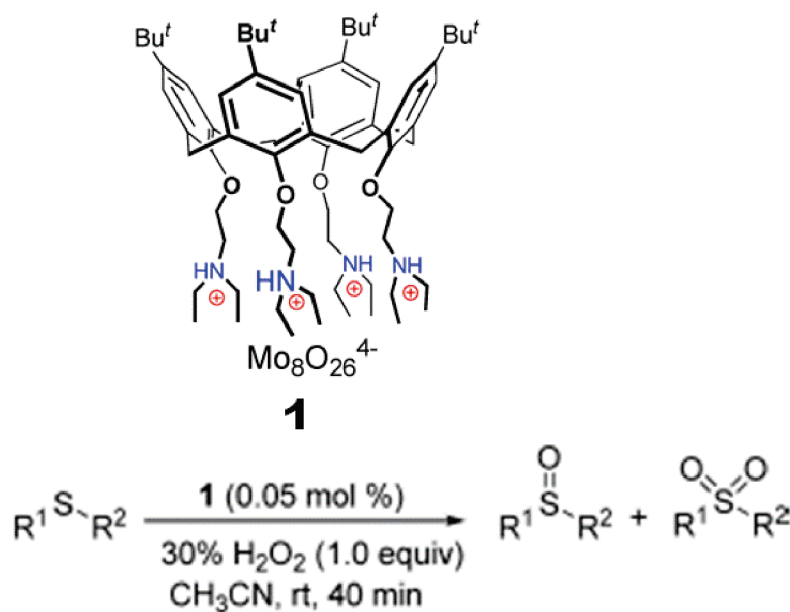


**Figure 2. 7-** The designed calix[4]arene tetra-ammonium octamolybdate, developed by Meninno et al. and its application toward the catalytic oxidation of thioethers.

Recently, Kastner et al. developed a redox-active hybrid organic–inorganic polyoxometalate surfactant showing solvent-dependent self-assembly to form nano-scale architectures. The POM-surfactant $H_6[P_2W_{17}O_{57}(H_{27}C_{17}O_4PS)_2]*3C_4H_9NO$ was prepared by the condensation of (4-((11-mercaptoundecyl)oxy)phenyl)phosphonic acid with the monolacunary Dawson-type anion, $[P_2W_{17}O_{61}]^{10-}$. In water, the hybrid formed regular micellar assemblies, but addition of DMF led to the disruption of the supramolecular species. Moreover, the supramolecular assemblies exhibited contrasting electronic structure and redox activity respect to their molecular building units, and were found to be stable under electrochemical reduction and reoxidation.

They created a three-electrode set-up: with a glassy carbon electrode serving as the working electrode, Ag/AgCl as reference electrode and Pt wire as the counter electrode. Two broad redox processes centred at $E_{1/2}$ =0.26 V and $E_{1/2}$=-0.11 V vs. NHE were observed for the hybrid. Differently, under identical

conditions and at the same concentration, the cyclic voltammogram of the free {P2W18} showed redox processes centered at 0.27 V and 0.10 V vs. NHE. This positive shift of the hybrid compared to {P2W18} (of ca. 400 mV) for the POM reduction potential in DMF was absent in the aqueous $H_2SO_4$ solution. The authors hypothesized that this contrasting redox behaviour may be due to intermolecular cooperativity or coulombic repulsion between metal oxide head groups in the supramolecular aggregates.[19]
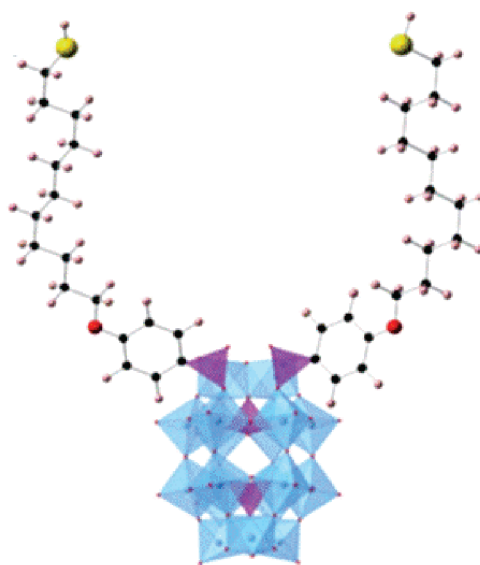


**Figure 2. 8- A**n example of POM-surfactant supramolecular complex developed by Kastner et al.

### 2.2.2    *Type II hybrid-POM catalysts*

Going to the most stable covalent hybrid POMs, an interesting example of a lacunary POM functionalized with a catalytically active organic ligand is given by Mirkhani et al. They investigated the catalytic activity of polyoxometalates hybridized with organometallic ligands, such as different metallosalen-polyoxometalates (M(salen)-POM), toward some oxidation reactions in the presence of hydrogen peroxide. In particular the authors focused their attention on the monolacunary Keggin $[SiW_{11}O_{39}]^{8-}$ functionalized by an organosilyl group bearing a pendant metallosalen moiety. Fe(salen)-POM, Ni(salen)-POM, and Co(salen)-POM systems have been studied in the epoxidation of olefins and

higher yields have been obtained with the M(salen)-POMs compared with the parent M(salen) complexes.[20–23]

Moreover, Fe(salen)-POM and Co(salen)-POMs have also been used for the oxidation of alkanes or primary and secondary benzyl halides.[22,23]
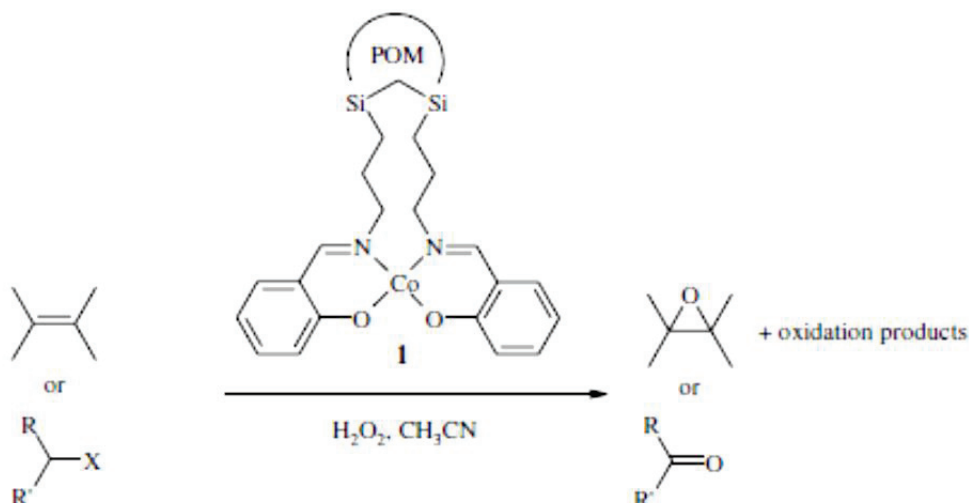


**Figure 2. 9**- Example of cobalt–Schiff base complex covalently linked to the Keggin polyoxometalate, employed by Mirkhani et al. in the alkene and benzyl halide oxidation in presence of hydrogen peroxide.

By reacting inorganic $H_3PW_{12}O_{40}$ with organic $[\text{п-}C_5H_5N(CH_2)_{15}CH_3]Cl$, Venturello and coworkers synthesized an organic-inorganic hybrid simultaneously acting as the catalyst and phase-transfer agent. Indeed, to increase the accessibility of lipophilic alkenes to the aqueous soluble catalyst precursors, the salts of quaternary ammonium modified by long-chain alkyl groups (C6−C18) were introduced into the systems as phase transfer agents. The $[\text{п-}C_5H_5N(CH_2)_{15}CH_3]_3PW_{12}$ effectively accelerates the oxidation of alkenes in biphasic systems using $CHCl_3$ as solvent and $H_2O_2$ as oxidant.[24,25]

With the aim to get a more robust catalyst for the epoxidation of olefins, a polyoxometalate was hybridized also with a metallo-porphyrin. The hybrid material, which is $[\{Gd_4Co_2(Co_4P_4W_{30})_2\}(Mn\text{-}OCPP)]$ (with Mn-OCPP corresponding to the metalloporphyrin $Mn^{III}Cl\text{-}5,10,15,20\text{-}tetrakis(3,5\text{--}biscarboxylphenyl)porphyrin$), is highly efficient toward the activation of

molecular oxygen. The authors exploited the immobilization of both the metalloporphyrin and POM moieties into the same frameworks of hybrid materials, finding that the collaborative work of multiple active sites in hybrid materials can achieve superior high efficiency in heterogeneous.

Indeed, knowing that both metalloporphyrins and POMs have been used as active species to initiate radical epoxidation of olefins with molecular oxygen in the presence of co-reductant aldehydes (such as benzaldehyde or isobutyraldehyde) [26,27], they decided to investigate the hybrid multi-active system toward this reaction. The heterogeneous catalyst exhibits high catalytic activity in the epoxidation of olefins in the presence of isobutyraldehyde (IBA), mainly for epoxidation of styrene to form (1,2-epoxyethyl)benzene (conversion >99%, selectivity =94%, TON =220000, and TOF=22000 h$^{-1}$).[28]
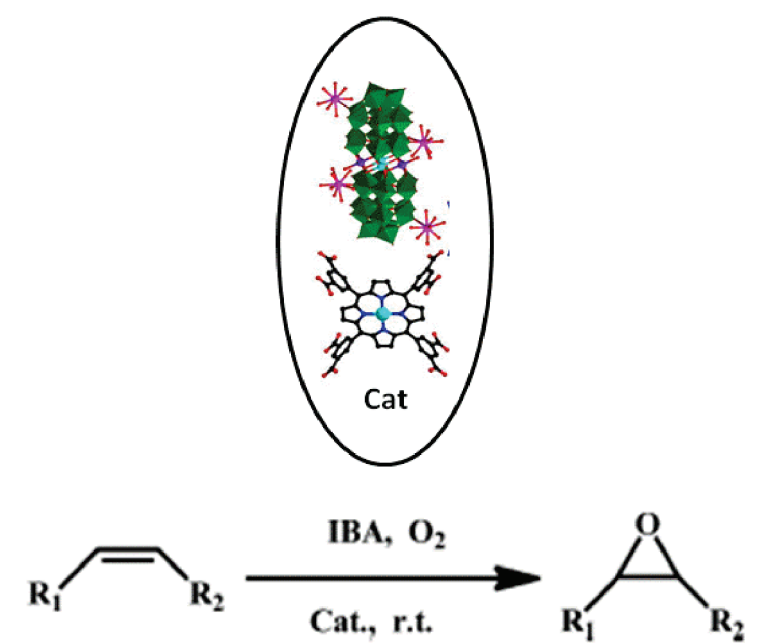


**Figure 2. 10-** Schematic representation of the two components of the hybrid system and catalyzed reactions scheme.

To impart a strong stability, Carraro and coworkers covalently functionalized the lacunary oxygen atoms of $\gamma$-SiW$_{10}$O$_{40}$ with organo moieties. They attached tunable organic moieties to influence the electron density on the proximal W atoms. In particular, the hybrid POM [$\gamma$-SiW$_{10}$O$_{36}$(PhPO)$_2$]$^{4-}$ was used as catalyst

toward the alkene epoxidation in the presence of $H_2O_2$, under microwave irradiation in acetonitrile and IL: the reaction in IL was faster.[29,30]
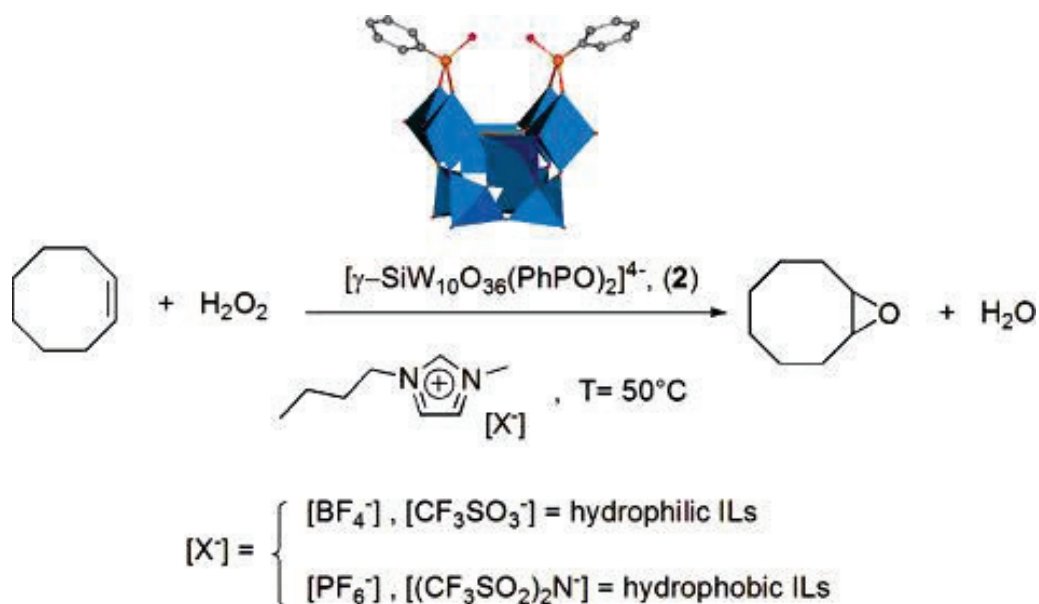


**Figure 2. 11-** Catalytic epoxidation of *cis*-cyclooctene by the hybrid POM with $H_2O_2$ in ILs, proposed by Berardi et al.

Lacôte, Thorimbert, Hasenknopf and coworkers were the first to graft carbonyl ligands (diolamides, diolureas, diolcarbammates) in the crown of a Dawson polyoxotungstovanadate.[31,32] These hybrid systems were good catalysts for the oxidation of sulfides. In addition, it is possible to fine-tune the chemoselectivity of the sulfide oxidation upon appropriate choice of cations and organic substituents. The chemoselectivity is a function of the proton content of the inorganic salt and of the electronic properties of the grafted organic substituents.

| ent. | R (POM) | cations[a] | 6[b] | 7[b] |
|---|---|---|---|---|
| 1 | − (1) | TBA$_{5.3}$H$_{3.7}$ | 60 | 40 |
| 2 | − (1) | TBA$_9$ | 70 | 30 |
| 3 | EtNH (3a) | TBA$_{2.85}$H$_{2.15}$ | 67 | 33 |
| 4 | EtNH (3a) | TBA$_5$ | 96 | 4 |
| 5 | $p$NO$_2$C$_6$H$_4$NH (3b) | TBA$_{4.7}$DMA$_{0.3}$ | 82 | 18 |
| 6 | $p$NO$_2$C$_6$H$_4$NH (3b) | TBA$_5$ | 93 | 7 |
| 7 | $p$CF$_3$C$_6$H$_4$NH (3c) | TBA$_{4.65}$DMA$_{0.35}$ | 93 | 7 |
| 8 | PhNH (3d) | TBA$_{3.45}$H$_{1.55}$ | 72 | 28 |
| 9 | PhNH (3d) | TBA$_{4.7}$DMA$_{0.3}$ | 87 | 13 |
| 10 | $p$MeOC$_6$H$_4$NH (3f) | TBA$_{4.7}$DMA$_{0.3}$ | 83 | 17 |
| 11 | $p$MeOC$_6$H$_4$NH (3f) | TBA$_5$ | 95 | 5 |
| 12 | BnO (3k) | TBA$_{4.7}$DMA$_{0.3}$ | 86 | 14 |
| 13 | PhO (3m) | TBA$_{4.6}$DMA$_{0.4}$ | 78 | 22 |
| 14 | PhO (3m) | TBA$_5$ | 96 | 4 |
| 15 | $p$MeOC$_6$H$_4$O (3o) | TBA$_{4.6}$DMA$_{0.4}$ | 72 | 28 |
| 16 | $p$MeOC$_6$H$_4$O (3o) | TBA$_5$ | 96 | 4 |
| 17 | $p$NO$_2$C$_6$H$_4$ (3s) | TBA$_{4.7}$DMA$_{0.3}$ | 79 | 21 |
| 18[c] | $p$NO$_2$C$_6$H$_4$ (3s) | TBA$_{4.7}$DMA$_{0.3}$ | 72 | 28 |
| 19 | $p$NO$_2$C$_6$H$_4$ (3s) | TBA$_5$ | 88 | 12 |
| 20 | $p$MeOC$_6$H$_4$ (3t) | TBA$_{4.65}$DMA$_{0.35}$ | 90 | 10 |
| 21 | $p$MeOC$_6$H$_4$ (3t) | TBA$_5$ | 95 | 5 |

**Figure 2. 12**- Oxidation reaction (on the top) catalyzed by the POM-based hybrid systems (on the middle) and table showing the chemoselectivity obtained changing the organic substituent or the proton-content of the POM (on the bottom).

## 2.3     Hybrid POMs toward catalytic Photo-Oxidation reactions

Considering also the interesting properties of some polyoxometalates toward photo catalysis, the hybridization of the inorganic scaffold through photo-active organic moieties was examined.[33] Indeed, the goal of this hybridization is to reduce the band-gap between the HOMO and LUMO: Ultraviolet wavelengths are generally necessary to drive the electronic transitions between frontier orbitals in totally inorganic POMs. Thanks to the presence of organic moieties, it is possible to employ the less energetic visible light to promote the reaction.

### 2.3.1    *Type I hybrid-POM photo-catalysts*

The electrostatic interaction between the tetracobalt Dawson-derived sandwich polyanion $[Co_4(H_2O)(OH)(P_2W_{15}O_{56})_2]$ and the tetracationic zinc porphyrins, $ZnTMPyP^{4+}$ or $ZnOETPyP^{4+}$, was employed by Schaming et al. to create functional hybrid POMs in aqueous solutions. In these complexes, porphyrins can be excited by visible light and then to give electrons to the polyoxometalate. Then, the photocatalytic reduction of silver ions in the presence of these complexes and propan-2-ol (as sacrificial H-donor) was observed in aerated and de-aerated aqueous solutions.[34]

The same idea, was employed by the Bonchio group to exploit the great potential of the $[Ru_4(\mu\text{-}O)_4(\mu\text{-}OH)_2(H_2O)_4(\gamma\text{-}SiW_{10}O_{36})_2]$ toward water oxidation,[15,35] in the presence of $Ru(bpy)_3^{2+}$[36] or metallo-porphiryns as sensitizers.[37] Their idea was to develop new three-components system for visible light-driven water oxidation.

For instance, the supramolecular POM@Zn(porphyrin) complex (where the porphyrin is the photosensitizer and the POM the water oxidation catalyst) was irradiated in the presence of persulfate as electron acceptor. The photophysical study revealed the photogeneration of a pentacation radical of the porphyrin, with a quantum yield up to 1.01, upon oxidative quenching of the excited triplet state by persulfate. The electron transfer from the water-oxidation catalyst to the pentacation radical (hole scavenging) then occurs, but it is slow (bimolecular rate constant, $k < 4 \times 10^7 \, M^{-1} \, s^{-1}$). Probably this is the main reason for the low efficiency of the system in experimental photocatalytic tests for water oxidation.[37]
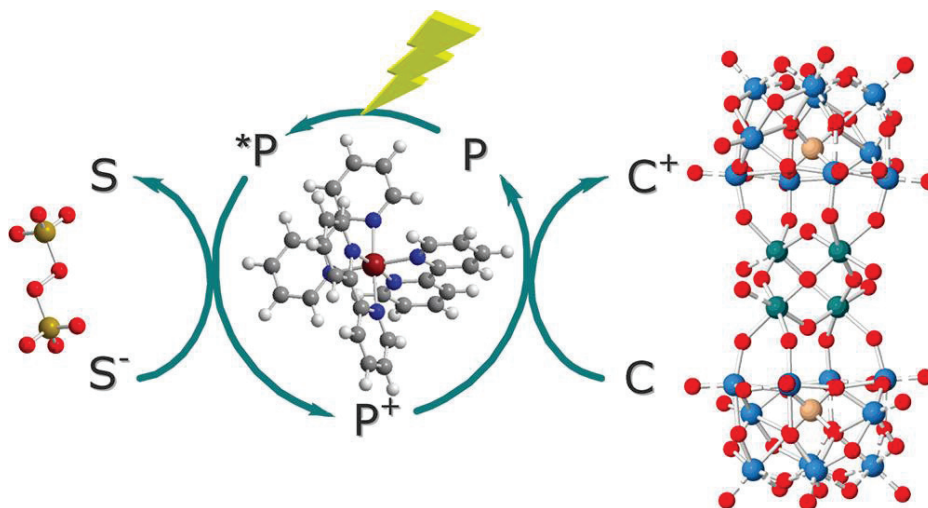
**Figure 2. 13**- Hybrid $Ru_4POM@Ru(bpy)_3$ ionic system used for the photo-oxidation of water, in presence of persulfate as electron acceptor.

Lacôte and co-workers used the lacunary Well-Dawson polyoxotungstate, $(\alpha_1/\alpha_2-[P_2W_{17}O_{61}Sn(CH_2)_2CO]$, to functionalize it with organo moieties and testing their catalytic activity.[38–41] Interestingly, they synthesized a polystyrene–POM composite latexes, showing that the inorganic clusters transferred their properties to the latexes and blue latexes could be reversibly formed upon photoreduction, which makes these materials photochromic. The POM mediated surface photoactivity of the PS-POM hybrids was attested with the photoreduction of silver ions. In the latter reaction, homogeneous and small silver NPs were exclusively formed at the surface of the PS spheres.[40]

Last year, Chen et al. presented a new hybrid system employing stepwise self-assembly pathway to combine the organic– inorganic hybrid units, $([Cd(phen)_3]^{2-})$ with Dawson-type inorganic polyanions. The new hybrid system results in a water-insoluble hybrid polytungstate, $(Hdma)_4[Cd(phen)_3][W_{18}O_{54}(PO_4)_2]*2H_2O$, that shows good catalytic activity for the photo-bleaching of rhodamine B by $H_2O_2$ under UV-light. The POM-hybrid system increases the degradation rate up to 98%, with respect to the background $H_2O_2$ direct oxidation.[42]

### 2.3.2    *Type II hybrid-POM photo-catalysts*

Examples of covalent POM-based donor–acceptor dyads reported thus far include pyrene and perylene,[43–45] ferrocenes,[46,47] Ru and Ir complexes [48,49] and porphyrins,[43,50–52] as sensitizers.

Proust and co-workers decorated Keggin and Dawson-type lacunary polyoxometalates, such as $[PW_{11}O_{39}]^{7-}$, and $[P_2W_{17}O_{61}]^{10-}$, by organometallic cyclometalated ruthenium(II) polypyridine complexes or organic pyrene chromophores, through post-functionalization of the hybrid disilylated POM platforms.
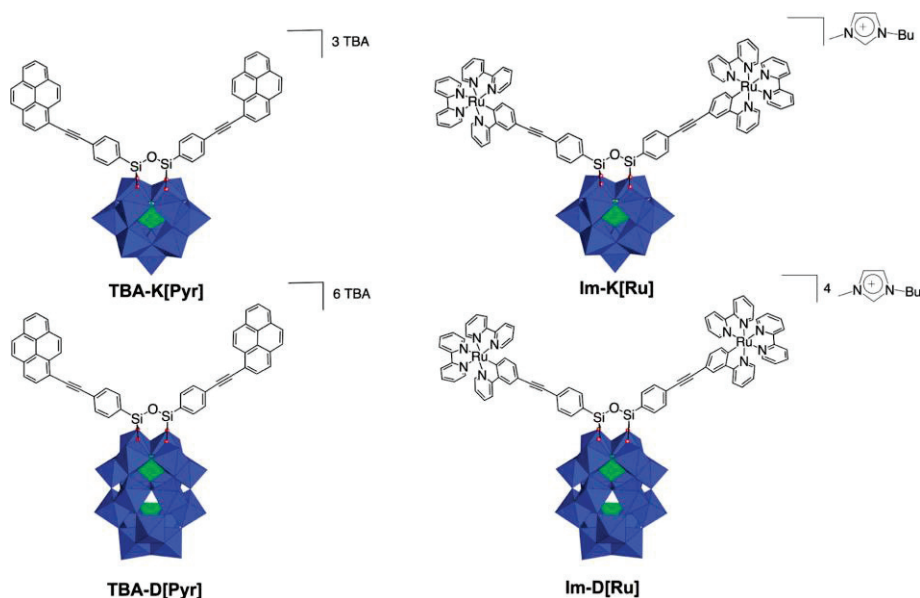


**Figure 2. 14**- Molecular Drawing of the Four Photoactive POM-Based Hybrids described by Proust's group.

They observed a poor electronic interaction between the two partners. The presence of the POM leads to luminescence quenching of the chromophores which was attributed to an intramolecular electron transfer from the chromophore to the POM. More interestingly a comparative study of the luminescence quenching on POM@Ru system showed that the electron transfer is more important in the covalently bonded hybrids than in systems where the POM and the ruthenium complexes are assembled via electrostatic interactions.[49]

A few months ago, the organic–inorganic hybrid polyoxometalate, $K_6[P_2W_{17}O_{57}(PO_5H_5C_7)_2]_6C_4H_9NO$, was found to exhibit enhanced redox behavior and photochemistry compared to its purely inorganic counterparts. The hybridization with electron-withdrawing moieties was shown to tune the frontier orbital energy levels and reduce the HOMO–LUMO gap, leading to direct visible-light photoactivation.[53]

In 2014 Zhang and coworkers synthesized the bipyridine bicapped/monocapped Keggin-type POMs, such as $[Co^{II}(bpy)_3]_6(H_2bpy)[(Co^{II}bpy)_2(PMo_8^{VI}Mo_4VO_{40})]^{3-}$ and $[(Co^{II}bpy)-(PMo_8^{VI}Mo_4VO_{40})]^4*16H_2O$, and showed their efficiency as molecular water oxidation catalyst under photocatalytic conditions.[54]
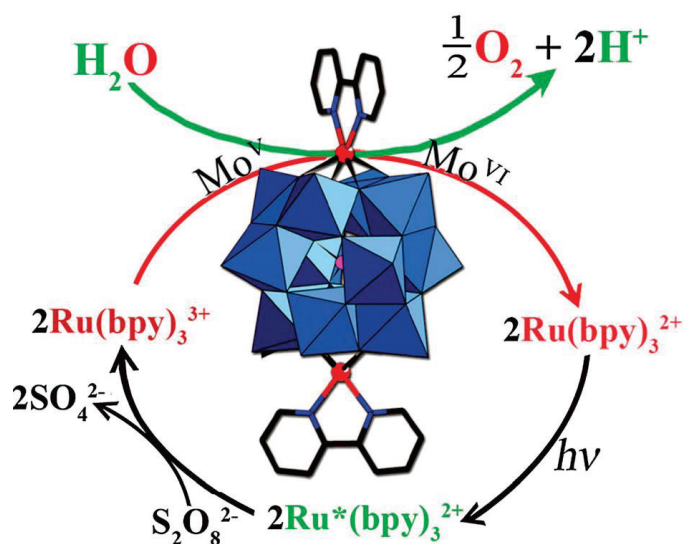


**Figure 2. 15-** Bicapped 2,2 bipyridine keggin POM catalyzes water oxidation to generate O2 under visible light irradiation, using $[Ru(bpy)_3]^{2+}$ as the photosensitizer and $S_2O_8^{2-}$ as the sacrificial electron acceptor

Bonchio's group functionalized the lacunary Keggin polyoxotungstate $[\gamma\text{-}SiW_{10}O_{36}]^{8-}$ with organosilyl fuller-pyrrolidines ligands, investigating their catalytic properties toward waste water treatment, under photocatalytic conditions. The hybrid POMs have been efficiently employed for the photooxidation of phenol and L-methionine in water (using visible light irradiation $\lambda > 375$ nm). Phenol (4 mM) was oxidized in 150 min with a Chemical

Oxygen Demand (COD) loss up to 30% (TON up to 50 - expressed as moles of substrate converted per mole of photocatalyst), while l-methionine methyl ester (15 mM) provided selective photo-oxygenation to the corresponding sulfoxide in 90 min (TON up to 200). Then the photocatalyst stability was evaluated and the catalyst could be reused three times.[55]
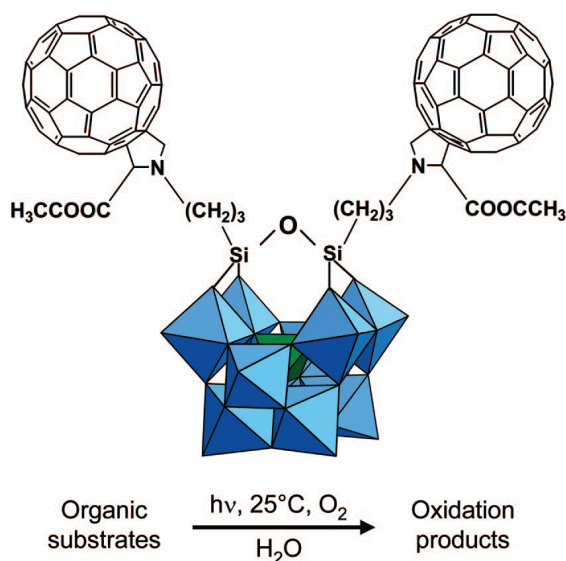


**Figure 2. 16**- Lacunary Keggin POM functionalized with organosilyl fuller-pyrrolidines moieties and general scheme of its applications toward the photooxidation in water of phenol and L-methionine substrates.

## 2.4      Other reaction types catalyzed by organo-POMs

*Synthesis of Azlactones*

Rostami and co-workers developed an ionic liquid-based POM: 1-butyl-3-methylimidazolium salts of $(W_{10}O_{32})^{4-}$ and $(PW_{12}O_{40})^{3-}$ polyanions, to be used as heterogeneous catalyst toward the synthesis of azlactone. The reaction of aldehydes with hippuric acid and acetic anhydride under solvent-free conditions (Erlenmeyer reaction) delivered the expected products. This important reaction, used to prepare aminoacids, in general is carried by heating and in the presence of sodium acetate. They proved that in this case the catalytic activity of the system arises from the creation of a favorable microenvironment, thanks to the interaction between anions and cations in [[bmim]$_3$PW$_{12}$O$_{40}$ and [bmim]$_4$W$_{10}$O$_{32}$ ]

(where bmin =1-butyl-3-methylimidazolium), with respect to the free simple POMs [$K_3PW_{12}O_{40}$ and $K_4W_{10}O_{32}$]. These catalysts were recycled several times without loss on their activities.[56]
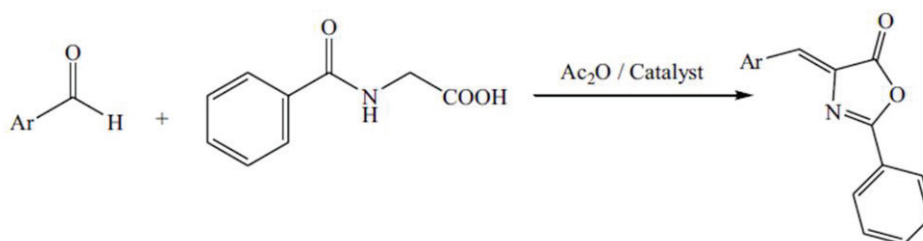


**Figure 2. 17-** Erlenmeyer synthesis of azlactone efficiently catalyzed by the POM-IL developed by Rostami et al.

*Addition of dicarbonyl compounds to nitro-olefins*

The lacunary $\alpha_2$-Dawson polyoxotungstate in the achiral isomeric form, ($\alpha_2$-[$P_2W_{17}O_{61}Sn(CH_2)_2CO$], was also recently functionalized with squaramide ligands. The catalyst is a bifunctional catalyst toward the addition of dicarbonyl derivatives onto nitroolefins. Indeed, the POM surface enhances the acidity of the squaramide ligand and its highly charged surface acts as a base in the organic medium, which helps to deprotonate the nucleophile while the squaramide activates the nitroalkenes via H-bonds.[41]
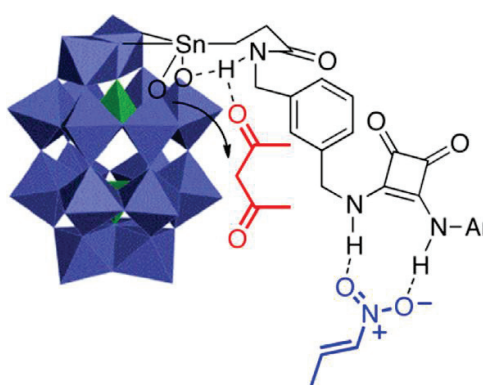


**Figure 2. 18-** Reaction mechanism proposed by Lachkar and Lacôte for the catalytic addition of dicarbonyl compounds to nitro-olephines catalyzed by the hybrid squaramide-POM.

*Allylations of imines and aldehydes*

The same group grafted a palladium complex on the Dawson POM $[P_2W_{15}V_3O_{62}]^{9-}$ through an organic ligand. Indeed, the Palladium atom was post-synthetically installed on the (pyridine)amide-substituted POM. This grafting generates a large family of electrophilic pincer-type hybrid polyoxometalates. The palladium-POM derivatives present dual catalytic properties. Unlike their parent inorganic polyanions, they catalyze allylations of imines and aldehydes, while retaining their oxidant character, which leads to single-pot dual site catalysis.[57]
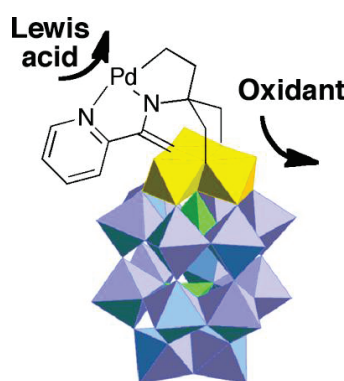


**Figure 2. 19**- Dual site POM based catalyst, presented by Riflade et al.

*Hydrogenation of alkenes*

In the Neumann groups a metal-organic–polyoxometalate hybrid compound with two functional centers was synthesized. It consists of a rhodium(I)bis(diphenylphospine) unit connected through two alkylene bridging groups to a lacunary Keggin type polyoxometalate. An effective, recyclable alkenes hydrogenation catalyst was obtained in both monophasic and aqueous biphasic systems.[58]
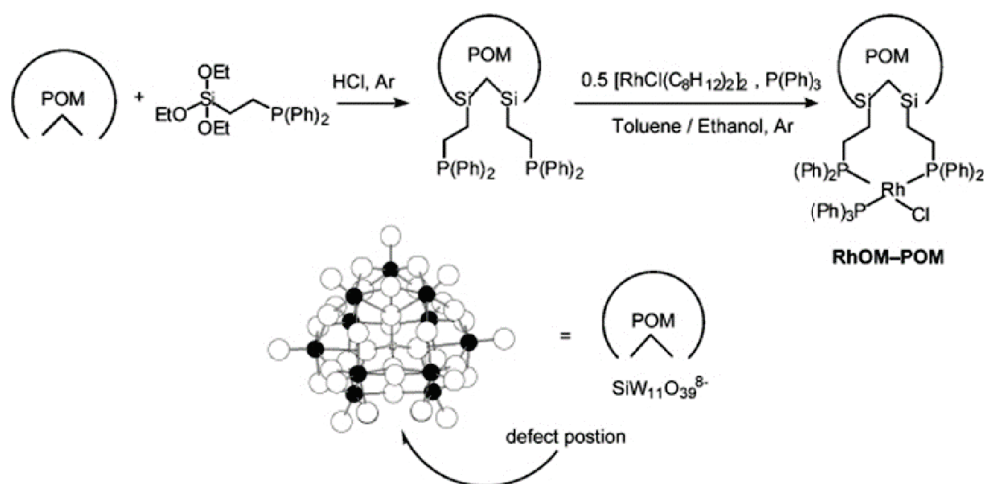
**Figure 2. 20-** Synthetic scheme for the preparation of the rhodium based metalorganic–polyoxometalate hybrid compound, developed by Neumann.

The Rh(I)metal-organic–polyoxometalate hybrid compound $Li_4\{SiW_{11}O_{39}[O(SiCH_2CH_2PPh_2)_2PPh_3Rh(I)Cl]\}$ was a ~ 50% more effective catalyst. Indeed, the catalytic efficiency of the Rh(I)metal-organic-POM catalyst in the monophasic system was compared, by the authors, to that of the classic $(Ph_3P)_3Rh(I)Cl$ Wilkinson's catalyst using 1-octene as substrate (1.0 mmol 1-octene, 4.0 mmol (Rh)OM–POM, 1 mL toluene– EtOH, 2 atm $H_2$). This higher activity was probably due to the presence of the alkyl chains in the phosphine ligands of the POM which could improve the stabilization of the intermediate Rh(III) species after oxidative addition of hydrogen. Catalyst recycle experiments showed that the water-soluble LiRhOM–POM could be recovered by phase separation from the product and reused without loss of activity.

*Cross-coupling reaction and dehalogenation*

The Bonchio group functionalized the Keggin polyanion $[\gamma\text{-}SiW_{10}O_{36}]^{8-}$ with imidazolium-based NHC palladium complexes. There, the interplay of the Pd binding domains with the inorganic scaffold provides multi-turnover catalysis, for the cross-coupling reactions of aryl halides with good performances under MW-assisted protocols. Depending on the reaction conditions, both cross-

coupling and dehalogenation of aromatic compounds were efficiently catalyzed. The proposed mechanism of the palladium-catalyzed dehalogenation involves the oxidative addition of the aryl halide to the $Pd^0$–NHC intermediate, and the formation of a $Pd^{II}$–hydride species[59]
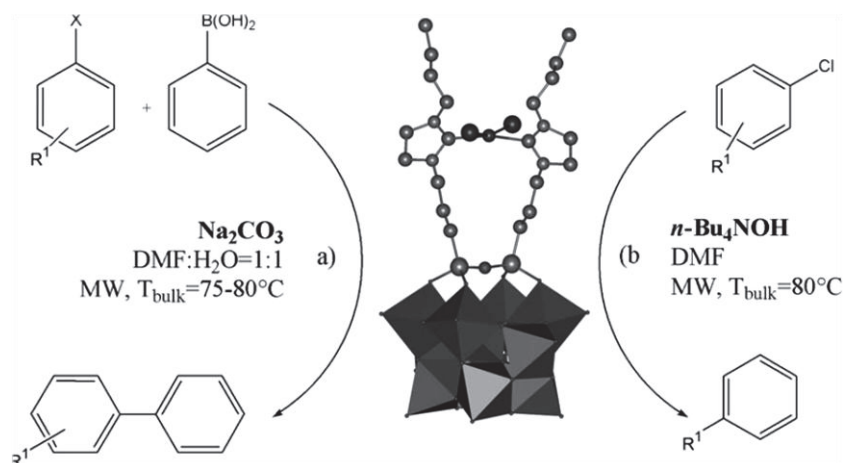


**Figure 2. 21-** Cross-coupling (path a) and dehalogenation reactions (path b) catalyzed by $PdBr_2(C_{10}H_{17}N_2Si)_2O(\gamma\text{-}SiW_{10}O_{36})^{4-}$ under MW irradiation.

*Cationic polymerization of styrene*

The catalytic efficiency of the POMs can be significantly improved also by enhancing the compatibility of the POMs with organic media, providing catalytic interfaces for biphasic reactions, as well as easier preparation, and better recyclability.[60]

Interestingly, the Polarz group functionalized a lacunary Keggin polyoxotungstate $[PW_{11}O_{39}]^{3-}$ with alkyl chains of different length, attached to the head group via siloxy bridges. The POM surfactants self-assemble into liquid crystalline phases or micelles in solution. They have been used efficiently for the emulsification of styrene and, its cationic polymerization, for which they are initiators.[61]
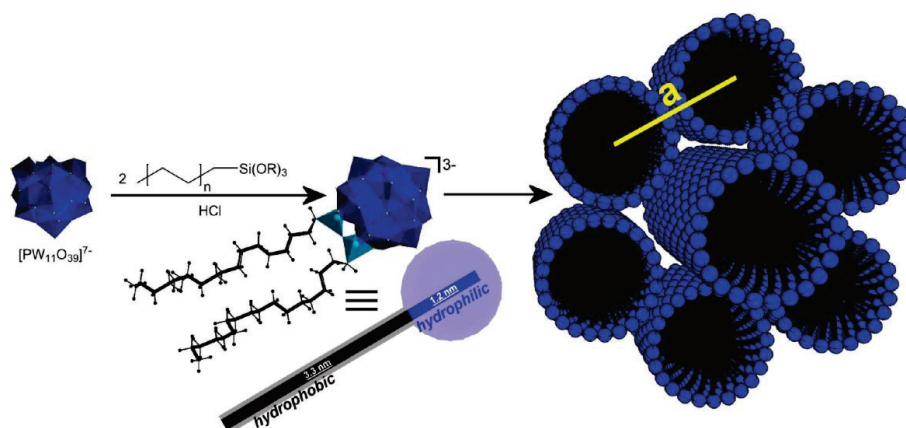
**Figure 2. 22**- Illustration of the synthetic pathway of the POM Surfactants presented by Landsmann et al.

*Acetylation reaction*

New hybrid complexes based on covalent interaction between porphyrins, such as 5,10,15,20-tetrakis(4-aminophenyl) porphyrinatozinc(II) and 5,10,15,20-tetrakis(4-aminophenyl)porphyrinatotin(IV) chloride, and a Lindqvist type polyoxometalate, $Mo_6O_{19}{}^{2-}$, were prepared by Araghi et al. and the catalytic activity of tin(IV)porphyrin−hexamolybdate hybrid material was investigated in the acetylation of primary, secondary and tertiary alcohols and phenols with acetic anhydride. The attachment of electron-withdrawing hexamolybdate substituents to the porphyrin ring decreased the electron density of the porphyrin ring which was therefore reduced more easily.[50]
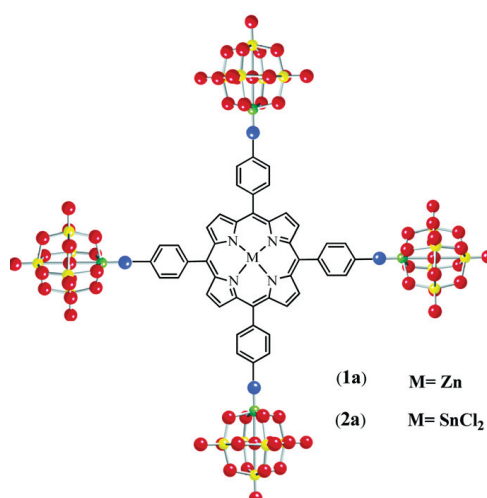


**Figure 2. 23-** Hybrid system based on Lindvist type polyoxomolybdate proposed by Araghi et al. for the efficient acetylation of alcohols.

## 2.5 Hybrid-POMs as asymmetric catalysts

Asymmetric catalysis continues to be a very attractive area which is related to multidisciplinary sciences due to its importance in both fundamental research and industrial applications. The design and construction of new asymmetric catalytic systems with high efficiency has been of great interest in last year. Much effort has been made to prepare chiral POMs and their derivatives. Indeed, because POMs have multiple possible catalytic sites, it is hard to achieve enantio-control in synthetic chemistry using POMs. In addition, the instability and rapid racemization in solution makes most POMs with chiral structures quickly lose the chiral information.[62,63] To overcome these disadvantages, different synthetic strategies have been presented to obtain chiral POM architectures. An important strategy is the functionalization with enantiomerically pure organo moieties.[64–71] Despite the big effort to study the chirality transfer between organic and inorganic moieties, only few asymmetric hybrid systems have been already employed to perform asymmetric catalysis.

*An overview on the catalytic applications of some chiral organo-POMs will be presented below.*

### 2.5.1 *Supramolecular assemblies*

A non covalent strategy was used by Li et al. in 2009 to assembly a chiral multidentate amine to a polyoxometalate, which is $H_3P_2W_{12}O_{40}$. The chiral amines, such as $C_2$-symmetric tetramine with a *trans*-1,2-diaminocyclohexane skeleton, were coordinated *via* electrostatic interaction to the POM surface. The catalytic activity of the amines toward the Diels–Alder reactions of α-substituted acroleins in aqueous solution afforded up to 96% yields, 95:5 *exo*/*endo* ratios, and 83% *ee*. The presence of the POM scaffold stabilizes the catalytic systems, which could be recycled and reused six times with only minimal losses of activity and selectivity.[72]
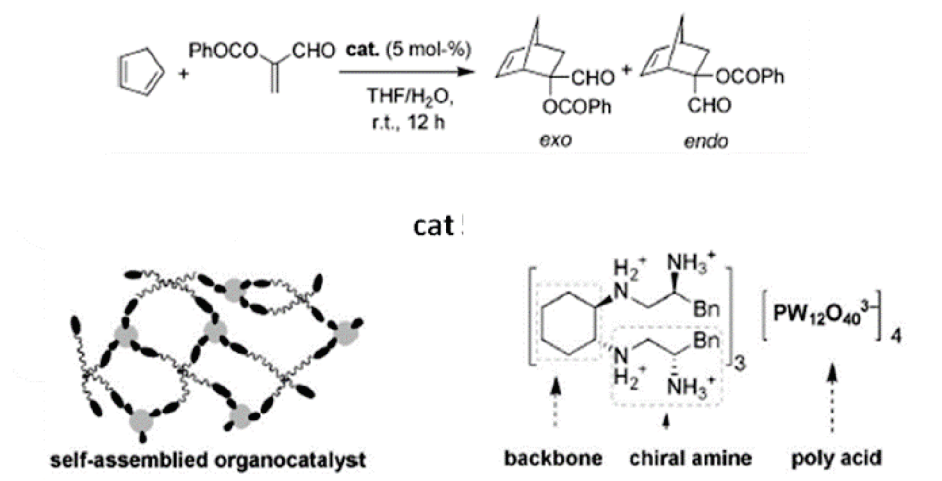
**Figure 2. 24**- Diels-Alder reaction catalyzed by the chiral self-assembled organo-POM catalyst presented by Li et al.

The same approach was used by Luo et al., which combined different achiral protonated polyoxometalate structures with chiral diamines to create an enamine-based catalyst. In that case the authors took profit from the intrinsic high acidity of POMs and the chiral information of chiral diamines to obtain easily recoverable catalysts, efficiently experienced toward asymmetric direct aldol reactions for a broad range of substrates. Up to 92% ee was obtained, using acetone and 2-Cl(Phenyl)aldehyde as substrates.[73]
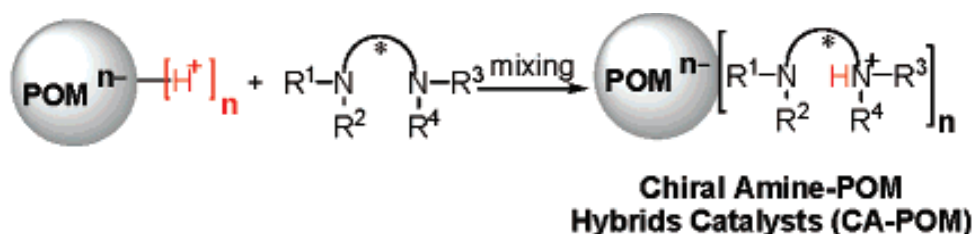


**Figure 2. 25**- Strategy for the POM-chiral diamines assembly

The supramolecular assembly was used also by the Wu group to develop a chiral POM-based system. There, a chiral amphiphilic cation with two stereocenters was employed to encapsulate a catalytically activated sandwich-type polyoxometalate, which is $Na_{12}[WZn_3(H_2O)_2(ZnW_9O_{34})_2]$, through electrostatic interactions. They found that the new chiral organic cation-encapsulated

81

polyoxometalate complexes self-aggregate into spherical supramolecular assemblies with a diameter of ca. 100 nm in the reaction solution, which lead to efficient asymmetric catalytic activities for the oxidation of thioethers, with up to 72% of enantiomeric excess. [74]
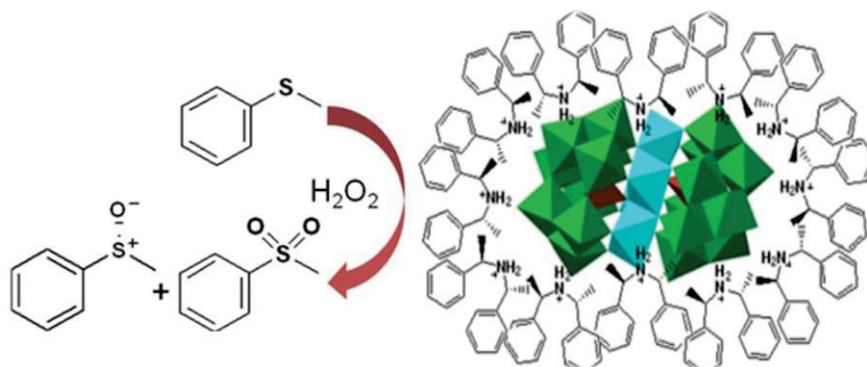


**Figure 2. 26**-Schematic illustration of the microreactir developed by Wang et al. and its asymmetric catalytic oxidation activity for methyl phenyl sulfide with H2O2 (30%).

Few years later the same group employed a similar strategy to encapsulate a catalytically efficient polyoxometalate with chiral surfactants bearing two long alkyl chains with terminal hydroxyl groups. Then, the new micro system was covalently immobilized into a silica matrix via a sol–gel process and, efficiently applied for oxidative kinetic resolution reactions of secondary alcohols, reaching up to 89% ee.[75]

Enantiopure dendritic POM frameworks were obtained by assembling chiral dendritic amines and acidic POM moieties in a collaboration between Bonchio's and Nlate's group. The selective oxidation of thioanisole to the corresponding chiral sulfoxide was tried, but only 14% ee was obtained. Nevertheless a chiral transfer between the organic cation and the inorganic scaffold was demonstrated.[76]

A few years later, Jahier and Nlate developed another chiral DENDRI-POM system based on L-proline derivatives. In particular, the charge of $[PW_{12}O_{40}]^{3-}$ was neutralized by three L-proline-derived tetrapropylammonium dendrons and

the system employed for different oxidation reactions. This DENDRI-POM oxidized methyl phenyl sulfide with low activity and very low *ee* (up to 4%), whereas aromatic alkenes were efficiently oxidized to the corresponding oxirane with up to 37% *ee*.[77]



**Figure 2. 27-** Catalytic oxidation of different substrates by proline-derived DENDRI-POM, using $H_2O_2$, presented by Jahier and Nlate.

A mixed covalently-anchored, electrostatically assembled hybrid system based on POMs was developed by Meng et al. in 2011. In that case the Keggin type $[PX_{12}O_{40}]^{3-}$ anion (X=Mo, W) was functionalized with chiral metallo-salen complexes. In particular the POM is covalently bonded to the $[Mn(salen)(CH_3OH)]$ segment *via* one terminal oxygen atom of its own, and interacts with the other two $[Mn(salen)(CH_3OH)(H_2O)]^+$ fragments through electrostatic forces. The catalytic activity and enantioselectivity of these hybrid compounds were experienced for the asymmetric epoxidation of substituted chromene using NaClO/4-phenyl pyridine N-oxide (PPNO) as oxidant in $CH_2Cl_2$ at 0°C, with a yield of 86% and enantiometic excess of 41%, in the case of Molybdate-POMs and, 83% of yield and 42% of ee for the polyoxotungstate

derivatives. However, these results were not so far from the ones obtained with pure metallo-salen complexes.[78]

A heterogeneous asymmetric catalytic system was presented by Han et al. They used the self-assembly strategy to encapsulate in the same Metallo Organic Framework both a catalytically active POM, ($[BW_{12}O_{40}]^{5-}$), and a chiral group, such as L- or D-pyrrolidin-2-ylimidazole. The coexistence of both the chiral directors and the oxidants within a confined space provided a special environment for the stereoselective formation of reaction intermediates. The catalytic system was efficiently used in the asymmetric dihydroxylation of aryl olefins, leading to up to 95% ee.[79]
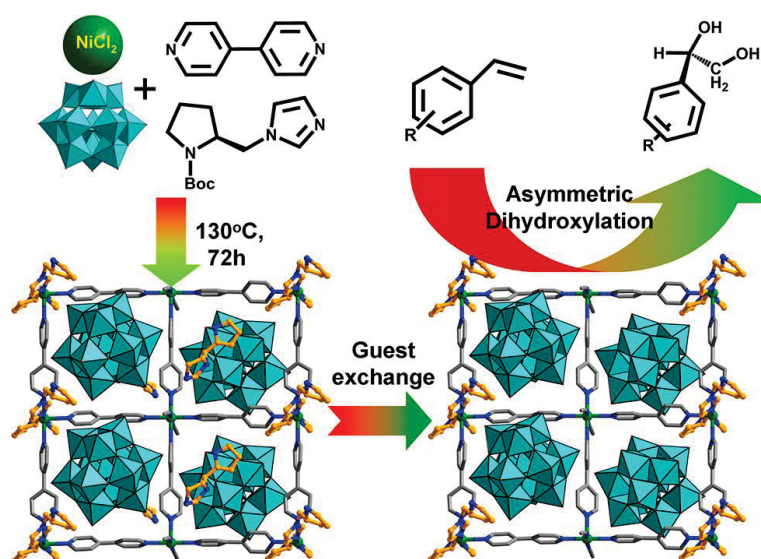


**Figure 2. 28-** Synthetic pathway presented by Han et al. for the development of asymmetric catalytic systems and experienced catalytic activity.

### 2.5.2    *Covalently linked asymmetric hybrid systems*

Up to now, only three examples of covalently linked hybrid POMs employed for asymmetric catalysis have been reported in literature.
The covalent pathway to create asymmetric hybrid systems was chosen by the Bonchio group. As seen in chapter I, they bis-functionalized the lacunary Keggin

POM, $[\gamma\text{-}SiW_{10}O_{36}]^{8-}$ with (R) or (S) 1-aminoethylphosphonic acid, to perform the enantioselective sulfoxidation of methyl p-tolylsulfide. The sulfoxide was recovered in 20% yield, 100% selectivity, and up to 24 % enantiomeric excess. Even if only a poor enantiomeric excess was recorded, the chirality transfer was demonstrated. In this case the chirality was coded in the organic substituent.[29]
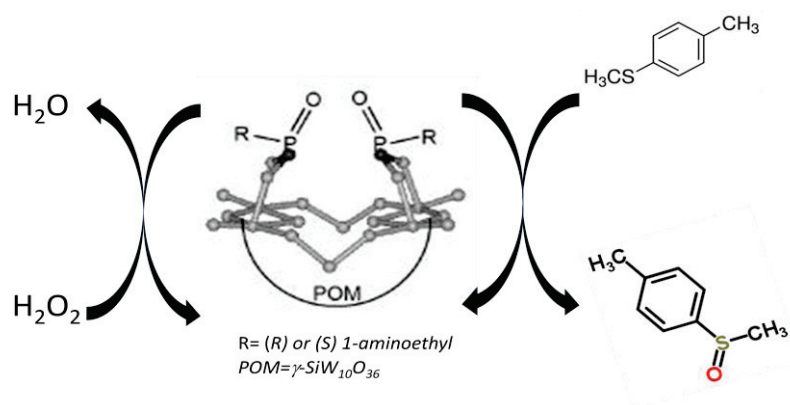


**Figure 2. 29-** Enantioselective oxidation reaction catalyzed by the chiral hybrid POM proposed by Carraro et al.

Thorimbert, Hasenknopf and Lacôte took an opposite approach. In that case a chiral $\alpha_1$-Dawson polyanion $(TBA)_6[\alpha_1\text{-}P_2W_{17}O_{61}\{SnCH_2CH_2C(=O)\}]$ bearing a lateral achiral side chain with a 4-aminopyridine end group was synthesized. The chirality information was present only on the inorganic framework.

This organopolyoxometalate catalyzed the addition of indenyl allyl silanes to cinnamoyl fluorides.
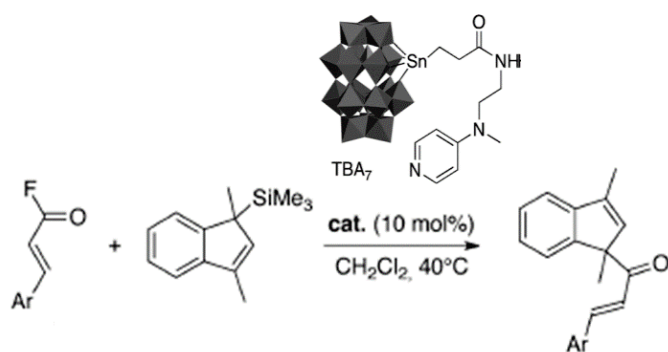


**Figure 2. 30-** Organo-POM catalyzed 1,2-additions of allylindenes to acyl fluorides. The possibility of chirality transfer was demonstrated by the authors.

The polyanionic framework influenced the organo-catalyst activity and selectivity since the reactivity was driven by the interaction of the cationic reactive intermediates with the POM negative surface. A moderate but nonzero chirality transfer from the chiral inorganic framework to the organic substrate was observed. The reaction carried out in the presence of the enantiopure hybrid-POM led to the product in 50% yield and a modest 8% ee determined by HPLC analysis. Even if the observed ee was much too low to qualify the hybrid system as a synthetically useful asymmetric catalyst in this reaction, it nonetheless established the possibility of chirality transfer from a POM to an organic substrate.[38]

More recently Thorimbert and coworkers have continued this approach, where a chiral lacunary Dawson POM, $[\alpha_1\text{-}P_2W_{17}O_{61}]^{10-}$ was functionalized by achiral imidazolidinone ligands. In that case the system was employed to perform efficiently Diels–Alder cyclo-addition reactions.
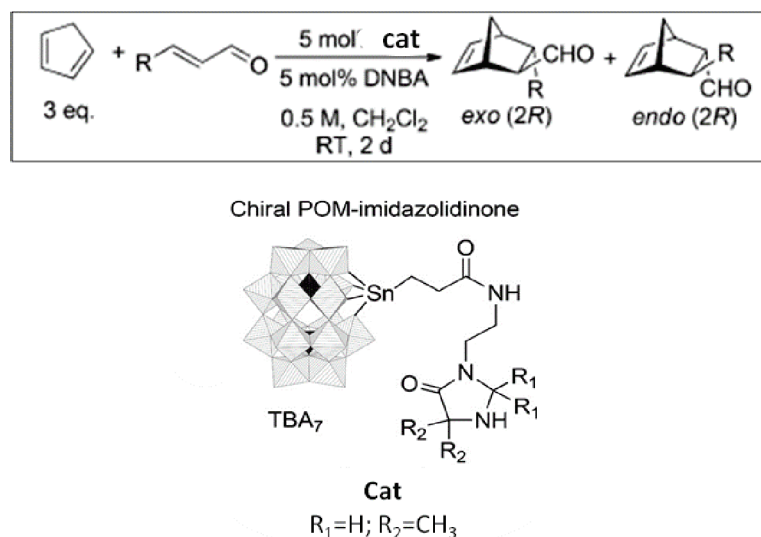


**Figure 2. 31-** Enantioselective Diels-Alder cicloaddition catalyzed by the chiral hybrid POM, $[\alpha_1\text{-}P_2W_{17}O_{61}]^{10-}$, functionalized with achiral imidazolidinone ligands.

The best enantioselective results were obtained when cyclopentadiene and 4-nitrophenylacrylaldehyde were used as partners. The reaction was quantitative and the cycloadduct was obtained with a *exo/endo* ratio 84:16, with

enantioselectivities of 86 and 78%, respectively. This was the first interesting example of synthetically useful chirality transfer from a chiral POM to an achiral substrate.[80]

## 2.6 Theoretical studies on hybrid-POMs

Computational chemistry on polyoxometalates has attracted growing interest in the last decades after the first theoretical study on a very simple POM appeared on 1991 with ab-initio Hartree-Fock (HF) methods to get the electronic structure of a decavanadate.[81] This was followed by the investigation on the basicity of the different oxygen atoms of the decavanadate.[82]

The main issues facing computational studies of POMs are i) their large sizes, ii) the presence of a high number of transition metals and iii) their high negative charge.

The use of Density Functional Theory (DFT) and Molecular Dynamics (MDs) now makes it possible to accurately investigate the properties of more complex systems based on polyoxometalate clusters, in the gas phase as well as in solution. Indeed, through these theoretical tools it is possible to get information about the basicity, NMR chemical shifts, spectroscopic and magnetic properties, etc. All this detailed knowledge helps to investigate the reactivity of the inorganic cluster and consequently understand their catalytic activity, for example in redox or acid-base reactions.[83–85]

However only a few papers investigate computationally the reactivity of organo-POMs and these theoretical tools are mainly exploited to get information about the electronic or optical properties of such hybrid complexes.

One of the first theoretical studies on hybrid POMs was carried out by Rohmer et al. in 1994, where *ab-initio* Hartree-Fock method was used to understand the host-guest interaction in the RCN@$(V_{12}O_{32})^{4-}$, (with R=H, CH$_3$, C$_6$H$_5$). [86,87] They report the maps of electrostatic potential obtained from *ab initio* SCF calculations on the cavitand polyoxometallic cage $V_{12}O_{32}$ and the guest molecules RCN,

finding that the stabilization energies range from-12.8 to-4.4 kcal*mol$^{-1}$ for the three systems considered.
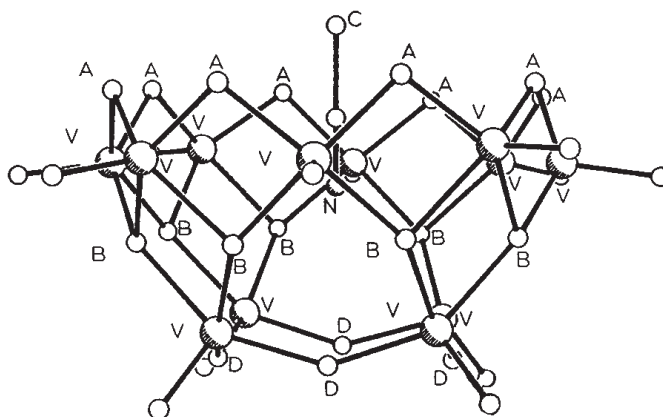


**Figure 2. 32-** Perspective plot of CH$_3$CN@(V$_{12}$O$_{32}$)$^{4-}$ analyzed by Rohmer et al.

Furthermore, the decomposition energy analysis showed that most of the stabilization should be attributed to an electrostatic origin, including direct coulombic interaction, polarization of the guest molecule and counter polarization of the vanadate host. This stabilization energy due to orbital interactions and charge transfer increases with the acceptor potentialities of the R substituent in the order: H < CH$_3$ < C$_6$H$_5$.

Easier and more accurate investigations of the properties of hybrid systems have taken hold with DFT. In general, DFT calculations on hybrid systems have been used to investigate the structural stabilities, or the electronic and optical properties of hybrid systems, the charge transfer between two domains and only more recently to probe catalytic pathways.

*In the next paragraph an overview about how DFT has been applied to hybrid POM systems will be given.*

## A.   DFT on hybrid POMs

*Lindvist hexamolybdates*

A great attention has been given to organo imido derivatives of the Lindvist hexamolybdate $[Mo_6O_{19}]^{2-}$. The first theoretical studies on this system were carried out by Wang, Su and coworkers in 2006. They used Time-Dependent DFT (TDDFT) to get information about the polarizability[88] and the electronic structure of different organo-imido hexamolybdate derivatives.

For the calculations, they used the standard ADF TZP basis set, which is a triple-$\zeta$ plus polarization STO basis set. Triple-$\zeta$ plus polarization basis sets were used to describe the valence electrons of all atoms, whereas for the transition-metal molybdenum atom, a frozen core composed of 1s to 3spd shells was described by single Slater functions. In calculations of the polarizability, second-order polarizability, and excitation properties, the RESPONSE and EXCITATION modules implemented in the ADF program were used on the basis of the optimized geometries.

They found that once anchored in the hexamolybdate structure, the organo-imido ligand possesses remarkably larger static third-order polarizability (-17882.6*10$^{-36}$ esu) compared with that of typical organic compounds. This variation can be traced to the different electronic transition characteristics of the hybrid. Moreover they observed that the diagonally-substituted derivatives have larger *polarizability* values than orthogonally-substituted derivatives and consequently a better charge transfer occurs in the orthogonally-substituted derivatives.[89,90]

Diagonally substituted organo-imido POM → R₃=O, R₁=R₂
Orthogally-substituted organo-imido POM → R₂=O, R₁=R₃
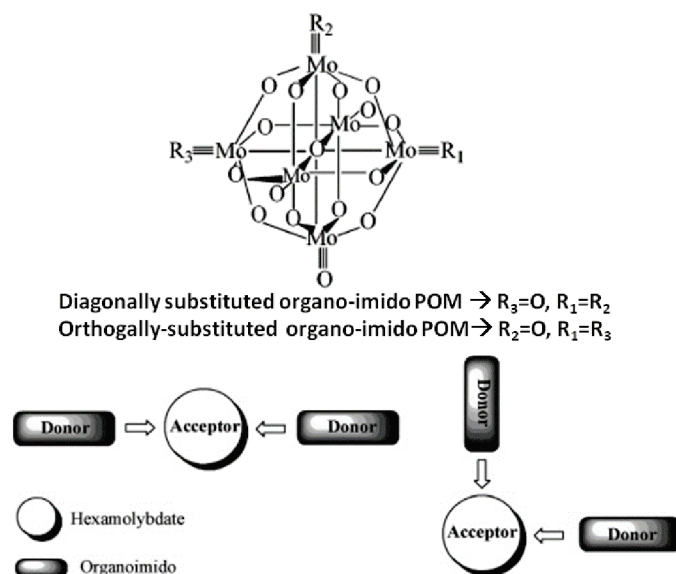
**Figure 2. 33**- Organo-imido hexamolybdate derivatives studied by Yang et al., in the diagonally- and orthogonally- substituted form.

Finally, the second-order nonlinear optical NLO response[91] of these organic–inorganic hybrid materials could be enhanced not only by including strong donor groups (-NH₂) but also by introducing a second phenyl group through N=N and C=C bonds.[92]

Time-dependent density functional theory studies have been also exploited by Zhang and coworkers to investigated the electron transfer occurring in organo-imido hexamolybdate containing a pyrene moiety on the imido ligand.

The results revealed that the strong electronic absorption at the visible region mainly comes from the optically allowed $\pi-\pi^*$ transitions of the pyreneimido component (S0 to S2 transition). The electron transfer process from the excited pyrene-imido moiety to the inorganic POM cluster is at the time scale of ~700 fs, and it could be ascribed to the internal conversion of singlet excited states from S2 state to S1 state.[45]
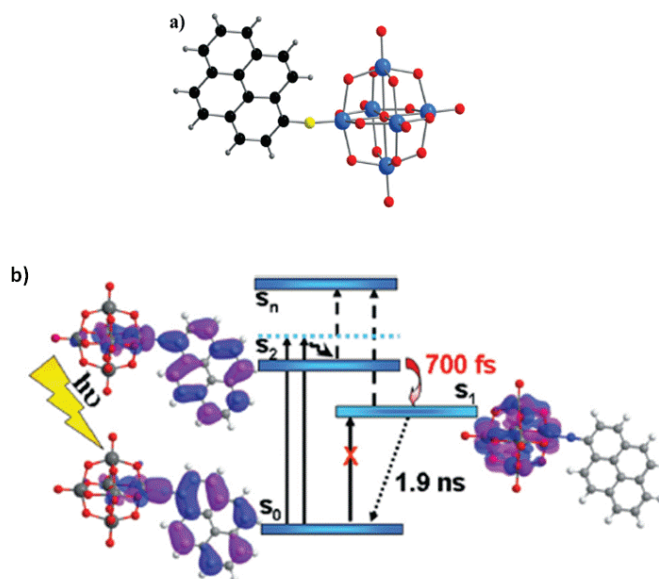
**Figure 2. 34-** a) Representation of the hybrid pyrene-imido POM studied and b) schematic representation of the charge transfer process

A series of hexamolibdate-based organic–inorganic hybrids containing double Donor–Acceptor–π–Acceptor (D-A1-π-A2) chains were designed by Su group's, with the aim to get new materials for dye sensitizer solar cells (DSSC).

The A1 spacers included thiophene, 1,2,3-triazole, 1,3,4-oxadlazole, and thienothiadiazole units or combinations of the same. The hexamolybdate cluster acted as an A2 spacer.
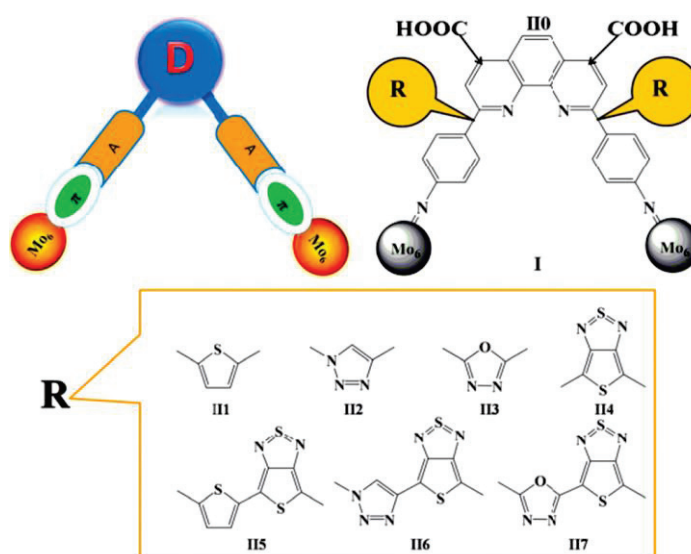


**Figure 2. 35-** Molecular structure of studied systems by Su group's.

In that case the electronic structures, absorption spectra, and electronic transition characteristics of the systems were studied using density functional theory (DFT) and time-dependent DFT (TDDFT) to understand how to improve the light absorption ability of the dyes. Indeed, the effective way to enhance the efficiency of $\pi$-type DSSCs is by improving light harvesting efficiency (LHE), hole injecting efficiency (HJE), dye regeneration efficiency (DRE) and reducing charge recombination efficiency (CRE). For TDDFT calculations, based on the optimized ground-state geometries, the range-separated hybrid functional CAM-B3LYP was employed and the LanL2DZ basis set was used for the transition metal Mo, whereas the nonmetal elements were described by the 6-31G(d) basis set in n,n-dimethylformamide.

They found that the HOMO levels of all designed systems were below the Valence Band of NiO and the LUMO levels were higher than the $I_2/I_3^-$ redox level, which benefits hole injection and dye regeneration. Introduction of the thienothiadiazole unit was found to be an effective way to improve the light absorption ability of the dyes. Indeed the absorption spectrum of the thiophene system (II5 in the Figure 2.35) shows a good overlap with sunlight, which contains near ultraviolet, visible and the near infrared wavelenghts.[93]

*Keggin-type hybrids*

Going to the Keggin cluster, recently Mirzaei et al. developed new hybrid systems based on the $H_4SiW_{12}O_{40}$ structure, hybridizing it with trinuclear lanthanide cluster of type $\{Na(H_2O)_3[Ln(HCAM)(H_2O)_3]_3\}^{4+}$, with Ln=Ce, La, Eu and $H_3$CAM=2,6-dicarboxy-4-hydroxypyridine. Spectroscopic studies about their luminescence properties were carried out revealing the role of strong anion–$\pi$ and hydrogen bonding interactions between the POM, which is a tetra-anion, and the aromatic pyridine ring. The DFT analysis was concentrated on the anion–$\pi$ interaction observed in the crystal packing of the hybrid inorganic–organic POM. The energies of the complexes studied were computed at the BP86-D3/def2-TZVP level of theory using the crystallographic coordinates, while for the W and La atoms the def2-SVP basis set was used.

The results confirmed that the effect of the coordination of the ligand to the metal centre is crucial for increasing the π-acidity of the aromatic ring, and consequently it increases its ability to establish anion–π interactions. Indeed, the interaction is not favorable in the absence of the La metal centre coordinated to the organic ligand ($\Delta E_1$ =+11.9 kcal*mol−1), while when the ligand is coordinated to the La centre the interaction energy is large and negative ($\Delta E_2$ =−41.6 kcal*mol−1), indicating a very favorable anion–π interaction.[94]
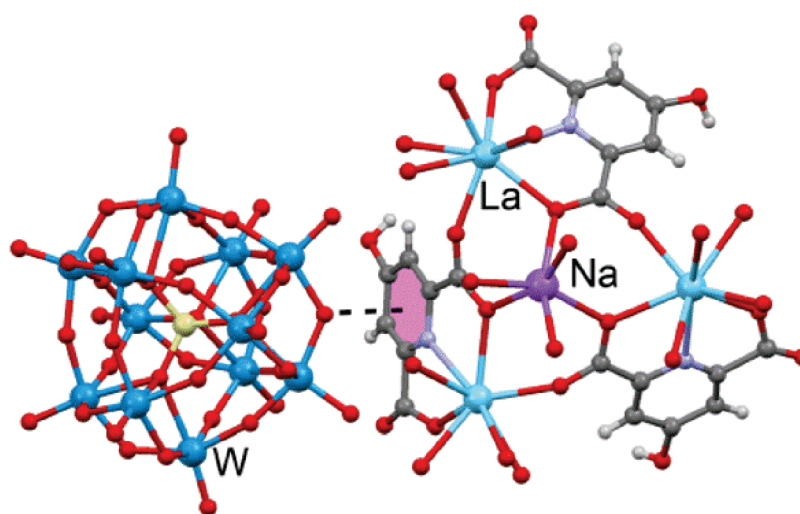


**Figure 2. 36-** Hybrid–POM structure developed by Mirzaei et al., revealing the anion–π interaction occurring in the hybrid system.

A similar idea was applied to the Keggin type POM, α-[MSiW$_{11}$O$_{39}$]$^{3-}$ (M =Nb$^V$or V$^V$), hybridized through coordination interaction with porphyrin rings. In that case the second-order non-linear optical properties (NLO) were investigated through time-dependent DFT. The NLO coefficients of all complexes were calculated with the ADF-RESPONSE module based on the optimized geometries, and to further interpretate the charge transfer between organic group and POM, the natural bond orbital (NBO) calculation at the B3LYP level was performed using the GAUSSIAN 09 (LanL2DZ basis set for W and V, Nb, Zn atoms and 6–31g(d) basis set for all non-metal elements).

The calculations showed that the complex exhibits remarkable molecular second-order NLO polarizability, especially for the Zn-substituted porphyrin coordinated to the Vanadium substituted Keggin cluster ($\gamma$=261.410 a.u). The general effects on NLO response changing the metal atom (M =Nb$^V$ or V$^V$), the metallo-porphyrin moiety and the π-conjugation in the hybrid system, were analyzed. The authors found that the substituted metal atom (M) with a large electronegativity, the metallo porphyrin, and the lengthening of π-conjugation are helpful in enhancing the optical non-linearity of these systems.[95]

Hill's group, similarly, electrostatically hybridized two and Keggin-type polyoxometalates, such as $[PW_{11}O_{39}]^{7-}$ and $[PW_{12}O_{40}]^{3-}$ with tris(bipyridine)ruthenium(II), $[Ru(bpy)_3]^{2+}$ as photosensitizer. In that case DFT studies helped them to investigate the frontier orbital occupancy and charge transfer process between the two moieties, finding that it can be achieved by photoexcitation of $[Ru(bpy)_3]^{2+}$ from its S0 (ground state) to S1 (the first excited state).[96]
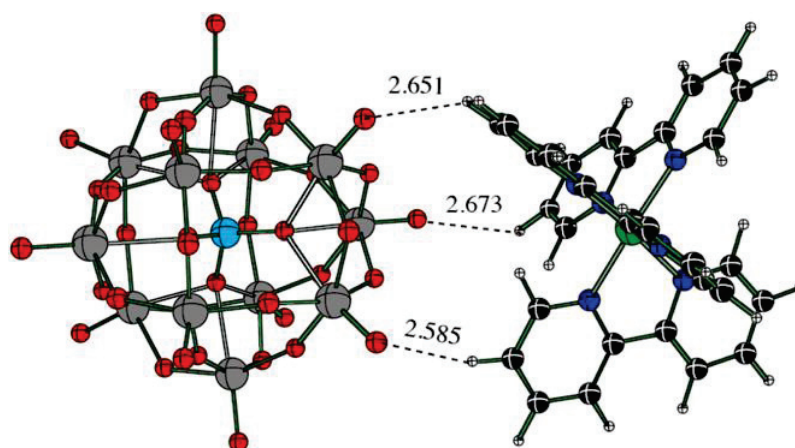


**Figure 2. 37-** Optimized structure and hydrogen bond distances (in Å) of the $\{[Ru(bpy)_3]^{2+}-- [PW_{12}O_{40}]^{3-}\}$ complex developed by Hill's group.

Non covalent interactions was exploited also by Liao et al. in 2016, when a Keggin-type polyoxometalate, $(H_2PW_{12}O_{40})$, was doped with naphthalenediimide (NDI) derivatives, known to be efficient electron-transfer

mediators due to their photoinduced or electrically induced electron transfer from their neutral organic moieties to anion radicals. The aim of this job was to create an efficient photosensitive POM-based hybrid material and the computational studies allow them to understand the charge-transfer pathway in the hybrid system. Indeed, experimentally the photochromism was found to be easily reversible in response to visible light, ultraviolet light or X-ray irradiation, indicative of an efficient charge-transfer pathway. DFT studies on the electronic band structure of compounds were performed using the Vienna *ab intio* simulation package (VASP) program. The electronic band structure revealed that POMs served as electron donors to generate unique anion-π interactions with π-electron-deficient NDIs through electronic effects. Then the non covalent interactions, such as the anion-π interactions, π-π contacts, and hydrogen bonds, offer the effective pathways for the charge-transfer interactions in the photochromic process: the POMs act as electron acceptors to form a reservoir of electrons. Furthermore the complicated charge-transfer processes explain the long lifetime of the two charge-separated states in this photosensitive polyoxometalate-based charge transfer hybrid material.[97]
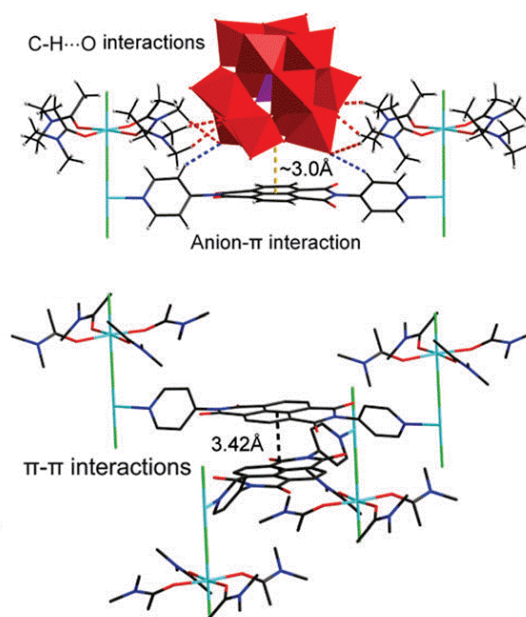


**Figure 2. 38-** Scheme revealing the main interactions between the POM and the NDI ligands, responsible of the charge transfer process.

Albelo et al. in 2010 used DFT methods to study the best way to create zeolitic Metal Organic Frameworks (MOFs) based on imidazole (im)[98] or benzenedicarboxylate (BDC)[99] or benezenetricarboxylate[100] as ligand and ε-type Keggin PolyOxoMetalates (POMs) as building units (such as ε-Keggin isomer anions, stabilized by four capping Zn(II) ions).

The general code TOBUNPOROUS[101] was used to automatically replace the Si tetrahedral centres of the parent $SiO_2$ zeolite structure by an ε-Zn Keggin anion with the appropriate orientation of the Zn metal centres. Each oxygen atom of the zeolite was then replaced by a suitably orientated imidazolate ligand lattice. Finally energy minimizations were carried out using the UFF (molecular mechanics) force-field.[102]

Using energy minimization methods they saw that the lattice energies follow a linear relationship with the topological density similar to that found in other zeolitic systems, such as ZIFs[103] and BDC Z-POMOFs[99], previously investigated by the same group. Typically, the very dense ZNI topology (showed in the Fig. 2.39) was found as the most stable one and the simulation results suggest that the imidazole ligand favors the stability of hypothetical Z-POMOFs containing sodalite cages.[98]
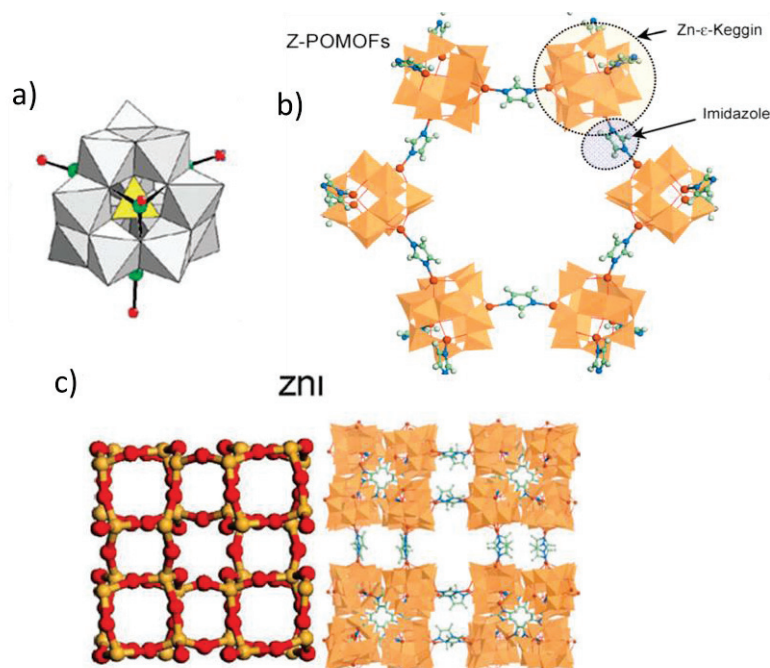


**Figure 2. 39-** a) Zn(II) capped ε-Keggin structure; b) hypothetical imidazolate Z-POMOF based on the ε-Keggin cluster and c) most stable simulated crystal structure of imidazole Z-POMOFs.

With the aim to develop new molecular optical switches, a covalently linked hybrid system benzo spiropyran-Keggin POM ($K_{Sn}$[BSPR]) was very recently synthesized and studied by Parrot et al. In that case DFT helped them to understand the role of the POM in the enhanced fluorescence of $K_{Sn}$[BSPR] compared to the reference BSPR compounds. Single points were processed on the optimized structured using the larger Def2-TZVP basis set and electronic transitions were computed in the time-dependent variant of DFT (TD-DFT) within the adiabatic approximation taking into account the 250 lowest-lying excited states.

From simulation supported by 2D $^1$H/$^1$H NOESY NMR experimental evidences, they saw that the two compounds adopt a similar conformation in which the nitroaryl moiety is folded and engages in C-H/$\pi$ interactions with the tolyl/aryltin unit. They concluded that the higher fluorescence of the closed form with respect to the reference BSPR compounds is probably due to the folding of the BSPR towards the POM, that allows a more easily accessible emitting state.[104]
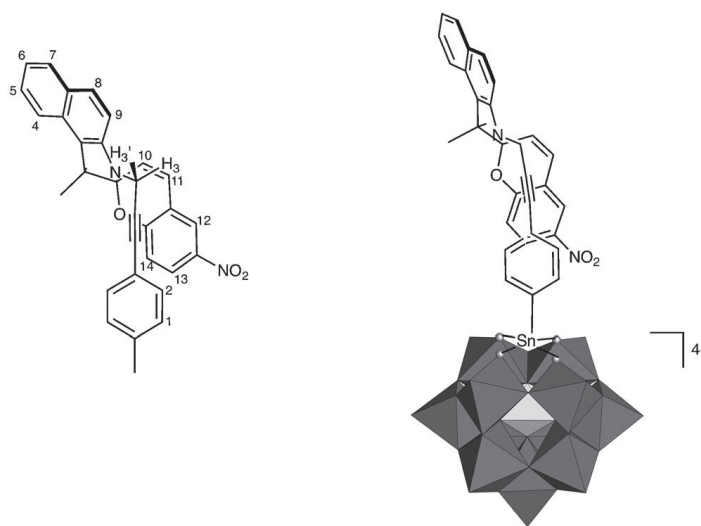


**Figure 2. 40-** Representation of energy-optimized structures of BSPR and $K_{Sn}$[BSPR] studied by Parrot et al.

Another interesting example about the use of DFT to understand the properties of hybrid-POM materials is given by the collaboration between the Neumann and Poblet groups. They investigated through DFT and TDDFT the

photoreduction mechanism of carbon dioxide to carbon monoxide catalyzed by the Re-organic hybrid POM $\{NaH[PW_{12}O_{40}]_3-ReIL(CO)_3DMA\}^{n-}$ (L =15-crown-5 phenanthroline, DMA =N,N-dimethylacetamide) following the energy potential profile of the reaction.
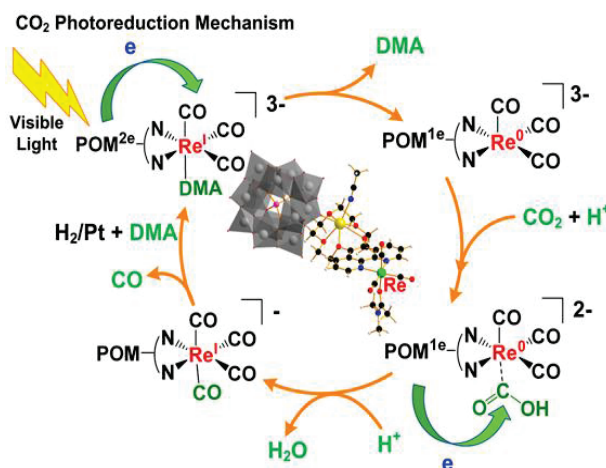


**Figure 2. 41**- Photoreduction mechanism of $CO_2$, (Re)organo-POM catalyzed.

Vibrational frequency calculations were performed for every optimized intermediate to verify that an energy minimum was attained. The excited state properties were obtained by means of TDDFT calculations.[105] The M06,[106] M062X,[106] X3LYP,[107] and CAM-B3LYP[108] functional were also used to simulate the visible spectrum. The visible spectrum and the electron density difference maps (EDDMs) were obtained with GaussSum 3.0.[109]

The reaction mechanism can be divided into several steps, including (i) photoexcitation and charge transfer, (ii) DMA release, (iii) $CO_2$ addition, (iv) protonation, and (v) CO release and regeneration of the catalyst. The charge transfer states, POM to Re complex, are efficiently induced by metal-centered excitations occurring on the reduced POM. Once one electron is transferred to the organometallic unit from the excited POM, the Re is able to bind and activate the $CO_2$ substrate.[110]
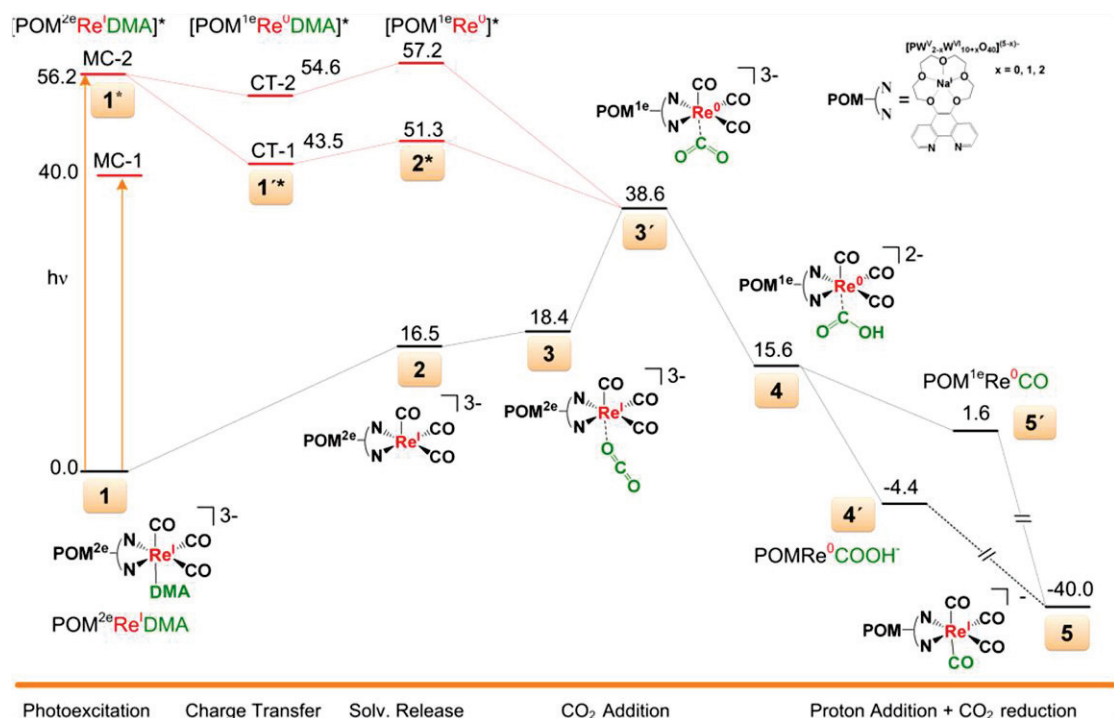
**Figure 2. 42-** Potential energy surface for the reduction of $CO_2$ to CO catalyzed by the hybrid rhenium-POM-hybrid compound.

Creating the potential energy pathway, optimizing all the intermediate structures, it is possible to observe that the reaction cannot take place in the ground state at room temperature, since the process has to overcome a barrier of at least 38 kcal*mol$^{-1}$. However, under photocatalytic conditions, once an electron is transferred from the POM to the Re center, the reaction is exergonic and it can take place.

## 2.7      Conclusions

*In this chapter we gave an outlook on the catalytic activity of different hybrid polyoxometalates. Hybrid-POM systems have been employed mainly toward oxidation reactions, but their interesting properties have been exploited also in other catalytic reactions, such as C-C cross coupling, cationic polymerizations, hydrogenations etc. In addition we also presented a brief overview of the use of theoretical methods (mainly DFT) to investigate some electronic properties of these hybrid systems, allowing a better understanding their reactivity.*

*In light of this, my thesis will be focused on the development of catalytic systems based on hybrid-POMs, extending the series of catalytic applications of these interesting complexes. (Chapter III)*

*Furthermore, considering the growing demand of efficient and enantioselective catalytic systems, Chapter IV is devoted to the presentation of the studies of intramolecular interactions between POM and polypeptide chains. This made possible to derive more general concept about the conformation of organo-POMs in solution and thus help the design of efficient chiral pockets around the catalytic site.*

## 2.8 Bibliography

[1] S.-S. Wang, G.-Y. Yang, *Chem. Rev.* **2015**, *115*, 4893–4962.

[2] D.-L. Long, R. Tsunashima, L. Cronin, *Angew. Chem. Int. Ed.* **2010**, *49*, 1736–1758.

[3] T. Minato, K. Suzuki, K. Kamata, N. Mizuno, *Chem. – Eur. J.* **2014**, *20*, 5946–5952.

[4] K. Sugahara, T. Kimura, K. Kamata, K. Yamaguchi, N. Mizuno, *Chem. Commun.* **2012**, *48*, 8422–8424.

[5] D.-L. Long, R. Tsunashima, L. Cronin, *Angew. Chem. Int. Ed.* **2010**, *49*, 1736–1758.

[6] Y. Ren, M. Wang, X. Chen, B. Yue, H. He, *Materials* **2015**, *8*, 1545–1567.

[7] Y.-F. Song, R. Tsunashima, *Chem. Soc. Rev.* **2012**, *41*, 7384.

[8] N. Mizuno, K. Yamaguchi, K. Kamata, *Catal. Surv. Asia* **2011**, *15*, 68–79.

[9] S. Favette, B. Hasenknopf, J. Vaissermann, P. Gouzerh, C. Roux, *Chem. Commun.* **2003**, 2664.

[10] S. Nlate, C. Jahier, *Eur. J. Inorg. Chem.* **2013**, *2013*, 1606–1619.

[11] C. Jahier, S. S. Mal, U. Kortz, S. Nlate, *Eur. J. Inorg. Chem.* **2010**, *2010*, 1559–1566.

[12] H. Yang, B. Jiang, Y. Sun, L. Zhang, Z. Sun, J. Wang, X. Tantai, *Chem. Eng. J.* **2017**, *317*, 32–41.

[13] H. Weiner, Y. Hayashi, R. G. Finke, *Inorg. Chem.* **1999**, *38*, 2579–2591.

[14] J. Ettedgui, R. Neumann, *J. Am. Chem. Soc.* **2009**, *131*, 4–5.

[15] A. Sartorel, M. Carraro, G. Scorrano, R. D. Zorzi, S. Geremia, N. D. McDaniel, S. Bernhard, M. Bonchio, *J. Am. Chem. Soc.* **2008**, *130*, 5006–5007.

[16] F. M. Toma, A. Sartorel, M. Iurlo, M. Carraro, P. Parisse, C. Maccato, S. Rapino, B. R. Gonzalez, H. Amenitsch, T. Da Ros, et al., *Nat. Chem.* **2010**, *2*, 826–831.

[17] S. Meninno, A. Parrella, G. Brancatelli, S. Geremia, C. Gaeta, C. Talotta, P. Neri, A. Lattanzi, *Org. Lett.* **2015**, *17*, 5100–5103.

[18] X.-M. Zhou, W. Chen, Y.-F. Song, *Eur. J. Inorg. Chem.* **2014**, *2014*, 812–817.

[19] K. Kastner, A. J. Kibler, E. Karjalainen, J. A. Fernandes, V. Sans, G. N. Newton, *J Mater Chem A* **2017**, DOI 10.1039/C7TA00408G.

[20] V. Mirkhani, M. Moghadam, S. Tangestaninejad, I. Mohammadpoor-Baltork, N. Rasouli, *Inorg. Chem. Commun.* **2007**, *10*, 1537–1540.

[21] V. Mirkhani, M. Moghadam, S. Tangestaninejad, I. Mohammadpoor-Baltork, E. Shams, N. Rasouli, *Appl. Catal. Gen.* **2008**, *334*, 106–111.

[22] V. Mirkhani, M. Moghadam, S. Tangestaninejad, I. Mohammadpoor-Baltork, N. Rasouli, *Catal. Commun.* **2008**, *9*, 219–223.

[23] V. Mirkhani, M. Moghadam, S. Tangestaninejad, I. Mohammadpoor-Baltork, N. Rasouli, *Catal. Commun.* **2008**, *9*, 2171–2174.

[24] C. Venturello, E. Alneri, M. Ricci, *J. Org. Chem.* **1983**, *48*, 3831–3833.

[25] C. Venturello, R. D'Aloisio, J. C. J. Bart, M. Ricci, *J. Mol. Catal.* **1985**, *32*, 107–110.

[26] A. M. Khenkin, A. Rosenberger, R. Neumann, *J. Catal.* **1999**, *182*, 82–91.

[27] H.-Y. Lan, X.-T. Zhou, H.-B. Ji, *Tetrahedron* **2013**, *69*, 4241–4246.

[28] S.-L. Zhu, X. Xu, S. Ou, M. Zhao, W.-L. He, C.-D. Wu, *Inorg. Chem.* **2016**, *55*, 7295–7300.

[29] M. Carraro, L. Sandei, A. Sartorel, G. Scorrano, M. Bonchio, *Org. Lett.* **2006**, *8*, 3671–3674.

[30] S. Berardi, M. Bonchio, M. Carraro, V. Conte, A. Sartorel, G. Scorrano, *J. Org. Chem.* **2007**, *72*, 8954–8957.

[31] J. Li, I. Huth, L.-M. Chamoreau, B. Hasenknopf, E. Lacôte, S. Thorimbert, M. Malacria, *Angew. Chem. Int. Ed.* **2009**, *48*, 2035–2038.

[32] J. Oble, B. Riflade, A. Noël, M. Malacria, S. Thorimbert, B. Hasenknopf, E. Lacôte, *Org. Lett.* **2011**, *13*, 5990–5993.

[33] J. J. Walsh, A. M. Bond, R. J. Forster, T. E. Keyes, *Coord. Chem. Rev.* **2016**, *306*, 217–234.

[34] D. Schaming, C. Costa-Coquelard, S. Sorgues, L. Ruhlmann, I. Lampre, *Appl. Catal. Gen.* **2010**, *373*, 160–167.

[35] Y. V. Geletii, B. Botar, P. Kögerler, D. A. Hillesheim, D. G. Musaev, C. L. Hill, *Angew. Chem. Int. Ed.* **2008**, *47*, 3896–3899.

[36] M. Natali, M. Orlandi, S. Berardi, S. Campagna, M. Bonchio, A. Sartorel, F. Scandola, *Inorg. Chem.* **2012**, *51*, 7324–7331.

[37] M. Natali, E. Deponti, D. Vilona, A. Sartorel, M. Bonchio, F. Scandola, *Eur. J. Inorg. Chem.* **2015**, *2015*, 3467–3477.

[38] C. Brazel, N. Dupré, M. Malacria, B. Hasenknopf, E. Lacôte, S. Thorimbert, *Chem. – Eur. J.* **2014**, *20*, 16074–16077.

[39] N. Dupré, C. Brazel, L. Fensterbank, M. Malacria, S. Thorimbert, B. Hasenknopf, E. Lacôte, *Chem. – Eur. J.* **2012**, *18*, 12962–12965.

[40] J. Lesage de La Haye, J.-M. Guigner, E. Marceau, L. Ruhlmann, B. Hasenknopf, E. Lacôte, J. Rieger, *Chem.- Eur. J.* **2015**, *21*, 2948–2953.

[41] D. Lachkar, E. Lacôte, *Comptes Rendus Chim.* **2016**, *19*, 113–116.

[42] W.-H. Chen, Z.-B. Hu, Z.-S. Zhang, Z.-H. Qiu, J.-H. Zhao, Y.-Z. Lai, J.-X. Mi, *J. Clust. Sci.* **2016**, DOI 10.1007/s10876-016-1108-6.

[43] K. J. Elliott, A. Harriman, L. L. Pleux, Y. Pellegrin, E. Blart, C. R. Mayer, F. Odobel, *Phys. Chem. Chem. Phys.* **2009**, *11*, 8767–8773.

[44] B. Matt, C. Coudret, C. Viala, D. Jouvenot, F. Loiseau, G. Izzet, A. Proust, *Inorg. Chem.* **2011**, *50*, 7761–7768.

[45] J. Gao, X. Liu, Y. Liu, L. Yu, Y. Feng, H. Chen, Y. Li, G. Rakesh, C. H. A. Huan, T. C. Sum, et al., *Dalton Trans.* **2012**, *41*, 12185–12191.

[46] J. L. Stark, V. G. Young, E. A. Maatta, *Angew. Chem. Int. Ed. Engl.* **1995**, *34*, 2547–2548.

[47] J. Kang, J. A. Nelson, M. Lu, B. Xie, Z. Peng, D. R. Powell, *Inorg. Chem.* **2004**, *43*, 6408–6413.

[48] B. Matt, J. Moussa, L.-M. Chamoreau, C. Afonso, A. Proust, H. Amouri, G. Izzet, *Organometallics* **2012**, *31*, 35–38.

[49] B. Matt, C. Coudret, C. Viala, D. Jouvenot, F. Loiseau, G. Izzet, A. Proust, *Inorg. Chem.* **2011**, *50*, 7761–7768.

[50] M. Araghi, V. Mirkhani, M. Moghadam, S. Tangestaninejad, I. Mohammdpoor-Baltork, *Dalton Trans.* **2012**, *41*, 11745–11752.

[51] M. Araghi, V. Mirkhani, M. Moghadam, S. Tangestaninejad, I. Mohammdpoor-Baltork, *Dalton Trans.* **2012**, *41*, 3087–3094.

[52] C. Allain, D. Schaming, N. Karakostas, M. Erard, J.-P. Gisselbrecht, S. Sorgues, I. Lampre, L. Ruhlmann, B. Hasenknopf, *Dalton Trans.* **2013**, *42*, 2745–2754.

[53] J. M. Cameron, S. Fujimoto, K. Kastner, R.-J. Wei, D. Robinson, V. Sans, G. N. Newton, H. H. Oshio, *Chem.- Eur. J.* **2017**, *23*, 47–50.

[54] C. Zhang, X. Lin, Z. Zhang, L.-S. Long, C. Wang, W. Lin, *Chem Commun* **2014**, *50*, 11591–11594.

[55] M. Bonchio, M. Carraro, G. Scorrano, A. Bagno, *Adv. Synth. Catal.* **2004**, *346*, 648–654.

[56] M. Rostami, A. Khosropour, V. Mirkhani, M. Moghadam, S. Tangestaninejad, I. Mohammadpoor-Baltork, *Appl. Catal. Gen.* **2011**, *397*, 27–34.

[57] B. Riflade, D. Lachkar, J. Oble, J. Li, S. Thorimbert, B. Hasenknopf, E. Lacôte, *Org. Lett.* **2014**, *16*, 3860–3863.

[58] I. Bar-Nahum, R. Neumann, *Chem. Commun.* **2003**, 2690–2691.

[59] S. Berardi, M. Carraro, M. Iglesias, A. Sartorel, G. Scorrano, M. Albrecht, M. Bonchio, *Chem. – Eur. J.* **2010**, *16*, 10662–10666.

[60] B. Zhang, P. Yin, F. Haso, L. Hu, T. Liu, *J. Clust. Sci.* **2014**, *25*, 695–710.

[61] S. Landsmann, C. Lizandara-Pueyo, S. Polarz, *J. Am. Chem. Soc.* **2010**, *132*, 5315–5321.

[62] X. Fang, T. M. Anderson, C. L. Hill, *Angew. Chem. Int. Ed.* **2005**, *44*, 3540–3544.

[63] N. Belai, M. T. Pope, *Chem. Commun.* **2005**, 5760–5762.

[64] K. Micoine, B. Hasenknopf, S. Thorimbert, E. Lacôte, M. Malacria, *Angew. Chem. Int. Ed.* **2009**, *48*, 3466–3468.

[65] B. Hasenknopf, K. Micoine, E. Lacôte, S. Thorimbert, M. Malacria, R. Thouvenot, *Eur. J. Inorg. Chem.* **2008**, *2008*, 5001–5013.

[66] M. Carraro, A. Sartorel, G. Scorrano, C. Maccato, M. H. Dickman, U. Kortz, M. Bonchio, *Angew. Chem. Int. Ed.* **2008**, *47*, 7275–7279.

[67] U. Kortz, M. G. Savelieff, F. Y. A. Ghali, L. M. Khalil, S. A. Maalouf, D. I. Sinno, *Angew. Chem. Int. Ed.* **2002**, *41*, 4070–4073.

[68] H.-Y. An, E.-B. Wang, D.-R. Xiao, Y.-G. Li, Z.-M. Su, L. Xu, *Angew. Chem. Int. Ed.* **2006**, *45*, 904–908.

[69] L. Shi, B. Li, L. Wu, *Chem Commun* **2015**, *51*, 172–175.

[70] M. Inoue, T. Yamase, *Bull. Chem. Soc. Jpn.* **1996**, *69*, 2863–2868.

[71] F. Xin, M. T. Pope, *J. Am. Chem. Soc.* **1996**, *118*, 7731–7736.

[72] J. Li, X. Li, P. Zhou, L. Zhang, S. Luo, J.-P. Cheng, *Eur. J. Org. Chem.* **2009**, *2009*, 4486–4493.

[73] S. Luo, J. Li, H. Xu, L. Zhang, J.-P. Cheng, *Org. Lett.* **2007**, *9*, 3675–3678.

[74] Y. Wang, H. Li, W. Qi, Y. Yang, Y. Yan, B. Li, L. Wu, *J. Mater. Chem.* **2012**, *22*, 9181.

[75] L. Shi, Y. Wang, B. Li, L. Wu, *Dalton Trans.* **2014**, *43*, 9177.

[76] C. Jahier, M. Cantuel, N. D. McClenaghan, T. Buffeteau, D. Cavagnat, F. Agbossou, M. Carraro, M. Bonchio, S. Nlate, *Chem. – Eur. J.* **2009**, *15*, 8703–8708.

[77] C. Jahier, S. Nlate, *Eur. J. Inorg. Chem.* **2012**, *2012*, 833–840.

[78] X. Meng, C. Qin, X.-L. Wang, Z.-M. Su, B. Li, Q.-H. Yang, *Dalton Trans.* **2011**, *40*, 9964.

[79] Q. Han, C. He, M. Zhao, B. Qi, J. Niu, C. Duan, *J. Am. Chem. Soc.* **2013**, *135*, 10186–10189.

[80] W.-J. Xuan, C. Botuha, B. Hasenknopf, S. Thorimbert, *Chem. – Eur. J.* **2015**, *21*, 16512–16516.

[81] M.-M. Rohmer, R. Ernenwein, M. Ulmschneider, R. Wiest, M. Benard, *Int. J. Quantum Chem.* **1991**, *40*, 723–743.

[82] J. Y. Kempf, M. M. Rohmer, J. M. Poblet, C. Bo, M. Benard, *J. Am. Chem. Soc.* **1992**, *114*, 1136–1146.

[83] J. M. Poblet, X. López, C. Bo, *Chem. Soc. Rev.* **2003**, *32*, 297–308.

[84] X. López, P. Miró, J. J. Carbó, A. Rodríguez-Fortea, C. Bo, J. M. Poblet, *Theor. Chem. Acc.* **2011**, *128*, 393–404.

[85] M.-M. Rohmer, M. Bénard, J.-P. Blaudeau, J.-M. Maestre, J.-M. Poblet, *Coord. Chem. Rev.* **1998**, *178–180, Part 2*, 1019–1049.

[86] M.-M. Rohmer, M. Benard, *J. Am. Chem. Soc.* **1994**, *116*, 6959–6960.

[87] M.-M. Rohmer, J. Devémy, R. Wiest, M. Bénard, *J. Am. Chem. Soc.* **1996**, *118*, 13007–13014.

[88] Polarizability is the ability to form instantaneous dipoles. It is a property of matter. Polarizabilities determine the dynamical response of a bound system to external fields, and provide insight into a molecule's internal structure., **n.d.**

[89] G. Yang, W. Guan, L. Yan, Z. Su, L. Xu, E.-B. Wang, *J. Phys. Chem. B* **2006**, *110*, 23092–23098.

[90] L. Yan, M. Jin, P. Song, Z. Su, *J. Phys. Chem. B* **2010**, *114*, 3754–3758.

[91] Nonlinear optics (NLO) is the branch of optics that describes the behavior of light in nonlinear media, that is, media in which the dielectric polarization P responds nonlinearly to the electric field E of the light. The nonlinearity is typically observed only at very high light intensities (values of the electric field comparable to interatomic electric fields, typically 108 V/m) such as those provided by lasers., **n.d.**

[92] M. R. S. A. Janjua, W. Guan, C. G. Liu, S. Muhammad, L. Yan, Z. Su, *Eur. J. Inorg. Chem.* **2009**, *2009*, 5181–5188.

[93] T. Zhang, W. Guan, L. Yan, T. Ma, J. Wang, Z. Su, *Phys. Chem. Chem. Phys.* **2015**, *17*, 5459–5465.

[94] M. Mirzaei, H. Eshtiagh-Hosseini, N. Lotfian, A. Salimi, A. Bauzá, R. Van Deun, R. Decadt, M. Barceló-Oliver, A. Frontera, *Dalton Trans* **2014**, *43*, 1906–1916.

[95] T. Zhang, N. Ma, L. Yan, S. Wen, T. Ma, Z. Su, *J. Mol. Graph. Model.* **2013**, *46*, 59–64.

[96] J. Song, Z. Luo, H. Zhu, Z. Huang, T. Lian, A. L. Kaledin, D. G. Musaev, S. Lense, K. I. Hardcastle, C. L. Hill, *Inorganica Chim. Acta* **2010**, *363*, 4381–4386.

[97] J.-Z. Liao, C. Wu, X.-Y. Wu, S.-Q. Deng, C.-Z. Lu, *Chem. Commun.* **2016**, *52*, 7394–7397.

[98] L. M. R. Albelo, A. R. Ruiz-Salvador, D. W. Lewis, A. Gómez, P. Mialane, J. Marrot, A. Dolbecq, A. Sampieri, C. Mellot-Draznieks, *Phys. Chem. Chem. Phys.* **2010**, *12*, 8632–8639.

[99] L. Marleny Rodriguez-Albelo, A. R. Ruiz-Salvador, A. Sampieri, D. W. Lewis, A. Gómez, B. Nohra, P. Mialane, J. Marrot, F. Sécheresse, C. Mellot-Draznieks, et al., *J. Am. Chem. Soc.* **2009**, *131*, 16078–16087.

[100] B. Nohra, H. El Moll, L. M. Rodriguez Albelo, P. Mialane, J. Marrot, C. Mellot-Draznieks, M. O'Keeffe, R. Ngo Biboum, J. Lemaire, B. Keita, et al., *J. Am. Chem. Soc.* **2011**, *133*, 13363–13374.

[101] A. R. Ruiz-Salvador, A. Go´mez, D. W. Lewis, C. Mellot-Draznieks, and L. M. Rodriguez-Albelo, Tobunporous, TOpological BUilding, of NanoPOROUs Solids University of Havana, Cuba, **2009**.

[102] C. J. Casewit, K. S. Colwell and A. K. Rappè, "Application of a universal force field to organic molecules- Journal of the American Chemical Society (ACS Publications)," **1992**.

[103] D. W. Lewis, A. R. Ruiz-Salvador, A. Gómez, L. M. Rodriguez-Albelo, F.-X. Coudert, B. Slater, A. K. Cheetham, C. Mellot-Draznieks, *CrystEngComm* **2009**, *11*, 2272–2276.

[104] A. Parrot, A. Bernard, A. Jacquart, S. A. Serapian, C. Bo, E. Derat, O. Oms, A. Dolbecq, A. Proust, R. Métivier, et al., *Angew. Chem. Int. Ed.* **2017**, *56*, 4872–4876.

[105] R. E. Stratmann, G. E. Scuseria, M. J. Frisch, *J. Chem. Phys.* **1998**, *109*, 8218–8224.

[106] Y. Zhao, D. G. Truhlar, *Theor. Chem. Acc.* **2008**, *120*, 215–241.

[107] X. Xu, W. A. Goddard, *Proc. Natl. Acad. Sci. U. S. A.* **2004**, *101*, 2673–2677.

[108] "A new hybrid exchange–correlation functional using the Coulomb-attenuating method (CAM-B3LYP)," can be found under http://www.sciencedirect.com/science/article/pii/S0009261404008620, **n.d.**

[109] N. M. O'boyle, A. L. Tenderholt, K. M. Langner, *J. Comput. Chem.* **2008**, *29*, 839–845.

[110] C. Ci, J. J. Carbó, R. Neumann, C. de Graaf, J. M. Poblet, *ACS Catal.* **2016**, *6*, 6422–6428.

# CHAPTER 3: HYBRID-POMs AS BRØNSTED ACID CATALYSTS

## 3.1 Introduction

Polyoxometalates have been extensively used as acid catalysts since the '70s, both under homogeneous and heterogeneous conditions.[1–5]

Indeed, besides their great applicability as oxidation catalysts, POMs in their protonated forms- called heteropolyacids (HPAs)- approach the superacidic behavior. Their molar catalytic activity can be 100-1000 times higher than that of $H_2SO_4$, in organic media. This makes it possible to carry out catalytic processes at a lower catalyst concentration and/or at a lower temperature.

In the last two decades, the broad utility of HPAs has been demonstrated on a wide variety of synthetically useful selective transformations of organic substances.[1] Several industrial processes based on HPA catalysts, such as the hydration of olefins (propene and butenes) or the polymerization of tetrahydrofuran, have been developed.[6]

The main characteristics that made HPAs extensively used in acid catalysis are:

- High efficiency;
- Resistance to oxidative degradation and hydrolysis;
- Stabilization of metal ions that are unstable in air;
- Environmental benignity.

Usually, tungsten HPAs are the catalysts of choice because of their stronger acidity, higher thermal stability, and lower oxidation potential compared to molybdenum ones.[7]

Besides, Polyoxometalates can have both Brønsted and/or Lewis acidic catalytic properties, depending on their chemical composition. For instance, the Lewis acidic pathway is preferred in the presence of transition metal-substituted lacunary POMs, where the catalytic site is the hetero-metal center.[8–10]

*In this chapter an overview of the most common Brønsted acid catalyzed reactions with totally inorganic POMs will be given, with a special focus on recyclable systems. Later our*

*studies, devoted to the development of first organo-POMs for Brønsted acid catalysis, will be presented.*

## 3.2      POMs as Brønsted acid catalysts

*A.         Friedel-Craft reactions*

In 2002, the Kozhevnikov group proved the catalytic activity of the Keggin $H_3PW_{12}O_{40}$ toward the Friedel-Craft acylation of anisole with acetic anhydride in a liquid phase. They used different silica-supported POMs, such as $H_3PW_{12}O_{40}$, $H_4SiW_{12}O_{40}$ and $H_3PMo_{12}O_{40}$, as heterogeneous catalysts, finding that polyoxotungstate $H_3PW_{12}O_{40}$ exhibits the highest activity, yielding up to 98% *para* methoxyacetophenone at 90–110°C, with only 2–4% of the *ortho* isomer. This matches the acidity trend of the three polyoxometalates tested.

Moreover, $H_3PW_{12}O_{40}$ was found to be 100 times more active than the zeolite H-beta, commonly used to catalyze this type of reactions. The catalyst was reusable, although a gradual decline of activity was observed due to the progressive coking of the catalyst. In contrast to anisole, the acylation of toluene with HPAs was far less efficient than with H-beta. Indeed, since the catalytic activity of the HPA arises from the non-chemical absorption of the substrate on the acid sites of the POM, in the case of toluene evidences provided that the reaction was inhibited by preferential adsorption of acetic anhydride on the catalyst.[11]
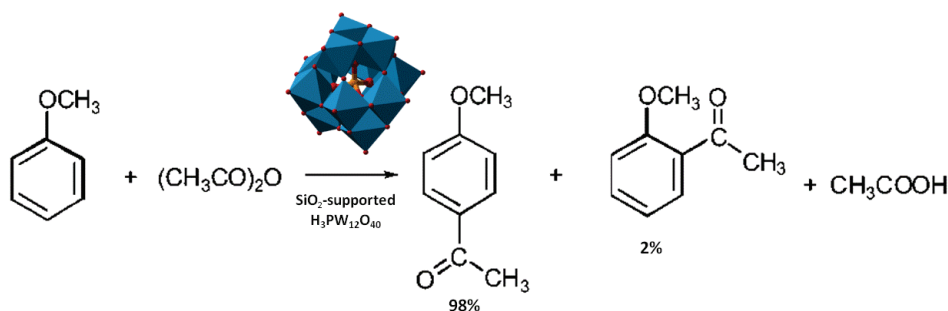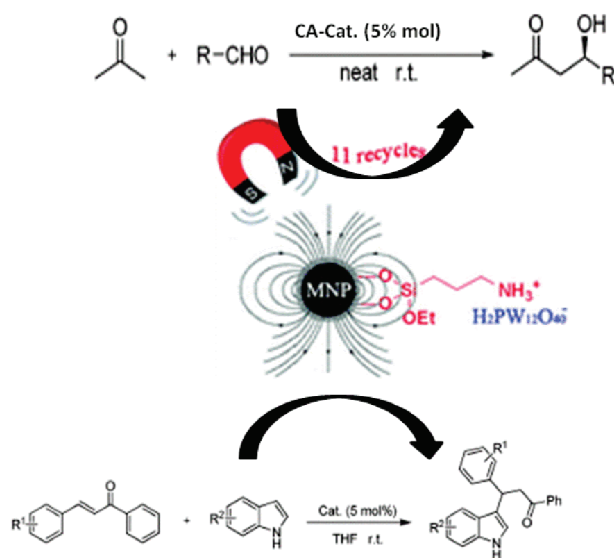


**Figure 3. 1-** Friedel-Craft reaction catalyzed by $SiO_2$-supported HPAs, presented by Kaur et al.

Friedel–Craft acylation of the more inert benzene with benzoic anhydride to produce benzophenone, was successively studied by Togawa et al. over various

ion-exchanged Keggin heteropoly acids (HPA). They found that in the presence of insoluble $Cs_{2.5}H_{0.5}PW_{12}$ the reaction proceeded quantitatively at 423K, opening the way to a chlorine-free fine process for this reaction.[12]

Zheng et al. successfully developed a non-covalently immobilized POM catalyst based on the Keggin $H_3PW_{12}O_{40}$, for Friedel–Craft reactions of indoles and chalcones in various solvents, using magnetic nanoparticles as supports. These immobilized acid catalysts are highly efficient in THF and could be reused for at least 11 times without loss in activity: a yield of 94% was achieved in 12h of reaction at room temperature, in THF.

In addition, the immobilization of chiral amines on the NPs was realized via non-covalent assembly with the POMs as the non-covalent anchors. The non-covalently assembled catalyst was efficiently employed for the enantioselective aldol reaction of acetone with 4-nitrobenzaldehyde, giving an 87% yield of aldol products in 91% ee after 24 h, in the presence of 0.33 mol % of catalyst. The yield and enantioselectivity were maintained even after 11 cycles. The TEM image of the catalyst after 10 recyclings indicated that the catalyst was quite robust and no significant aggregation was found [13]



**Figure 3. 2**- Friedel-Craft reaction catalyzed by Magnetic NPs-supported (MNP) Keggin $H_3PW_{12}O_{40}$

*B.    Mannich reaction*

The same POM, $H_3PW_{12}O_{40}$, was efficiently employed for Mannich reactions. In particular, in 2006 Azizi et al. employed the two Keggin HPAs, $H_3PW_{12}O_{40}$ and $H_3PMo_{12}O_{40}$ as catalysts for the one-pot, three-component Mannich reaction of ketones with aromatic aldehydes and different amines, in water at room temperature. This afforded the corresponding *β*-amino carbonyl compounds in good yields (up to 95%) but moderate diastereoselectivity (72:28 *anti/syn*). In this case, the efficiency of HPAs was interesting mainly because of the low catalyst loading, improved yields and clean reaction. Besides, the reaction products were often insoluble in water, and then easily filtered off.
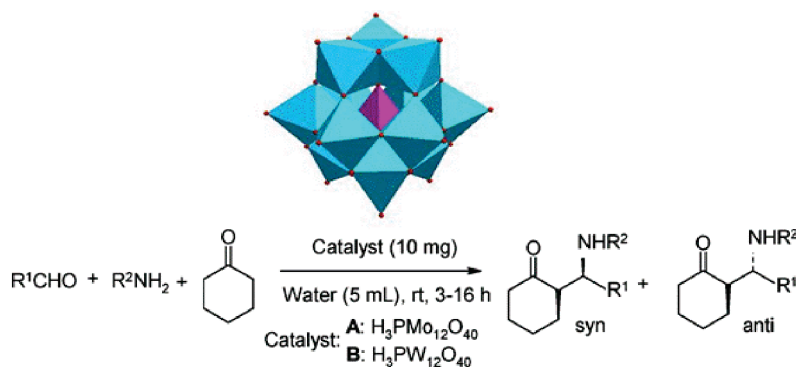


**Figure 3. 3-** One pot, three-component Mannich reaction catalyzed by $H_3PW_{12}O_{40}$ and $H_3PMo_{12}O_{40}$.

The Mannich reaction, as well as Diels-Alder reactions, was also efficiently catalyzed by several lanthanide complexes of the monolacunary Dawson polyoxotungstate, $TBA_5H_2(\alpha_1-LnP_2W_{17}O_{61})$, (Ln =La, Sm, Eu, Yb, Hf). In this case a totally Lewis acidic pathway was demonstrated by the authors.[9,10,14,15] The POM $TBA_5H_2(\alpha_1-HfP_2W_{17}O_{61})$ also catalyzed the Mukaiyama aldol reaction. In contrast to the former reaction, the Lewis acid generated a proton in the presence of adventitious water, indicating that the reaction goes through an indirect Brønsted acidic pathway.
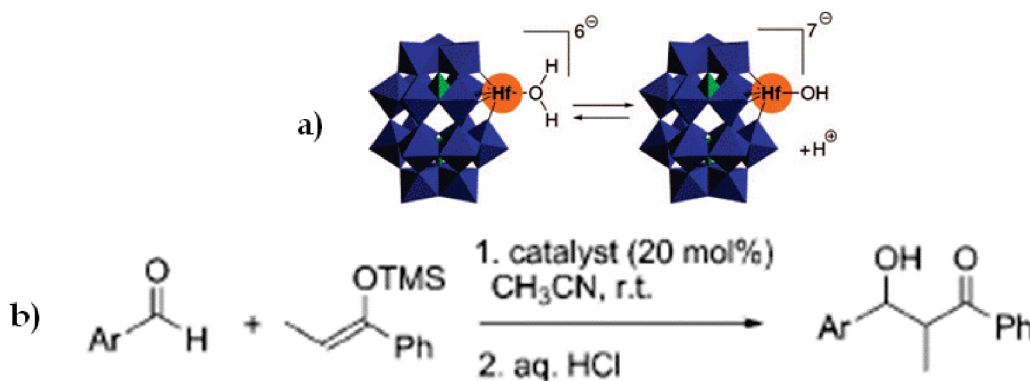
**Figure 3. 4-** a) The Hf-substituted lacunary Dawson polyoxotungstate coordinates a water molecule, with a consequent release of proton that catalyzes the b) Mukaiyama rearrangement with an indirect Bronsted acidic pathway.

## C.    Esterifications

The Parida group intercalated molybdophosphoric acid and tungstophosphoric acid in Zn−Al hydrotalcite-like materials at different concentrations (5−20 wt %). The catalysts were tested in the liquid phase esterification of acetic acid using *n*-butanol under spontaneous condition. In particular and in contrast to what precedes, the molybdophosphoric acid-intercalated samples showed better catalytic activity than their tungstophosphoric acid counterparts, givings 84.15% conversion of 1-butanol and 100% selectivity for n-butyl acetate with a rate constant of $12.6 \times 10^{-5}$ s$^{-1}$.[16]

The polyoxotungstate $H_3PW_{12}O_{40}$ was also heterogenized on mesoporous $Ta_2O_5$ for the esterification of lauric acid and myristic acid, the trans-esterification of tripalmitin, and the direct use of soybean oil for biodiesel production under mild conditions. Its activity was higher than that of $H_3PW_{12}O_{40}$ or $Ta_2O_5$ alone and the improved activity of the composite catalyst was mainly attributed to the strong interaction of the Keggin units and surface hydroxyl groups of $Ta_2O_5$.[17,18]
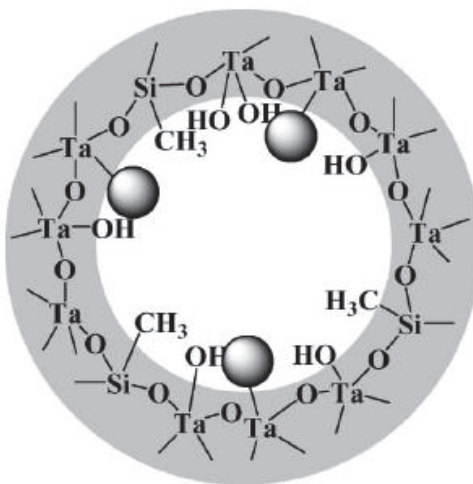
**Figure 3. 5-** Schematic representation of the $Ta_2O_5/SiO_2$-supported $H_3PW_{12}O_{40}$ catalyst for (trans)esterification reactions.

## D. Hydrolysis of esters

An example of the reverse hydrolysis of esters by similar catalysts was reported by Liu's group, who constructed a series of MOF−POM catalysts by filling a MOF with Keggin POMs, eg. $H_nXM_{12}O_{40}$ (with X=Si, Ge, P, As and M=W, Mo) into a copper-linked MOF. These POMOFs are extremely water-resistant, have high stability and tolerate thermal and acid−base conditions. They were efficiently applied as catalysts for the hydrolysis of esters in excess water, and could be used repeatedly without POM leaching from the channel or skeleton decomposition. [19]
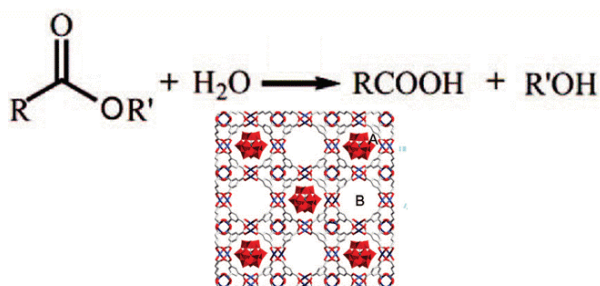


**Figure 3. 6-** POMOF system employed for the hydrolysis of esters

The same idea was followed by the Inumaru group: a water-tolerant, highly active solid acid catalyst for the hydrolysis of esters was prepared by immobilizing

$H_3PW_{12}$ in the hydrophobic nanospaces of organo-modified mesoporous silica. The resulting catalyst has a higher activity than the hydrophobic $Cs_{2.5}H_{0.5}PW_{12}$, and many other inorganic acids. It is also slightly higher than those of $H_3PW_{12}$ and $H_2SO_4$ (6 times higher than that of $H_2SO_4$ per acidic proton).

The Parac-Vogt group found that the highly negatively charged heptamolybdate anion $[Mo_7O_{24}]^{6-}$,[20,21] as well as polyoxovanadate $[HV_{10}O_{28}]^{5-}$,[22] could efficiently catalyze the cleavage of the phosphodiester bond in bis(4-nitrophenyl) phosphate (BNPP), a commonly used DNA model substrate. In particular for both systems, the reaction rate was accelerated by nearly 4 orders of magnitude compared to the rate of uncatalyzed cleavage at pH 5.
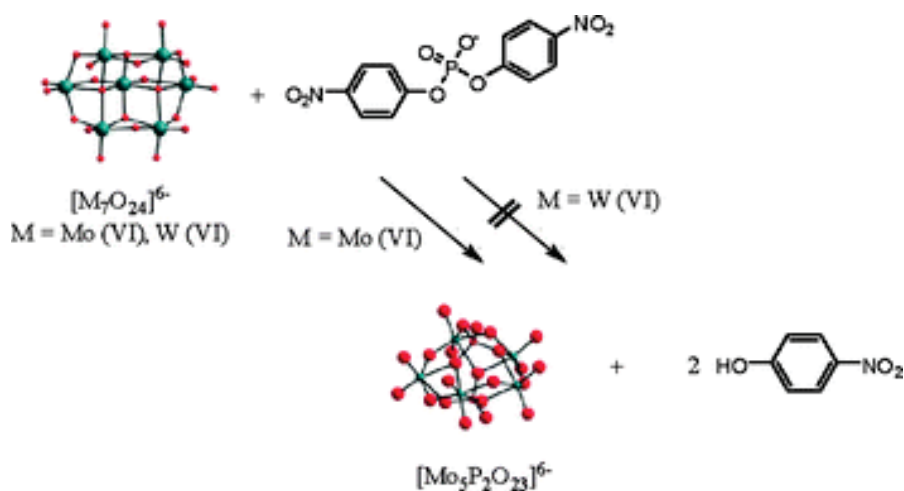


**Figure 3. 7**- Polyoxomolybdate used by Cartuyvels et al. for the hydrolysis of phosphodiester bonds.

The authors initially suggested that the phosphodiester bond was hydrolyzed by the POM acting as a Brønsted acid. However, further work leds them to consider that the origin of the hydrolytic activity of both HPAs toward the hydrolysis of phosphodiester bonds is most likely due to its high lability and its dissociation into smaller fragments, that could bind the substrate into the polyoxometalate skeleton. This may lead to bond strain and polarization of the P−O ester bond and its activation toward external attack by water.

## 3.3       The first organo-POM as Brønsted acid catalyst

### 3.3.1       Introduction

The Brønsted acid activity of POMs stems from the presence of protons on the negatively charged POM surface. The high polarization of this bond enables their interaction with other substrates. Nevertheless, it is difficult to establish the precise catalytic proton position on the POM surface, since protons can have more than one possible binding site.

The structural characterization of the HPA proton sites is thus an important key toward understanding the catalytic activity.

Moreover, the structural diversity and tunability of totally inorganic POMs is relatively narrow and they also have a limited solubility in organic solvents. Thus, their use with sensitive organic substrates remains limited.

In that context, there was an opening for POM organo-hybrids.

*The aim of my Ph.D. is to develop POM-based catalysts for asymmetric reactions. In light of this, it is crucial to localize the active site, in order to successively design a chiral pocket around it.*

During his Ph.D. thesis Dr. David Lachkar developed hybrid Brønsted acid POMs, by grafting different diolamide ligands on the Dawson polyoxotungstovanadate $TBA_5H_4(P_2V_3W_{15}O_{61})$.[23] In particular, he synthesized various phenyl diolamide and pyridine diolamide hybrids, by changing the substituent on the aromatic ring.[24]
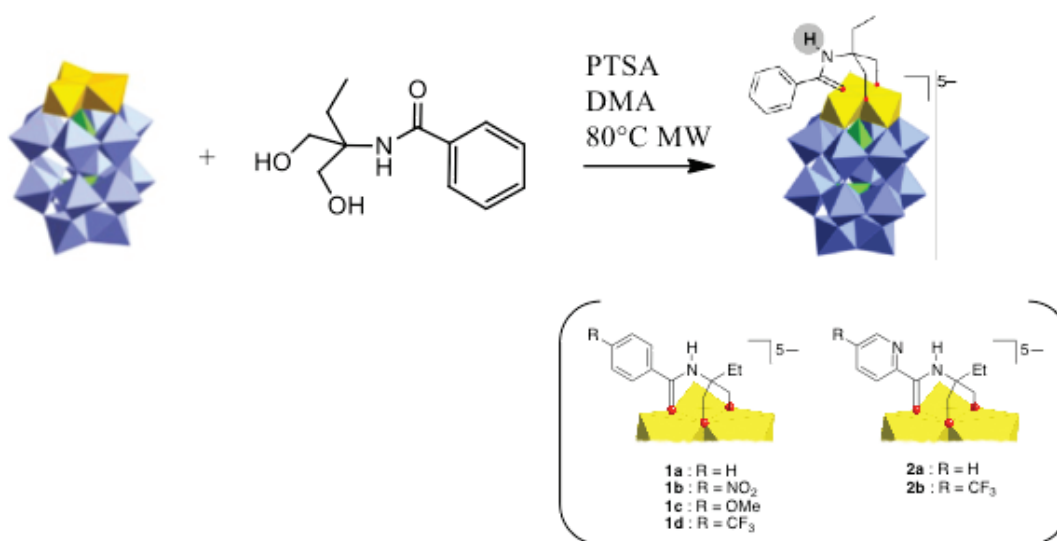
**Scheme 3. 1-** List of diolamides@POM derivatives synthesized by Dr.Lachkar

The underlying assumption was that since POMs are good electron reservoirs, they might stabilize the negative charge derived from deprotonation of the amide, by delocalization on the POM surface. This aspect is relevant because it can promote the catalysis stabilizing the intermediate steps in the catalytic cycle.
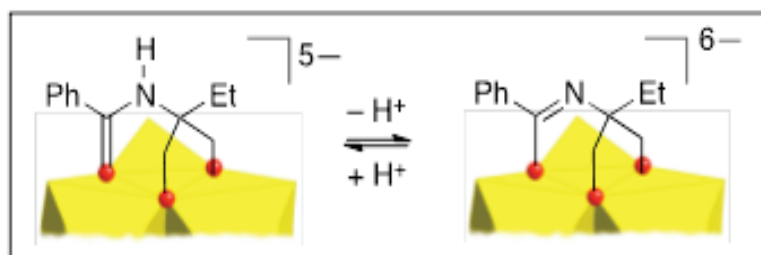


**Scheme 3. 2-** General scheme for the deprotonation of diolamides@ POM derivatives.

In light of the above, Dr. Lachkar tested all the catalysts in the organo-catalytic quinoline reduction in the presence of Hantzsch esters as stoichiometric reductant. The mechanism features a proton transfer (Brønsted acid catalysis) from the catalyst to the quinoline nitrogen, forming an ion-pair, followed by the reduction of the substrate via a hydride transfer from the ester. All the organo-POMs considered were active toward the catalytic reaction, with a yield after 13h that

depends from the substituent on the phenyl ring: the more electronwithdrawing the substituents (such as $CF_3$- $NO_2$-) the faster is the reaction.

For example, the reaction yield was estimated after 13h for all the catalysts used and it was found at 96% with *p*-$CF_3$(Ph)diolamide@POM (the faster) and 81% with *p*-OMe(Ph)diolamide@POM (the slower). Moreover the organo ligands were inactive toward the reaction, and the simple POM ($TBA_5H_4P_2V_3W_{15}O_{61}$) with 4 protons as counterions on its surface, didn't succeed to match the reaction yield of the slower active organo-POM (Y=62%) after 13h.[23]

In light of these interesting results, we decided to investigate the precise position of the catalytic proton. Since the ^{1}H-NMR of the organo-POMs showed a big downfield shift of the amidic proton signal, once the diolamide ligand is anchored into the POM surface, it is reasonable to suppose that the amidic proton was not bonded anymore to the amidic nitrogen, but free to migrate around the negatively charged polyoxometalate surface or on the close basic site of the pyridine derivatives (for the pyridine substrates).
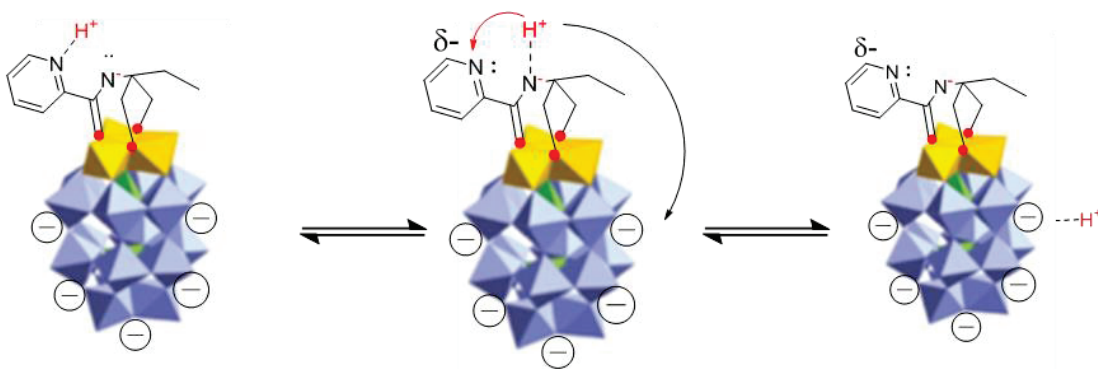


**Figure 3. 8-** Schematic representation of the conceivable amidic proton migration on the basic sites of the hybrid complexes.
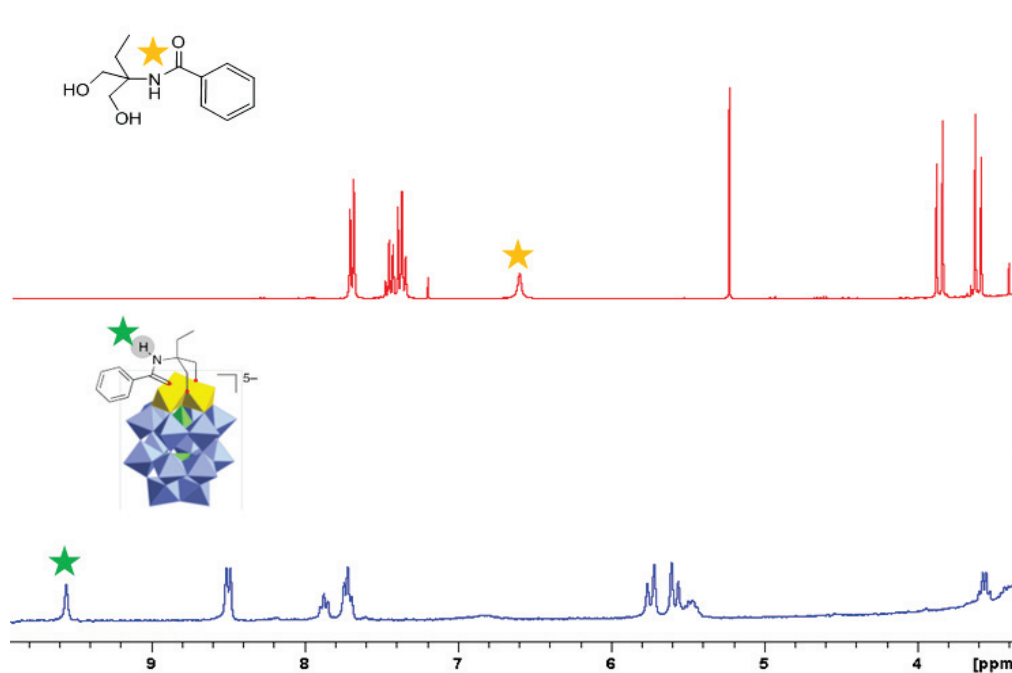
**Figure 3. 9-** ¹H-NMR superposition spectra of free (Ph)diolamide and (Ph)amide@POM. [Spectra recorded at 300 MHz, in CD₃CN, at 298K; concentration samples 10 mM].

We sought help from NMR to validate or reject this hypothesis.

### 3.3.2     High field NMR studies

We first recorded the ¹H-NMR spectrum of all the hybrids to investigate the increment in the acidity of the amidic protons of the POM-grafted diolamides, with respect to the free diolamide ligands.

| Entry | Hybrid-POM | δ (ppm) amidic proton |
|-------|-----------|----------------------|
| 1 | (Ph)amide@POM (**1a**) | 9.32 |
| 2 | $p$-NO₂(Ph)amide@POM (**1b**) | 9.86 |
| 3 | $p$-OMe(Ph)amide@POM (**1c**) | 9.15 |
| 4 | $p$-CF₃(Ph)amide@POM (**1d**) | 9.68 |
| 5 | (Py)amide@POM (**2a**) | 10.40 |
| 6 | $p$-CF₃(Py)amide@POM (**2b**) | 10.40 |

**Table 3. 1-** ¹H-NMR chemical shifts of the amidic protons in the all hybrid-POM structures. Recorded at 300 MHz, in CD₃CN, at 10mM in concentration.

As it is can be seen in table 3.1, the chemical shifts range from 9.15 ppm for the POM functionalized with an electron-rich Phenyl ring (**1c**) to 9.86 ppm for the *p*-NO$_2$(Ph) derivative (**1b**), with POM **1a** at 9.32 ppm and **1d** at 9.68 ppm. The chemical shift for the pyridine derivatives **2a** and **2b** was found at 10.40 ppm.

The electronic nature of the arene substituent influences the $^1$H-NMR chemical shifts. The amide signals are much further downfield shifted when an electrowithdrawing group is present in the Phenyl ring (**1b-1d**), since they are likely to pull electron density from the iminium (making the N-H more polarized). Conversely, the resonance of the amidic proton in the *p*-OMe(Ph)urea@POM (**1c**) was found more high-field shifted compare to the (Ph)derivative, as expected in presence of a donating group. For the pyridine-substituted POMs **2a,b**, the amidic proton signals were even further downfield shifted. This can be a consequence of the presence of the electron-poor heteroaromatic ring, which pull electrons and/or of a difference in anisotropy cones compared to arenes.

This suggests that an increment in the acidity of the amidic proton happens once the organic moiety is grafted onto the vanadate crown, since the chemical shift for a general amidic proton is situated at around 7 ppm, and in parallel the iminium resonance form of the amide is stabilized by the POM structure. All of this would only be possible if the H is on the amide.

To definitively prove if the proton is on the amide site or on the POM surface, we decided to monitor the amide resonance with 2D $^1$H-$^{15}$N HSQC experiments at natural nitrogen isotopic abundance on the (Ph)amide@POM (**1a**), (Py)amide@POM (**2a**) and *p*-CF$_3$(Py)amide@POM (**2b**).

In the $^1$H-$^{15}$N HSQC experiment it is possible to observe the $^{15}$N resonance of nitrogen that are directly bound to a proton.
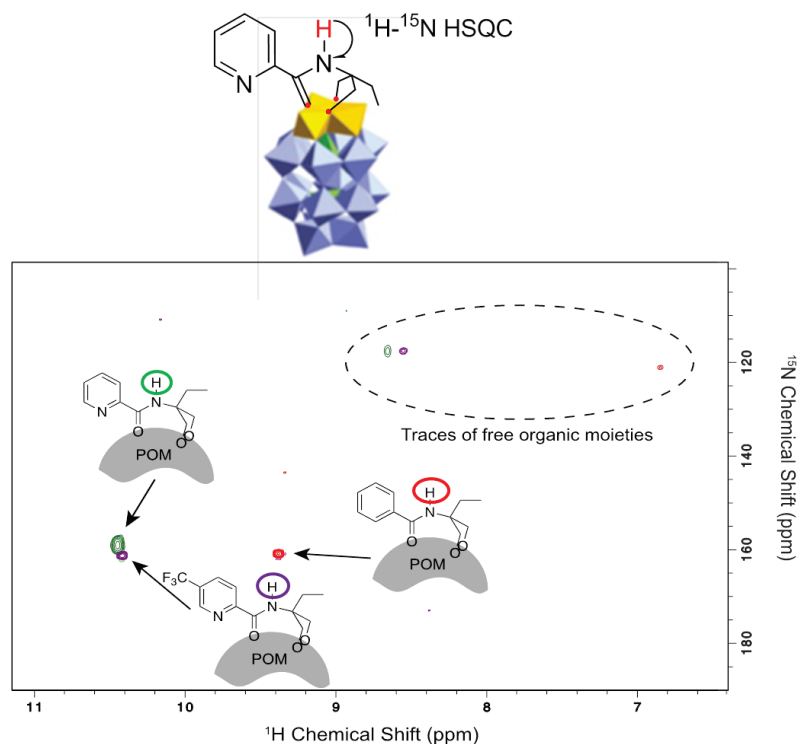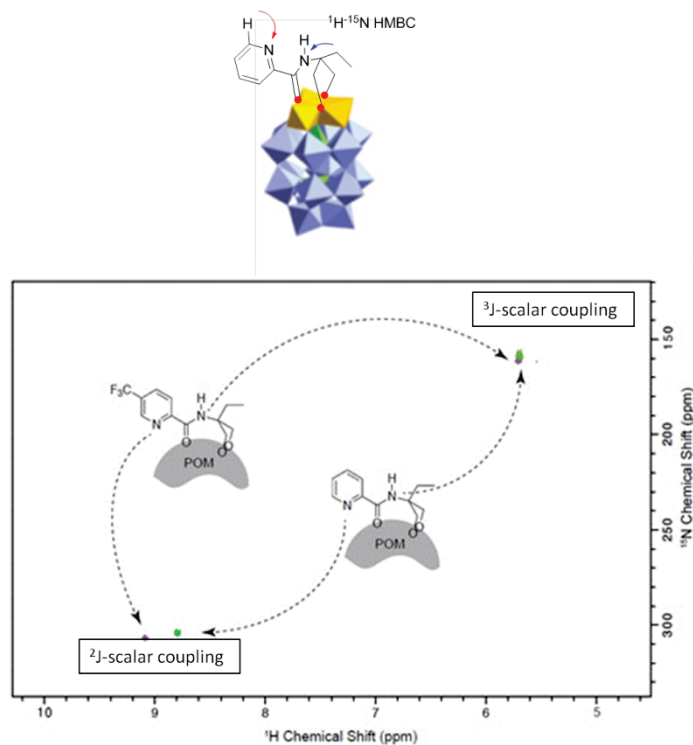
**Figure 3. 10-** 2D $^1$H-$^{15}$N HSQC superposition spectra of **1a, 2a, 2b**. Spectra recorded at 600MHz, in CD$_3$CN, at 298K. Concentration samples: **1a**=5 mM (red), **2a**=2.3 mM (green), **2b**=7.5 mM (purple).

Figure 3.9 shows the overlap of the HSQC spectra acquired on the POMs **1a**, **2a** and **2b**. Strong cross-peaks were observed for the amide with a $^{15}$N chemical shift of about 160 ppm and $^1$H chemical shifts ranging from 9.4 for **1a** to 10.4 ppm for **2a** and **2b**. In the same spectrum it is possible to observe some weak cross-peaks at around 120 ppm for nitrogen and 6.9 ppm for **1a**, 8.6–8.7 ppm for **2a,b**. Comparison with authentic samples showed that these crosspeaks correspond to remaining traces of the free diolamide ligands of **1a**, **2a,b** that did not get anchored to the POM scaffold during the synthesis.

In both the free diolamides and the organo-POMs, the proton resonances of the amide in the pyridine derivatives are downfield shifted from 1 to 1.5 ppm compared to their analogous benzamide derivative. Furthermore, there were no cross peaks corresponding to the pyridine nitrogen of **2a** and **2b** (expected signal at ~200 ppm for a protonated pyridine). The $^{15}$N resonances shift from about 120 ppm in the free ligands to about 160 ppm in the organo-POMs and they do not vary much in the different POMs. Simultaneously, the $^1$H signals are also strongly downfield shifted (2 ppm average shift) in the organo-POMs, as mentioned above.

The observation of crosspeaks demonstrates that the target proton remains bound to the amidic nitrogen in the POMs, as does the significant ^{1}H chemical shift difference between **1a** and **2a,b**. This observation certainly reflects the different magnetic and chemical environment of the amide when substituted by a phenyl ring, relative to an electronically different pyridine ring. This difference would likely be less pronounced if the protons were attached to the metal oxide surface, far from the substituents.

To exclude the possibility that the pyridinium proton would not be observed because of a rapid exchange with the residual water in the solvent, we acquired also 2D ^{1}H-^{15}N HMBC spectra, for the two (pyridine)amides@POM derivatives **2a** and **2b**. The 2D ^{1}H-^{15}N HMBC experiment correlates the nitrogen spin with the non-exchangeable protons attached to carbon that is bound to nitrogen *via* the weak long-range [1]H-[15]N [2]J or [3]J-scalar couplings. In this manner, it is also possible to determine the ^{15}N chemical shift of the pyridine nitrogen independently from its protonation state and to clearly assess if it is protonated or not.



**Figure 3. 11-** Superposition of the 2D ^{1}H-^{15}N HMBC spectra of the hybrid-POM **2a** and **2b**. Concentration samples: **2a**: 2.3 mM, **2b**: 7.5 mM. The crosspeaks for the hybrid POM **2a** is reported in green, for the hybrid **2b** is reported in purple. Spectra recorded at 600MHz, in CD$_3$CN, at 298K.

We observed a correlation between the aromatic proton of the pyridines and the nitrogen resonance at 303.8 ppm for **2a** and 306.6 ppm for **2b**. This chemical shift value is very close to the expected chemical shift of the free pyridine (302 ppm in CHCl₃) and it is far from the chemical shift observed for the protonated pyridinium ions (204 ppm in CHCl₃ for the pyridinium chlorohydrate).[25] This unambiguously indicates that the pyridine is not protonated in organo-POMs **2a** and **2b**.

### 3.3.3    DFT calculations

In order to further validate the hypothesis of a real catalytic amidic proton, we performed some DFT calculations at the BP86/LANL2DZ level of theory within the Gaussian09 suite of programs.[26] An implicit solvent correction was added to model the acetonitrile.

First of all a geometry optimization was carried out for the protonated and deprotonated hybrid-POM molecules. The example for **1a** is shown in Figure 3.11.
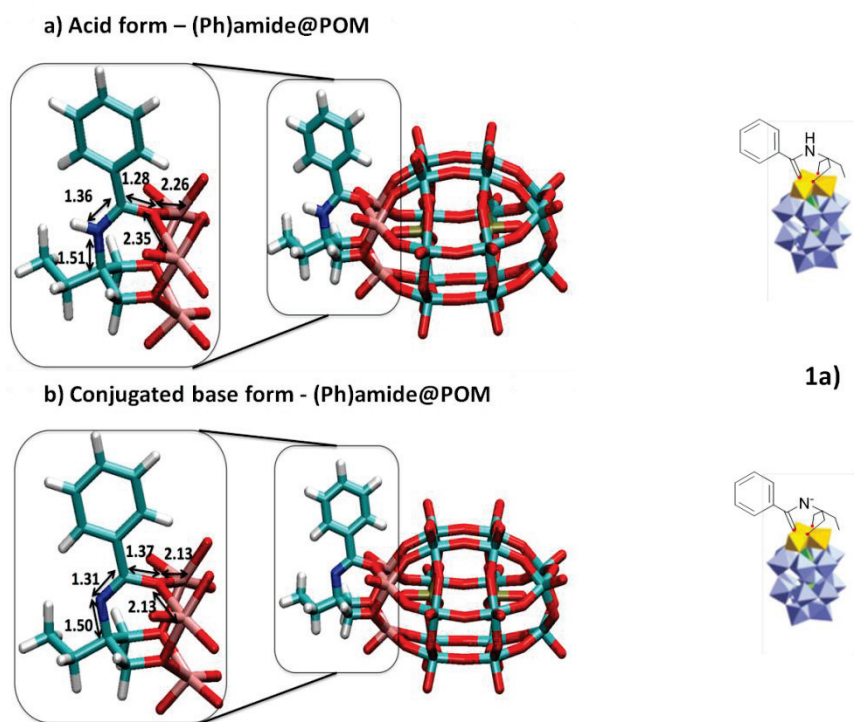


**Figure 3. 12-** Optimized geometries with explicit bond lengths (in Å) of the acid form (a) and conjugate base form (b) for (Ph)diolamide@POM (1a).

In the protonated form *(acid)*, the HN-C(Ph)=O bond length was calculated at 1.36 Å, and that of the C=O bond was 1.28 Å. The phenyl group appears slanted and the V-O(=C)-V bridge is distorted, with the V=O bond facing the C=H of the phenyl longer than the V=O bond on the other side (2.26 Å vs.2.35 Å). The N=C bond connecting the amide group to the diol part is 1.51 Å long. In the deprotonated form (*Conjugated base)*, the N-C(Ph)=O bond length shortens to 1.31 Å, while the C=O bond is lengthened (1.37 Å). The phenyl group is much less slanted, and the V-O(=C)-V bridge is symmetrical (equal V=O bond lengths at 2.13 Å). The N=C bond connecting the amide group to the diol part is unchanged (1.50 Å).

This trend is similar for all the systems calculated (see the Table 3.2), including the pyridine derivatives.



**Figure 3. 13-** Optimized geometries with explicit bond lengths of the acid form (a) and conjugate base form (b) for (Py)amide@POM (2a).

123

a) Acid form - P-NO$_2$(Ph)amide@POM



b) Conjugated base form - P-NO$_2$(Ph)amide@POM

**1b)**
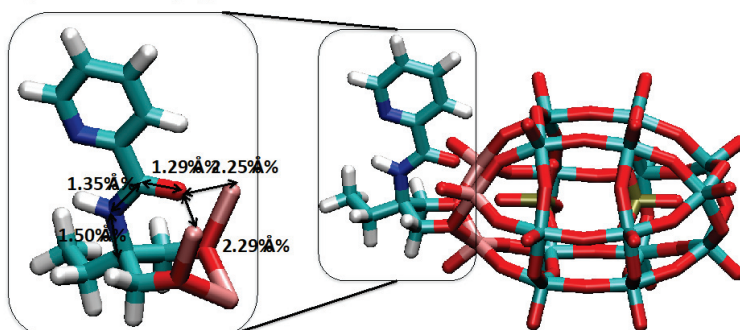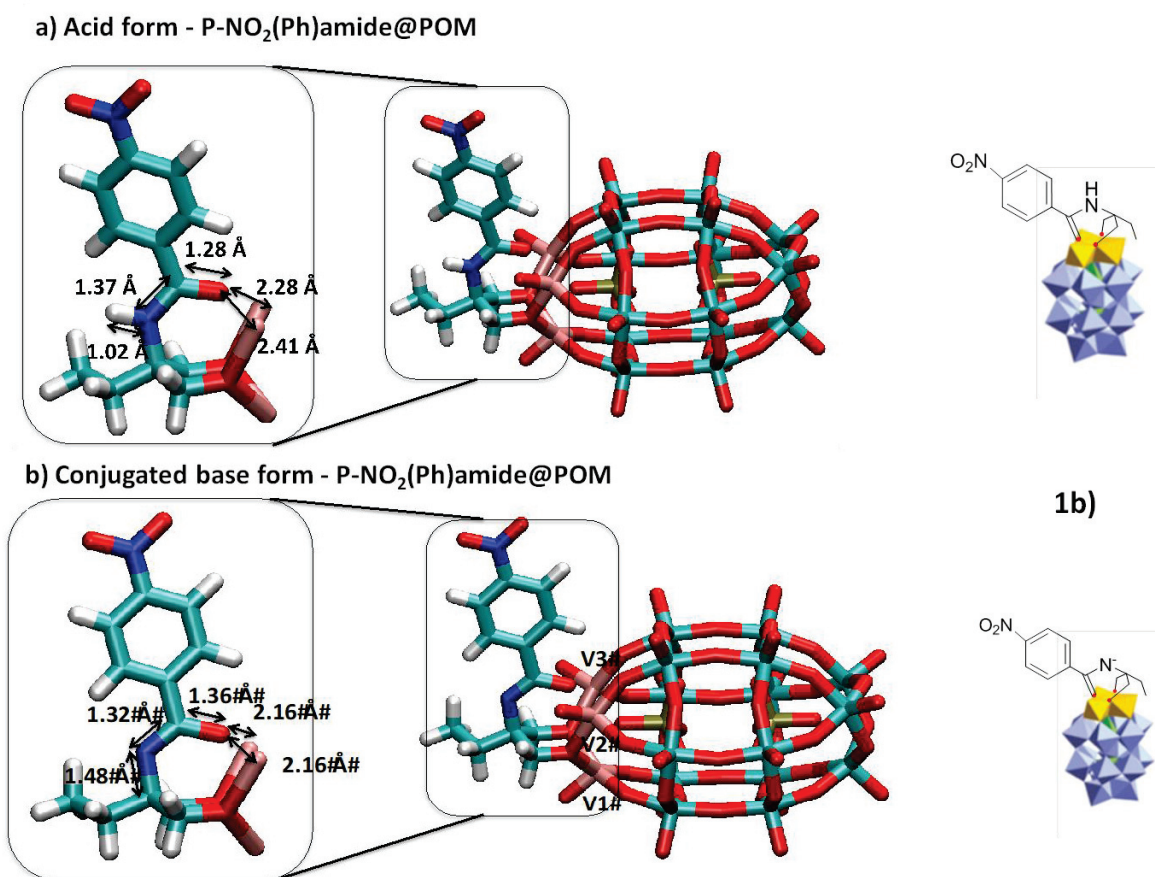


**Figure 3. 14**- Optimized geometries with explicit bond lengths of the acid form (a) and conjugate base form (b) for *p*-NO$_2$(Ph)amide@POM (1b).
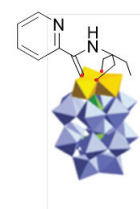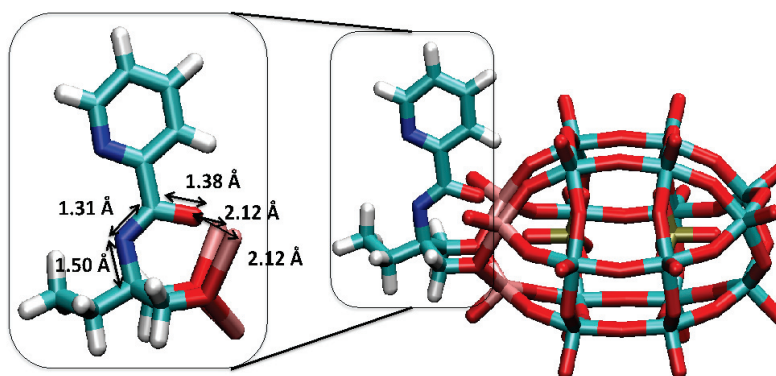
124

| | | d(C-N) | d(N=C) | d(C=O) | d(N-H) | d(O-V2) | d(O-V3) |
|---|---|---|---|---|---|---|---|
| H | Base | 1.50 | 1.31 | 1.37 | | 2.13 | 2.14 |
| | H | 1.51 | 1.36 | 1.28 | 1.02 | 2.26 | 2.33 |
| Ph **1a** | Base | 1.50 | 1.31 | 1.37 | | 2.13 | 2.13 |
| | H | 1.51 | 1.36 | 1.28 | 1.02 | 2.26 | 2.35 |
| Ph-*p*OMe **1d** | Base | 1.50 | 1.31 | 1.38 | | 2.12 | 2.12 |
| | H | 1.51 | 1.36 | 1.29 | 1.02 | 2.25 | 2.26 |
| Ph-*p*NO$_2$ **1b** | Base | 1.48 | 1.32 | 1.36 | | 2.16 | 2.16 |
| | H | 1.50 | 1.37 | 1.28 | 1.02 | 2.28 | 2.41 |
| Ph-*p*CF$_3$ **1c** | Base | 1.49 | 1.31 | 1.38 | | 2.14 | 2.14 |
| | H | 1.51 | 1.36 | 1.29 | 1.02 | 2.27 | 2.37 |
| Pyridine **2a** | Base | 1.50 | 1.31 | 1.38 | | 2.12 | 2.12 |
| | H | 1.50 | 1.35 | 1.28 | 1.03 | 2.25 | 2.29 |
| Pyridine-CF$_3$ **2b** | Base | 1.50 | 1.31 | 1.38 | | 2.13 | 2.13 |
| | H | 1.50 | 1.35 | 1.28 | 1.03 | 2.23 | 2.35 |

**Table 3. 2-** Optimized bond lengths (in Å) characterizing the C=O insertion of the organic appendage into the POM for all the amides@POM complexes.

The calculated bond lengths are fully consistent with our initial hypothesis that in the protonated form, the C=N bond has less double-bond character, and is longer. The C=O bond is also shorter because of the conjugation with the C=N.
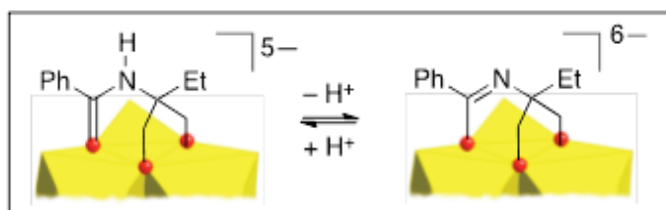


**Scheme 3. 3-** Schematic representation of the deprotonation of the amide@POM derivatives.

Moreover, as it is possible to see a steric strain appears between the POM and the phenyl group, which results in a distortion. The organic ligand "pulls" the oxygen to escape this tension, resulting in longer V=O bonds, and a loss of symmetry. Upon deprotonation, the C=N bond is considerably shortened, while the C=O bond is lengthened. This reflects the increase of the imidate form, as expected since more electron density is accommodated on the oxygen and on the POM. The C=O bond lengthening also releases the strain, with a V-O-V crown back to normal.

We then simulated the $^1$H-NMR chemical shifts of the amide protons of all hybrid-POMs (in their N-protonated forms), using the GIAO protocol, at the PBE1PBE/ LANL2DZ//BP86/ LANL2DZ level of theory.
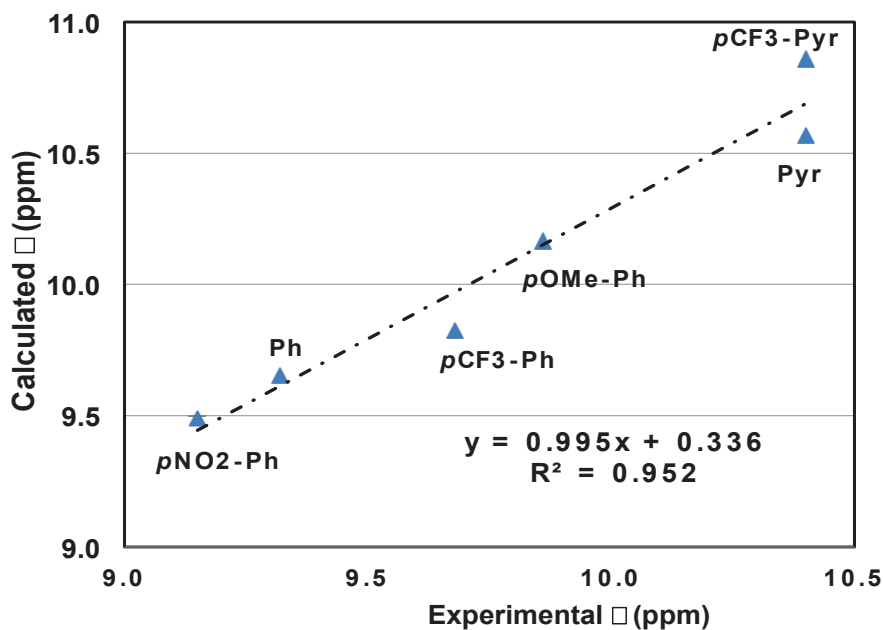


**Figure 3. 15**- Correlation between experimental vs. computed $^1$H-NMR shifts. The level of theory is PBE1PBE/LANL2DZ//BP86/ LANL2DZ

The calculated values were in very good linear agreement with the observed shifts with a systematic deviation of 0.33 ppm.

We also calculated the proton affinities for all our hybrid-POMs.

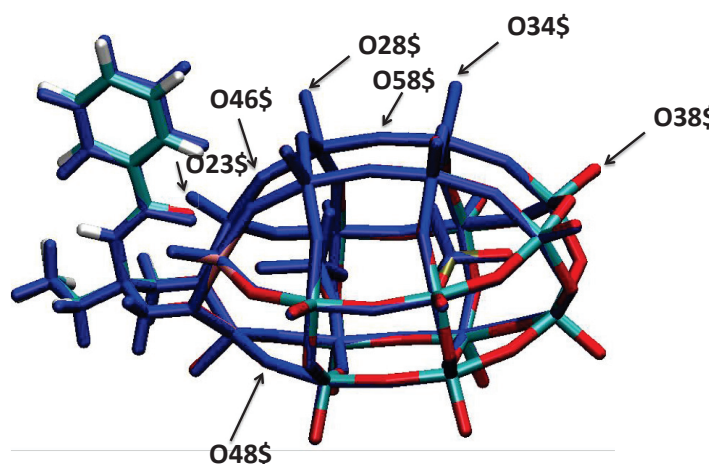| | N | Terminal O1 O23 | Terminal O2 O28 | Terminal O3 O34 | Terminal O4 O38 | Bridging O5 O46 | Bridging O6 O48 | Bridging O7 O58 |
|---|---|---|---|---|---|---|---|---|
| (Ph)amide@POM (**1a**) | 0.0 | 27.3 | 25.3 | 29.6 | 29.3 | 19.5 | 23.3 | 25.1 |
| *p*-NO$_2$(Ph)amide@**P**OM (**1b**) | 0.0 | 23.7 | 21.4 | 22.6 | 23.5 | 16.0 | 19.4 | 22.6 |
| *p*-OMe(Ph)amide@POM (**1c**) | 0.0 | 24.9 | 25.7 | 23.9 | 24.8 | 17.1 | 24.8 | 22.5 |
| *p*-CF$_3$(Ph)amide@POM (**1d**) | 0.0 | 28.8 | 26.9 | 28.3 | 29.2 | 21.2 | 25.0 | 28.4 |
| (Py)amide@POM (**2a**) | 0.0 | 33.8 | 30.6 | 32.0 | 32.9 | 27.8 | 28.6 | 30.6 |
| *p*-CF$_3$(Py)amide@POM (**2b**) | 0.0 | 31.3 | 28.0 | 29.2 | 30.1 | 22.6 | 26.1 | 27.9 |

**Table 3. 3-** Calculated proton affinities (in kcal/mol) along the series of substituted POM **1a-d** and **2a-b**, relative to the proton affinity of the amide nitrogen set at 0.0 kcal/mol, and cartoon representation (superimposing the acid and basic form in color and blue sticks, respectively) for the compound **1a** to indicate the numbering scheme for the oxygen atoms.

This was carried out to explore the possibility of a protonation on the oxygen atoms present on the POM structure. The proton affinity at the nitrogen position is more favorable by at least 25.3 kcal*mol$^{-1}$ compared to terminal oxygens and by at least 19.5 kcal*mol$^{-1}$ compared to a bridging oxo. This means that according to calculations, the POM surface is not basic enough to deprotonate the inserted amide.

All these models confirm that the proton prefers to be located on the amidic nitrogen, not on the POM structure.

Finally, we used DFT to estimate the charge transfer between the inorganic and organic parts of the hybrid-POMs. Indeed, since it was not possible to extimate the pKa of our systems, computational methods allow us to estimate the partial atomic charges distribution in the molecule which is related to the protonation/deprotonation process. The partial charge distribution in the molecule, indeed, varies with protonation/deprotonation of the acid/base active sites. Three different population analysis (Mulliken, ESP, NPA) were carried out and the obtained data are collected in the table below.

| | Mulliken | | | ESP | | | NPA | | |
|---|---|---|---|---|---|---|---|---|---|
| | Base | Acid | Diff. | Base | Acid | Diff. | Base | Acid | Diff. |
| (Ph)amide@POM (**1a**) | 0.98 | 1.62 | 0.64 | 0.46 | 0.78 | 0.32 | 1.09 | 1.82 | 0.73 |
| *p*-NO$_2$(Ph)amide@POM (**1b**) | 1.00 | 1.66 | 0.64 | 0.45 | 0.72 | 0.27 | 1.05 | 1.78 | 0.73 |
| *p*-OMe(Ph)amide@POM (**1c**) | 0.91 | 1.56 | 0.63 | 0.64 | 0.45 | 0.23 | 1.06 | 1.78 | 0.72 |
| *p*-CF$_3$(Ph)amide@POM (**1d**) | 0.93 | 1.00 | 0.66 | 0.04 | 0.44 | 0.48 | 1.11 | 1.85 | 0.74 |
| (Py)amide@POM (**2a**) | 0.97 | 1.58 | 0.61 | 0.48 | 0.63 | 0.15 | 1.08 | 1.80 | 0.72 |
| *p*-CF$_3$(Py)amide@POM (**2b**) | 0.93 | 1.55 | 0.62 | 0.59 | 0.71 | 0.12 | 1.06 | 1.77 | 0.72 |

**Table 3. 4-** Assessment of the difference of charge transfer between the POM unit and the organic grafted moiety, with three different population analysis.

The difference between the acidic and basic moities is higher for compounds with a donating substituent, which proves its role to stabilize the form with an H$^+$.

Moreover, no significative difference in the atomic charge distribution was found between the Phenyl-substituted amides@POM and the pyridine-substituted ones. This confirms that in presence of the electron-poor pyridine ring, the down-field shift of the amidic proton resonance is probably due to a difference in the anisotropy cones compared to arenes, with respect to the electrowithdrawing property of the pyridine ring.

### 3.3.4    Conclusions

*To summarize, we demonstrated that the catalytic activity as Brønsted acid, along all the series of hybrid diolamides@POM synthesized by Dr. David Lachkar, arises from the conjugation between the organic ligand and the polyoxometalate structure. Indeed, the acidity of the amide proton is exalted upon grafting to the vanadium-oxide crown of a Dawson vanadotungstate, thanks to the electro-withdrawing character of the POM, and its ability to act as electron reservoir.*

*Moreover, the catalytic proton is located on the amidic nitrogen, opening the way for the successive creation of a chiral pocket around it, to perform asymmetric reactions.*

## 3.4 Ureas@POM as Brønsted acid catalysts

### 3.4.1 Introduction

In light of the interesting results showed in the previous part, we decided to synthesize a new series of organo-POMs by grafting various diolurea derivatives into the crown of the same Dawson polyoxotungstovanadate.

The double hydrogen-bonding motif is a powerful tool in organocatalysis for the activation of carbonyl groups and related compounds through weak hydrogen-bond interactions.[27] Considering the various molecular scaffolds that have proved effective as bidentate hydrogen-bond donors, urea- and thiourea-derived catalysts are certainly amongst the most competent structures.[28–30]

Our idea was to test how the inorganic scaffold can tune the catalytic acid activity of the ureic protons. Indeed, ureas have an extra nitrogen atom that makes them very different from amides: where the amide-inserted derivatives will react as a regular Brønsted acid, the ureas could react by H-bonding activation only.

In general, during the course of a reaction, hydrogen bonding can be used to stabilize anionic intermediates and/or transition states. Alternatively, some catalysts can bind small anions, enabling the formation of reactive electrophilic counterions. More acidic donors can act as general or specific acids, which activate electrophiles by protonation.[31]

In biological systems, hydrogen bonding plays a key role in many enzymatic reactions, both in orienting the substrate molecules and lowering barriers to hard reaction.

New reactions catalyzed by hydrogen bond donors are being discovered, including asymmetric variants of common organic reactions useful for synthesis,[31] such as aldol additions,[32] Diels-Alder cycloadditions,[33,34] Mannich reactions, Friedel-Crafts alkylations,[35] Strecker reactions[36] and more recently N-H arylation.[37]

In 2011, Oble et al. developed a family of carbonyl-inserted organo POMs, based on amides, ureas, carbamates, and thiocarbamates, by grafting the organic moiety into the vanadate crown of the Dawson $[P_2V_3W_{15}O_{61}]^{9-}$.[38]

In that case they investigated the influence of the organic substituent on the oxidation power of the polyoxometallic structure. The organo-POMs were employed for the oxidation of sulfides, finding that the chemoselectivity depends primarily on the proton content of the POM, but it was also influenced by the organic substituent.
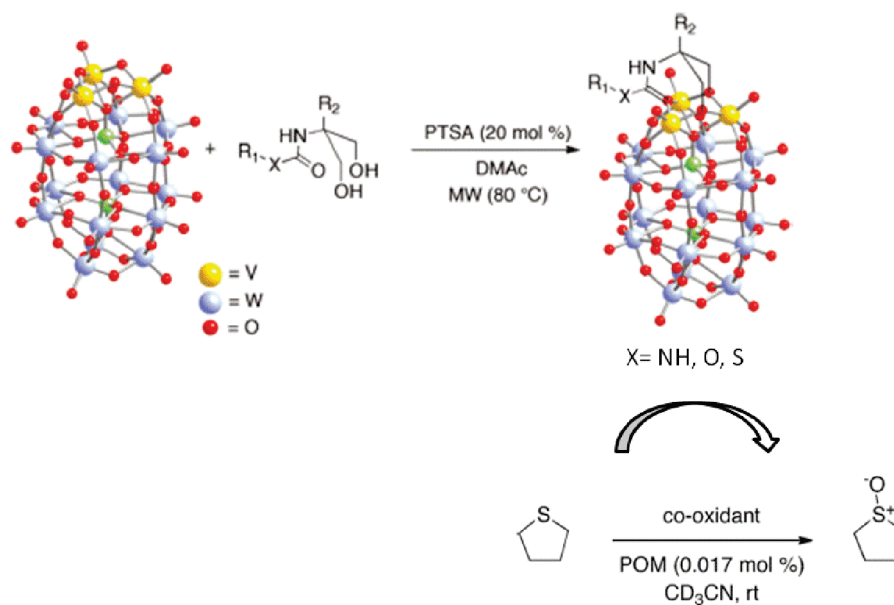


**Figure 3. 16-** Carbonyl-inserted organo-POMs employed for the oxidation of sulfides by Oble et al.

Inspired by this new family of carbonyl-inserted organo-POMs, we decided to investigate whether they could act as urea catalysts for organo-catalyzed addition.

*In the next paragraphs, the synthesis of new POM@ureas derivatives will be shown followed by their application as H-bonding activation catalysts in the Friedel-Craft alkylation of Indoles with trans-β-nitrostyrene.*

131

### 3.4.2    Synthesis of urea-inserted organo-polyoxotungstovanadates

We started with the synthesis of the diolurea ligands to be grafted onto the inorganic scaffold.

Four different diolurea ligands have been synthesized. We changed the substituents on the Phenyl ring, to cover the entire range of electronic properties, which might affect the catalytic activity of the urea group (**1-2**). Moreover, with the aim to synthesize a dimeric catalyst, the hexamethylene bis-diolurea (**3**) was also synthesized, followed by the respective single site derivative hexamethyldiolurea (**4**).

The synthetic strategy relies on the reaction between the 2-amino-2-ethyl-1,3-propane diol and the respective (bis)isocyanates, in THF.
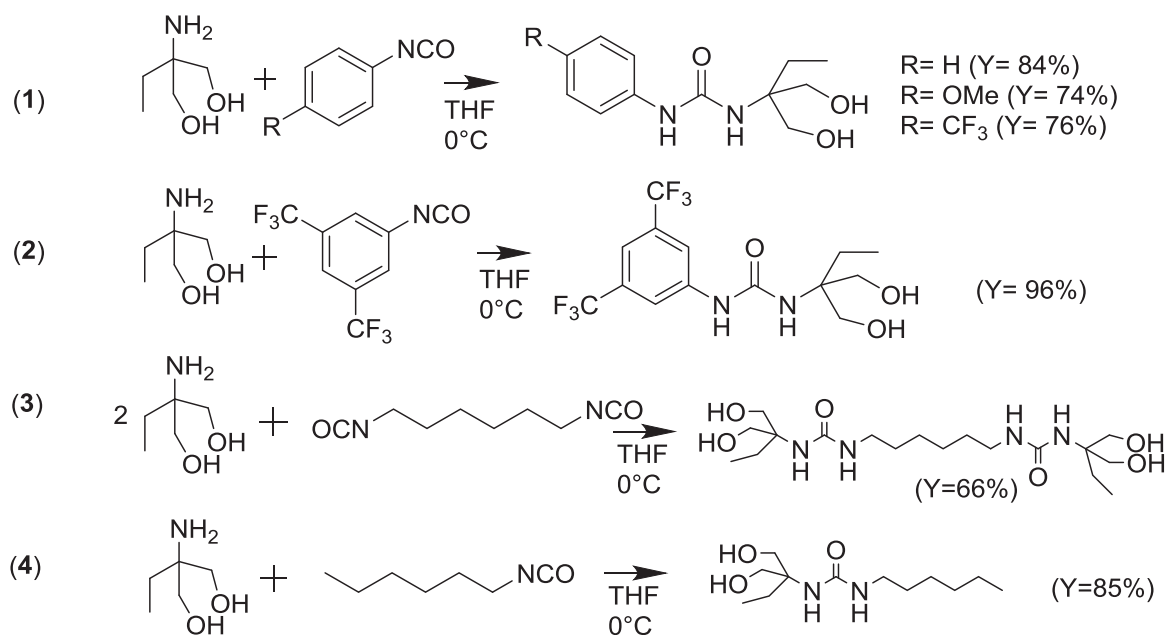


**Scheme 3. 4-** Ureic ligands synthesis

The reaction products were isolated through centrifugation after having been precipitated from the reaction solution with brine and thus were obtained pure in high yields.

Successively these ligands were grafted into the polyoxotungstovanadate with our established method.[38] The polyoxometalate (1eq) is solubilized in a microwave vial with 600 μL of dimethylacetammide (DMA) in presence of 1,5eq of diolurea

and 0.2eq of p-toluensulfonic acid (PTSA). The mixture is then heated at 80°C under microwave irradiation for ~105 minutes.



R=Ph (Y= 90%)
R=p-OMe(Ph) (Y= 95%)
R=p-CF$_3$(Ph) (Y= 89%)
R=3,5bisCF$_3$(Ph) (Y= 87%)
R=hexamethyl (Y= 92%)

R= (Y= 75%)
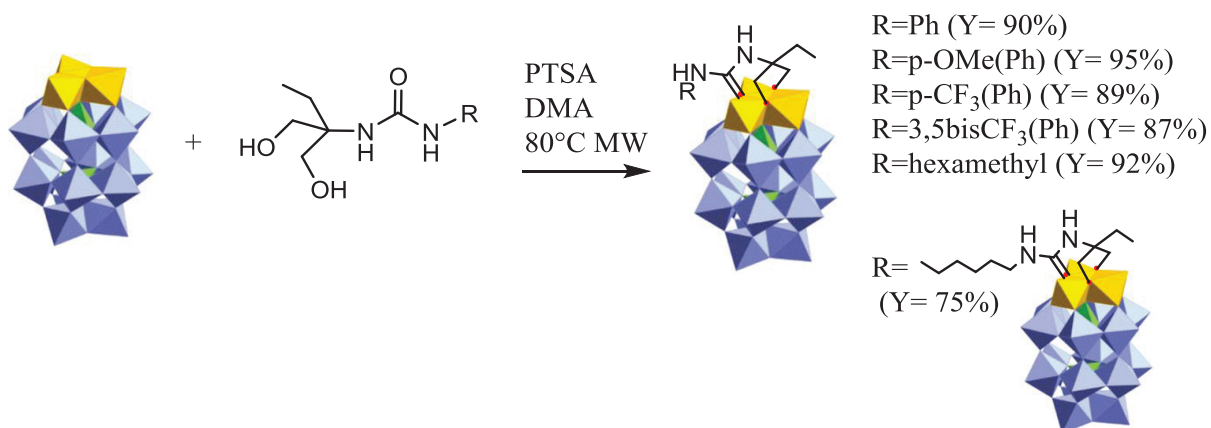
**Scheme 3. 5**- Synthetic pathway for the grafting of diolurea ligands into the vanadate crown of polyoxotungstovanadate. Reaction conditions: 1eq POM + 1.5 eq diolurea + 0.2 eq PTSA in 600 μl of DMA, under MW irradiation for ~105 minutes at 80°C.

All the $^1$H-NMR spectra of the isolated products showed the expected downfield shift of the doublet signals of the two CH$_2$ groups directly bound to the grafted oxygen atoms of the diol and an important downfield shift of the ureic protons signals, with respect to the corresponding free diolurea (more details in the next paragraph).

Moreover, following the same strategy two different diolthiourea ligands were synthesized: (Ph)thiodiolurea, *p*-OMe(Ph)thiodiolurea.

The idea was to try to insert the sulfur atom inside the vanadate crown maintaining the electronic conjugation between the organic and inorganic scaffold through the sulfur atom.

Unfortunately, after the microwave irradiation to graft them into the POM crown, the $^1$H-NMR suggested us that only the two oxygen atoms of the diolthiourea were anchored onto the vanadate, while the C=S group remained free. No shift in the H-N ureic signals was found after the MW irradiation, with respect to the free-thiourea moiety, sign that no insertion of the C=S into the POM had taken place.
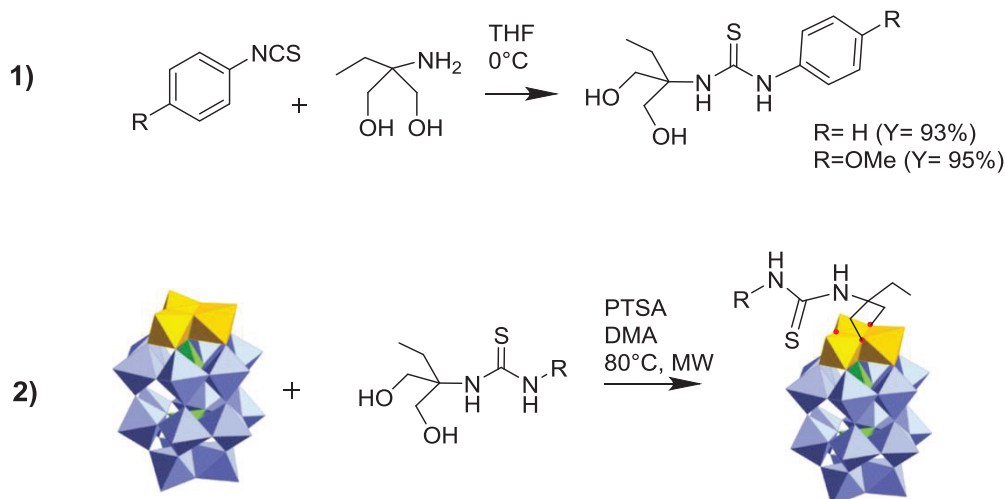
**Scheme 3. 6**- Synthetic reaction scheme for R-Thiourea@POM. The sulfur atom isn't grafted in the POM structure after the MW irradiation.

A second coupling reaction on this derivative was done in presence of benzyl alcohol (1eq) to see if it was possible to obtain a mixed triol.

After 105 minutes of MW irradiation the $^{31}$P-NMR showed 4 peaks. We then tried to perform a recrystallization in diethyl ether vapours to separate the different hybrid complexes. The obtained yellow crystals were dissolved and analyzed by NMR: they presented only 2 peaks in the $^{31}$P-NMR spectrum and the $^{1}$H-NMR showed that in the collected POM-derivative only one benzyl alcohol group was present as organic moiety. It seems that the benzyl alcohol displaces the (Ph)thiourea moiety anchoring itself on the POM vanadate.
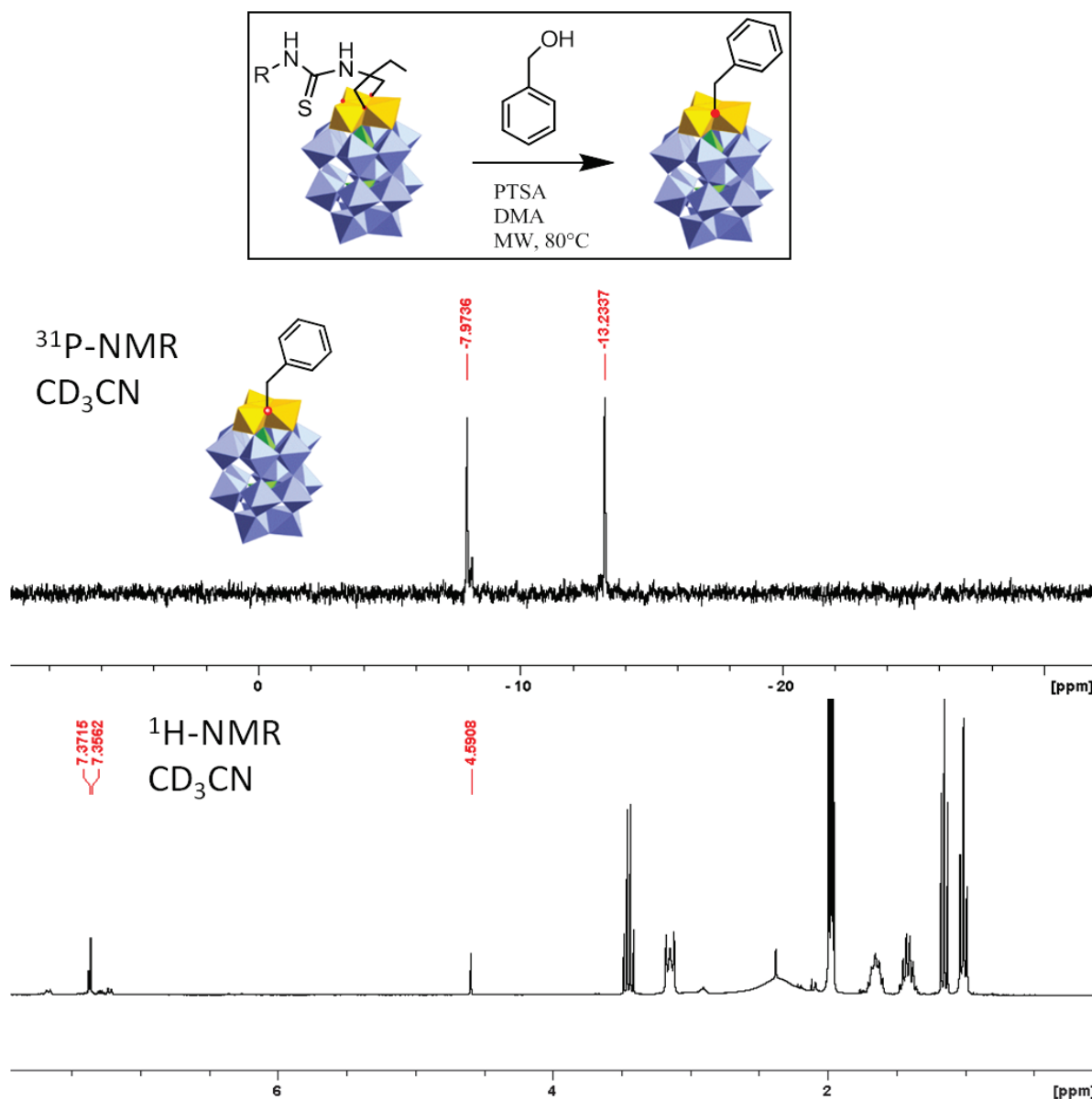
**Figure 3. 17-** Coupling reaction scheme between (Ph)thiourea@POM and benzyl alcohol. The ³¹P-NMR and ¹H-NMR spectra, after the work-up and the re-crystallization in diethyl ether vapors, show that only the benzyl alcohol is grafted on the POM.

Since the grafting of the benzyl alcohol alone was not our aim, we did not investigated more in detail the obtained product.

When (Ph)diolurea was added to the benzyl alcohol@POM only the normal (Ph)urea@POM was observed: the (Ph)diolurea moiety removes the benzyl alcohol.
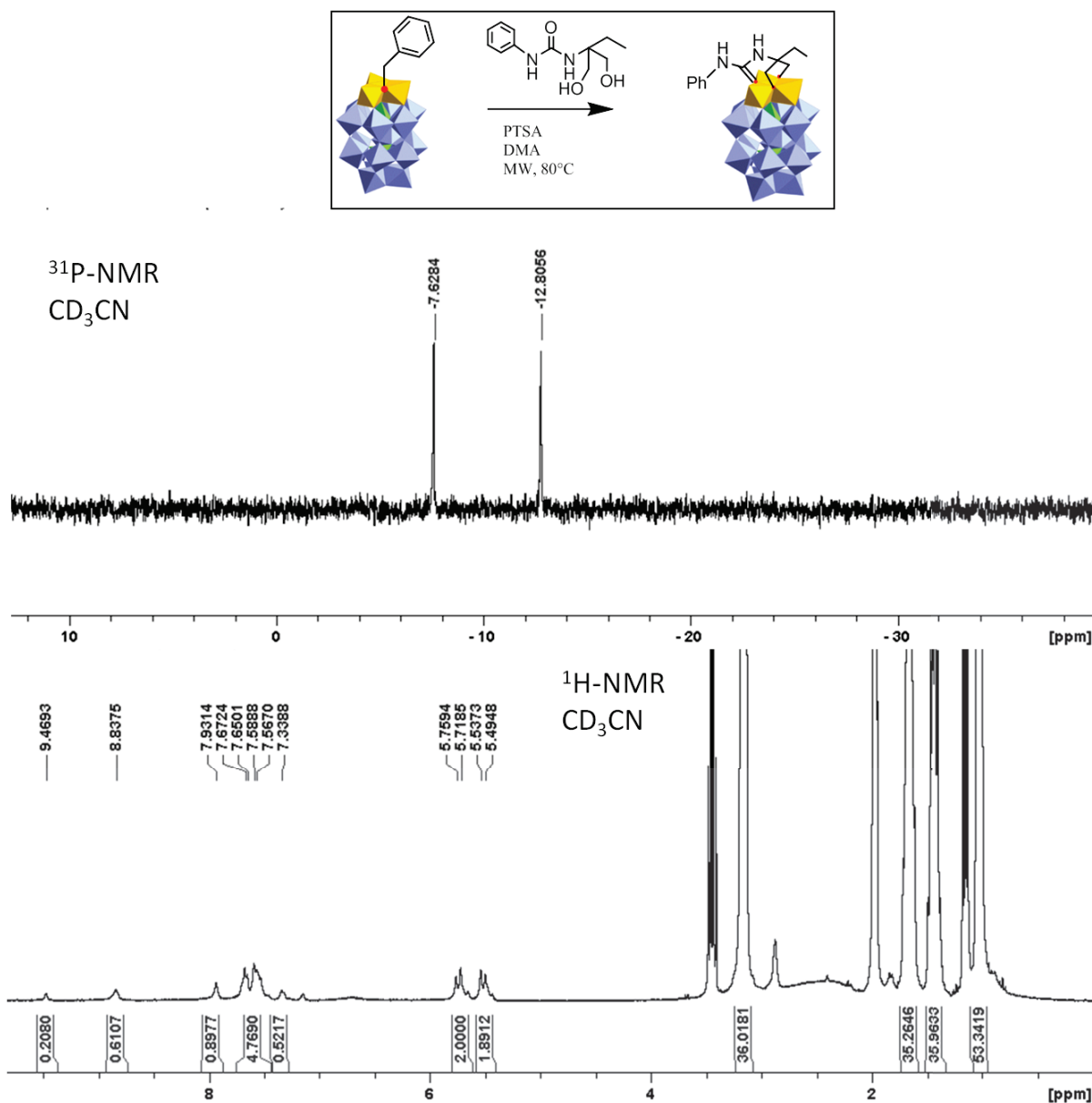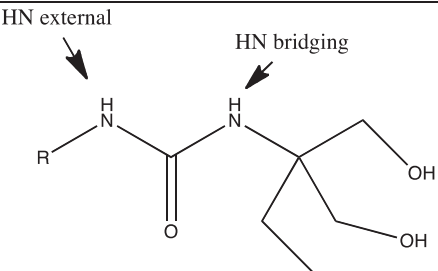
**Figure 3. 18-** Coupling reaction scheme between (Ph)CH₂@POM and (Ph)diolurea. The ³¹P-NMR and ¹H-NMR spectra after the work-up show that only the (Ph)diolurea is grafted on the POM.

Because we had no clear structure with the thio-derivatives we focus our ottention only on the catalytic activity of the POM@diolurea.

### 3.4.3 Investigation of the catalytic activity

The ¹H-NMR spectrum of these new organo-POMs shows an important downfield shift of the ureic proton signals once the organic ligand is anchored to the vanadate crown of the inorganic molecule. The ¹H-NMR resonances of the ureic

protons in the free and grafted form are collected in the table below. 2D $^1$H-$^1$H COSY, $^1$H-$^{13}$C HMBC sequences have been used to definitively assign the ureic protons resonances.

| Organic ligand | δ shift for free diolurea | | δ shift for urea@POM | |
|---|---|---|---|---|
| | HN bridging | HN external | HN bridging | HN external |
| (Ph)diolurea | 5.43 | 7.38 | 9.64 | 8.63 |
| *p*-OMe(Ph)diolurea | 5.33 | 7.05 | 9.23 | 8.45 |
| *p*-CF$_3$(Ph)diolurea | 5.67 | 7.86 | 9.79 | 8.80 |
| 3,5-bis-CF$_3$(Ph)diolurea | 5.76 | 8.07 | 10.1 | 9.10 |
| (Hexamethyl)diolurea | 5.29 | 5.18 | 7.18 | 6.85 |
| Hexamethylen-bis-diolurea | 5.30 | 5.14 | 7.21 | 6.90 |

**Table 3. 5-**Ureic proton resonances for the free ligands and the respective urea-grafted POM. Spectra recorded at 600 MHz. Concentration samples 10mM, in CD$_3$CN at 298K.

Table 3.5 shows that the chemical shift for the bridging ureic protons ranges from 5.29 ppm for the (hexamethyl)diolurea and 5.76 ppm for the 3,5bis-CF$_3$(Ph)urea when the urea is free, and 7.18 ppm for the (hexamethyl)urea@POM and 10.1 ppm for the 3,5bis-CF$_3$(Ph)urea@POM, when the organic ligand is grafted into the POM crown. In the same manner the chemical shift of the external ureic proton ranges from 5.14 ppm for the (hexamethylen)diolurea derivative and 8.07 ppm for the 3,5bis-CF$_3$(Ph)diolurea to 6.85 ppm for the hexamethylurea@POM and 9.10 ppm for the 3,5bis-CF$_3$(Ph)urea@POM. A first observation of the chemical shifts of the aromatic derivatives after the grafting into the POM crown suggests that the diolurea group electronically interacts with the POM vanadate crown, which electrowithdraws the electron density on the ureic proton and downfield shifting the proton resonances.

The down field shift of the ureic proton signals could indicate an increase in the acidity of the two protons upon grafting.

Considering the H-bonding activation properties of the ureas, we decided to test our organo-POM catalysts toward a benchmark reaction, generally catalyzed by electron-poor substituted (thio)urea: the Friedel-Crafts alkylation of indole with trans-β-nitrostyrene (TBNS).[35]
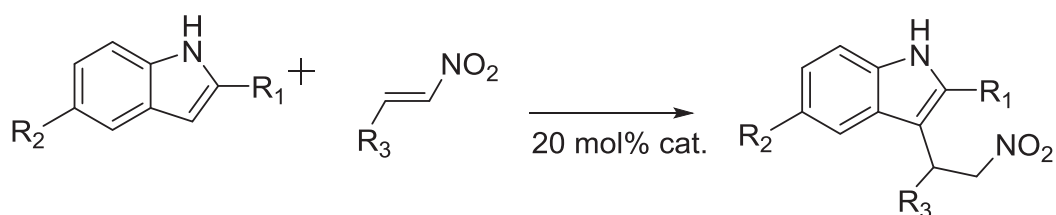


**Scheme 3. 7-** Friedel-Crafts alkylation of indole with TBNS generally catalyzed by (thio)urea as organo-catalyst.

The proposed catalytic process provides the activation of the nitro-group of the TBNS through hydrogen-bonds with the urea protons of the catalyst, this induces the polarization of the bonds in the olefinic substrate which in turn promotes the nucleophilic insertion of the indole ring into the β-carbon of the TBNS.

## A. *NMR investigation of the catalytic activity*

The first step of the catalysis is the interaction between the two hydrogen atoms of the urea moiety and the nitro-group of the TBNS. We tried to monitor this interaction through a $^1$H-NMR titration: if we observe a shift of the ureic proton signals upon addition of TBNS this could evidence an interaction of the ureic protons with the nitro group.[39]

We thus titrated a CD$_3$CN solution of *p*-OMe(Ph)urea@POM, (Ph)urea@POM, *p*-CF$_3$(Ph)urea@POM, 3,5bis-CF$_3$(Ph)urea@POM and the relative free diolurea ligands at 298 K with trans-β-nitro styrene, monitoring the $^1$H-NMR spectrum after each addition (additions from 0.25eq to 2eq of TBNS).

The titration with TBNS of *p*-OMe(Ph)urea@POM, (Ph)urea@POM, free OMe(Ph)urea and free (Ph)urea did not lead to any observable change in the ^{1}H-NMR spectrum of the catalyst as is shown in the Figure 3.19 below. This does not confirm the presence of an interaction but it also does not exclude it: it is still possible that the interaction is weak for the sensitivity of the NMR technique.
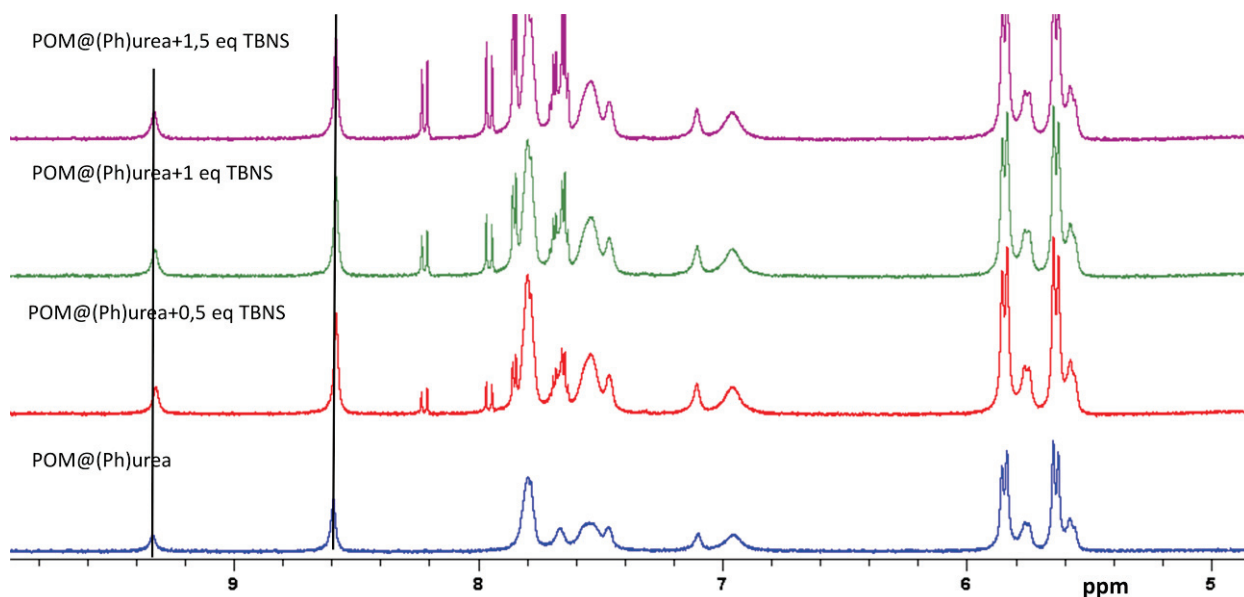


**Figure 3. 19**- ^{1}H-NMR spectra superposition of titrated $CD_3CN$ solution of POM@(Ph)urea (8mM) with a $CD_3CN$ solution of TBNS. Spectral width between 5 and 10 ppm to investigate the ureic proton signals shift. The vertical black lines are centered on the ureic proton signals of the catalyst. (Spectra recorded at 600 MHz, in $CD_3CN$, at 298K).

Conversely, when we investigate the electron poorer *p*-CF$_3$(Ph)urea@POM, 3,5bis-CF$_3$(Ph)urea@POM, free *p*-CF$_3$(Ph)diolurea and free 3,5bis-CF$_3$(Ph)urea we observed relevant NMR shifts. In all this four investigated systems the ureic protons signals were slightly affected during ^{1}H-NMR titration with TBNS. Interestingly, the titration of the two free ligands showed that the ureic protons signals were significantly influenced by the presence of the TBNS. The interaction between ureic protons and TBNS is possible but when the urea is grafted on the POM it becomes much less important.

This suggests that the urea@POM are less Brønsted acid than the respective ligands!

The superposition spectra of the titrated solutions of *p*-CF$_3$(Ph)urea and *p*-CF$_3$(Ph)urea@POM with TBNS are shown in the Figure 3.20 below.

The ureic protons signals of the free ligand are more affected by the presence of the TBNS, with a downfield shift of ~10 Hz for the signal at 5.67 ppm, after the addition of 1.5 equivalents of TBNS. Concerning the titration of *p*-CF$_3$(Ph)urea@POM, the ureic protons signals are still affected but much less, with the signal at 8.98 ppm that is downfield shifted of about 3 Hz after the addition of 1.5 equivalents of TBNS, while the second ureic proton signal at 7 ppm is too broad to be correctly exploited.
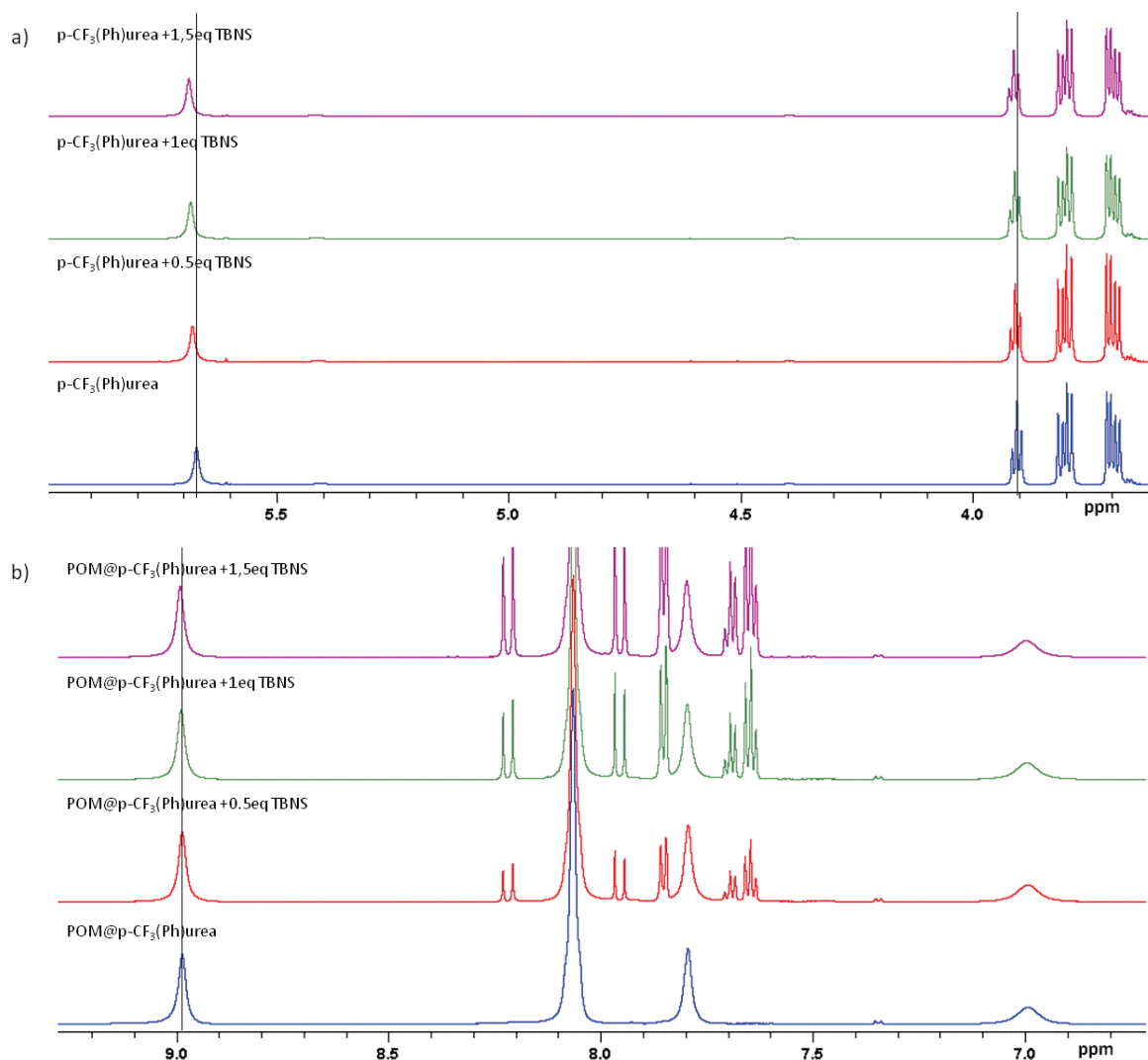


**Figure 3. 20-** $^1$H-NMR titration with TBNS of a) free *p*-CF$_3$(Ph)urea (8mM) and b) *p*-CF$_3$(Ph)urea@POM (8mM). Spectra recorded at 600 MHz, in CD$_3$CN, at 298K. We reported the region comprised between 6 and 3.5 ppm for a) and between 6.8 and 9.3 ppm for b) to evidence the ureic resonances. The vertical black lines are centered on the ureic proton signals of the catalyst.

A similar trend was observed for the 3,5bis-CF$_3$(Ph)diolurea and 3,5bis-CF$_3$(Ph)urea@POM: the ureic proton signals of the free ligand are more affected (downfield of ~8.5 Hz for the peak at 8.07 ppm) with respect to the organo-POM (downfield shifts is possible but it is hardly measurable because the resonances are too broad, probably because of the presence of water).

Even if the shifts of the ureic signals were only slightly affected, we decide to estimate the binding constant between the urea moiety and the nitro-group of the TBNS for the $p$-CF$_3$(Ph)urea and 3,5bis-CF$_3$(Ph)urea free ligand and the $p$-CF$_3$(Ph)urea@POM derivative.

Indeed, in a regime of fast exchange in the NMR time scale, the NMR shift is related to the relative concentration of bound and free form, thus with an NMR titration is possible to derive information about binding constant. The equation below allows one to inversely relate the signal shift in the frequency of the titrated solution ($\Delta\omega$) to the concentration of the added compound (C$_{TBNS}$).

$$C_L = C_{CM} * \Delta\omega_M / \Delta\omega_{P-} K_d$$

Where C$_L$ is the concentration of the added compound, C$_{CM}$ is the concentration of the titrated compound, $\Delta\omega_M$ is the chemical shift of the proton involved in the complexation in the starting material (ureic proton shift in the starting sample), $\Delta\omega_P$ is the difference in the resonance frequence of the proton involved in the complexation during the titration, and K$_d$ is the dissociation constant.[39,40]

Then, plotting the inverse ratio of the variation in resonance frequency of the ureic proton $\Delta\omega_P$, to the concentration of the added TBNS C$_L$, the intercept along the y axis of the corresponding linear correlation gives us information about the dissociation constant K$_d$ and consequently the association constant between the two compounds involved in the titration.

The plot obtained in the case of the titration of the $p$-CF$_3$(Ph)urea@POM with TBNS is reported in the Figure 3.21 below.
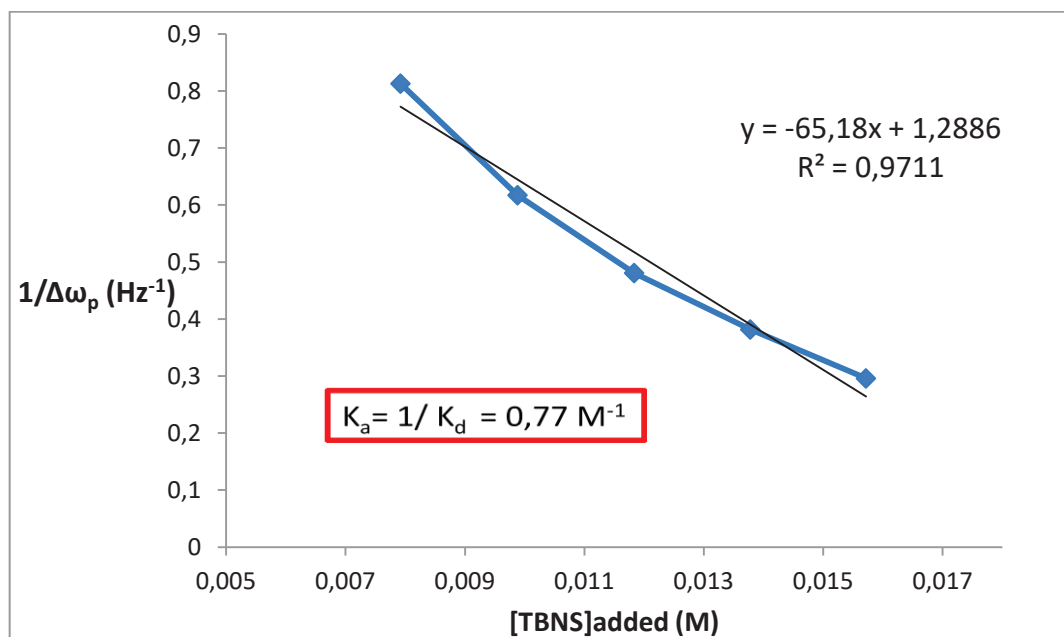
**Figure 3. 21**- Plot of the linear correlation between the inverse of the frequency shift of the ureic proton of *p*-CF$_3$(Ph)urea@POM and the concentration of the added TBNS, that cause the signal shift.

A small association constant of 0.77 M$^{-1}$ was estimated in this case. The free ligand had a binding constant almost one order of magnitude higher in the case of the corresponding free ligand *p*-CF$_3$(Ph)urea (4.43 M$^{-1}$). It was 3.85 M$^{-1}$ for the free 3,5bis-CF$_3$(Ph)urea. For the corresponding POM derivative (3,5bis-CF$_3$(Ph)urea@POM) a small shift of the ureic protons signals was observed, but the signals were too broad to estimate the $\Delta\omega$ in Hz.

The small association constants between the catalysts and the olefin substrate estimated through NMR titrations suggest a labile interaction between the two molecules. At this stage, a labile interaction could have a positive and/or a negative consequence for catalysis:

- The two molecules do not interact efficiently to perform the catalytic Friedel-Crafts alkylation of indoles, probably because of the negative charge of the inorganic catalyst and the partial negative charge of the nitro group of the olefinic substrate, which would be a negative factor;

-       The small association constant found here is a sign of a promising catalytic activity, considering that the substrate does not remain attached to the catalyst surface, allowing easy turnover, which would be a positive factor.

## B.    Catalysis

We started trying to perform the reaction between TBNS and Indole at room temperature under air in presence of (Ph)urea@POM as catalyst.

After 9 days however no conversion of the TBNS was observed by $^1$H-NMR. The same happens in presence of the corresponding free ligand which did not catalyze the reaction under these conditions.

Then the temperature was raised and the same test performed at 50°C under air, in the presence of the same catalysts: also in this case no conversion of the substrates was observed through $^1$H-NMR after 5 days.

Finally we performed the reaction in a dry solvent in a closed Schlenk tube under argon, at 50°C: in these conditions a conversion of the reagent was recorded after 24h. We selected these conditions for the rest of our studies. We believe water is the main inhibitor in the previous unsuccessfull runs. Water solvate the nitro group of the substrate, thus limiting the substrate-catalyst interaction or influence the catalyst solubility in the organic media.

It is important to highlight that the amount of catalyst used (2%) is kept small with respect to the general protocol followed for similar organo-catalyzed reactions (20%).[35] This is done to be sure of the homogeneous environment in the reaction mixture, and also because of the high molecular weight of the catalyst. On the other hands this represents a very low loading for an organo-catalyzed reaction.
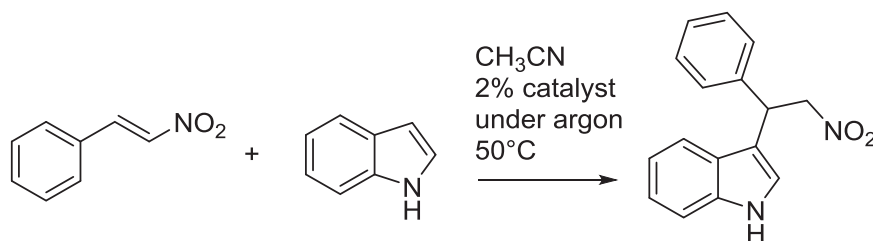
**Figure 3. 22**- Benchmark reaction chose to test the catalytic activity of the syntesized organo-POMs toward the acid H-bonding activation of the olefinic substrate.

Gratifyingly, all the organo-POMs catalysts resulted active toward the Friedel-Crafts alkylation of the Indole with the trans-β-nitrostyrene.

| Used Catalyst | TBNS Conversion estimated through $^1$H-NMR | | | | Yield |
|---|---|---|---|---|---|
| | 24h | 48h | 72h | 96h | |
| *p*-OMe(Ph)urea@POM | 6% | 13% | 33% | 46% | |
| (Ph)urea@ POM | 7% | 25% | 44% | 66% | |
| *p*-CF$_3$(Ph)urea@POM | 18% | 52% | 99% | | 92% |
| 3,5bis-CF$_3$(Ph)urea@ POM | 16% | 54% | 98% | | |
| (hexamethyl)urea@POM | - | 14% | 37% | 48% | |
| Hexamethylen@bis-POM-urea | 11% | 26% | 42% | 56% | |

**Table 3. 6**- TBNS conversion in presence of different catalysts. <u>Reaction conditions</u>: 60 mg TBNS (0.4mmol), 72 mg Indole (0.6mmol), 2% cat(8μmol). Dissolved in 1 ml of CH$_3$CN-dry in a conditionated schlenk tube. Under argon at 50°C. Product obtained through FC using n-hexane:ethyl acetate 90:10 as eluent.

As it is possible to see from the Table 3.6 all the POMs performed the catalysis. The reaction time depends on the nature of the grafted urea.
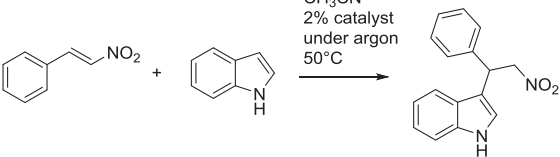
The stronger is the electrowithdrawing substituents on the aromatic ring, the more active is the catalyst toward the Friedel-Crafts alkylation. In particular, the *p*-CF$_3$(Ph)urea@POM and the 3,5bis-CF$_3$(Ph)urea@POM succeeded to totally convert the TBNS substrate after 72h, while the other organo-POM derivatives, with an electrodonating group in the aromatic ring or an alkyl chain, require more time to totally convert the substrate.

When the catalysis was carried out in presence of 1% of Hexamethylen@bis-POM-urea as catalyst an interesting improvement of TBNS conversion was recorded

with respect to the single site derivative (POM@(hexamethyl)urea, 2%), although the improvement was not linear. This is an interesting sign of the possibility to develop double site catalysts to improve the catalytic efficiency.

The difference in the TBNS conversion rate obtained in the presence of different organo-POMs as catalyst (for example, with electrowithdrawing/electrodonating substituents on the phenyl ring), is already a sign that the catalytic activity arises from the ureic protons of the grafted organic ligand. Indeed, if the catalytic activation of TBNS was due to the protons present as counterions around the polyoxometalate surface, no difference in the TBNS conversion rate should be recorded with a change in the organic moiety, since it is too far from the catalytic site to be able to influence it.
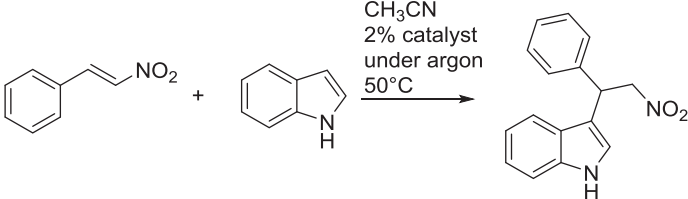
To effectively establish the role of the interplay between the organic and inorganic part of the organo-polyoxometalates, some control experiments were also performed. First of all we tested all the free diolurea ligands toward the Friedel-Crafts alkylation of Indole, in the same reaction conditions, estimating also in this case through ^{1}H-NMR the trans-β-nitrostyrene conversion during the reaction.



| Used Catalyst | TBNS Conversion estimated through ^{1}H-NMR | | |
|---|---|---|---|
| | 24h | 48h | 72h |
| *p*-OMe(Ph)diolurea | - | - | 6% |
| (Ph)diolurea | - | - | 7& |
| *p*-CF$_3$(Ph)diolurea | - | - | 5% |
| 3,5bis-CF$_3$(Ph)diolurea | - | - | 6% |
| (hexamethyl)diolurea | - | - | 6% |
| Hexamethylen-bis-diolurea | - | - | 9% |

**Table 3. 7**- TBNS conversion in presence of the different free diolurea ligands as catalysts. <u>Reaction conditions</u>: 60 mg TBNS (0.4mmol), 72 mg Indole (0.6mmol), 2% cat (8μmol). Dissolved in 1 ml of CH3CN-dry in a conditionated schlenk tube. Under argon at 50°C.

As it is possible to see from the Table 3.7, all the organo ligands are almost inactive, giving a substrate conversion of max 9% after 72h of reaction, while the less active organo-POM (*p*-OMe(Ph)urea@POM) reaches 33% conversion of TBNS in the same time (see Table 3.3). Moreover, also in the case of the free urea-ligand the reaction in presence of 1% of hexamethylen-bis-diolurea as catalyst shows a TBNS convertion (9%) higher than the one obtained with the double amount of the respective single-site catalyst (2% of hexamethyl diolurea). As we have seen for the respective hybrid-POMs the catalytic effiency is slightly improved with the double-site catalyst.

We thus tested the catalytic activity of the totally inorganic scaffold. Indeed, as mentioned before, four protons are present as counterions around the inorganic scaffold and they are generally available to perform Brønsted acid catalysis, as we have previously described in the introduction, even if less efficiently.



| Used Catalyst | TBNS Conversion estimated through $^1$H-NMR | | | |
|---|---|---|---|---|
| | 24h | 48h | 72h | 96h |
| TBA$_5$H$_4$P$_2$W$_{15}$V$_3$O$_{62}$ | 9% | 21% | 35% | 41% |
| TBA$_5$H$_4$P$_2$W$_{15}$V$_3$O$_{62}$+p-CF$_3$(Ph)diolurea | 10% | 15% | 25% | 39% |
| TBA$_9$P$_2$W$_{15}$V$_3$O$_6$ | - | - | - | - |
| Without catalyst | - | - | - | - |

**Table 3. 8-** TBNS conversion in presence of the inorganic scaffold as catalyst (in its protonated and totally deprotonated form, and in presence of a physical mixture of the inorganic molecule and the organic ligand). Reaction conditions: 60 mg TBNS (0.4mmol), 72 mg Indole (0.6mmol), 2% cat (8μmol). Dissolved in 1 ml of CH$_3$CN-dry in a conditionated schlenk tube. Under argon at 50°C.

As expected, the totally inorganic scaffold with four protons on its surface is able to perform the Brønsted catalysis toward the Friedel-Crafts alkylation of the indole. However, it is important to highlight that it achieves a lower TBNS

146

conversion in 96h of reaction than the less active organo-POM (POM@*p*-OMe(Ph)urea). The former gives a 41% while the latter reaches 46%.

The same reaction was carried out in the presence of a physical mixture of POM and free *p*-CF$_3$(Ph)diolurea as catalyst. In that case, the TBNS followed a rate conversion similar to the one obtained in presence of the inorganic molecule alone, sign that the free ligand alone is not acidic enough to perform the H-bonding activation of the nitro-olefin.

We also decided to perform the catalysis in the absence of catalyst but in the presence of the totally deprotonated form of the polyoxometalate. The first observation was that in the absence of any catalyst the Friedel-Crafts reaction doesn't proceed after 96h, and the same happens in the presence of the totally deprotonated POM. The latter was obtained by eluiting a CH$_3$CN solution of our starting POM TBA$_5$H$_4$P$_2$V$_3$W$_{15}$O$_{61}$ on a column prepared with a cationic-exchange Amberlist resin loaded with TBA salts. The elemental analysis confirmed us that TBA$_9$P$_2$V$_3$W$_{15}$O$_{61}$ was obtained after the elution.

All these control experiments confirmed that the catalytic activity arises from the interplay between the organic and inorganic parts of the hybrid-POM. With its electrowithdrawing character the polyoxometalate likely increases the polarization of the N-H bonds, allowing the H-bonding activation of the nitro group of the TBNS, and the consequent C-C coupling to the Indole.

To probe more in detail the catalytic process of the Friedel-Crafts alkylation reaction, we performed the same reaction changing the indole substrate. Indeed, if the catalysis follows the general catalytic pathway for these types of reactions, the insertion of an electrodonating group on the indole ring should increase the reaction rate (the opposite in presence of an electrowithdrawing group), since it could stabilize the partially cationic intermediate generated on the 2-position of the pyrrole ring, once the hetero-aromatic ring is subject to the electrophilic attack. [35]
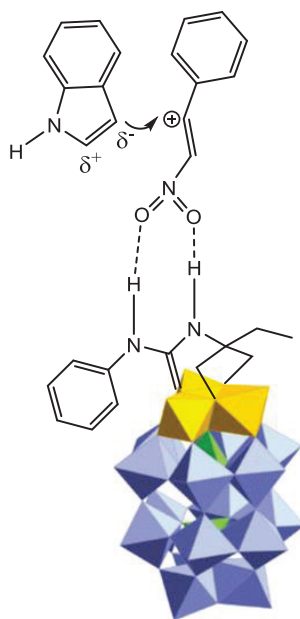
**Figure 3. 23-** Catalytic mechanism aspected for the Friedel-Crafts alkylation of Indole catalyzed by our organo-POMs.

Then, three reactions were carried out in presence of *p*-CF$_3$(Ph)urea@POM as catalyst, using 6-(OMe)Indole, 6-Cl(Indole) and N-methyl Indole as substrates. The TBNS conversion was followed through $^1$H-NMR and the data are collected in the table below.



| Used Catalyst: *p*-CF$_3$(Ph)urea@POM | | | | | | |
|---|---|---|---|---|---|---|
| **Indole substrate** | | **TBNS Conversion estimated through $^1$H-NMR** | | | | **Yield** |
| **R$_1$** | **R$_2$** | **24h** | **48h** | **72h** | **96h** | |
| OMe | H | 28% | 82% | 92% | 99% | 97% |
| Cl | H | 7% | 16% | 63% | 94% | 94% |
| H | Me | 13% | 49% | 61% | | |

**Table 3. 9-** TBNS conversion obtained changing the electronic properties of the indole substrate, in the presence of *p*-CF$_3$(Ph)urea@POM as catalyst. <u>Reaction conditions</u>: 60 mg TBNS (0.4mmol), 72 mg Indole (0.6mmol), 2% cat (8µmol). Dissolved in 1 ml of CH$_3$CN-dry in a conditionated schlenk tube. Under argon at 50°C.

The first observation is that, as expected, the reaction works in the presence of the organo-POM catalyst with all the tested indole substrates.

In particular, when an electrodonating group is present on the phenyl ring of the indole substrate [6-OMe(Indole)], the TBNS conversion rate is faster (82% of conversion after 48h), with respect to the reaction carried out on the simple indole substrate with the same catalyst (52% conversion after 48h- see table 3.3). The opposite happens when an electrowithdrawing substituent is present in the indole: the reaction rate resulted lower in presence of the 6-(Cl)indole (only 16% of TBNS converted after 48h), with respect to the same reaction with indole as substrate.

When the nitrogen of the indole ring is methylated the reaction is slower (only 61% of TBNS is converted after 72h). We believe this shows that our organo-POMs may act as a dual activation catalyst, whereby the urea activates the nitro-olefin and an oxo of the crown directs the approach of the indole by H-bonding, resulting in a rate increase.
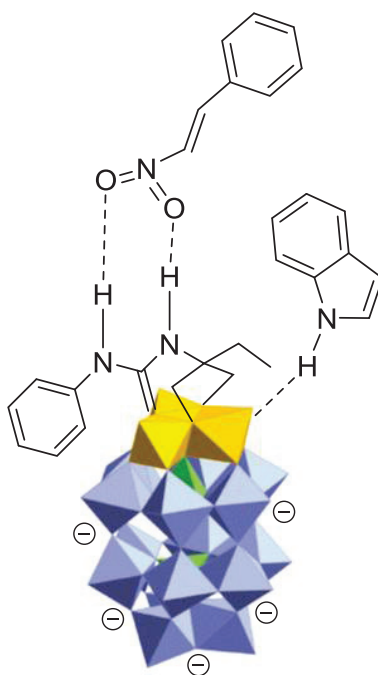


**Figure 3. 24-** Proposed mechanism for the catalytic Friedel-Crafts alkylation of Indoles with TBNS, highlighting the probable role of the nitrogen-bound proton of the Indole.

Another interesting observation of our organo-POMs catalysts was their stability after the catalytic process. Indeed, we observed that the ^{31}P-NMR of the reaction mixture, at the end of the catalysis, presented the same two peaks as the pristine organo-POM. We thus investigated the recycling of the catalyst: the example of the (Ph)urea@POM is presented below.

The catalyst was isolated from the reaction mixture through precipitation with diethylether and successive centrifugation at 5000 rpm. The ^{31}P-NMR spectra of the isolated brown powder showed two single peaks at -7.38 and -13.44 ppm, sign of the maintained stability of the starting inorganic POM structure.
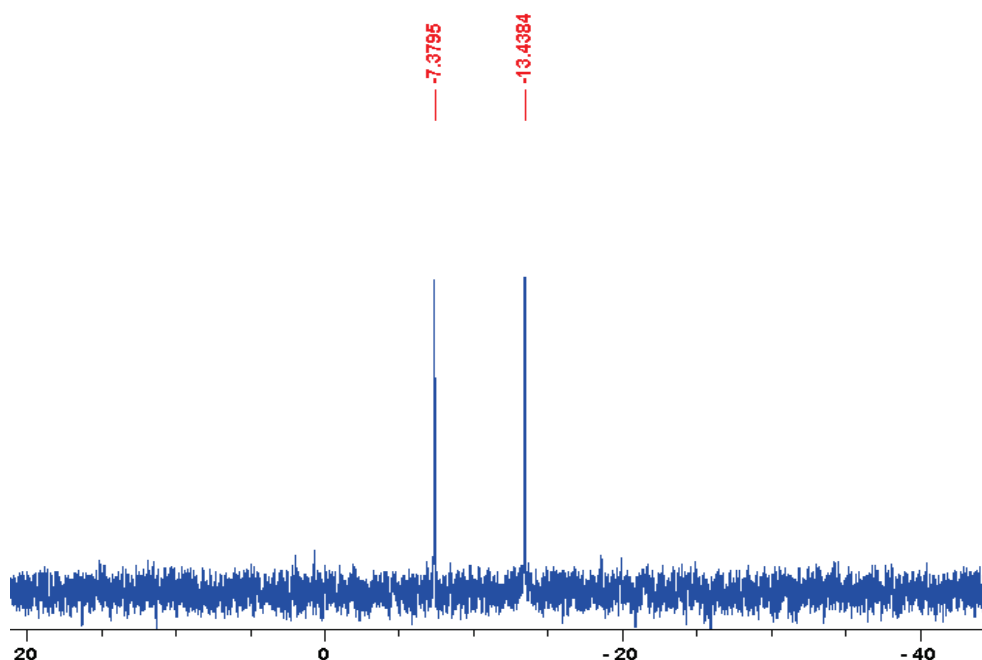


**Figure 3. 25**- ^{31}P-NMR of the recycled (Ph)urea@POM (1mM). Spectrum recorded at 300 MHz, in CD$_3$CN at 298 K

The TBNS conversions during four consecutive catalysis are reported in the plot below. The catalyst was isolated each time through precipitation with diethylether and centrifugation at 5000 rpm.
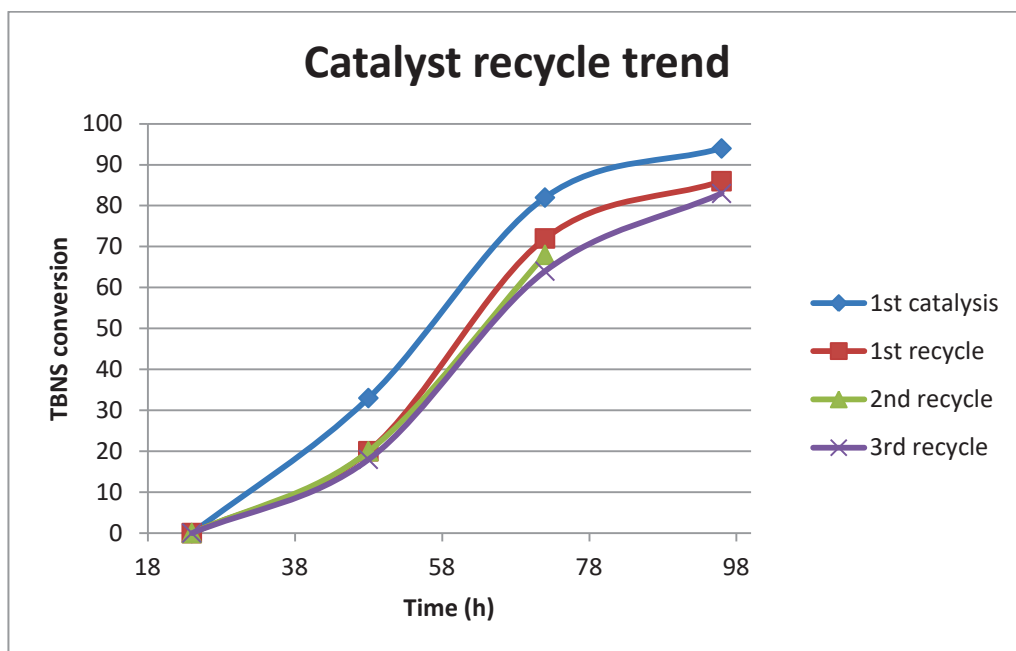
**Figure 3. 26-** TBNS conversion trend, recorded through ¹H-NMR, obtained using a recycled (Ph)urea@POM as catalyst. <u>Reaction conditions</u>: 60 mg TBNS (0.4mmol), 72 mg Indole (0.6mmol), 2% cat(8μmol). Dissolved in 1 ml of CH₃CN-dry in a conditionated schlenk tube. Under argon at 60°C.

The superposition of the TBNS conversion along the reaction time for the three consecutive catalytic reactions, using the recycled catalyst, shows that no significant loss in the activity of the organo-POM is recorded: after the 3rd recycling only 12% of the catalytic activity was lost. These results confirmed the great power of the polyoxometalates to be recycled without any important loss in the catalytic activity.
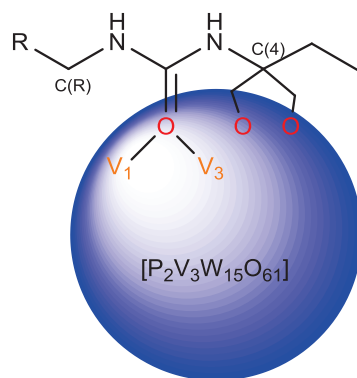
In light of these interesting catalytic results DFT studies were carried out to better understand the catalytic mechanism.

## C. DFT studies

First of all we optimized the structures of the synthesized hybrid-POMs by DFT, at the BP86/LANL2DZ level of theory.
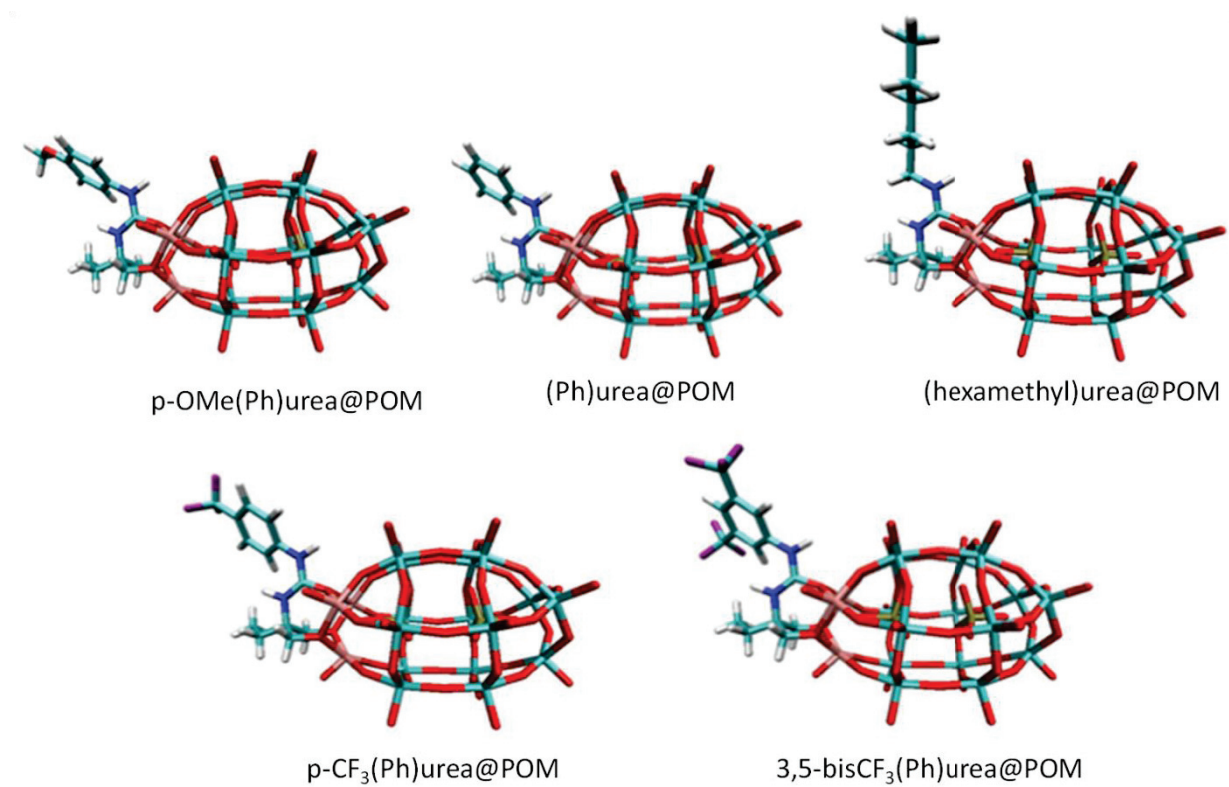
**Figure 3. 27-** Cartoon representation of the different urea@POM optimized structures.



| | d(O-V1) | d(O-V3) | d(N-C(4)) | d(N-C(R)) | d(N-C(O))[a] | d(C=O) | d(N-H (R)) | d(N-H (C(4))) |
|---|---|---|---|---|---|---|---|---|
| **Ph** | 2.15 | 2.15 | 1.51 | 1.45 | 1.36 | 1.34 | 1.03 | 1.03 |
| *p*OMe | 2.15 | 2.14 | 1.50 | 1.45 | 1.36 | 1.34 | 1.03 | 1.03 |
| **Hexamethyl** | 2.13 | 2.14 | 1.50 | 1.49 | 1.35 | 1.34 | 1.02 | 1.02 |
| *p*CF₃ | 2.16 | 2.16 | 1.51 | 1.43 | 1.37 | 1.33 | 1.03 | 1.03 |
| **bis-CF₃** | 2.16 | 2.16 | 1.51 | 1.43 | 1.37 | 1.33 | 1.03 | 1.03 |

**Table 3. 10-** Schematic representation of the ureic ligands grafted into the inorganic framework (on the top). Optimized bond lengths in Å, characterizing the C=O insertion of the organic ligands into the POM (on the bottom). a)bond length N-C(=O) from the substituent side (C(R)).

As it is possible to see from the Table 3.10, the bond lengths are quite constant along all the series of investigated aromatic-substituted hybrid-POMs. The N-H bond lengths remain the same for all the complexes (1.3 Å). Only slightly differences are observed for the other bonds. In particular, when electrowithdrawing substituents are present in the organo moiety (*p*CF$_3$ or bis-CF$_3$ derivatives) the N-C(R) bonds became shorter (1.43 Å), with respect to 1.45 Å found for *p*OMe and Ph derivatives. Simultaneously, the N-C(=O) bond length is lengthened- 1.37 Å for the *p*CF$_3$ or bis-CF$_3$ derivatives- against 1.36 Å for the *p*OMe and Ph derivatives. The same trend is found for the C=O bond length, which is slightly shorter (1.33 Å) for *p*CF$_3$ or bis-CF$_3$ derivatives, with respect to the *p*OMe and Ph derivatives (1.34 Å).

Different is the case for alkyl-substituted urea@POM. When the aromatic ring is substituted with hexamethyl moiety, the H-N bond length becomes slightly shorter (1.02 Å instead of 1.03 Å), as well as the N-C(=O) bond (1.35 Å, with respect to 1.36/1.37 Å found for the aromatic-substituted hybrids) and parallely the N-C(R) bond length, from the substituent side, became longer (1.49 Å, with respect to 1.43 or 1.45 Å in the other systems). The latter reflects the loss in the conjugation (less sp$^2$ character) with the C=O when the alkyl chain is present with respect to the aryl one.
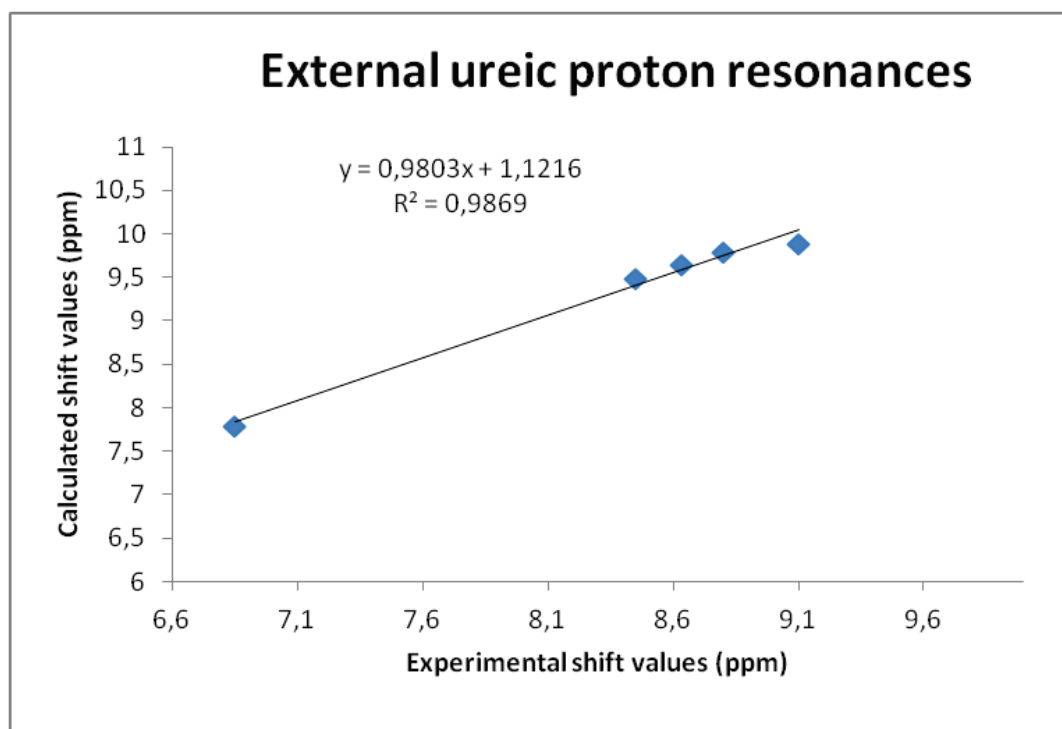
Once the structures were optimized, NMR simulations were run to compare the ureic protons resonances with the experimental values. We then simulated the $^1$H-NMR chemical shifts of the amide protons of all hybrid-POMs using the GIAO protocol, at the PBE1PBE/6-311G**/LANL2DZ//BP86/LANL2DZ level of theory. I include basis set for the organic moiety to compute the NMR displacements.

A first observation of the calculated ureic proton shifts evidences that while the calculated shifts for the external protons are ~1 ppm up-fielded with respect to the respective experimental values, the bridging ureic proton shifts result ~1ppm down-fielded with respect to the experimental values, with the only exception of the bridging proton of the hexyl derivative.

| POM derivative | Bridging ureic proton shifts | | External ureic proton shifts | |
|---|---|---|---|---|
| | Calculated | Experimental | Calculated | Experimental |
| 3,5-bisCF$_3$(Ph)urea@POM | 8.61 | 10.1 | 9.89 | 9.1 |
| $p$CF$_3$(Ph)urea@POM | 8.88 | 9.79 | 9.79 | 8.8 |
| Hexylurea@POM | 8.17 | 7.18 | 7.79 | 6.85 |
| (Ph)urea@POM | 8.72 | 9.64 | 9.65 | 8.63 |
| $p$OMe(Ph)urea@POM | 8.43 | 9.79 | 9.45 | 8.45 |

**Table 3. 11**- Calculated/Experimental ureic proton shift values.

A plot of the theoretical/experimental ureic protons shifts is given in the figures below.



**External ureic proton resonances**

$y = 0{,}9803x + 1{,}1216$
$R^2 = 0{,}9869$

Calculated shift values (ppm)

Experimental shift values (ppm)

**Figure 3. 28**- Plot of the Experimental/Calculated resonances of the ureic protons of the synthesized urea@POM. Linear correlation for the resonances of the external ureic protons.

As it is possible to see from the Figure 3.28, for the external ureic protons a quite good agreement between the calculated and experimental values can be proposed with a deviation in the linear correlation of ~1 ppm.
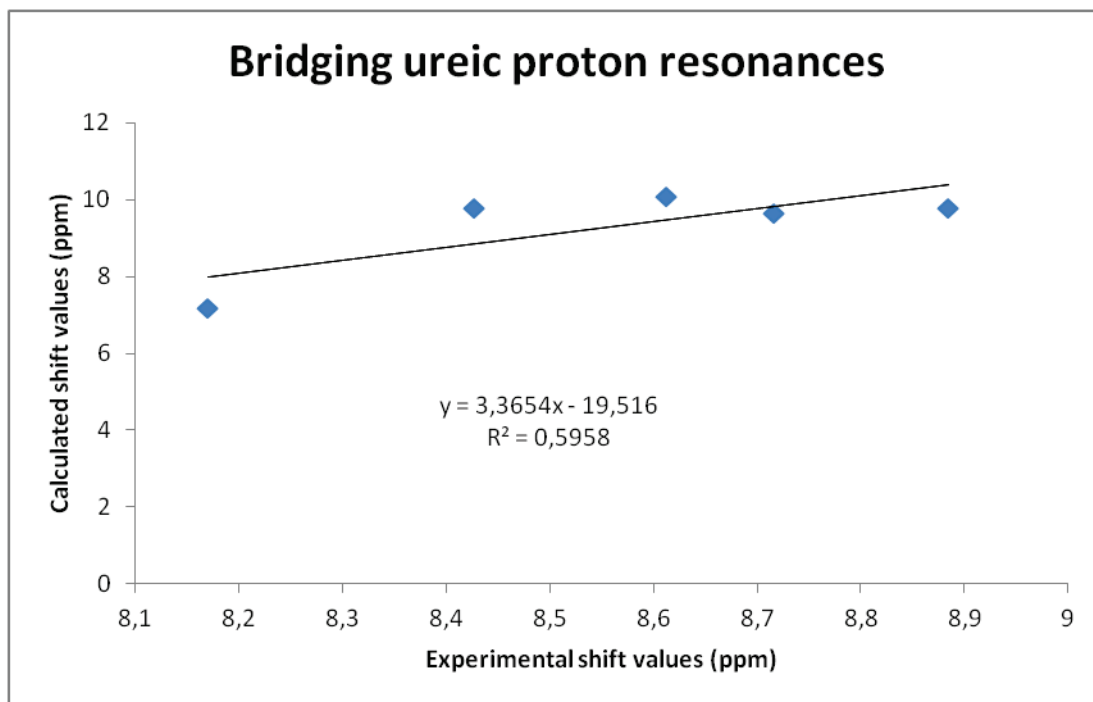


**Figure 3. 29-** Plot of the Experimental/Calculated resonances of the ureic protons of the synthesized urea@POM. Linear correlation for the resonances of the bridging ureic protons.

Different was the case of bridging ureic protons. In this case the deviation in the linear correlation between the experimental and calculated resonance values was quite big. We are currently seeking to increase the level of theory to improve the numerical agreement with the experimental measurements.

We are estimating the charge transfer between the organic and inorganic part of the hybrid in manner to better quantify the improvement in the catalytic activity of the N-H, thanks to the presence of POM which likely acts as electron reservoir as we have seen in the hybrid system investigated before (amides@POM).

### 3.4.4    Conclusions

*A new family of organo-catalytically active hybrid-POM, thanks to the interplay between the organic urea and inorganic moiety has been studied. The catalytic activity arises from the hydrogen-bonding activation by the urea protons of a series of hybrid-POMs. It was demonstrated on the Friedel-Crafts alkylation of indoles with trans-β-nitrostyrene. The electronic conjugation with the polyoxometalate scaffold, which acts as electron-reservoir, improves the ureic protons acidity in the organo moiety (N-H activation) and consequently it allows the Friedel-Crafts alkylation of indole, when the free urea ligands are inactive. A parallel activity is due to the nature of the urea ligand which influences the reaction rate, since electrowithdrawing groups can also improve the acidity of the ureic protons.*

*A secondary activation of the reaction by the POM has been induced. The latter likely wants the approach of the indole via its N-H bond that enters an H-bonding interaction with one of the oxygen atoms of the crown.*

*The catalyst could be successively recycled without any significant loss in the activity even after 3 cycles.*

## 3.5     General Conclusions

In this chapter, we investigated the catalytic acid activity of two families of organo-POMs: amide@POM and urea@POM.

The first family of hybrid POMs (amide@POM) active as Brønsted acid catalyst have been successful developed.[41]

We demonstrated through NMR and DFT simulations that in both cases (amide@POM and urea@POM) the activity as Brønsted acid catalysts arises from the interplay between the organic and inorganic part of the hybrid molecule.

The urea@POM hybrids have been efficiently tested toward the Friedel-Crafts alkylation of Indole in presence of trans-β-nitrostyrene, while the free urea ligands were not able to perform this catalysis. In the amide@POM an achiral proton transfer occurs while the ureas work by using non-covalent interactions.

Last but not least, we have seen that in both families the catalytic site is well confined in the organo moiety. This could open the way to the successive creation of a chiral pocket around it to perform asymmetric acid catalysis.

*In the next chapter we will start our preliminary studies toward the creation of the chiral pocket. Indeed, since the polyoxometalate surface is highly negative charged, it is important to understand how it will interact with the organic ligands targeted to create the chiral pocket.*

## 3.6        Bibliography

[1]    I. V. Kozhevnikov, *Chem. Rev.* **1998**, *98*, 171–198.

[2]    Y.-F. Song, R. Tsunashima, *Chem. Soc. Rev.* **2012**, *41*, 7384.

[3]    D.-L. Long, R. Tsunashima, L. Cronin, *Angew. Chem. Int. Ed.* **2010**, *49*, 1736–1758.

[4]    N. Mizuno, M. Misono, *Chem. Rev.* **1998**, *98*, 199–218.

[5]    J. Jiang, O. M. Yaghi, *Chem. Rev.* **2015**, *115*, 6966–6997.

[6]    M. Misono, N. Nojiri, *Appl. Catal.* **1990**, *64*, 1–30.

[7]    I. V. Kozhevnikov, *Russ. Chem. Rev.* **1987**, *56*, 811–825.

[8]    C. Boglio, G. Lemière, B. Hasenknopf, S. Thorimbert, E. Lacôte, M. Malacria, *Angew. Chem. Int. Ed.* **2006**, *45*, 3324–3327.

[9]    C. Boglio, K. Micoine, P. Rémy, B. Hasenknopf, S. Thorimbert, E. Lacôte, M. Malacria, C. Afonso, J.-C. Tabet, *Chem. – Eur. J.* **2007**, *13*, 5426–5432.

[10]  N. Dupré, P. Rémy, K. Micoine, C. Boglio, S. Thorimbert, E. Lacôte, B. Hasenknopf, M. Malacria, *Chem. – Eur. J.* **2010**, *16*, 7256–7264.

[11]  J. Kaur, K. Griffin, B. Harrison, I. V. Kozhevnikov, *J. Catal.* **2002**, *208*, 448–455.

[12]  T. Tagawa, J. Amemiya, S. Goto, *Appl. Catal. Gen.* **2004**, *257*, 19–23.

[13]  X. Zheng, L. Zhang, J. Li, S. Luo, J.-P. Cheng, *Chem. Commun.* **2011**, *47*, 12325–12327.

[14]  C. Boglio, G. Lemière, B. Hasenknopf, S. Thorimbert, E. Lacôte, M. Malacria, *Angew. Chem. Int. Ed.* **2006**, *45*, 3324–3327.

[15]  E. Derat, E. Lacôte, B. Hasenknopf, S. Thorimbert, M. Malacria, *J. Phys. Chem. A* **2008**, *112*, 13002–13005.

[16]  J. Das, K. M. Parida, *J. Mol. Catal. Chem.* **2007**, *264*, 248–254.

[17]  L. Xu, Y. Wang, X. Yang, X. Yu, Y. Guo, J. H. Clark, *Green Chem.* **2008**, *10*, 746–755.

[18]  L. Xu, Y. Wang, X. Yang, J. Hu, W. Li, Y. Guo, *Green Chem.* **2009**, *11*, 314–317.

[19]  C.-Y. Sun, S.-X. Liu, D.-D. Liang, K.-Z. Shao, Y.-H. Ren, Z.-M. Su, *J. Am. Chem. Soc.* **2009**, *131*, 1883–1888.

[20]  L. V. Lokeren, E. Cartuyvels, G. Absillis, R. Willem, T. N. Parac-Vogt, *Chem. Commun.* **2008**, 2774–2776.

[21]  E. Cartuyvels, G. Absillis, T. N. Parac-Vogt, *Chem. Commun.* **2007**, 85–87.

[22]  N. Steens, A. M. Ramadan, G. Absillis, T. N. Parac-Vogt, *Dalton Trans.* **2009**, *39*, 585–592.

[23]  D. Lachkar, *Synthèses, Études Structurales et Applications Catalytiques d'Organo-Polyoxométallates*, Paris 11, **2014**.

[24]  J. Li, I. Huth, L.-M. Chamoreau, B. Hasenknopf, E. Lacôte, S. Thorimbert, M. Malacria, *Angew. Chem. Int. Ed.* **2009**, *48*, 2035–2038.

[25]  R. O. Duthaler, J. D. Roberts, *J Am Chem Soc* **1978**, 4969.

[26]   Gaussian 09, Revision A.02, M. J. Frisch, G. W. Trucks, H. B. Schlegel, G. E. Scuseria, M. A. Robb, J. R. Cheeseman, G. Scalmani, V. Barone, G. A. Petersson, H. Nakatsuji, X. Li, M. Caricato, A. Marenich, J. Bloino, B. G. Janesko, R. Gomperts, B. Mennucci, H. P. Hratchian, J. V. Ortiz, A. F. Izmaylov, J. L. Sonnenberg, D. Williams-Young, F. Ding, F. Lipparini, F. Egidi, J. Goings, B. Peng, A. Petrone, T. Henderson, D. Ranasinghe, V. G. Zakrzewski, J. Gao, N. Rega, G. Zheng, W. Liang, M. Hada, M. Ehara, K. Toyota, R. Fukuda, J. Hasegawa, M. Ishida, T. Nakajima, Y. Honda, O. Kitao, H. Nakai, T. Vreven, K. Throssell, J. A. Montgomery, Jr., J. E. Peralta, F. Ogliaro, M. Bearpark, J. J. Heyd, E. Brothers, K. N. Kudin, V. N. Staroverov, T. Keith, R. Kobayashi, J. Normand, K. Raghavachari, A. Rendell, J. C. Burant, S. S. Iyengar, J. Tomasi, M. Cossi, J. M. Millam, M. Klene, C. Adamo, R. Cammi, J. W. Ochterski, R. L. Martin, K. Morokuma, O. Farkas, J. B. Foresman, and D. J. Fox, Gaussian, Inc., Wallingford CT, 2016., **2016**.

[27]   P. R. Schreiner, *Chem. Soc. Rev.* **2003**, *32*, 289–296.

[28]   A. Wittkopp, P. R. Schreiner, *Chem. – Eur. J.* **2003**, *9*, 407–414.

[29]   P. R. Schreiner, A. Wittkopp, *Org. Lett.* **2002**, *4*, 217–220.

[30]   D. P. Curran, L. H. Kuo, *J. Org. Chem.* **1994**, *59*, 3259–3261.

[31]   A. G. Doyle, E. N. Jacobsen, *Chem. Rev.* **2007**, *107*, 5713–5743.

[32]   *Comprehensive Asymmetric Catalysis | Eric N. Jacobsen | Springer*, **n.d.**

[33]   H. Xu, S. J. Zuend, M. G. Woll, Y. Tao, E. N. Jacobsen, *Science* **2010**, *327*, 986–990.

[34]   A. Wittkopp, P. R. Schreiner, *Chem. – Eur. J.* **2003**, *9*, 407–414.

[35]   R. P. Herrera, V. Sgarzani, L. Bernardi, A. Ricci, *Angew. Chem. Int. Ed.* **2005**, *44*, 6576–6579.

[36]   M. S. Sigman, E. N. Jacobsen, *J. Am. Chem. Soc.* **1998**, *120*, 4901–4902.

[37]   S. S. So, S. Oottikkal, J. D. Badjić, C. M. Hadad, A. E. Mattson, *J. Org. Chem.* **2014**, *79*, 4832–4842.

[38]   J. Oble, B. Riflade, A. Noël, M. Malacria, S. Thorimbert, B. Hasenknopf, E. Lacôte, *Org. Lett.* **2011**, *13*, 5990–5993.

[39]   Ivano Bertini, Claudio Luchinat, Giacomo Parigi, *Solution NMR of Paramagnetic Molecules, Volume 2- 1st Edition*, **2001**.

[40]   S. A. Kadam, K. Haav, L. Toom, T. Haljasorg, I. Leito, *J. Org. Chem.* **2014**, *79*, 2501–2513.

[41]   D. Lachkar, D. Vilona, E. Dumont, M. Lelli, E. Lacôte, *Angew. Chem. Int. Ed.* **2016**, *55*, 5961–5965.

# CHAPTER 4: Conformation studies of Polyglycine@POM hybrids in solution

## 4.1 Introduction

As we have seen in the first chapter, polyoxometalates have potential applications in medicine. The antiviral, anti-tumor and antibiotic activity of some polyoxometallic structures is described in literature.[1-6] All the POM bio-activities stem from the interaction between the inorganic cluster and essential biomolecules or organelles, e.g. the viral cell membrane. For example, the mechanism of the anti-tumor effect of POM has been suggested to involve the induction of cell apoptosis and inhibition of ATP generation.[5] In another example, POMs have also been reported to interact with the basic fibroblast growth factor, and may lead to a tumor angiogenesis inhibitor.[7-9]

With POMs, crucial factors that influence the interaction and reactivity with biomolecules can be tuned reasonably easily. Indeed, the polarities, redox potentials, surface charge distribution, shape and acidity of POMs can be controlled by synthesis. In this context, the covalent attachment of organic groups to POMs via linkages that are compatible with physiological conditions (long half-lives in $H_2O$ or buffers at pH=7), could be used to modulate bioavailabilities or increase the recognition of key biomacromolecules.[10]

The precise understanding of the interactions between the inorganic framework and biomolecules is thus of prime importance for the design of POM-based drugs, as it could be a way to predict the POM biological properties.

In light of this interest in peptide-based biomimetic catalysts, it is important to better understand the relation between POMs and aminoacids or peptides.

*In the next paragraph the covalently linked POM-aminoacids and related peptides synthetized over the past years will be presented, to better understand how the organic part interacts with the inorganic cluster. Then, our peptide@POM hybrids will be introduced, followed by our studies of the intramolecular interactions between the two moieties in solution.*

## 4.2 Literature: a short review

### 4.2.1 Aminoacids@POM derivatives

In 1999, Cindric et al. reported the synthesis of a POM functionalized with three glycinate ligands through coordination to the molybdenum oxide. Starting from molybdenum(VI) oxide and vanadium(V) oxide in aqueous solution and adding glycine and potassium chloride, they obtained the hybrid compound, $K_2[HMo_6^{VI}V^VO_{22}(NH_3CH_2COO)_3]*8H_2O$. The X-ray analysis revealed that the compound was based on six $MoO_6$ edge-sharing octahedra connected into a ring centered by a $VO_4$ tetrahedron. The $MoO_6$ octahedra were in pairs linked by the bridging glycine-carboxylato ligands (see Figure 4.1-a).[11]

Seven years later, the same group synthesized three new compounds based on γ-octamolybdates containing aminoacids, such as alanine, and peptides, which was a diglycine ligand: $Na_4[Mo_8O_{26}(alaO)_2]*18H_2O$, $Na_4[Mo_8O_{26}(glyglyO)_2]*15H_2O$ and $Na_4[Mo_8O_{26}(glyglyO)_2]*12H_2O$. The X-ray diffraction revealed that the DL-alanine and glycylglycine ligand were coordinated to the molybdenum atom in γ-octamolybdate $[Mo_8O_{26}]^{4-}$ anions via monodentate carboxylate-oxygen atom, and a different packing structure was obtained depending on the ligand (Figure 4.1-b). The new hybrids were screened for the possible antiproliferative activity on a panel of five tumor cell lines, showing a differential cell-growth inhibition in a dose-dependent manner, selectively on hepatocellular carcinoma cell line (HepG2) and breast cancer cell line (MCF-7).[12]
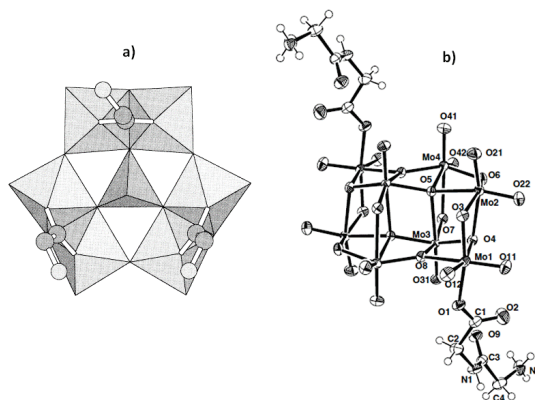
**Figure 4. 1-** Biomolecules-based hybrid POMs, presented by Cindrìc et al. a) Polyhedral representation of $K_2[HMo_6^{VI}V^VO_{22}(NH_3CH_2-COO)_3]*8H_2O$; b) glycylglycine coordinated via carboxylate oxygen atom in the γ-octamolybdate anions. (The other two structures, containing DL-ala and glycylgycine ligands, presented the same structural and coordination feature).

In 2002, the Kortz group presented a list of eighteen aminoacid-containing polyoxometalates. In particular they synthesized different heteropolymolybdates by changing the internal heteroatom (As$^{III}$, Sb$^{III}$, Bi$^{III}$, Se$^{IV}$, and Te$^{IV}$) and functionalized them by several amino acids, which are glycine ($HO_2CCH_2NH_2$), β-alanine ($HO_2C(CH_2)_2NH_2$), 4-aminobutyric acid ($HO_2C(CH_2)_3NH_2$), L-alanine (L-$HO_2CCHCH_3NH_2$) and L-lysine (L-$HO_2CCH-\{(CH_2)_4NH_2\}NH_2$). The general formula of the compounds synthesized is $[XMo_6O_{21}(O_2CRNH_3)_3]^{n-}$ (n=2, if X=Se$^{IV}$, Te$^{IV}$; n=3, if X=As$^{III}$, Sb$^{III}$, Bi$^{III}$; R=$CH_2$, $C_2H_4$, $C_3H_6$, $CHCH_3$, $CH(CH_2)_4NH_2$). The X-ray analysis showed that in all the polyanions three amino acids were bound to the polyoxomolybdate framework by their carboxylate group.
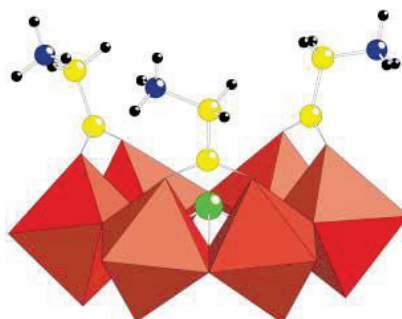


**Figure 4. 2-** Representation of one aminoacid-based hybrid POM synthesized by Kort et al. $(Se^{IV}Mo_6O_{21}(O_2CCH_2NH_3)_3)^{2-}$. $MoO_6$ octahedra are shown in red and the balls represent selenium (green), carbon (yellow), nitrogen (blue), and hydrogen (black).

They tried also to bind aminoacids containing bulkier functional groups, such as L-asparagine, but they weren't able to isolate pure products, probably because of steric interactions. More interestingly, the structures of the synthesized compounds were investigated through NMR in solution. However, NMR did not allow to distinguish free from the bound amino acids. Indeed, the molybdenum only weakly coordinate the carboxylate oxygen atoms (as it is possible to deduce from the bond distance in the solid $d_{Mo-OC}$=2.260-2.322 Å). In aqueous solution the coordination of the amino acids are probably labile, which would lead to a fast exchange, in the NMR time scale, between free and bound forms.[13]

The chiral lysine ligands (D- and L-form) were coordinated via their carboxylate-oxygen atoms at the vacant sites on the centrosymmetric octamolybdate $\gamma$-$[Mo_8O_{26}]^{4-}$ anion, by Inoue and Yamase in 1995.

Each octamolybdates coordinated two lysine ligands, $Na_2[Mo_8O_{26}(D\text{-}lysH_2)_2]\cdot 8H_2O$ and $Na_2[Mo_8O_{26}(L\text{-}lysH_2)_2]\cdot 8H_2O$, and it was found that the ligands retain their configuration with a resultant formation of optically-active octamolybdate species.[14] The same coordination behavior on the $\gamma$-$[Mo_8O_{26}]^{4-}$ anion was obtained by the same authors in presence of adenosine-5′-monophosphoric acid.[15]

The reaction of the same molybdate and DL-proline at pH 3.4 resulted in the formation of $Na_4[Mo_8O_{26}(proO)_2]*22H_2O$ (pro =proline), by the Parac-Vogt group. Also in this case the X-ray analysis revealed that two proline ligands were attached to the molybdenum(VI) ions via monodentate coordination of the carboxylate groups. In solution the structure seemed to be stable at native pH=3.4 while at physiological pH, the polyoxometalate framework was completely dissociated into the monomeric $MoO_4^{2-}$ unit. In addition, the $Na_4[Mo_8O_{26}(proO)_2]*22H_2O$ complex was found to be active toward the hydrolysis of ATP. The hydrolytic activity was tested by authors at different pH values. At pH=3.4 the hydrolysis gave adenosine monophosphate and adenosine diphosphate in nearly equal amounts, while at pH 5.8 the adenosine diphosphate was the only product of hydrolysis after 24 h of reaction. At neutral pH, the

hydrolysis of ATP was slower, but it gave the 75% of adenosine diphosphate after 48 h of reaction.[16]
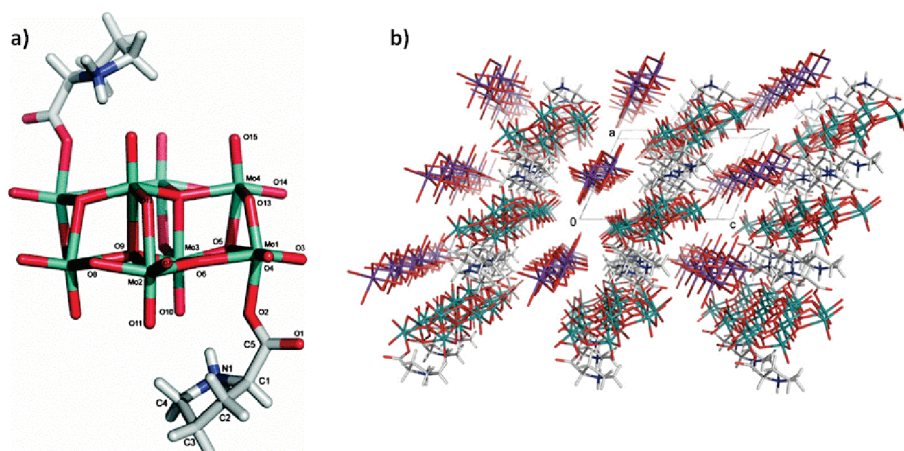


**Figure 4. 3-** a) Molecular structure of the $Na_4[Mo_8O_{26}(proO)_2]*22H_2O$ complex, and b) the corresponding package in the solid state.

A giant metal–oxide based wheel-type cluster containing cystine ligands at the inner wall of their cavities was obtained by Müller et al. by replacing $H_2O$ ligands.
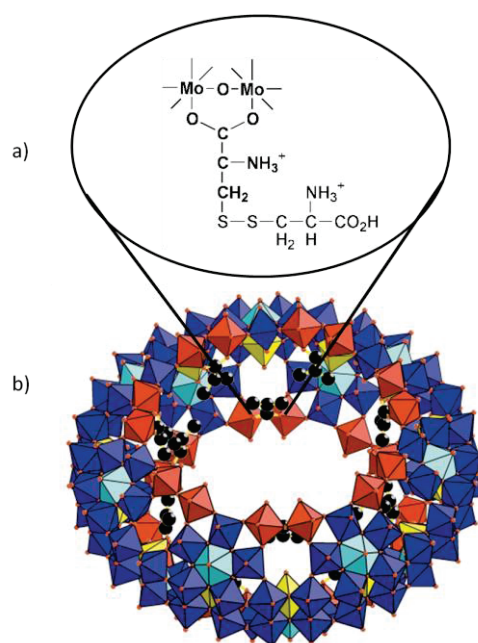


**Figure 4. 4-** a) Zoom on the coordination through the carboxylate group of the cystine aminoacid to the molybdenum center and b)representation of the Cystin-based giant wheel type cluster anion, obtained by Müller et al.. The carbon atoms of the organic ligand are represented in black.

The giant hybrid POM was obtained by reaction of an acidified aqueous solution of sodium molybdate $Na_2MoO_4$ with cysteine, which acts as the reducing agent at *ca.* 55 °C, at rather low pH values ($\approx$ 1.5). The resulting $Na_3[Mo_{154}O_{462}H_{14}(H_2O)_{48}(HO_2C–(NH_3^+)HC–CH_2–S–S–CH_2–CH(NH_3^+)–COO_2)_{11}]*xH_2O$ (x $\approx$ 250) contains nanosized ring-shaped clusters which captured the oxidation product of cysteine ($H_2cystine^+$) in the inner cavity. The 11 $H_2cystine+$ ligands, coordinated to {Mo2} units through their carboxylate functions, were found to be located quite disordered near the inner wall of the cavity [17]

Sadakane et al. employed the chiral Ce(III)-substituted Dawson $\alpha_1$-$[P_2W_{17}O_{61}]^{7-}$ to bind different aminoacids. They proposed coordination of the amino acid to the cerium center by the carboxylate group in a monodentate fashion, interestingly accompanied by hydrogen bonding involving the amino group. This locked the ligand enough to observe the complexation equilibria in solution.
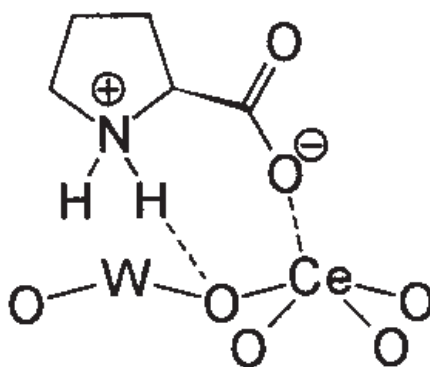


**Figure 4. 5**- Representation of the possible interaction between $\alpha_1$-$[P_2W_{17}O_{61}Ce]^{7-}$ and Amino Acids. Here the example of L-proline.
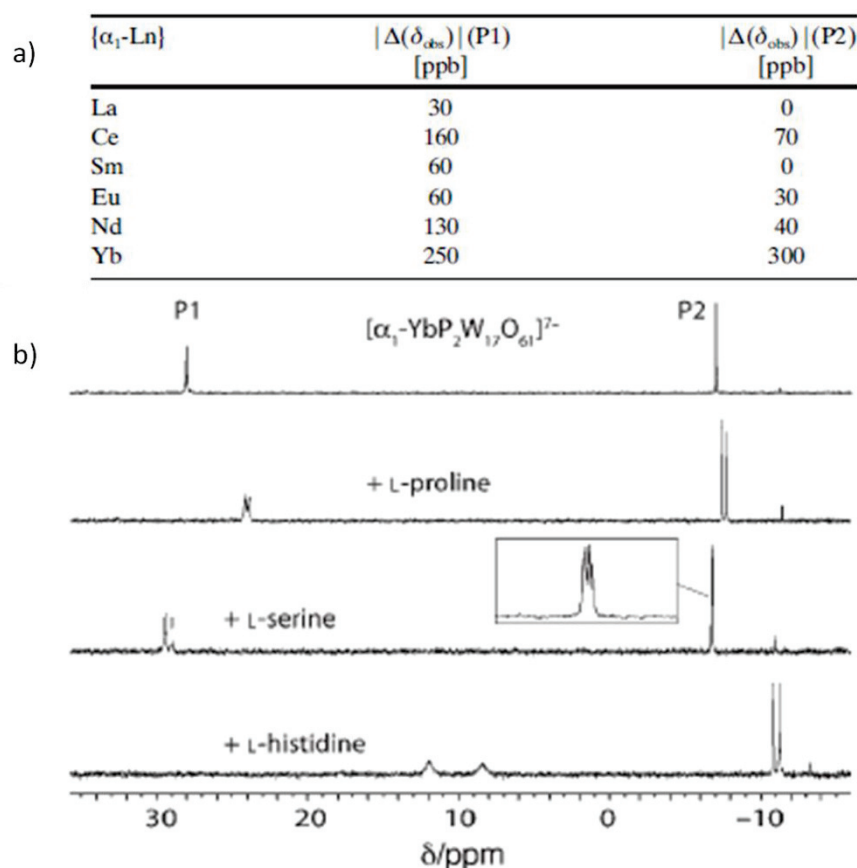
In particular they studied the stereoselective interactions between the chiral aminoacid and the chiral polyoxometalate.

The addition of chiral amino acids to aqueous solutions of $\alpha_1$-$[P_2W_{17}O_{61}Ce]^{7-}$ resulted into the splitting of the ^{31}P-NMR signals as a result of diastereomer formation. While no such splitting was observed with glycine or DL-proline, or

when chiral amino acids were added to the corresponding complex of the achiral $\alpha_2$-isomer of $[P_2W_{17}O_{61}]^{10-}$. Then they used NMR analysis of the $^{31}P$-NMR spectra, to calculate the binding constants of the two diastereomeric adducts of $\alpha_1$-$[P_2W_{17}O_{61}Ce]^{7-}$ with L-proline which resulted to be 7.3±1.3 and 9.8±1.4 $M^{-1}$.

Following the same idea, Boglio et al. synthesized a series of lanthanides-substituted $[\alpha_1$-$LnP_2W_{17}O_{61}]^{7-}$ (with Ln=La$^{III}$, Ce$^{III}$, Sm$^{III}$, Eu$^{III}$, Nd$^{III}$, Yb$^{III}$) and coordinated the metal atom to different amino acids, with the aim to promote the enantiomeric resolution of the POM. The authors started to record the $^{31}P$-NMR spectra of all the series of Ln-substituted POM in the presence of increasing concentrations of L-proline. The $^{31}P$ signals were splitted into two resonances for all the series of lanthanides, except for La- and Sm- substituted POM where only one signal was present. Moreover, the amplitude of the splitting increased linearly with the amount of ligand. The Yb-substituted $\alpha_1$-POM presented the biggest splitting of the $^{31}P$-NMR signals and so they used this POM to study the influence of different amino acids (L-Pro, L-Val, L-Ser, L-Asp, L-Glu, L-Orn, L-Lys, L-Arg, L-Hys). Then, $^{31}P$-NMR spectra of $\{\alpha_1$-Yb$\}$ in the presence of 20 equivalents of a variety of amino acids were recorded by the authors. The chiral discrimination depended also on the nature of the amino acid. In general they saw that chiral discrimination was rather weak with amino acids bearing carboxyl groups in their side chain (aspartate versus glutamate), while the most pronounced resolution effects were obtained with L-arginine and L-histidine. Indeed, the two amino acids with protonated side chains under experimental conditions establishes electrostatic attraction between the negatively charged POM and the positively charged side chain.[18]

a)

| {$\alpha_1$-Ln} | $\|\Delta(\delta_{obs})\|$ (P1) [ppb] | $\|\Delta(\delta_{obs})\|$ (P2) [ppb] |
|---|---|---|
| La | 30 | 0 |
| Ce | 160 | 70 |
| Sm | 60 | 0 |
| Eu | 60 | 30 |
| Nd | 130 | 40 |
| Yb | 250 | 300 |

b)

P1    $[\alpha_1\text{-}YbP_2W_{17}O_{61}]^{7-}$    P2

+ L-proline

+ L-serine

+ L-histidine

30      20      10      0      -10

δ/ppm

**Figure 4. 6**-a) Table showing the chiral differentiation by $^{31}P$ NMR of {$\alpha_1$-Ln} in the presence of 20 equivalents of L-proline. b) $^{31}P$ spectra of $[\alpha_1\text{-}Yb(H_2O)_4P_2W_{17}O_{61}]^{7-}$ and in the presence of 20 equivalents of L-proline, L-serine, and L-histidine.

### 4.2.2    Peptides@POM

In 2003[19] and 2005[20], Bareyt et al. succeed to efficiently functionalize the monolacunary Dawson $[\alpha_1/\alpha_2\text{-}P_2W_{17}O_{61}]^{7-}$ with organo-tin chains ($SnCH_2CH_2COOH$) easily post-functionalizable with amino-derivatives for the peptide bonds formation. The authors evidenced that the coupling of chiral amines, such as Tyrosine or Phenyl alanine, to the chiral organotin-substituted $\alpha_1$-derivative allows the isolation of diastereomers, which feature in some cases split $^1H$, $^{13}C$, and $^{31}P$ NMR spectra. A mechanism for the diastereomeric differentiation was proposed by the authors, as probably due to a hydrogen-bonding interaction between the acid protons present in the lateral chain and the oxygen naturally

present on the polyoxometallic surface, which allow to lock the structure. But no evidences of this behavior are still known.
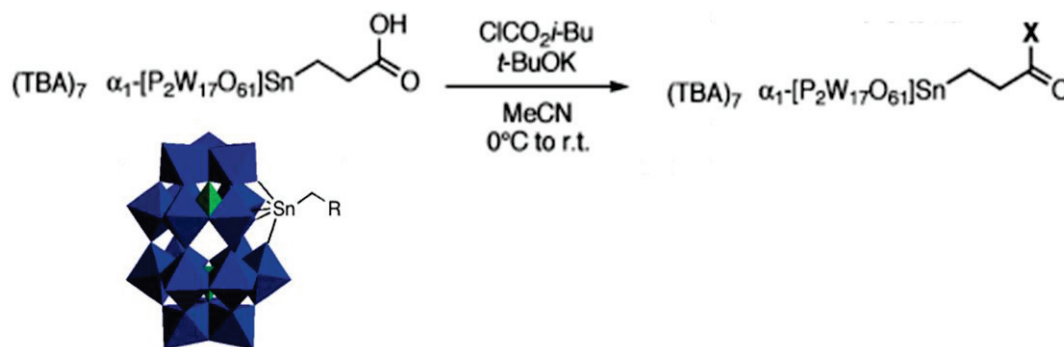


**Figure 4. 7-** a) General scheme for the post-functionalization of the $\alpha_1$-derivative with functional organic lateral chains, such as aminoacids.

Following the same strategy in 2008 and in 2009, the same group inserted in the organo-tin monolacunary $[P_2W_{17}O_{61}(SnCH_2CH_2COOH)]^{7-}$ different aminoacids[21] and oligopeptide chains.[22] They exploited the intramolecular acylation by the oxo-ligand of the POM surface to monoacylate the activated carbonyl group of the lateral chain. Then the nucleophylic attack by amino-derivatives to the carbonyl activated moiety allows to post-functionalize the hybrid-POM.



**Figure 4. 8-** General Strategy for Regioselective Acylation of Oxo Ligands (LG =Leaving Group)

Moreover, they demonstrated through $^{31}$P-NMR and circular dichroism that when chiral tripeptides were inserted in the lateral chain, it was possible to kinetically resolve (until 99% ee) the racemic mixture of the two organo-POM enantiomers,

since the peptidic chain prefers to interact first with one enantiomer of the POM with respect to the other.[22]
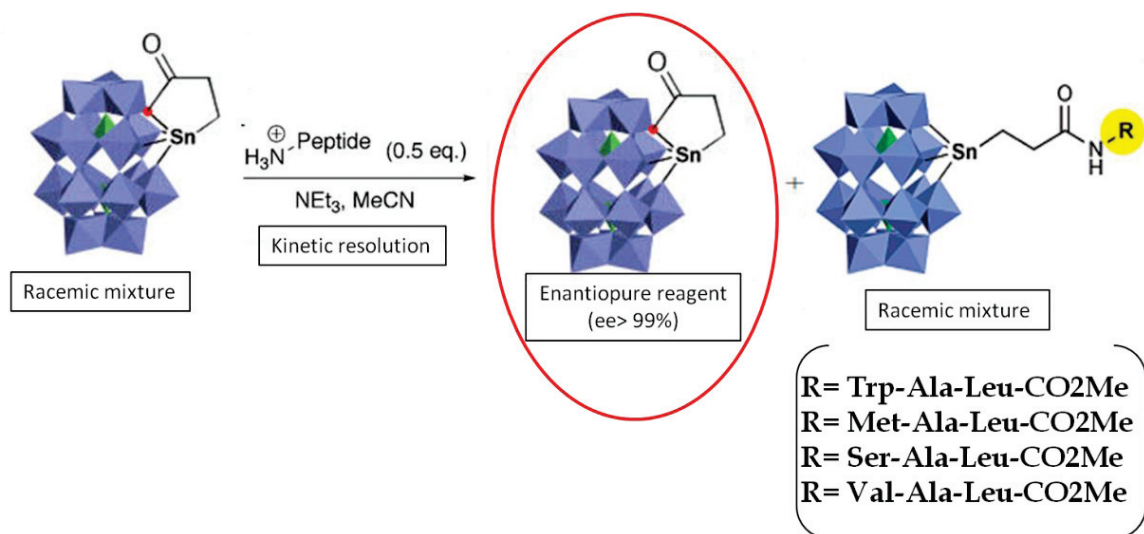


**Figure 4. 9-** $\alpha_1$-tripeptides substituted lacunary Dawson POM, $\alpha_1$-$[P_2W_{17}O_{61}]^{10-}$, presented by Micoine et al. efficiently employed for the kinetic resolution of the chiral substituted-POM.

Successively in 2014, the Cronin group presented the integration of POM clusters into peptide chains. They started with the synthesis of N-hydroxysuccinimide (NHS) ester activated Mn-Anderson precursors ($[MnMo_6O_{18}(O(CH_2)_3C)_2]_3^-$), which was grafted at the N terminus of peptide chains. This Fmoc-protected carboxylic group of the NHS was then employed to bind different aminoacids or small oligomers, such as Glycine, Phenylalanine, di- and tri- phenylalanine, until a 15 amino acid peptide

($H_2N$-Ala-Asn-Thr-Leu-Ser-Ser-Thr-Ala-Ser-Thr-Leu-Glu-Ser-Tyr-Leu-OH).
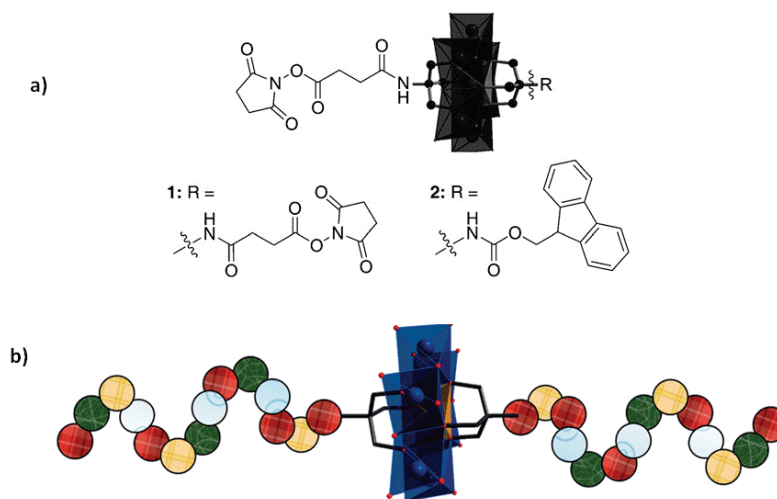
**Figure 4. 10-** a) N-hydroxysuccinimide-functionalized Mn-Anderson POM used as precursor to incorporate peptidic chains. b) Schematic representation of the integration of POM clusters into peptide chains.

In particular, for this last complex, containing 30 aminoacid residues, a structural modification in the peptidic chain structure was observed due to the presence of the inorganic cluster. Indeed, the CD spectrum showed signals that was characteristic of an α-helix arrangement with two troughs at 208 nm and 222 nm. It was not clear if this feature resulted from a regular secondary structure in only a part of the molecule, or if the cluster inclusion leads the entire peptide chain to adopt a helical arrangement.[23]

## 4.3 Intramolecular Peptides@POM interaction in solution: elucidation of the conformation

### *4.3.1 Introduction*

Considering that polyoxometalates are highly negatively charged oxo clusters, electrostatic and/or hydrogen bonding are the main expected interactions between the latter and organo ligands or biomolecules. When we are in the presence of covalently attached organo-POMs intramolecular interactions between the two moieties could also happen, which certainly influence the activity of the hybrid molecules. For example toward the catalytic reactivity[24] or the approach to biological recognition sites, or that of small molecules.[25,26]

For example, we showed before that Micoine et al. presented a tripeptides-functionalized chiral POM to be able to discriminate between both enantiomers of the chiral polyoxotungstate $[\alpha_1\text{-}P_2W_{17}O_{61}\{SnCH_2CH_2C(=O)\}]^{6-}$. The authors suggested that probably the enantiomeric resolution arises from a strong enough interaction between the tripeptide and the POM surface, which leads to a diastereomeric transition states at the origin of the chiral resolution of the racemic platform.[22]
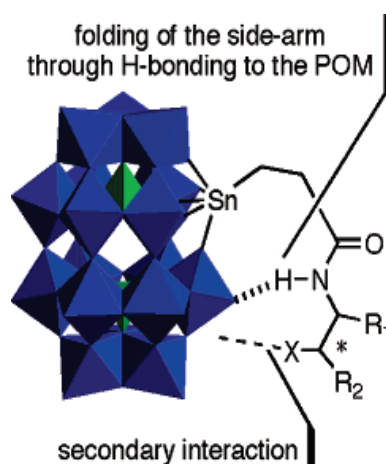


**Figure 4. 11**- Probable H-bonding interaction between the lateral chain and the POM surface responsible for the kinetic diastereomeric resolution.

174

Conversely, Thorimbert and coworkers demonstrated the possibility of chirality transfer from an organo-POM, where chirality was only coded in the inorganic framework, to substrates in a Diels-Alder reaction. This was made possible by the proximity of the organic chain to the chiral POM surface.[27]
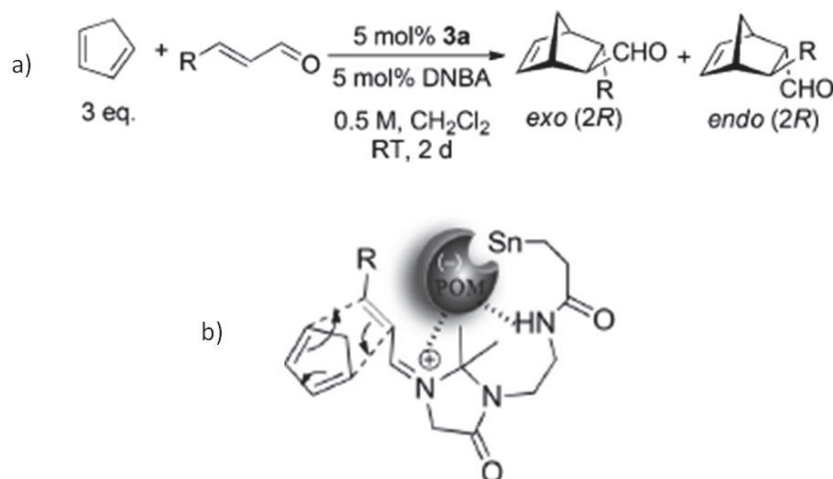


**Figure 4. 12**- a) Diels–Alder reaction between cyclopentadiene and crotonaldehyde with POM-Imidazolidinone as catalysts; b) Proposed substrates approach mechanism to the catalyst which achieve the chirality transfer from the inorganic framework.

Similarly more recently, Lachkar et Lacôte suggested that the catalytic activity of an $\alpha_2$-Dawson polyoxotungstate functionalized with squaramides in the lateral chains was exalted probably thanks to a "supramolecular" interaction between the H-bond donors on the lateral chain of the hybrid (the squaramide), and the POM surface, leading to an increase in the acidity of the squaramide protons.[24]
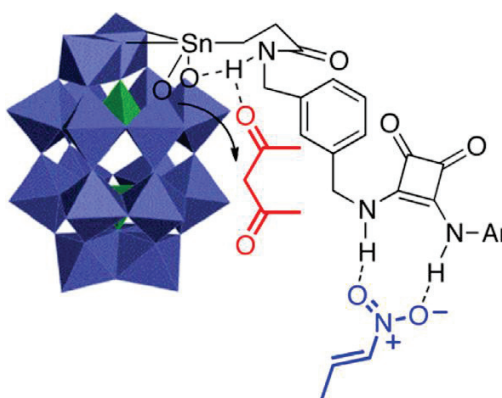


**Figure 4. 13**- Proposed model for the POM@squaramide-catalyzed addition of dicarbonyl compounds to nitro-olefins.

From what precedes, one sees that the organic/POM-surface interaction can play a role. However, to date there is still a lack of understanding of how exactly organo-POMs fold in solution and to predict the solution behavior of the hybrids could be an important tool.

With the aim to clearly assess how a peptide lateral chains could interact in solution with the POM surface, and eventually use this knowledge to create a chiral pocket around the catalytic site of the organo-polyoxotungstovanadate presented in the previous chapter, we will now focus our attention on the two series of polyglycine organo-polyoxotungstate introduced by Dr. David Lachkar during his Ph.D. thesis.[28]

*In the next paragraphs the high-field NMR studies and Molecular Dynamics simulations that allowed us to elucidate the real conformation of these hybrids in solution will be presented.*[1]

### 4.3.2    *Synthesis of the Polyglycines@POM*

During his Ph.D. thesis Dr. David Lachkar prepared two series of organo-POMs, covalently functionalizing the $\alpha_1$ or $\alpha_2$ monolacunary Dawson polyoxotungstates $[P_2W_{17}O_{61}]^{10-}$ with peptidic chains ranging from 3 to 6 residues, following the established method of the research group.[20]

In particular, the lacunary $\alpha_1$ and $\alpha_2-[P_2W_{17}O_{61}]^{10-}$ polyoxoanions were monofunctionalized with an organotin chain; then polyglycine chains of different lengths (from 3 to 6 glycine residues) were covalently bound to the carbonyl group, generating peptide-POM conjugates with 4 to 7 H-bond donating sites.

---

[1] The below text has been taken from the submitted publication Vilona et al., with some implementations for a better understanding.
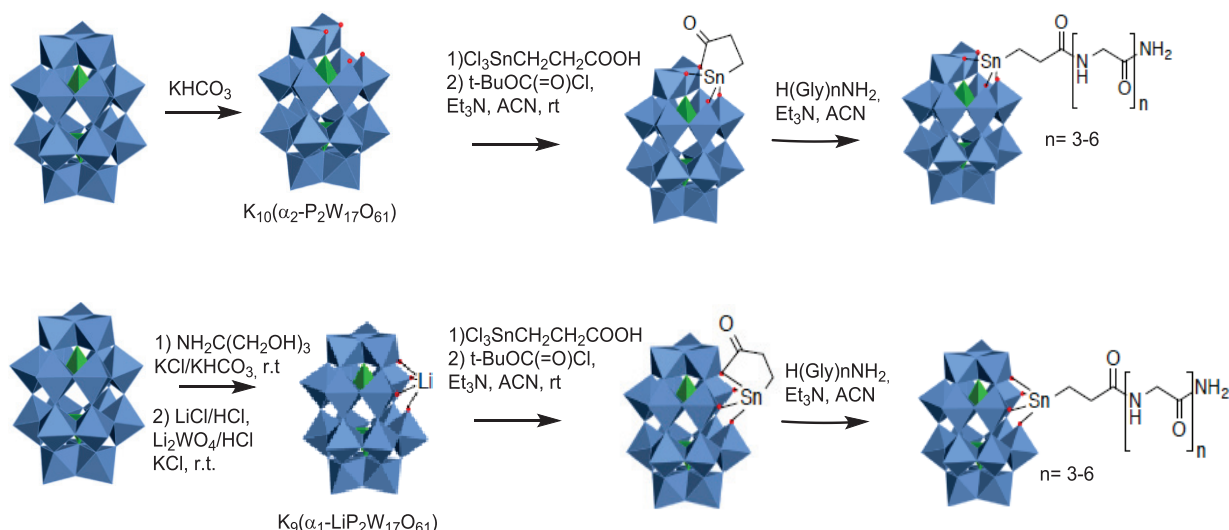
**Figure 4. 14**- $\alpha_1/\alpha_2$- polyglycines@POM synthetic pathway.

As a reminder, in the $\alpha_1$ compounds, the lateral chain is grafted to the 6W belt of the POM, where one $WO^{4+}$ unit has been replaced by a functional organostannane, leading to chiral structures. The substituent is located in the 3W cap in the $\alpha_2$ series. A plan of symmetry makes the resulting structure achiral.
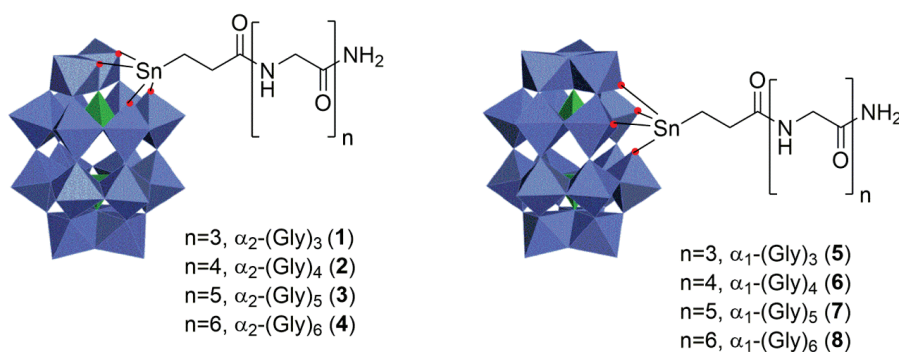


**Figure 4. 15**- Compact structures of the studied POM@polyglycines derivatives. Achiral $\alpha_2$-serie on the left, Chiral $\alpha_1$-serie on the right.

### 4.3.3    High-field NMR studies

To map if the polyglycine chains interact with the POM surface we decided to monitor the amidic protons shifts in $CD_3CN$. 1D $^1$H-NMR spectra at 1 GHz of magnetic field were thus recorded for all the organo-POMs and all the resonances

corresponding to amide protons could be assigned through 2D sequences ($^1$H-$^1$H COSY, $^1$H-$^{13}$C HSQC, $^1$H-$^{13}$C HMBC), which enabled the sequential assignment.
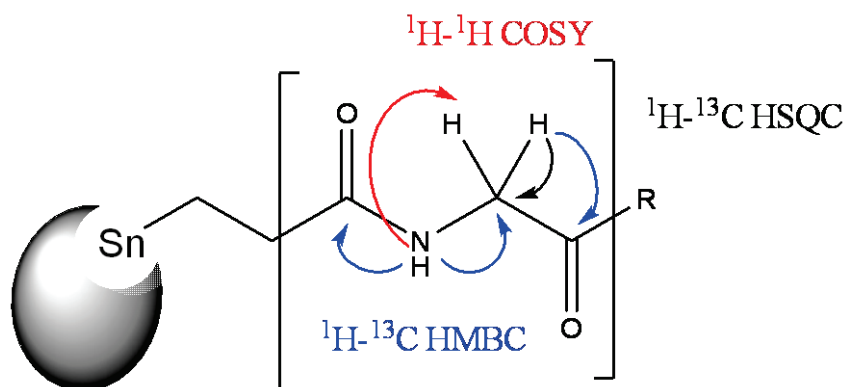


**Figure 4. 16-** General scheme about how it is possible to sequentially assign the proton and carbon shifts

The assigned amidic proton resonances for all the hybrid-POMs are collected in the Table 4.1.

The first observation is that the amide resonances are distributed over a 3.4 ppm range, from approx. 5.9 to 9.3 ppm. Furthermore the fine structure is often well resolved with two exceptions for POMs **1** and **8**. However, generally speaking, the signals for $\alpha_1$ POMs **5-8** were sharper than those of $\alpha_2$ POMs **1-4**.

The chemical shifts of the amide proton directly connected to the POM side chain (column HN-1) do not vary much, ranging from 8.68 ppm in **4** to 8.97 ppm in **6**. Given that the variation of δ-NH for H-1 and H-3 is small (less than 0.3 ppm), it comes as a surprise that the values for HN-4 span a much larger range from 7.81 ppm for **6** to 9.25 ppm for **4**.
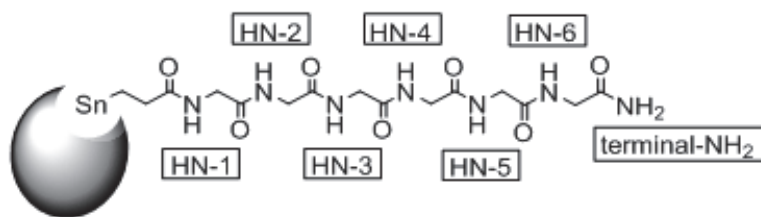
| POM | $\delta_{HN-x}$ (ppm)[a] | | | | | | |
|---|---|---|---|---|---|---|---|
| | x =1 | x =2 | x =3 | x =4 | x =5 | x =6 | terminal-$NH_2$ |
| $\alpha_2$-(Gly)$_3$ (**1**) | 8.70 | 7.95 | 7.65 | - | - | - | 7.46/5.69 |
| $\alpha_2$-(Gly)$_4$ (**2**) | 8.70 | 7.80 | 7.78 | 8.67 | - | - | 6.84/5.45 |
| $\alpha_2$-(Gly)$_5$ (**3**) | 8.73 | 7.81 | 7.98 | 8.94 | 7.53 | - | 7.21/5.63 |
| $\alpha_2$-(Gly)$_6$ (**4**) | 8.68 | 7.70 | 7.87 | 9.25 | 7.66 | 8.47 | 6.75/5.54 |
| $\alpha_1$-(Gly)$_3$ (**5**) | 8.94 | 7.95 | 7.87 | - | - | - | 7.05/5.62 |
| $\alpha_1$-(Gly)$_4$ (**6**) | 8.97 | 8.07 | 7.97 | 7.81 | - | - | 7.01/5.90 |
| $\alpha_1$-(Gly)$_5$ (**7**) | 8.82 | 7.85 | 8.11 | 8.10 | 7.52 | - | 6.96/5.77 |
| $\alpha_1$-(Gly)$_6$ (**8**) | 8.76 | 7.84 | 8.17 | 8.21 | 7.75 | 7.68 | 6.96/5.76 |

| POM | $^3J_{NH(x)-CH}$ (Hz)[a] | | | | | |
|---|---|---|---|---|---|---|
| | x =1 | x =2 | x =3 | x =4 | x =5 | x =6 |
| $\alpha_2$-(Gly)$_3$ (**1**) | br | br | br | - | - | - |
| $\alpha_2$-(Gly)$_4$ (**2**) | nd[b] | nd[b] | nd[b] | nd[b] | - | - |
| $\alpha_2$-(Gly)$_5$ (**3**) | 5.6 | 6.1 | 5.7 | 5.7 | 6.3 | - |
| $\alpha_2$-(Gly)$_6$ (**4**) | 5.8 | 6.2 | 6.1 | 5.9/6.1 | 6.2 | 6.2 |
| $\alpha_1$-(Gly)$_3$ (**5**) | 5.5/5.8 | 5.9/6.2 | 6.1 | - | - | - |
| $\alpha_1$-(Gly)$_4$ (**6**) | 6.0 | 5.7 | 6.2 | 6.1/6.2 | - | - |
| $\alpha_1$-(Gly)$_5$ (**7**) | 5.6/5.8 | 6.2 | nd[b] | nd[b] | 6.2 | - |
| $\alpha_1$–(Gly)$_6$ (**8**) | 5.2 | 5.5 | 5.3 | br | br | 5.8/6.0 |

[a] in CD$_3$CN, at 298K, 3.3 mM; [b] superimposed signals.

**Table 4. 1**- ^{1}H-NMR shifts of amide protons in all the POM@polyglycines (on the top). Coupling constant of the triplet signals (on the bottom). Spectra recorded at 1 GHz.

In addition, in the majority of cases we could determine $^3J$ constant between the amide proton and the α−carbon protons (columns $^3J_{NH-CH}$ in table 4.1), suggesting that the backbone dihedral angles were not changed much along the series.[29] Taken together, these observations show that the peptide chains are folded towards the POM surface in a reasonably rigid way at the NMR timescale. Indeed, if there was no interaction between the lateral chain and the POM scaffold, the isolated glycine peptides/oligomers would adopt a random coil structure, with a marked rotational freedom, resulting in a broad signal: the chemical shifts would be averaged for all the amide protons. On the contrary, in a rigid structure, all protons experience different chemical and magnetic environments and thus different chemical shifts.

In particular, for the amide protons the distribution of chemical shifts is sensitive to the presence of hydrogen bonds and the difference between the observed chemical shift value and that of the random coil is also an indication of the strength of the hydrogen bond interaction.[21]

Similarly, a rigid structure would feature fixed dihedrals angles, leading to well defined $^3J$ couplings values, which were observed here. Going more in detail, in the cases of $\alpha_2$-Gly$_3$ (**1**) and $\alpha_1$-Gly$_6$ (**8**), which exhibit broadened but split signals one can therefore infer that the folding is a little looser, likely because of the presence of some residual conformational dynamics, but still present.

To exclude the possibility of intermolecular interactions between two different hybrid-POM molecules generating dimeric (or more) structures, we decided to perform concentration studies. Indeed, if dimerization equilibrium is present – as opposed to folding – this will be displaced toward the monomer at lower concentrations, leading to a variation of the observed δ-NH. We then recorded $^1$H-NMR spectra at different concentrations (0.33 mM; 0.82 mM; 1.65 mM; 2.47 mM; 3.3 mM) for organo-POMs **1**, **3**, **5**, **7**. We chose these organo-POMs to have a representatives with short lateral chains $\alpha_n$-Gly$_3$ (**1**, **5**) or with a longer chain $\alpha_n$-Gly$_5$ (**3**, **7**), in both the $\alpha_1$ and $\alpha_2$ series.
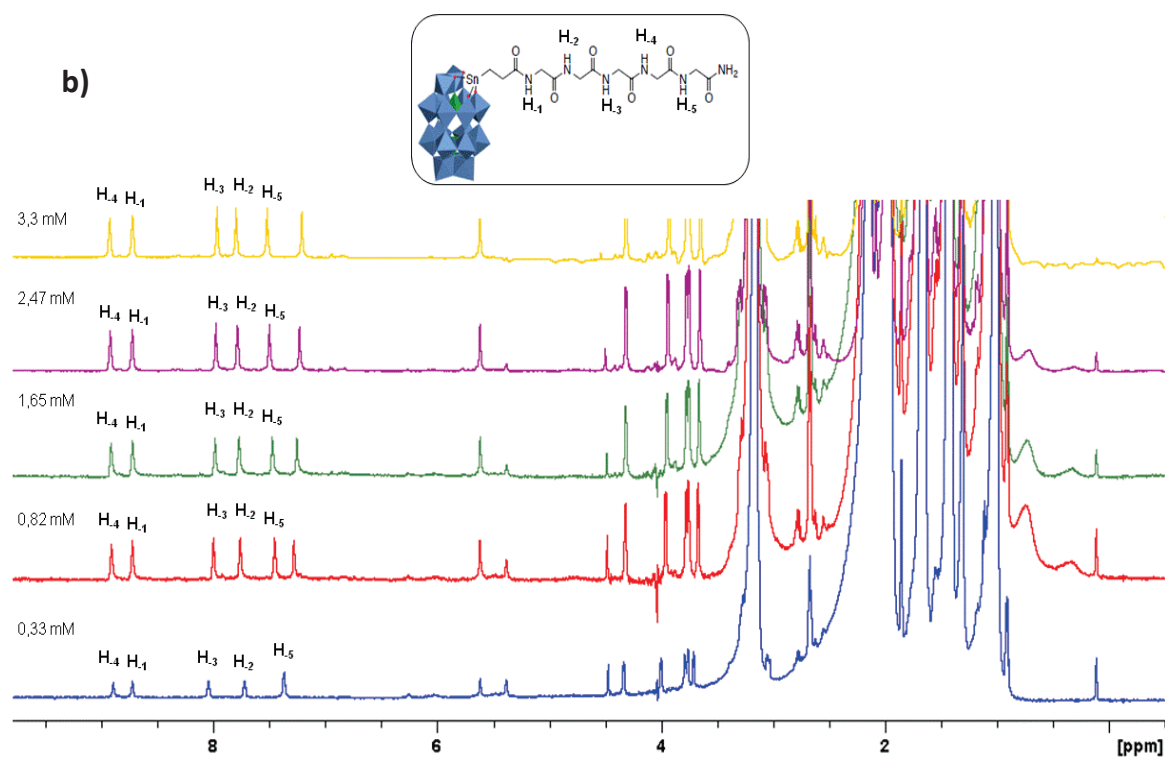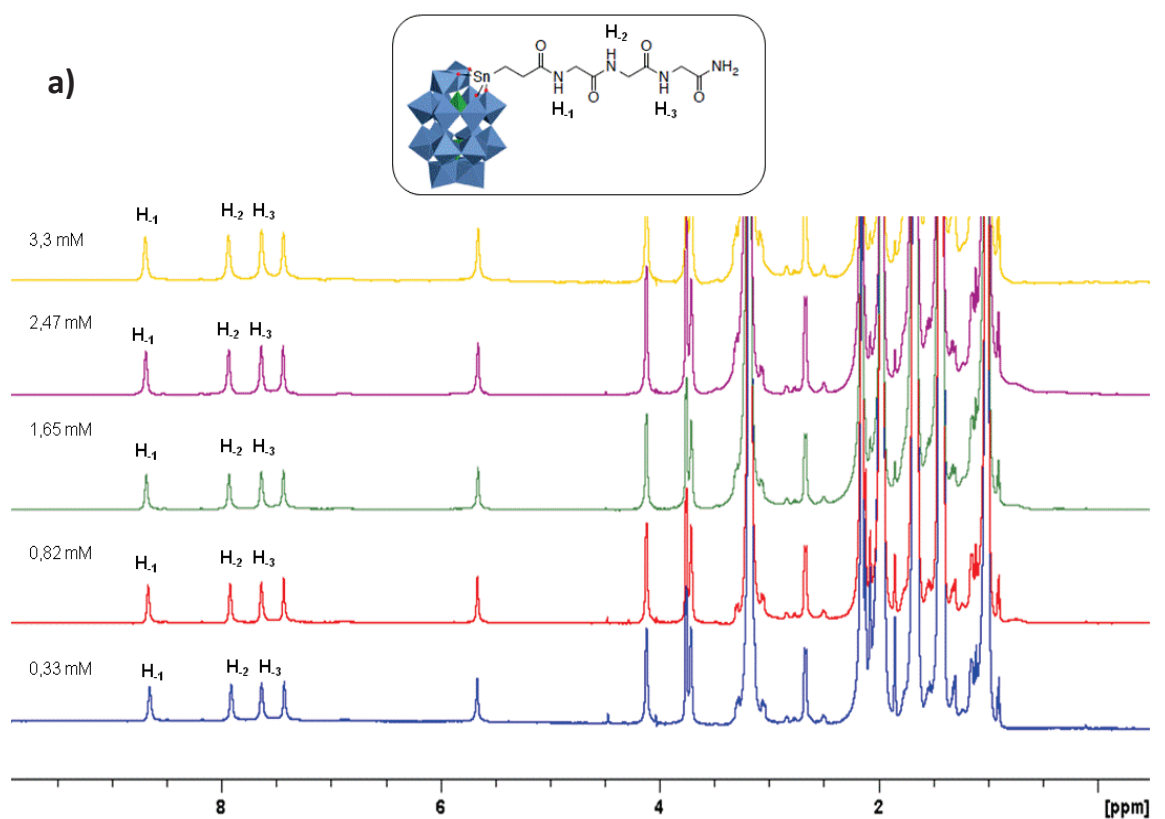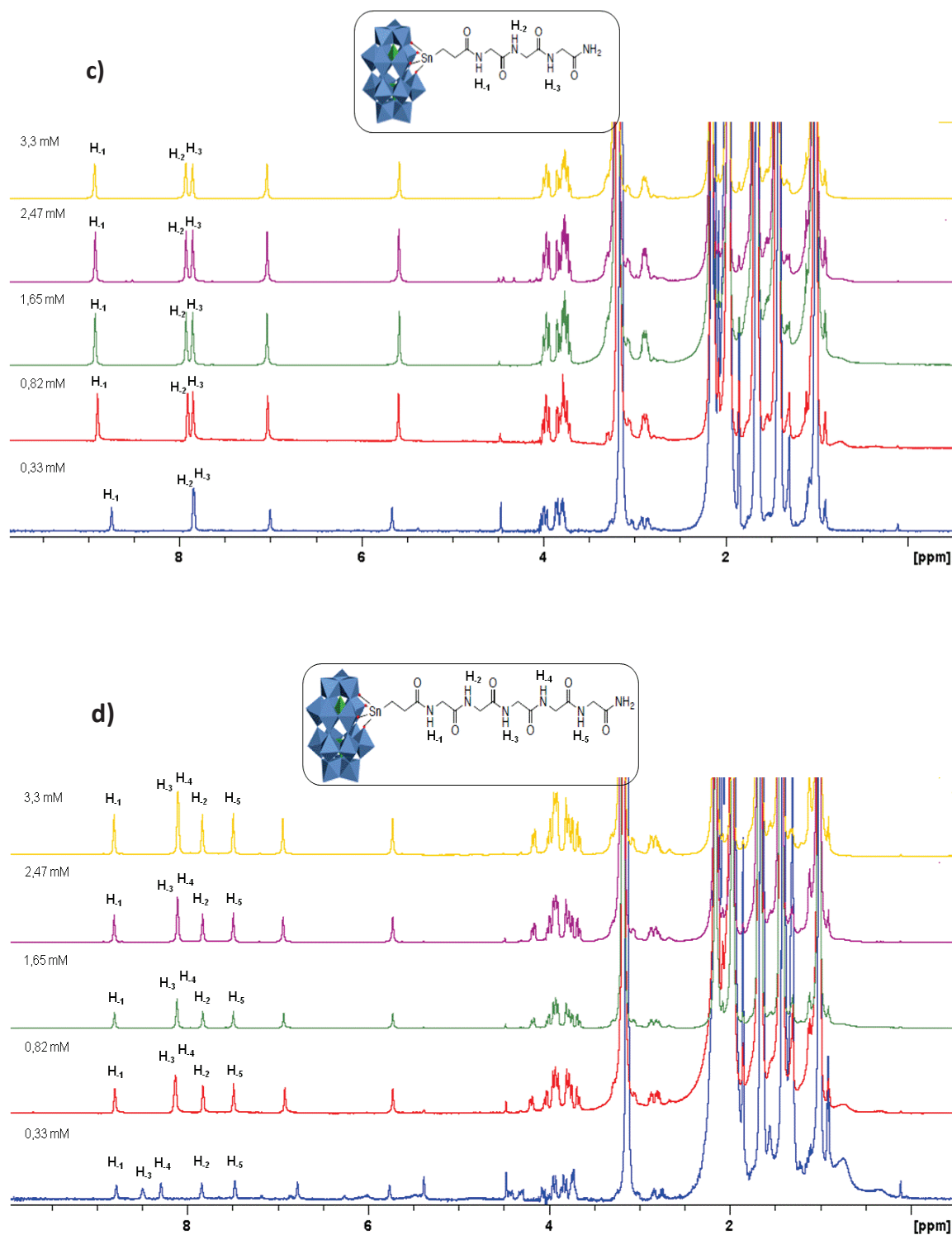
**Figure 4. 17-** $^1$H-NMR spectra superposition of the synthesized glycines@POM at different concentrations. a) $\alpha_2$-Gly$_3$, **1**; b) $\alpha_2$-Gly$_5$, **3**; c) $\alpha_1$-Gly$_3$, **5**; d) $\alpha_1$-Gly$_5$, **7**. Spectra recorded at 600 MHz, in CD$_3$CN at 298K.

No significant change of the amide shift was observed for $\alpha_2$-Gly$_3$ (Figure 4.17-a). For $\alpha_2$-Gly$_5$ (Figure 4.17-b), $\alpha_1$-Gly$_3$ (Figure 4.17-c) and $\alpha_1$-Gly$_5$ (Figure 4.17-d), only very minor deviations were observed (coalescence of signal for two protons). We think that these small deviations are caused by adventitious water. The absence of any meaningful change shows that there are no intermolecular interactions and that POMs **1-8** are monomeric in solution.

To confirm the monomeric nature of POM we performed also $^{15}$N-NMR relaxation measurements to determine the hydrodynamic radius on two exemplary molecules: POMs **3** ($\alpha_2$-Gly$_5$) and **7** ($\alpha_1$-Gly$_5$). The longitudinal relaxation time ($^{15}$N T1) is sensitive to the overall molecular correlation time ($\tau_R$), that itself depends on the hydrodynamic radius of the molecule (Equation (1) below):

$$
\begin{aligned}
R_1 = \frac{1}{T_1} = \frac{1}{10}\left(\frac{\mu_0}{4\pi}\right)^2 \frac{(\gamma_H \gamma_N \hbar)^2}{r_{HN}{}^6} & \left(\frac{\tau_R}{1+(\omega_H-\omega_N)^2\tau_R{}^2} + \frac{3\tau_R}{1+\omega_N{}^2\tau_R{}^2}\right.\\
& \left.+ \frac{6\tau_R}{1+(\omega_H+\omega_N)^2\tau_R{}^2}\right) + \frac{2(\gamma_N B_0 \Delta\sigma)^2}{15}\left(\frac{\tau_R}{1+\omega_N{}^2\tau_R{}^2}\right)
\end{aligned}
$$

(1)

where $\tau_R$ is the rotational correlation time, $\gamma_H$, $\gamma_N$, $\omega_H$ and $\omega_N$ are the gyromagnetic ratio and the angular Larmor Frequencies for the proton and the nitrogen, respectively. $B_0$ is the strength of the magnetic field, $\mu_0$ is the vacuum magnetic permeability, $\Delta\sigma$ is the chemical shift anisotropy (here we used $\Delta\sigma =$ –160 ppm for amide nitrogens), $r_{HN}$ is the proton nitrogen distance, that in amide group is about 104 pm.

Equation (1) can be solved for each experimental $^{15}$N T$_1$ data in order to obtain the values of $\tau_R$. In turn, the rotational correlation time can be used to estimate the hydrodynamic volume through the Stokes-Einstein relation:

$$
\tau_R = \frac{4\pi\eta r^3}{3kT} = \frac{\eta V}{kT}
$$

(2)

where $r$ is the hydrodynamic radius, $\eta$ is the solvent viscosity (here 0.3450 mPa*s for acetonitrile at 298 K), $k$ is the Boltzmann constant and $T$ is the temperature. This radius estimates as an approximate sphere the size of the molecule, but is precise enough to distinguish between the volume of a monomeric or a dimeric structure of the molecule.[30]

The analysis of the $^{15}$N T1 measurements revealed a rotational correlation time of about 0.4 ± 0.1 ns for both **3** and **7**. This corresponds to an hydrodynamic radius of the order of 11.9 ± 0.7 Å, which is in very good agreement with the radius of about 11 Å expected for the monomeric molecule. Furthermore, minimal differences in $^{15}$N T1 were observed for α$_1$-POM **7** along the peptide chain, supporting the observation that the molecule is compact with the peptide chain fully zipped on the POM surface. Indeed, if the peptide chain was not fully zipped on the POM surface, each HN residue should have its own flexibility, which is minor for anchored residues an is larger for not anchorated residues. This different flexibility will reflect in different T1 values, which are related to the re-orientational time of the particular residue in the peptide chain, which is combined with the rotational motion of the entire molecule. When the HN-residues of the lateral chain are fully zipped on the POM, their re-orientation values are similar since the peptide residues re-oriented themselves at the same time, during the rotational motion of the molecule.

| Amide Position in the α$_1$-(Gly)$_5$ POM derivative. | $^{15}$N R$_1$ (s$^{-1}$) | $^{15}$N T$_1$ (s) | $\tau_R$ (ns) | Amide Position in the α$_2$-(Gly)$_5$ POM derivative. | $^{15}$N R$_1$ (s$^{-1}$) | $^{15}$N T$_1$ (s) | $\tau_R$ (ns) |
|---|---|---|---|---|---|---|---|
| Gly-1 | 1.3 | 0.79 | 0.55 | Gly-1 | 1.3 | 0.78 | 0.55 |
| Gly-2 | 1.4 | 0.72 | 0.63 | Gly-2 | 1.7 | 0.59 | 0.88 |
| Gly-3* | 1.3 | 0.76 | 0.55 | Gly-3 | 1.1 | 0.89 | 0.40 |
| Gly-4* | 1.3 | 0.76 | 0.55 | Gly-4 | 1.3 | 0.76 | 0.55 |
| Gly-5 | 1.1 | 0.95 | 0.40 | Gly-5 | 0.85 | 1.18 | 0.24 |

**Table 4. 2**- $^{15}$N T1 for the amide protons for the α$_1$-(Gly)$_5$ and α$_2$-(Gly)$_5$. For each relaxation time is also reported the calculated rotational correlation time $\tau_R$ from equation 1 and 2. Concentration sample 3.3 mM in CD$_3$CN, spectra recorded at 600 MHz, at 298K. (*) These two resonances were overlapped in the spectra and fitted together.

To investigate the influence of the temperature on the folding of the peptide chain around the POM surface, we decided to collect ^{1}H-NMR spectra of the $\alpha_2$-Gly$_5$ (**3**) at different temperatures in CD$_3$CN. One can see that the chemical shifts of the amides closest to the polyoxometalate (HN-1, HN-2) are barely affected over a 90 K range (240-330 K), while the external ones (HN-4, HN-5 and H$_2$N) are more strongly affected. Nonetheless, the signals do not coalesce into a broad singlet, indicating that the polyglycine chain is still wrapped around the metal oxide cluster at 330 K.
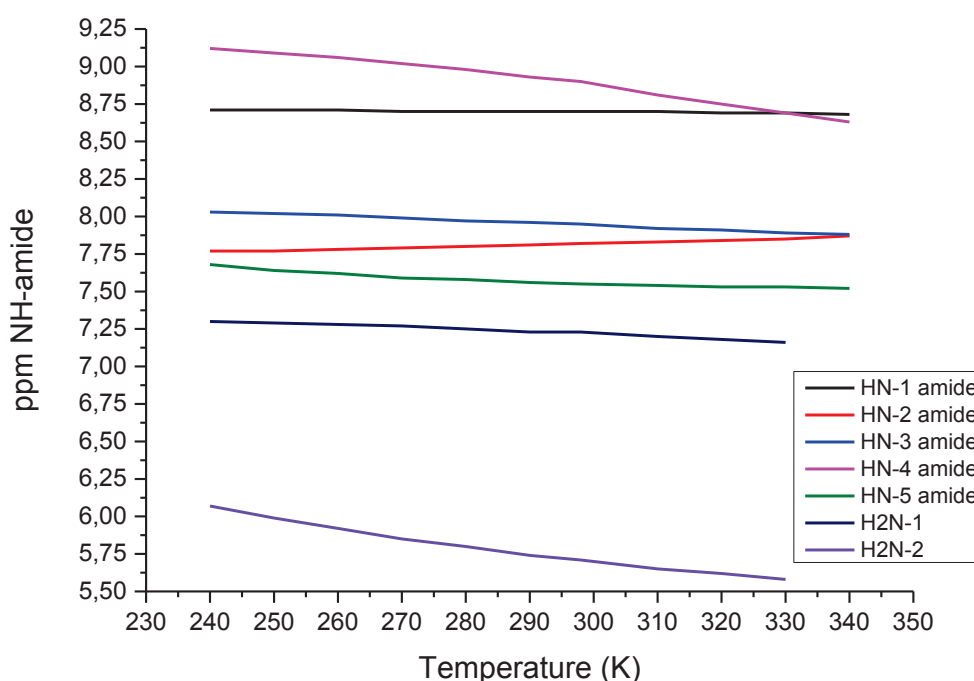


**Figure 4. 18**- Evolution of the proton amide shift with temperature for $\alpha_2$-Gly$_5$ (3) in CD$_3$CN. Concentration sample 3.3 mM. Spectra recorded at 1 GHz, in CD$_3$CN.

These contrasting temperature evolution patterns suggest a *zip-like* folding of the peptide in which a strong association arises from several cooperative interactions where Gly1 and Gly2 are tightly locked to the POM surface, and direct the wrapping of the remaining residues. Indeed the slope of the chemical shift vs. temperature curves is flat for the more "internal" signals (HN-1 and HN-2) while

it increases – albeit in a limited way – for the more external protons (HN-4, HN-5 and H$_2$N).

To investigate the influence of the solvent in the folding of the lateral chain, we decided to record the ^{1}H-NMR spectrum of $\alpha_2$-Gly$_5$ (**3**) in the more polar $d_6$-DMSO.

In DMSO the signals of the same protons are compacted in a small chemical shift range (0.4 ppm) around 8 ppm. Indeed, on the contrary to what has been observed in CD$_3$CN, in this more polar solvent the H-bonds to the POM surface are broken because the amides interact more strongly with the solvent, leading the lateral chain of the hybrid-POM to behave like its random coil parent.
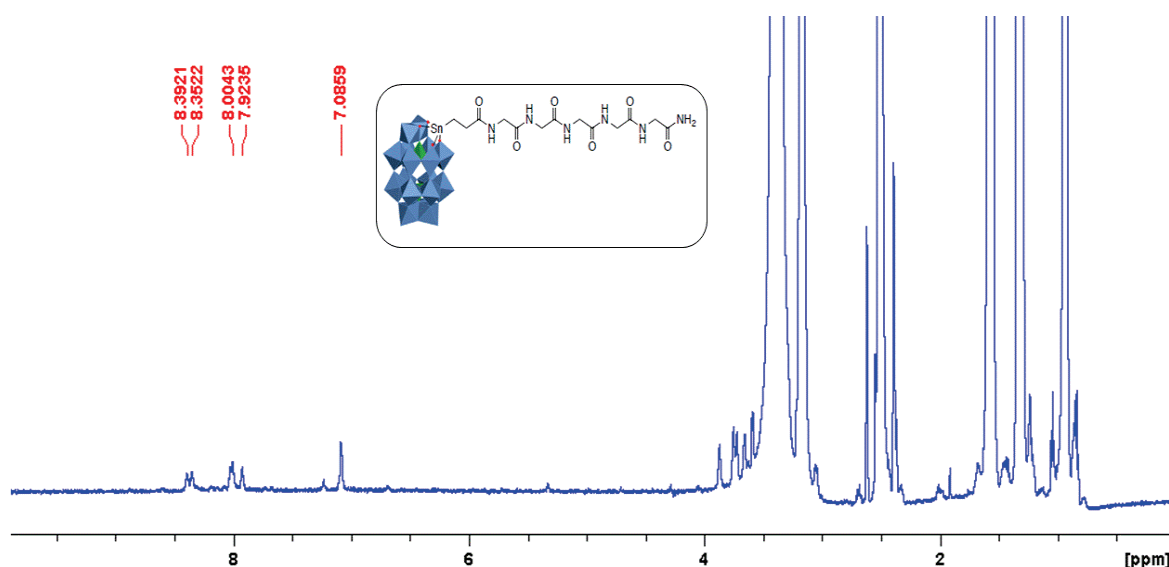


**Figure 4. 19**- ^{1}H-NMR spectrum of $\alpha_2$-Gly$_5$ in d$_6$-DMSO. Spectrum recorded at 600 MHz, 298K, 3.3 mM.

In light of all these observation in solution, we can deduce that the rigidity of the overall structure is due to a network of H-bonds interaction between the amide protons of the peptide chain and the oxygen atoms present on the POM surface, which lead to the folding of the polyglycine around the negatively charged POM via a *zip-like* arrangement.

### *4.3.4 Molecular Dynamics Simulations*

To accurately map where and how the polyglycine chains wrap onto the metal oxide surface, we sought insights from classical molecular dynamics performed with Amber12 Molecular Dynamic software package.[31] As shown in the Figure 4.20 as general example for $\alpha_1$-$Gly_6$, all the simulations were started from a β-sheet optimized conformation for the peptidic chain, at the BP86/6-31G(d)/Lanl2dz level of theory, with an implicit solvent model (IEFPCM) to account for acetonitrile solvation. The Gaussian09 software Revision D.01 was used for the quantum chemical calculations.[32]
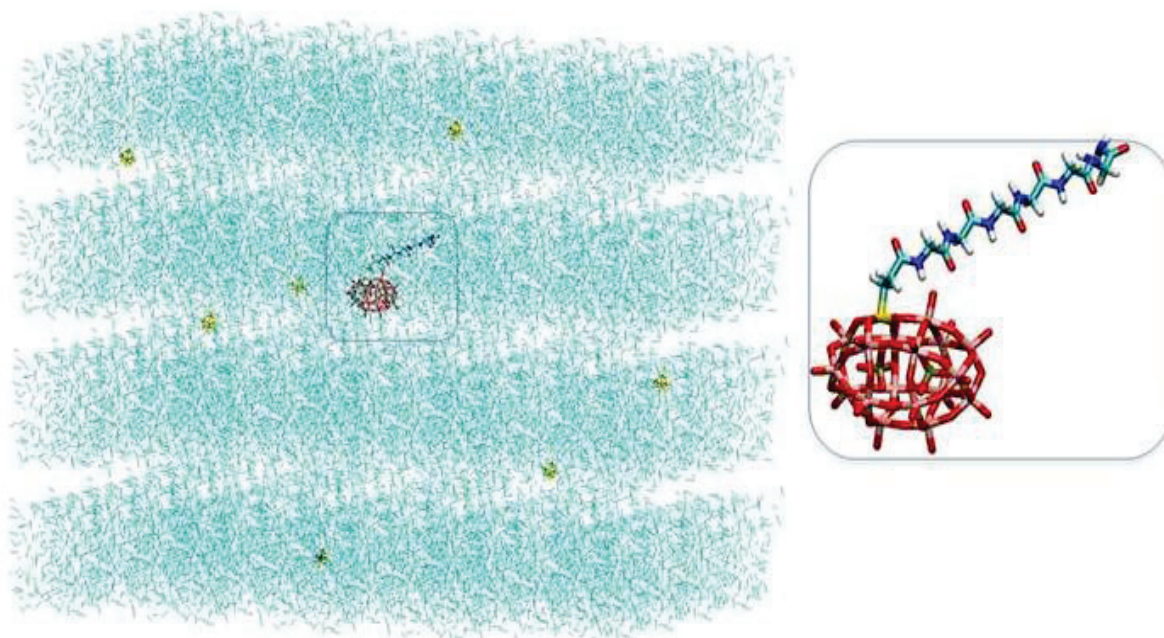


**Figure 4. 20**- $\alpha_1$- $Gly_6$. ~ 1000 molecules (7 Tetramethylammonium counteranions, in yellow). The acetonitrile solvent is represented in cyan lines. The polyglycine chain is started from a β-sheet conformation.

All 8 POMs underwent folding quickly (less than 250 ns) at 300 K. This characterizes a strong pattern of non-covalent interactions that dictates the wrapping.
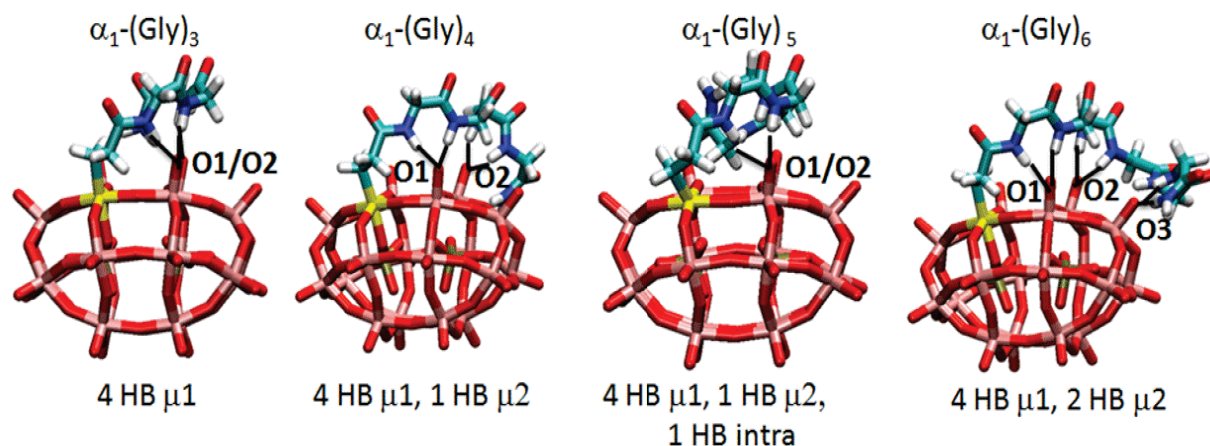
**Figure 4. 21**- Cartoon representation for the folded hybrid-POMs of the $\alpha_1$-(Gly)n serie. The number of HB is given. Acetonitrile and counterions are omitted.

Interestingly, the four $\alpha_1$-POMs (Figure 4.21) were found to fold the fastest, within less than 1 ns. In agreement with the NMR probe, all amide protons develop interactions with the POM. Two $\alpha_1$ oxygens interact with two hydrogen atoms each: along our dynamics, the pincer-like association for $Gly_1$ and $Gly_2$ is characterized by respective average distances of $1.76 \pm 0.1$ Å and $1.98 \pm 0.2$ Å (Table 4.3).

Along the $\alpha_1$ series, the pattern is conserved for the first hydrogen atoms of Gly-1 and Gly-2. The POM-(C=O)N-H interactions tend to be more labile as the chain expands and one moves further down the polyglycine chain (away from the POM).

| $\alpha_1$-Gly$_3$ | | $\alpha_1$-Gly$_4$ | | $\alpha_1$-Gly$_5$ | | $\alpha_1$-Gly$_6$ | |
|---|---|---|---|---|---|---|---|
| HH-OBC | 1.76±0.08 Å | HE-OBC | 1.99±0.14 Å | HE-OBC | 2.05±0.17 Å | HE-OBC | 2.16±0.18 Å |
| HK-OBC | 1.98±0.19 Å | HH-OBC | 93±0.14 Å | HH-OBC | 1.82±0.10 Å | HH-OBC | 1.85±0.11 Å |
| HN-OBC | 2.80±1.09 Å | HK-OAG | 2.06±0.14 Å | HK-OAG | 1.92±0.11 Å | HK-OAG | 2.04±0.17 Å |
| HO-OBA | 4.57±1.00 Å | HN-OAH | 1.93±0.15 Å | HN-OAH | 1.85±0.11 Å | HN-OAH | 1.91±0.18 Å |
| | | HQ-OAZ | 3.59±0.5 Å | HQ-OBH | 2.11±0.23 Å | HQ-OBB | 2.54±0.35 Å |
| | | HR-OAR | 2.46±0.44 Å | HV-OCN | 2.72±0.44 Å | HT-OBB | 1.95±0.34 Å |
| | | | | | | HW-OBB | 3.89±0.70 Å |
| | | | | | | HX-OBB | 2.64±0.83 Å |

| $\alpha_2$-Gly$_3$ | | $\alpha_2$-Gly$_4$ | | $\alpha_2$-Gly$_5$ | | $\alpha_2$-Gly$_6$ | |
|---|---|---|---|---|---|---|---|
| HE-OBF | 3.96±0.36 Å | HE-OAY | 2.49±0.31 Å | HE-OBF | 6.24±0.49 Å | HE-OCM | 4.34±1.38 Å |
| HH-OBF | 2.56±0.30 Å | HH-OAY | 7.97±1.66 Å | HH-OBF | 9.58±1.34 Å | HH-OCM | 4.25±0.96 Å |
| HK-OBA | 3.62±2.68 Å | HK-OBG | 1.90±0.16 Å | HK-OBG | 11.48±1.44 Å | HK-OBB | - |
| HN-OAM | >3 Å | HN-OBG | 2.20±0.22 Å | HN-OBG | 7.14±3.20 Å | HN-OBF | 7.88±1.34 Å |
| HO-OBA | 2.49±0.61 Å | HQ-OBB | 4.46±0.96 Å | HQ-OBA | 1.99±0.34 Å | HQ-OAR | 2.98±2.93 Å |
| | | HR-OBA | 5.73±0.58 Å | HT-OBB | 7.51±5.27 Å | HT-OAN | 3.56±3.48 Å |
| | | HR-OCM | - | HU-OBB | 6.21±4.29 Å | HW-OBB | 7.59±3.39 Å |
| | | | | | | HX-OBB | 7.28±3.38 Å |

**Table 4. 3-** Hydrogen-bonding map distances between each amidic proton of the lateral chain and the corresponding interacting oxygen of the POM surface, for all the hybrid-POMs. The fluctuation of the value during the molecular dynamics is given.

This confirms the *zip-like* folding mechanism/scenario hypothesized from the high-field NMR investigation, where the internal amides fold first, providing a starting lock to the conformation. This orientates the remaining amides, which follow suit. The interaction pattern between the more external glycines and the POM is therefore more opportunistic. Weaker electrostatic interactions through

one-to-one hydrogen bonds are typically at a distance of 2.7 ± 0.6 Å. Intrapeptide hydrogen bonds also progressively come into play, but only if no accessible oxygen from the metal oxide is available. The former induce less energetic stabilization. Counter-intuitively, the W–O–W bridging $\mu_2$ oxygen atoms are not the preferred surface oxo H acceptors.

The bridging oxos are generally the more basic sites in a POM because of their larger *s* character. This effect is however less pronounced in polyoxotungstates.[21] Klemperer reported that silylation of a terminal oxo was favored when steric strain was too important.[33] In our case, the constraints imposed by the $(CH_2)_2$–C=O spacer orientates the peptidic chain towards the terminal W=O $\mu_1$ oxos.

The folding behavior of the $\alpha_2$ organo-POMs is more complex. First of all, it takes more than 100 ns to complete the folding, except for $\alpha_2$-(Gly)$_3$, when the $\alpha_1$ equivalents took only a fraction of that time.

| Entry | | Time to stabilize the hydrogen bond (ns) [ns total acquisition production] | | | | | |
|---|---|---|---|---|---|---|---|
| 1 | $\alpha_2$-Gly$_3$ [300ns] | **HE-OBF** ~20ns | **HH-OBF** ~20ns | **HK-OBA** ~20ns | | | |
| 2 | $\alpha_2$-Gly$_4$ [300ns] | **HE-OAY** ~125ns | **HH-OAY** ~125ns | **HK-OBG** ~125ns | **HN-OBG** ~125ns | | |
| 3 | $\alpha_2$-Gly$_5$ [300ns] | **HE-OBF** ~200ns | **HH-OBF** ~200ns | **HK-OBG** - | **HN-OBG** ~200ns | **HQ-OBA** ~200ns | |
| 4 | $\alpha_2$-Gly$_6$ [300ns] | **HE-OCM** ~133ns | **HH-OCM** ~133ns | **HK-OBB** - | **HN-OBF** ~133ns | **HQ-OAR** ~133ns | **HT-OAN** ~133ns |

**Table 4. 4**- Folding time for $\alpha_2$-$(P_2W_{17}O_{61})SnCH_2CH_2(NHCH_2CO)xNH_2$.

This characterizes a less direct, probably weaker, interaction pattern as the peptidic chain samples more oxo ligands before finding the best suited ones.
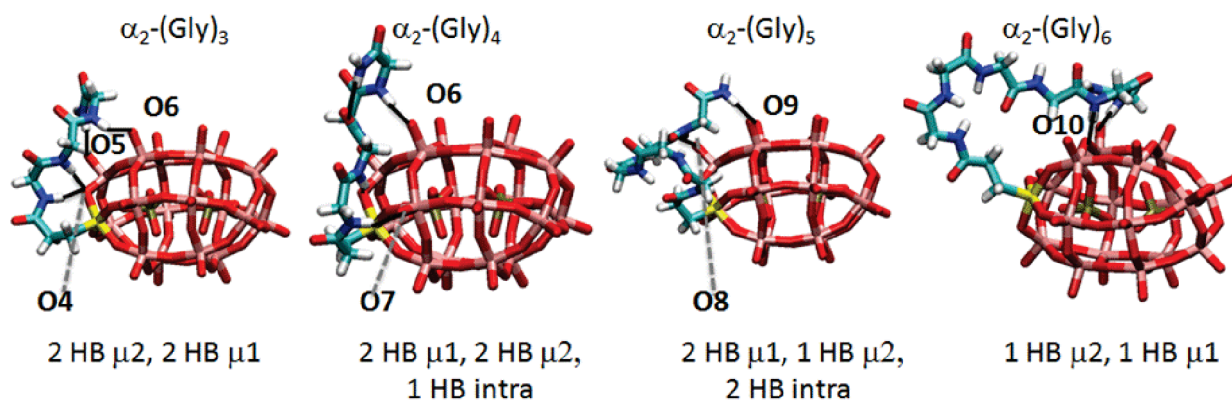
**Figure 4. 22**- Cartoon representation for the folded hybrid-POMs of the $\alpha_2$-(Gly)n serie. The number of HB is given. Acetonitrile and counterions are omitted.

The HN-1 and HN-2 hydrogen atoms end up "clamping" a lateral $\mu2$ oxygen atom. However, the distance remains rather long $2.5 \pm 0.3$ Å (Table 4.3) to the strongest interacting hydrogen. This is far from the optimal value of $1.8 \pm 0.1$ Å with the $\mu1$ oxos, as seen previously. The first two internal glycines are geometrically constrained because of their different grafting point on the POM structure, and they do not find a satisfying partner there. Consequently, when the chain of the $\alpha_2$-(Gly)$_n$ hybrids grows, they prefer entering into more energetically favorable β-turn intrapeptide conformations rather that locking on the POM surface, as shown in the cartoon representation in Figure 4.22. This positions the "farthest" amides close to the POM surface, with which they develop H-bonds. Longer polyglycine chains (n=5 and 6) thus spend even more time to explore the free energy surface (FES), yet our simulations still converge towards a well-defined folded structure. This was verified starting from several different orientations and initial velocities.

Our analysis reveals that the nature of the proximal oxygen with which the key first amide proton interacts ($\mu1$ in the belt, $\mu2$ in the crown [O1, O2 *vs.* O4 O5 and O6]) is the decisive factor that directs the folding of the polyglycine chain.

To further support our findings we performed calculations of NMR shifts on a series of eight structures, reoptimized at the DFT level.[32] A quantitative agreement could however not be reached due to the inherent dynamics of the pendulum-like motion of the protons around the µ1 oxos at the NMR timescale, which are especially strong for the shorter chain hybrids.
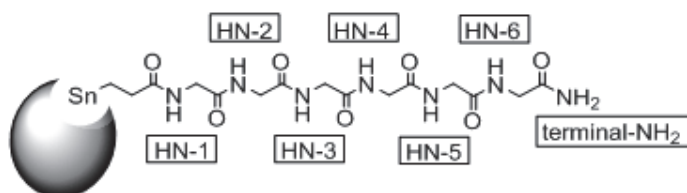


| POM | $\delta_{HN-x}$ (ppm) | | | | | | |
|---|---|---|---|---|---|---|---|
| | x =1 | x =2 | x =3 | x =4 | x =5 | x =6 | terminal-NH$_2$ |
| $\alpha_2$-(Gly)$_3$ | 10.87 | 10.15 | 9.75 | - | - | - | 9.64/5.34 |
| $\alpha_2$-(Gly)$_4$ | 9.59 | 8.33 | 10.24 | 9.68 | - | - | 9.55/5.64 |
| $\alpha_2$-(Gly)$_5$ | 11.01 | 8.78 | 11.10 | 8.73 | 10.44 | | 9.95/5.53 |
| $\alpha_2$-(Gly)$_6$ | 6.36 | 6.46 | 7.35 | 7.06 | 9.63 | 10.25 | 6.31/5.59 |
| $\alpha_1$-(Gly)$_3$ | 5.78 | 7.12 | 4.12 | - | - | - | 5.66/5.48 |
| $\alpha_1$-(Gly)$_4$ | 9.80 | 9.46 | 8.68 | 9.95 | - | - | 10.57/6.27 |
| $\alpha_1$-(Gly)$_5$ | 10.24 | 10.41 | 7.65 | 12.26 | 6.97 | - | 10.94/5.72 |
| $\alpha_1$-(Gly)$_6$ | 9.27 | 10.26 | 7.70 | 9.10 | 7.11 | 9.28 | 9.01/5.93 |

**Table 4. 5**- Calculated ^{1}H-NMR shifts of amide protons, in the POM@polyglycine derivatives.

We investigated more cautiously the case of $\alpha_2$-(Gly)$_6$ because it has less clamp-like 3 atoms bonds, and thus should be less prone to pendulum motion. We observed that this molecule shows significant differences also in the shifts and line-widths of the glycine CH$_2$ protons of the α-carbon. This behavior indicates that sizeable conformational equilibria are retained in solution for this particular POM.

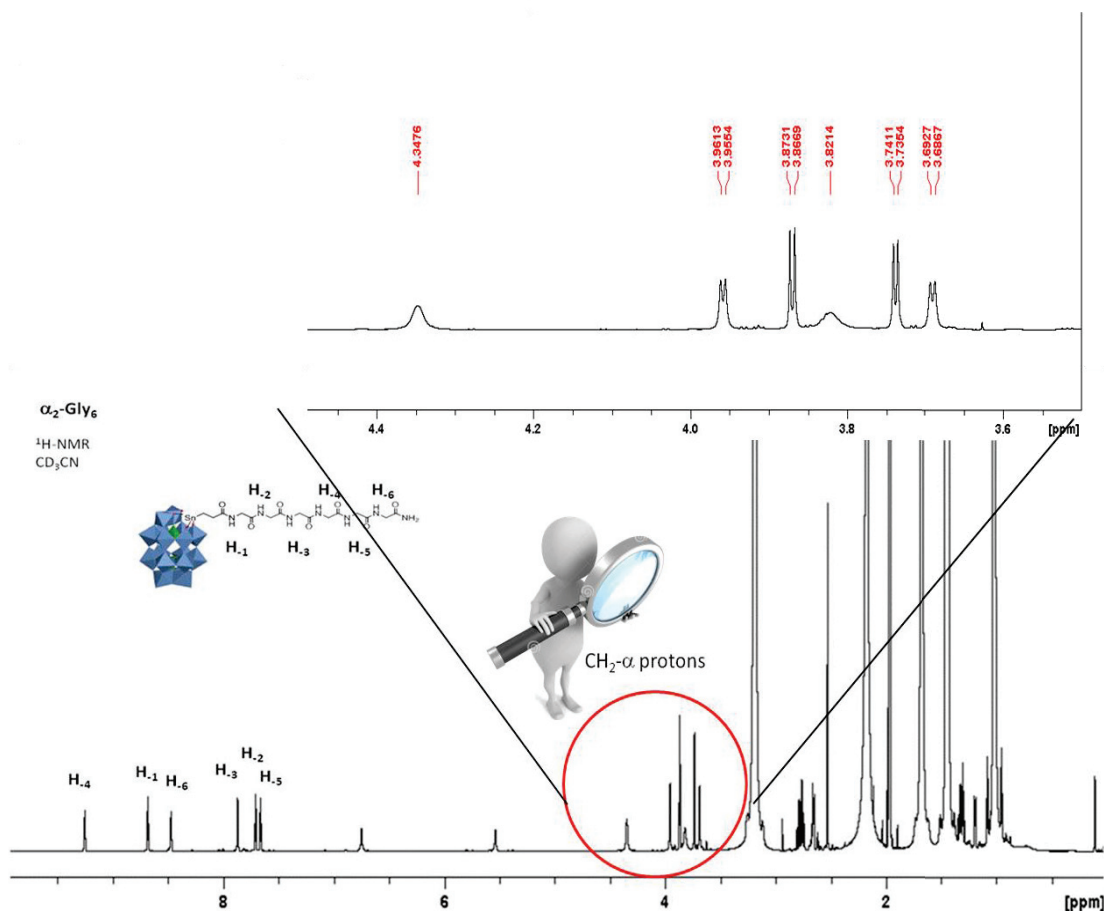**Figure 4. 23-** $^1$H-NMR spectrum of $\alpha_2$-Gly$_6$, highlighting the $\alpha$-protons peaks region.

Indeed, when we look at the 1D spectrum of the $\alpha_2$-POM(Gly)$_6$ it is possible to see a different situation concerning the protons of the $\alpha$-carbon in the peptide. As expected for a rigid structure, we are clearly in presence of 6 separate resonances for the 12 HA protons, with one resonance per residue. Four of them are split only by the $^3$J vicinal coupling with the HN (negligible geminal coupling), while two of them are weaker and broad, one at around 4.35 ppm, which correspond to the protons on the $\alpha$-carbon of Gly-2, and 3.82 ppm, which correspond to the protons of the $\alpha$-carbon of Gly-3. This situation can occurs only if the peptide chain is "zipped" on the POM but it remains highly flexible, with the conformational equilibrium that continuously flips the "equatorial and axial positions" and averages the chemical shifts of the two methylene protons. The resonances of the $\alpha_2$-POM(Gly)$_6$ are strongly affected by the dynamics, and not only the CH$_2$ but

193

also the amidic HNs. So, it is not surprising if the agreement with the DFT calculation is poor.
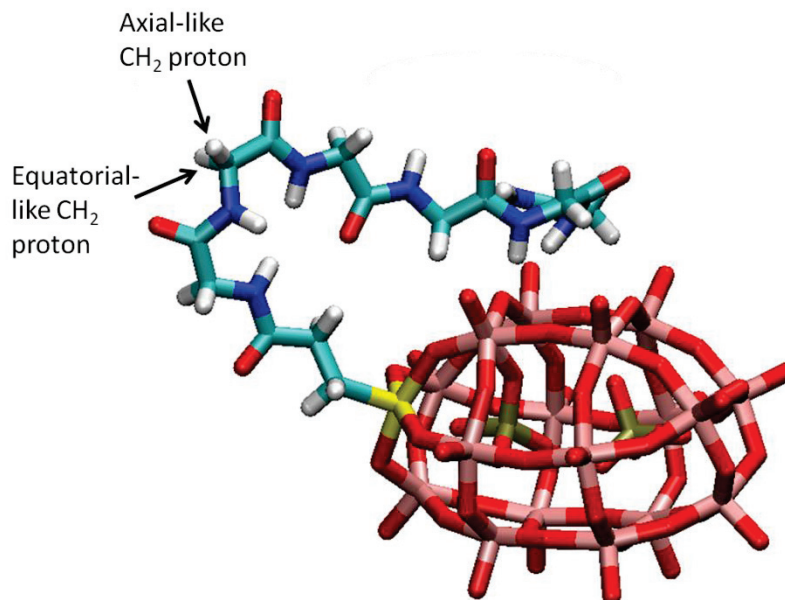


**Figure 4. 24**- $\alpha_2$-POM(Gly)$_6$ optimized structure at the end of the MD simulation. The lateral peptide chain isn't completely locked around the POM surface, reflecting a certain mobility of the amidic protons and a-CH2 protons.

This fits with the proposed clamp-like structure that retains some flexibility in this case, but it makes the agreement between computational and experimental shifts much harder.

As stated before, intrapeptide interactions do not appear in the $\alpha_1$ series, and only in POM $\alpha_2$-(Gly)$_6$. To establish whether and how this translates to longer chains, we decided to model oligopeptide conjugates $\alpha_1$-(Gly)$_{15}$ and $\alpha_2$-(Gly)$_{15}$. However, starting from 6 glycine residues in the lateral chain, solubility issues become important as the hybrid-POM becomes insoluble in $CH_3CN$. Because we showed that the solvent was crucial, it was pointless to look for a NMR solvent that made the organo-POM soluble. Since we could not assess this experimentally we turned to Molecular Dynamics simulations.

In this case, we found that along the $\alpha_1$-POM serie the polyglycine chain wrapped itself around the first three glycines that are themselves folded around the POM

surface. This happened via β-turn intrapeptide interactions (Gly$_4$ to Gly$_7$ and Gly$_7$ to Gly$_{10}$).

α$_2$-Gly$_n$ derivatives behave differently. Indeed in this case after 300 ns of simulation any folding of the lateral chain around the polyoxometallic framework was observed. The amidic protons of the lateral chain don't succeed to sample oxygen atoms on the POM surface, preferring to adopt a random conformation directed rather by intrapeptide interactions. Probably, more simulation time was necessary for the amidic protons of the α$_2$-POMs serie to lock into the oxygens on the POM surface.
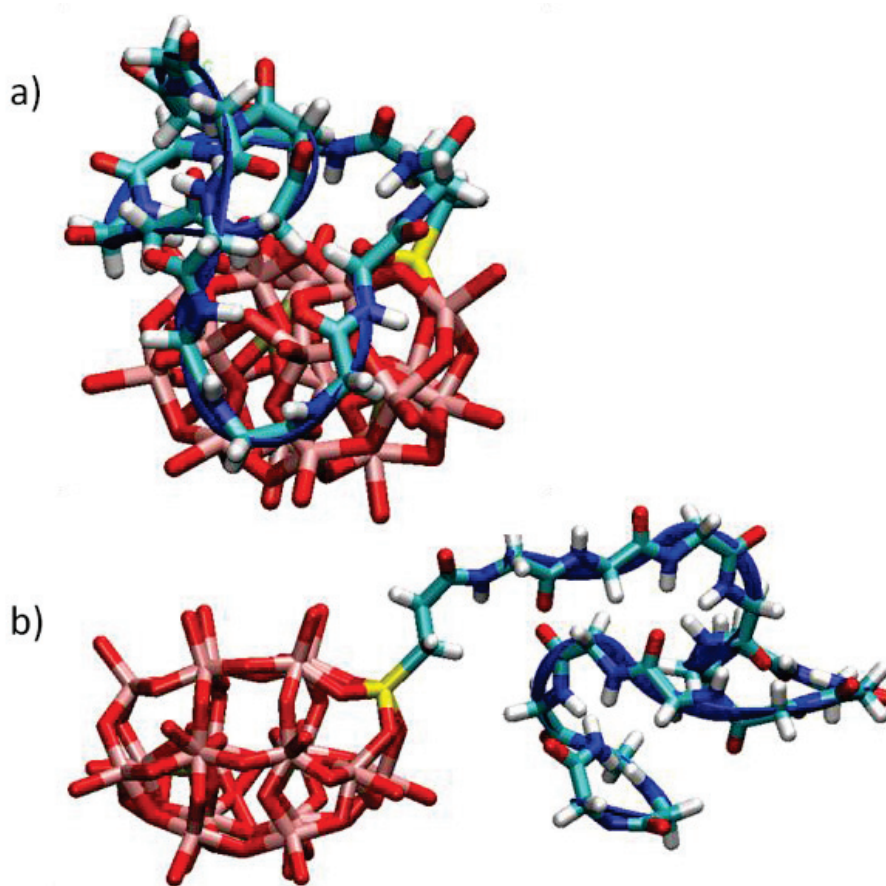


**Figure 4. 25-** Cartoon representation of the modeled hybrid POM-oligopeptides conjugate: a) α$_1$-(Gly)$_{15}$ and b) α$_2$-(Gly)$_{15.}$ Acetonitrile and counterions are omitted.

In any case, it can be seen that even in a much longer chain, the POM framework succeeds in rigidifying the normally flexible oligopeptide. Longer chain peptides do not find space around the metal-oxide surface of the cluster wrapping instead

themselves around the initial loop, like a ball of a wool, via β-turns, creating a more rigid structure.

### *4.3.5 Conclusions*

*To conclude, we have evidenced that polyglycine side-chains in several mono-substituted Dawson polyoxotungstates fold toward the metal-oxide surface with which they establish zip-like hydrogen-bond networks. The structures obtained are rigid in acetonitrile but not in the more polar DMSO. They were evidenced by high-field NMR and could be modeled to precisely pinpoint the cartography of the interaction. This led us to evidence that the topography of the hybrid ($\alpha_1$ or $\alpha_2$ series) is a key parameter that determines where and how the chain folds. Longer chain peptides do not find space around the metal-oxide surface but wraps themselves around the initial loop, via β-turns.*

*In all cases, the POM acts as a rigidifier for otherwise flexible oligomers and this bodes well for the conception of POM-based artificial enzymes.*[34]

## 4.4 General Conclusions

In this chapter we investigated for the first time the behavior in solution of a polyoxotungstate covalently functionalized with polyglycine chains of different length (3-6). We demonstrated, thanks to a mix of experimental/theoretical approach, that simultaneous weak H-bonding interactions, between the amidic protons of the peptide chain and the oxygen atoms naturally present on the POM surface, allow to rigidify the hybrid structure even in solution. The zip-like folding mechanism of the lateral chain around the POM surface and the influence of the polyoxometalate configuration toward the interaction pathway were elucidated. We are planning to explain this feature to create a peptide-based chiral pocket around a well-defined catalytic site on the POM.

## 4.5 Bibliography

[1]  J. T. Rhule, C. L. Hill, D. A. Judd, R. F. Schinazi, *Chem. Rev.* **1998**, *98*, 327–358.

[2]  B. Hasenknopf, *Front. Biosci. J. Virtual Libr.* **2005**, *10*, 275–287.

[3]  H. Yanagie, A. Ogata, S. Mitsui, T. Hisa, T. Yamase, M. Eriguchi, *Biomed. Pharmacother. Biomedecine Pharmacother.* **2006**, *60*, 349–352.

[4]  D. A. Judd, J. H. Nettles, N. Nevins, J. P. Snyder, D. C. Liotta, J. Tang, J. Ermolieff, R. F. Schinazi, C. L. Hill, *J. Am. Chem. Soc.* **2001**, *123*, 886–897.

[5]  T. Yamase, *J. Mater. Chem.* **2005**, *15*, 4773–4782.

[6]  R. Prudent, V. Moucadel, B. Laudet, C. Barette, L. Lafanechère, B. Hasenknopf, J. Li, S. Bareyt, E. Lacôte, S. Thorimbert, et al., *Chem. Biol.* **2008**, *15*, 683–692.

[7]  Crans, D. C., *Comments Inorg Chem* **1994**, 35–76.

[8]  H. Stephan, M. Kubeil, F. Emmerling, C. E. Müller, *Eur. J. Inorg. Chem.* **2013**, *2013*, 1585–1594.

[9]  Q. Wu, J. Wang, L. Zhang, A. Hong, J. Ren, *Angew. Chem. Int. Ed.* **2005**, *44*, 4048–4052.

[10] H.-K. Yang, Y.-X. Cheng, M.-M. Su, Y. Xiao, M.-B. Hu, W. Wang, Q. Wang, *Bioorg. Med. Chem. Lett.* **2013**, *23*, 1462–1466.

[11] M. Cindrić, N. Strukan, M. Devčić, B. Kamenar, *Inorg. Chem. Commun.* **1999**, *2*, 558–560.

[12] M. Cindrić, T. K. Novak, S. Kraljević, M. Kralj, B. Kamenar, *Inorganica Chim. Acta* **2006**, *359*, 1673–1680.

[13] U. Kortz, M. G. Savelieff, F. Y. A. Ghali, L. M. Khalil, S. A. Maalouf, D. I. Sinno, *Angew. Chem. Int. Ed.* **2002**, *41*, 4070–4073.

[14] M. Inoue, T. Yamase, *Bull. Chem. Soc. Jpn.* **1995**, *68*, 3055–3063.

[15] M. Inoue, T. Yamase, *Bull. Chem. Soc. Jpn.* **1996**, *69*, 2863–2868.

[16] E. Cartuyvels, K. Van Hecke, L. Van Meervelt, C. Görller-Walrand, T. N. Parac-Vogt, *J. Inorg. Biochem.* **2008**, *102*, 1589–1598.

[17] A. Müller, S. K. Das, C. Kuhlmann, H. Bögge, M. Schmidtmann, E. Diemann, E. Krickemeyer, J. Hormes, H. Modrow, M. Schindler, *Chem. Commun.* **2001**, 655–656.

[18] C. Boglio, B. Hasenknopf, G. Lenoble, P. Rèmy, P. Gouzerh, S. Thorimbert, E. Lacôte, M. Malacria, R. Thouvenot, *Chem.- Eur. J.* **2008**, *14*, 1532–1540.

[19] S. Bareyt, S. Piligkos, B. Hasenknopf, P. Gouzerh, E. Lacôte, S. Thorimbert, M. Malacria, *Angew. Chem. Int. Ed.* **2003**, *42*, 3404–3406.

[20] S. Bareyt, S. Piligkos, B. Hasenknopf, P. Gouzerh, E. Lacôte, S. Thorimbert, M. Malacria, *J. Am. Chem. Soc.* **2005**, *127*, 6788–6794.

[21] C. Boglio, K. Micoine, É. Derat, R. Thouvenot, B. Hasenknopf, S. Thorimbert, E. Lacôte, M. Malacria, *J. Am. Chem. Soc.* **2008**, *130*, 4553–4561.

[22]K. Micoine, B. Hasenknopf, S. Thorimbert, E. Lacôte, M. Malacria, *Angew. Chem. Int. Ed.* **2009**, *48*, 3466–3468.

[23]C. Yvon, A. J. Surman, M. Hutin, J. Alex, B. O. Smith, D.-L. Long, L. Cronin, *Angew. Chem. Int. Ed.* **2014**, *53*, 3336–3341.

[24]D. Lachkar, E. Lacôte, *Comptes Rendus Chim.* **2016**, *19*, 113–116.

[25]C. Jahier, M. Cantuel, N. D. McClenaghan, T. Buffeteau, D. Cavagnat, F. Agbossou, M. Carraro, M. Bonchio, S. Nlate, *Chem. – Eur. J.* **2009**, *15*, 8703–8708.

[26]Y. Yan, H. Wang, B. Li, G. Hou, Z. Yin, L. Wu, V. W. W. Yam, *Angew. Chem. Int. Ed.* **2010**, *49*, 9233–9236.

[27]W.-J. Xuan, C. Botuha, B. Hasenknopf, S. Thorimbert, *Chem. – Eur. J.* **2015**, *21*, 16512–16516.

[28]D. Lachkar, *Synthèses, Études Structurales et Applications Catalytiques d'Organo-Polyoxométallates*, Paris 11, **2014**.

[29]M. Karplus, *J. Am. Chem. Soc.* **1963**, *85*, 2870–2871.

[30]"Nuclear Spin Relaxation in Liquids: Theory, Experiments, and Applications," can be found under https://www.crcpress.com/Nuclear-Spin-Relaxation-in-Liquids-Theory-Experiments-and-Applications/Kowalewski-Maler/p/book/9780750309646, **2006**.

[31]D.A. Case, D.S. Cerutti, T.E. Cheatham, III, T.A. Darden, R.E. Duke, T.J. Giese, H. Gohlke, A.W. Goetz, D. Greene, N. Homeyer, S. Izadi, A. Kovalenko, T.S. Lee, S. LeGrand, P. Li, C. Lin, J. Liu, T. Luchko, R. Luo, D. Mermelstein, K.M. Merz, G. Monard, H. Nguyen, I. Omelyan, A. Onufriev, F. Pan, R. Qi, D.R. Roe, A. Roitberg, C. Sagui, C.L. Simmerling, W.M. Botello-Smith, J. Swails, R.C. Walker, J. Wang, R.M. Wolf, X. Wu, L. Xiao, D.M. York and P.A. Kollman; Amber, University of California, San Francisco, **2015**.

[32]Gaussian 09, Revision A.02, M. J. Frisch, G. W. Trucks, H. B. Schlegel, G. E. Scuseria, M. A. Robb, J. R. Cheeseman, G. Scalmani, V. Barone, G. A. Petersson, H. Nakatsuji, X. Li, M. Caricato, A. Marenich, J. Bloino, B. G. Janesko, R. Gomperts, B. Mennucci, H. P. Hratchian, J. V. Ortiz, A. F. Izmaylov, J. L. Sonnenberg, D. Williams-Young, F. Ding, F. Lipparini, F. Egidi, J. Goings, B. Peng, A. Petrone, T. Henderson, D. Ranasinghe, V. G. Zakrzewski, J. Gao, N. Rega, G. Zheng, W. Liang, M. Hada, M. Ehara, K. Toyota, R. Fukuda, J. Hasegawa, M. Ishida, T. Nakajima, Y. Honda, O. Kitao, H. Nakai, T. Vreven, K. Throssell, J. A. Montgomery, Jr., J. E. Peralta, F. Ogliaro, M. Bearpark, J. J. Heyd, E. Brothers, K. N. Kudin, V. N. Staroverov, T. Keith, R. Kobayashi, J. Normand, K. Raghavachari, A. Rendell, J. C. Burant, S. S. Iyengar, J. Tomasi, M. Cossi, J. M. Millam, M. Klene, C. Adamo, R. Cammi, J. W. Ochterski, R. L. Martin, K. Morokuma, O. Farkas, J. B. Foresman, and D. J. Fox, Gaussian, Inc., Wallingford CT, 2016., **2016**.

[33]V. W. Day, W. G. Klemperer, D. J. Maltbie, *J. Am. Chem. Soc.* **1987**, *109*, 2991–3002.

[34] D. Vilona, D. Lachkar, E. Dumont, M. Lelli, E. Lacôte, *Submitted* **2017**.

# CHAPTER 5: General Conclusions and Perspectives

This thesis project was focused in the development of hybrid polyoxometalates for sustainable asymmetric acid catalysis. The first part of the research was devoted to the study of organo POMs able to perform acid catalysis.

The second part was employed to understand how the polyoxometalate could intramolecularly interact with polypeptide chains, with the aim to rationally design chiral pockets around the catalytic site.

- Starting with a family of POM@amides, already tested as Brønsted acid catalysts toward the organo-catalytic quinoline reduction, it was demonstrated that the catalytic activity arises from the proton of the inserted amide of the organo-POMs. The electrowithdrawing character of the polyoxometalate exalts the acidity of the amidic proton, which is otherwise unable to catalyse the quinoline reduction. This is because the POM is an electron *reservoir* that can stabilize the negative charge generated from the deprotonation. Through NMR characterizations and DFT calculations we demonstrated that the catalytic proton remains confined on the amidic nitrogen, upon grafting of the organic-ligand.[1]
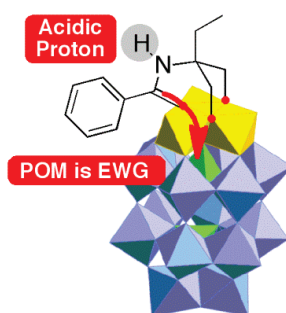


**Figure 5.1-** POM@amides: the first organo-POM efficiently employed as Bronsted acid catalyst.

- A new family of hybrid-POMs able to perform the Brønsted catalysis thanks to the interplay between organic and inorganic part, was developed.
  In this case the Dawson polyoxotungstovanadate $[P_2V_3W_{15}O_{62}]^{9-}$ was functionalized with different diolurea ligands. The activity as H-bonding

activation catalyst was demonstrated toward the Friedel-Craft alkylation of Indole with trans-β-nitrostyrene, where the free diolurea moiety was almost inactive. The catalyst was easily recycled 3 times, without any important loss in its activity. NMR titrations were performed to investigate the catalytic mechanism, and the calculated binding constants demonstrated that the hybrid-POMs do not interact strongly with the substrate with respect to the free urea. This probably allows the faster catalytic turnover. We also evidenced a likely secondary activation of the substrate *via* the oxygens of the crown. Finally DFT calculations are in progress to quantify the charge transfer between the inorganic scaffold and the organic moiety and consequently the improvement in the catalytic activity.[2]
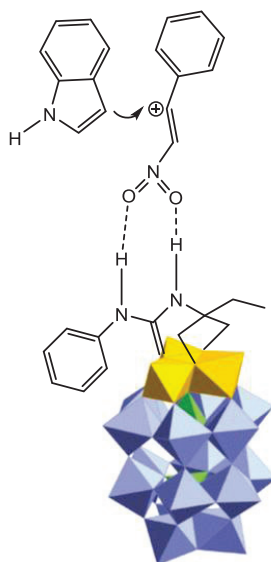


**Figure 5.2-** POM@ureas a efficient catalyst for hydrogen-bond activation reactions.

- Finally, a family of hybrid-polyoxotungstate, covalently functionalized with polyglycine chains of different lengths (3-6) residues, was chosen as benchmark to investigate the intramolecular interactions POM/peptides in solution.

  High-field NMR characterizations and Molecular Dynamics simulations allowed us to elucidate the folding of the lateral chain around the negative charged POM surface, thanks to hydrogen-bonding interactions. The zip-like

folding mechanism was proposed using NMR experiments and successively confirmed through Molecular dynamics simulations. The latter allowed us also to map each NH---O interaction between the amidic proton of the peptide and the oxygen atoms naturally present on the POM surface. Moreover, the influence of the POM topography ($\alpha_1$ or $\alpha_2$ lacunary POM) was established.[3]
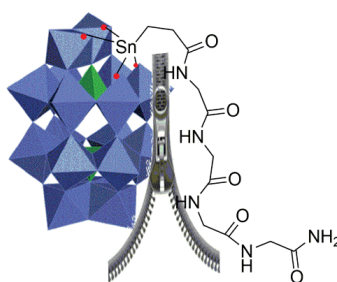


**Figure 5.3-** Intramolecular H-bonding interactions in solution in POM@polyglicines: a zip-like folding mechanism.

The natural perspective opened by this work concerns the development of a chiral pocket around the catalytic proton in the diolamide/diolurea ligand before to graft them into the POM crown, to perform asymmetric acid catalysis.

[1]   D. Lachkar, D. Vilona, E. Dumont, M. Lelli, E. Lacôte, *Angew. Chem. Int. Ed.* **2016**, *55*, 5961–5965.
[2]   D.Vilona, M. Lelli, E. Dumont, E. Lacôte; In preparation, **2017**.
[3]   D. Vilona, D. Lachkar, E. Dumont, M. Lelli, E. Lacôte, *Submitted* **2017**.

# CHAPTER 6: Experimental details

# 6.1 Organo-POMs as Brønsted acid catalysts

## *6.1.1 Density functional calculations*

Geometry optimizations were started from available crystal structures [5,6] and substitution made manually for each substituent before performing a full geometry re-optimization.

The geometries of the substituted organo-POMs were optimized in the framework of density functional theory (DFT), using the Becke88-Perdew86 (BP86) exchange correlation functional and alongside with the double-ζ LANL2DZ basis set. This choice is common for polyoxometalate structural determination.[7]

For the NMR shift calculations, single-point DFT-GIAO (Gauge-Independent Atomic Orbital) calculations were carried out using the hybrid PBE0 functional. The Gaussian 09 Revision D01 suite of programs was used throughout to perform quantum chemical calculations, both geometry optimizations and spectroscopic determination.[8]

The charge transfer between the organic appendage and the POM unit was evaluated according to the ESP (based on the evaluation of the electrostatic potential) charges.

Proton affinities (PA) for POM@amides derivatives were estimated as the difference between electronic energies $PA=E(RH+)-E(R)$ on the nitrogen atom: on the amide, and on several $\mu_1$ terminal and $\mu_2$ bridging oxygens.

### 6.1.2    *NMR details*

1D $^1$H, $^{19}$F, $^{31}$P, $^{13}$C NMR spectra were recorded at 9.4 T (300, 282, 121.5, and 75 MHz for $^1$H, $^{19}$F, $^{31}$P, $^{13}$C respectively), using a Bruker AVANCE 300 spectrometer equipped with a BBFO probe. The 2D NMR $^1$H–$^{15}$N HSQC and HMBC spectra were acquired at 14.1 T (600.3 MHz for proton, 150.9 MHz for $^{13}$C and 60.8 MHz for $^{15}$N Larmor frequencies) using an Avance III NMR Bruker instrument equipped with a Triple resonance TCI cryoprobe.

Standard sequences were used for $^1$H-$^{15}$N HSQC and $^1$H-$^{15}$N HMBC. The $^1$H $\pi/2$ radiofrequency (RF) pulse was calibrated to 8.0 ms, and the $^{15}$N $\pi/2$ RF pulse was 35.0 ms. The gradient selected Echo-Antiecho quadrature was used for 2D HSQC and Magnitude Mode for 2D HMBC. The 2D $^1$H-$^{15}$N HSQC were acquired with 512 x 128 complex points, with acquisition times of 53.2 ms and 17.5 ms in the direct and indirect dimensions, respectively, and the recycle delay was 4.0 s. The 2D $^1$H-$^{15}$N HMBC were acquired with 2048 x 476 complex points, with acquisition times of 170.39 ms and 24.47 ms in the direct and indirect dimensions, respectively, and the recycle delay was 4.0 s.

All the experiments where acquired at 298 K, and the $^1$H and $^{13}$C chemical shifts are referenced to TMS, while $^{31}$P is referenced to phosphoric acid and $^{15}$N has been referenced to liquid $NH_3$. Chemical shifts are reported in ppm, using, for $^1$H and $^{13}$C, solvent residual peak as internal standard references. Coupling constants (*J*) are given in Hertz (Hz), multiplicity (s =singlet, d =doublet, t =triplet, q =quartet, m =multiplet).

**NMR as a tool to calculate the association constant**

*Theory*

Consider a metal complex *CM*, where *C* is a multidentate ligand that leaves an empty coordination position on the metal, in the presence of a monodentate

ligand $L$. The paramagnetic effects observed on a nucleus of $L$ can then be used to obtain information on its dissociation constant:

$$K = \frac{[CM][L]}{[CML]} = \frac{(C_{CM} - [CML])(C_L - [CML])}{[CML]}$$

where $C_{CM}$ and $C_L$ are the total concentrations of all the metal-containing and ligand-containing species respectively, and $[CML]$ is the equilibrium concentration of the adduct. Under fast exchange conditions, the molar fraction of bound ligand $f_M$ can be

expressed as:

$$
\begin{aligned}
f_M &= \frac{[CML]}{C_L} = \frac{\Delta\omega_p}{\Delta\omega_M} = \frac{R_{1p}}{R_{1M}} = \frac{R_{2p}}{R_{2M}} \\
&= \frac{K + C_{CM} + C_L - \left[(K + C_{CM} + C_L)^2 - 4C_{CM}C_L\right]^{1/2}}{2C_L}
\end{aligned}
$$

Therefore, measurements of either $\Delta w_p$, $R1_p$, or $R2_p$ at various concentrations of $C_L$ and/or $C_{CM}$ allow a two-parameter fitting of the data in terms of $K$ and $\Delta w_M$, $R1_M$, or $R2_M$. If the experimental conditions are such that $[CML]$ is always much smaller than $CL$ (i.e. large excess of $L$ with respect to $CM$), then the equation becomes:

$$K = \frac{(C_{CM} - [CML])\, C_L}{[CML]}$$

and consequently, simplifying the $f_M$ equation expressed above:

$$f_M = \frac{[CML]}{C_L} = \frac{C_{CM}}{K + C_L}.$$

In the very fast exchange regions, the observed paramagnetic effects on the chemical shift $\Delta\omega_p$ and the relaxation rates $R1_p$, $R2_p$, are simply proportional to the full paramagnetic effects in the metal binding site:

$$\Delta\omega_p = f_M \Delta\omega_M$$

Then we can write that:

$$C_L = C_{CM}\frac{\Delta\omega_M}{\Delta\omega_p} - K = C_{CM}\frac{R_{1M}}{R_{1p}} - K = C_{CM}\frac{R_{2M}}{R_{2p}} - K$$

For constant $C_{CM}$, a plot of $1/\Delta\omega_p$, $1/R1_p$ ($=T1_p$), or $1/R2_p$ ($=T2_p$) against $C_L$, gives a straight line, where $\Delta\omega_M$, $R1_M$, or $R2_M$ can then be obtained from the slope, and $K$ can be found from the intercept on the $y$ axis.

*These equation are valid when the ligand is in fast exchange.*[9]

## 6.2    Hybrid-POMs synthesis and catalysis

### A.  Ligands synthesis

#### ✓  Diolamide ligands

The diolamides synthesis was repeated, when necessary, following the synthetic procedure already described by Dr. David Lachkar in his thesis,[6] as well as the organo catalytic quinoline reduction in presence of the organo-POM as catalyst.[10]

#### ✓  Diolurea ligands

The (Ph)-, pCF$_3$(Ph)- and pOMe(Ph)- diolurea ligands were synthesized following the procedure presented by Oble et al. in 2011.[5]

The synthesis of 3,5bisCF$_3$(Ph)-, hexamethyl-, hexamethylen-bis- diolurea ligands is described below.
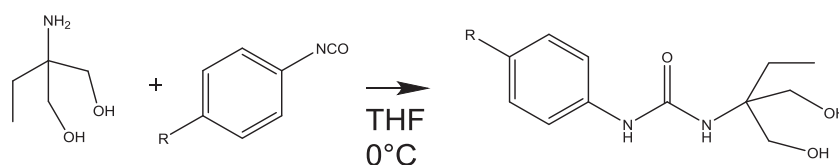


**General procedure- A:** Isocyanate (1,2 equiv) was slowly added to a solution of 2-amino-2-ethyl-1,3-propanediol (119 mg, 1 mmol, 1 equiv) in THF (4 mL) at 0 °C. The mixture was then left to reach room temperature and stirred until the 2-amino-2-ethyl-1,3-propanediol was completely consumed (3-16 h). The solvent was evaporated and the crude material was purified by centrifugation in a brine solution and dried under vacuum.
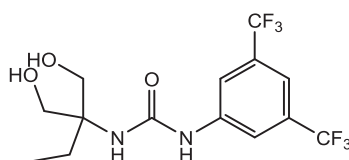
✓ **1-(1,1-bis-hydroxymethyl-propyl)-3-(3,5-bis-CF₃(Phenyl))urea**: Prepared according to the *general procedure – A*. Reaction time: over-night.

The crude white residue was purified by centrifugation in a brine solution and dried under vacuum to afford the diolurea as a white solid (99% yield)

IR: ṽ=3380 (m, br), 2974 (m), 1674 (vs), 1656 (s), 1578 (w), 1530 (vs), 1474 (s), 1444 (s), 1385 (vs), 1278 (s), 1190 (m), 1136 (m), 1078 (s), 1036 (vs) cm⁻¹.

$^1$H-NMR (300 MHz, CD₃OD): δ =7.99 (s, 2H, arom.), 7.47 (s, 1H, arom.), 3.72 (dd, J=10.88 Hz, 4H, *CH2*OH), 1.79 (q, J=7.58 Hz, 2H, *CH2*CH3), 0.95 (t, J=7.47 Hz, 3H, CH2*CH3*).

$^{13}$C-NMR (75.49 MHz, CD₃OD): δ =157.26 (C=O), 143.67 (C arom.), 133.29 (C arom.) 132.90 (C arom.), 126.68 (CF3), 123.11 (CF3), 118.89 (C arom.), 115.62 (C arom.), 64.69 (CH2OH), 61.56 (NHC), 25.32 (*CH2*CH3), 8.16 (CH2*CH3*).

$^{19}$F-NMR (282.90 MHz, CD₃OD)=δ =-64.56 ppm.

Electrospray mass spectrometry see below for full details:

| Entry | Charge | Simulated m/z | Observed m/z | Composition |
|-------|--------|---------------|--------------|-------------|
| **1** | 1+ | 375,11 | 375.11 | H[$C_{14}H_{16}F_6N_2O_3$] |
| **2** | 1+ | 397.1 | 397.09 | Na[$C_{14}H_{16}F_6N_2O_3$] |
| **3** | 1+ | 771.21 | 771.20 | Na[$C_{14}H_{16}F_6N_2O_3$]₂ |
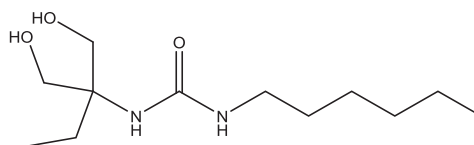
✓ **1-(1,1-bis-hydroxymethyl-propyl)-3-(hexamethyl)urea:** Prepared according to the general procedure – A. Reaction time: 6 hours.

The crude residue was purified by centrifugation in a brine solution and dried under vacuum to afford the urea as a colorless oil (85% yield).

IR: ν =3355 (br m), 2929 (m), 2858 (m), 1636 (s), 1567 (s), 1462 (s), 1379 (m), 1262 (m), 1052 (s), 798 (m) cm$^{-1}$.

$^{1}$H NMR (300 MHz, CD$_3$CN): δ =5.29 (br, 1H, NH), 5.18 (s, 1H, NH), 4.44 (br, 2H, OH), 3.55 (dd, J =6.13, 2.6 Hz, 2H, C*H*HOH), 3.44 (d, J =6.13, 2.6 Hz, 2H, CH*H*OH), 3.06 (q, J =7.6 Hz, 2H, NHC*H*$_2$R), 1.63 (q, J =8.18 Hz, 2H, C*H*2Me), 1.48-1.38 (m, 4H, NHCH2C*H*2C*H*2R), 1.38-1.27 (m, 4H, NHRC*H*2C*H*2CH3), 0.95-0.82 (m, 6H, CH2C*H*3 + NHRC*H*3).

$^{13}$C NMR (75.49 MHz, CD$_3$CN): δ =159.1 (C=O), 64.4 (CH2OH), 59.9 (CNH), 39.5 (CH2NH), 30.94 (*CH*2CH2NH), 29.5(*CH*2CH2CH2Me), 25.9 (*CH*2Me), 24.5(*CH*2CH2CH2CH2NH), 22.0 (*CH*2CH2CH2CH2CH2NH), 13.0(CH3), 6.8(CH2*CH3*).

Electrospray mass spectrometry see below for full details:

| Entry | Charge | Simulated m/z | Observed m/z | Composition |
|-------|--------|---------------|--------------|-------------|
| 1 | 1+ | 247,20 | 247.20 | H[C$_{12}$H$_{26}$N$_2$O$_3$] |
| 2 | 1+ | 269,18 | 269,2 | Na[C$_{12}$H$_{26}$N$_2$O$_3$] |
| 3 | 1+ | 515.37 | 515.4 | Na[C$_{12}$H$_{26}$N$_2$O$_3$]$_2$ |
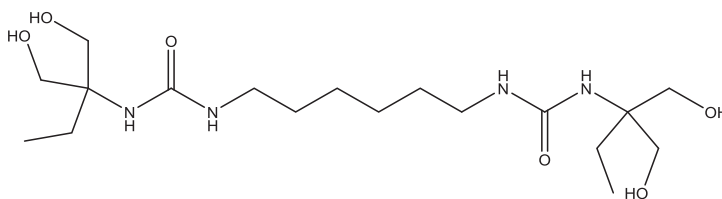
✓ **Hexamethylene- 1,1'-bis-(1,1-bis-hydroxymethyl-propyl)-3-urea:** Prepared according to the general procedure – A. Reaction time: over-night.

The crude residue was purified by centrifugation in a brine solution and dried under vacuum to afford the urea as a white solid (66% yield).

<u>IR</u>: ν =3316 (br), 2934 (m), 2859 (m), 1617 (s), 1567 (s), 1462 (w), 1273 (m), 1046 (s) cm-1.

<u>$^1$H NMR</u> (300 MHz, CD$_3$CN): δ =5.3 (s, 2H, NH), 5.14 (s, 2H, NH), 4.39 (s br, 4H, OH), 3.53 (d, J=8.8 Hz, 4H, C*H2*OH), 3.46 (d, J =8.7 Hz, 4H, C*H2*OH), 2,97 (t, J=6.99 Hz, 4H, C*H2*NH), 1.59 (q, J=7.79 Hz, 4H, C*H2*CH3), 1.42-1.32 (m, 4H, C*H2*CH2NH), 1.30-1.21 (m, 4H, C*H2*CH2CH2NH), 0.77 (t, J =7.6 Hz, 3H, CH2*CH3*).

<u>$^{13}$C NMR</u> (75 MHz, MeOD): δ =161.4 (C=O), 65.2 (*CH2*OH), 61.1 (*C*NH), 40.7 (*CH2*NH), 31.1 (*CH2*CH2NH), 27.6 (*CH2*CH3), 25.6 *(CH2*CH2CH2NH), 7.9 (CH2*CH3*).

Electrospray mass spectrometry see below for full details:

| Entry | Charge | Simulated m/z | Observed m/z | Composition |
|-------|--------|---------------|--------------|-------------|
| **1** | 1+ | 407.28 | 407.28 | H[C$_{12}$H$_{26}$N$_2$O$_3$] |
| **2** | 1+ | 429.27 | 429.27 | Na[C$_{12}$H$_{26}$N$_2$O$_3$] |
| **3** | 1+ | 835.53 | 835.54 | Na[C$_{12}$H$_{26}$N$_2$O$_3$]$_2$ |

## B. Hybrid POM synthesis
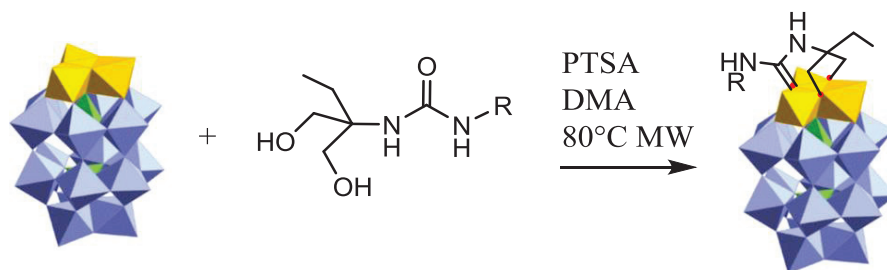


**General procedure for the POM functionalization-B**

TBA$_5$H$_4$[P$_2$V$_3$W$_{15}$O$_{62}$] (300 mg, 0.058 mmol, 1 equiv.), p-toluen sulfonic acid (PTSA 2.2 mg, 0.012 mmol, 0.3 equiv.) and the diol (0.069 mmol, 1.2 equiv.) were dissolved in dimethylacetamide (DMA, 0.6 mL) in a sealed microwave vial containing a stirring bar. The reaction was heated to 80 °C under µW for ~1h (with stirring). The reaction mixture was then quickly transferred to a round-bottom flask with a minimal amount of acetonitrile and the combined solvents were removed under reduced pressure. The crude yellow oil was dissolved with a minimal amount of acetonitrile (ca 1ml) and then transferred to a round-bottom 50 mL glass centrifuge tube and diethyl ether (30 mL) was added to precipitate the product as a yellow powder (sometimes a yellow-brown paste also formed which transformed into the same powder upon trituration with a spatula). After centrifugation, the colorless supernatant was removed from the tube, and the powder was air-dried. It was then redissolved in a minimal amount of acetonitrile (less than 0.5 mL is required), precipitated with ethanol (30 mL), triturated if needed, and centrifuged again. The orange supernatant was discarded and the remaining solid was triturated in diethyl ether. The ether was removed by centrifugation. The resulting powder was then finely dried under vacuum to afford the pure functionalized POMs.
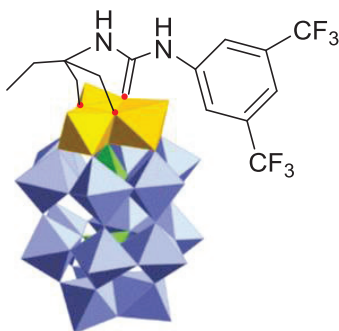
✓ **POM@3,5bisCF₃(Ph)urea:** Prepared according to general procedure – B. Reaction time: 1h15m. The product was isolated as a yellow powder (92% yield).

<u>IR</u>: υ =3451 (br), 2961 (m), 2872 (m), 1627 (s), 1483 (w), 1379 (m), 1088 (m), 1065 (m), 1022 (m), 954 (s), 915 (s), 827 (s) cm-1.

<u>$^1$H NMR</u> (600 MHz, CD₃CN): δ =8.01 (s, 1H, arom.), 7.87 (s, 2H, arom.), 5.59 (d, J=7.45 Hz, 2H, CH2OV), 5.45 (d, J=7.17 Hz, 2H, CH2OV), 3.42 (q, J=7.33 Hz, 2H, *CH*2CH3), 3.21-3.14 (m, 42.7H, N(C*H*2CH2CH2CH3)4), 1.71-1.63 (m, 43.2H, N(CH2C*H*2CH2CH3)4), 1.49-1.39 (m, 42.9H, N(CH2C*H*2CH2CH3)4), 1.06-0.98 (m, 63H, N(CH2C*H*2CH2CH3)4+CH2*CH3*).

<u>$^{13}$C NMR</u> (151.2 MHz, CD₃CN): δ =173 (C=O), 170.8 (CH arom), 163.9 (CH arom), 132.8 (CF3), 90.5 (CH2OV), 65.4 (CNH), 58.4 (N(CH2CH2CH2CH3)4), 35.9 (*CH*2CH3), 23.5 (N(CH2CH2CH2CH3)4), 19.5 (N(CH2CH2CH2CH3)4), 13.1(N(CH2CH2CH2CH3)4), 6.4 (CH2*CH3*).

<u>$^{19}$F NMR</u> (282.90 MHz, CD₃CN): d=-63.54 ppm.

<u>$^{31}$P NMR</u> (121.2 MHz, CD₃CN): δ =-7.90 (s, 1P),-13.57 (s, 1P) ppm.

<u>Elemental analysis</u> calc. for TBA5C14H14N2F6O62P2V3W15 (5498.40 g.mol-1): C 20.5, H 3.5, N 1.70; found: C 19.13, H 3.28, N 1.43.

<u>Electrospray mass spectrometry</u> see below for full details:

| Entry | Charge | Simulated m/z | Observed m/z | Composition |
|---|---|---|---|---|
| **1** | 4- | 1132,88 | 1133,1 | $(TBA)P_2W_{15}V_3O_{62}C_{14}H_{14}N_2F_6$ |
| **2** | 3- | 1591,33 | 1590,9 | $(TBA)_2P_2W_{15}V_3O_{62}C_{14}H_{14}N_2F_6$ |
| **3** | 2- | 2508,26 | 2507,9 | $(TBA)_3P_2W_{15}V_3O_{62}C_{14}H_{14}N_2F_6$ |
| **4** | 3- | 1510,83 | 1510,8 | $(TBA)HP_2W_{15}V_3O_{62}C_{14}H_{14}N_2F_6$ |
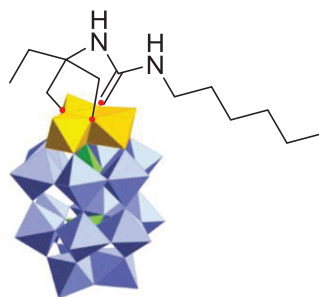
✓ **POM@hexamethylurea:** Prepared according to general procedure – B. Reaction time: 1h45m. The product was isolated as a yellow powder (92% yield).

<u>IR</u>: υ=3450, 2959, 2871, 1632, 1573, 1483, 1379, 1087, 953, 902, 815, 731 cm$^{-1}$.

<u>$^1$H NMR</u> (600 MHz, CD$_3$CN): δ =7.08 (s, 1H, NH) 6.73 (s, 1H, NH), 5.56 (d, J=HZ, 2H, CH2OV), 5.36 (d, J=HZ, 2H, CH2OV), 3.74 (t, J=HZ, 2H CH2NH), 3.29-3.11 (m, H, N(CH2C*H2*CH2CH3)4), 1.79-1.59 (m, H, N(CH2C*H2*CH2CH3)4), 1.53-1.33 (m, H, N(CH2C*H2*CH2CH3)4), 1.12-0.95 (m, H, N(CH2C*H2*CH2CH3)4).

<u>$^{13}$C NMR</u> (151.2 MHz, CD$_3$CN): 167.1 (C=O), 91.2 (CH2OV), 60.0 (CNH), 58.5 (N(CH2CH2CH2*Me*)4), 42.4 (*CH2*NH), 32.0 (*CH2*CH2NH), 30.0 (*CH2*CH2CH2NH), 29.2(*CH2*CH2CH2CH2NH), 26.5 (*CH2*CH3), 23.8 (N(CH2CH2CH2*CH3*)4), 22.8 (*CH2*(CH2)4NH), 19.8 (N(CH2CH2CH2*CH3*)4), 13.5 (RCH2*CH3*), 13.05 (N(CH2CH2CH2*CH3*)4), 6.4 (CH2*CH3*).

<u>Elemental analysis</u> calc. for TBA5C12H24N2O62P2V3W15 (5418.29 g.mol-1): C 20.59, H 3.80, N 1.83; found: C 20.36, H 3.76, N 1.78.

<u>Electrospray mass spectrometry</u> see below for full details.

| Entry | Charge | Simulated m/z | Observed m/z | Composition |
|---|---|---|---|---|
| 1 | 4- | 1100,89 | 1100,9 | $(TBA)P_2W_{15}V_3O_{62}C_{12}H_{24}N_2$ |
| 2 | 3- | 1548,69 | 1548,6 | $(TBA)_2P_2W_{15}V_3O_{62}C_{12}H_{24}N_2$ |
| 3 | 2- | 2444,30 | 2444,0 | $(TBA)_3P_2W_{15}V_3O_{62}C_{12}H_{24}N_2$ |
| 4 | 2- | 2202,78 | 2202,2 | $(TBA)H_2P_2W_{15}V_3O_{62}C_{12}H_{24}N_2$ |
| 5 | 2- | 2323,545 | 2323,8 | $(TBA)_2HP_2W_{15}V_3O_{62}C_{12}H_{24}N_2$ |
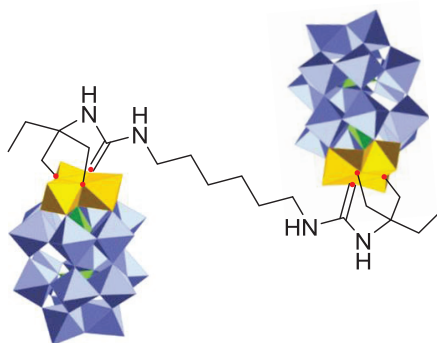
✓ **Hexamethylen@bis-POM-urea:** Prepared according to general procedure – B. Reaction time: 2h20m. The product was isolated as a yellow powder (75% yield).

IR: υ =3451, 2960, 2871, 1632, 1571, 1433, 1379, 1067, 954, 904, 815, 731 cm–1.

$^1$H NMR (600 MHz, CD$_3$CN): δ =7.21 (s, 1H, NH.), 6.90 (s, 1H, NH.), 5.54 (d, J=5.14 Hz, 2H, CH2OV), 5.36 (d, J=5.14 Hz, 2H, CH2OV), 3.73 (s br, 4H, CH2NH), 3.23-3.18 (m, 56.3H, CH2NH+N(C*H2*CH2CH2CH3)4), 1.72-1.64 (m, 103.4, CH2CH2NH + N(CH2C*H2*CH2CH3)4), 1.50-1.41 (m, 96H, CH2CH2CH2NH +N(CH2CH2C*H2*CH3)4), 1.06- 0.89 (m, 140H, CH2*Me* + N(CH2CH2CH2*CH3*)4).

$^{13}$C NMR (151.2 MHz, CD$_3$CN): δ =167.3 (C=O), 91.2 (CH2OV), 65.4 (CNH), 59.9 (*CH2*NH), 58.7 (N(CH2CH2CH2*CH3*)4), 41.9 (*CH2*CH2NH), 29.3 (*CH2*CH2CH2NH), 25.8(*CH2*CH3), 23.4 (N(CH2CH2CH2*CH3*)4), 19.5 (N(CH2CH2CH2*CH3*)4), 13.0 (N(CH2CH2CH2*CH3*)4), 6.7 (CH2*CH3)*.

$^{31}$P NMR (121.2 MHz, CD$_3$CN): δ =-7.39 (s, 1P),-13.42 (s, 1P).

Elemental analysis calc. for TBA10C18H34N4O124P4V6W30 (10660.94 g.mol-1): C 20.00, H 3.70, N 1.80; found: C 19.18, H 3.60, N 1.94.

Electrospray mass spectrometry see below for full details:

| Entry | Charge | Simulated m/z | Observed m/z | Composition |
|---|---|---|---|---|
| 1 | 5- | 1889,70 | 1889,8 | TBA$_5$(P$_2$W$_{15}$V$_3$O$_{62}$)$_2$C$_{17}$H$_{34}$N$_4$ |
| 2 | 4- | 2422,75 | 2422,9 | TBA$_6$(P$_2$W$_{15}$V$_3$O$_{62}$)$_2$C$_{17}$H$_{34}$N$_4$ |
| 3 | 3- | 3311,18 | 3310,18 | TBA$_7$(P$_2$W$_{15}$V$_3$O$_{62}$)$_2$C$_{17}$H$_{34}$N$_4$ |
| 4 | 5- | 1845,79 | 1846.0 | TBA$_4$Na(P$_2$W$_{15}$V$_3$O$_{62}$)$_2$C$_{17}$H$_{34}$N$_4$ |

### C. General procedure for Friedel-Craft alkylation reaction[11]
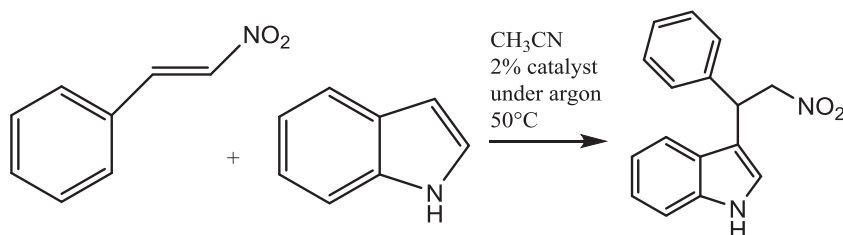


A dry-CH$_3$CN solution of trans-β-nitrostyrene (1 equiv) and the desired hybrid-POM catalyst (2% mol) is placed in a Schlenck tube under argon atmosphere and stirred at 50°C. Then, a dry-CH3CN solution of the Indole (1,5 equiv) is slowly added through a septum and the solution is kept under argon, at 50°C for 5 days.

The trans-b-nitrostyrene conversion was estimated through 1H-NMR all 24h. An internal standard (1,1'-2,2' tetrachloroethan) was used to quantify the trans-b-nitrostyrene conversion.

Finally, the solvent was removed under reduced pressure and the residue was purified on FC-silica gel using n-hexane:ethyl acetate 90:10 as eluent.

# 6.3 POM@polypeptides intra-molecular interactions in solution

### 6.3.1 *NMR details*

The 1D spectra ^{1}H-NMR, ^{13}C-NMR and 2D NMR ^{1}H-^{1}H COSY, ^{1}H–^{13}C HSQC and ^{1}H-^{13}C HMBC spectra were acquired at 23.5 T (1 GHz for proton, 251.6 MHz for [13]C Larmor frequencies) and 14.1 T (600 MHz for proton, 150.9 MHz for [13]C Larmor frequencies) using an Avance III NMR Bruker instrument equipped with a Triple resonance TCI cryoprobe, ^{31}P-NMR is acquired at 11.7 T (202 MHz).

Standard sequences were used for ^{1}H-^{1}H COSY, ^{1}H-^{13}C HSQC and ^{1}H-^{13}C HMBC. The ^{1}H and [13]C $\pi/2$ radiofrequency (RF) pulse were calibrated to 12.0 μs and 16.6 μs, respectively. The gradient selected Echo-Antiecho quadrature was used for 2D HSQC and Magnitude Mode for 2D HMBC. Typical 2D ^{1}H-^{13}C HSQC were acquired with 1024 x 512 complex points, with a maximum acquisition times of 121.9 ms and 42.3 ms in the direct and indirect dimensions, respectively, and the recycle delay was 2.0 s. The 2D ^{1}H-^{13}C HMBC were acquired with 2048 x 1024 complex points, with acquisition times of 227.2 ms and 32.2 ms in the direct and indirect dimensions, respectively, and the recycle delay was 1.5 s.

All the experiments where acquired at 298 K, and the ^{1}H and ^{13}C chemical shifts are referenced to TMS. Chemical shifts are reported in ppm, using, for ^{1}H and ^{13}C, solvent residual peak as internal standard references. Coupling constants (*J*) are given in Hertz (Hz), multiplicity (s =singlet, d =doublet, t =triplet, dd=double doublet, q =quartet, m =multiplet).

**NMR Determination of the hydrodynamic radius**

The determination of the molecular hydrodynamic radius makes possible to determine if the investigated POM derivative is prevalently present is solution as monomer of dimer or eventually small oligomers. This can be done on the

bases of the analysis of the NMR ^{15}N relaxation data, and in particular of the longitudinal relaxation time [15]N $T_1$. In solution, ^{15}N longitudinal relaxation time is dominated by the dipolar and the CSA mechanisms that are both modulated by the molecular rotation correlation time through the following equation[12]

$$R_1 = \frac{1}{T_1}$$

$$= \frac{1}{10}\left(\frac{\mu_0}{4\pi}\right)^2 \frac{(\gamma_H \gamma_N \hbar)^2}{r_{HN}^6}\left(\frac{\tau_R}{1+(\omega_H-\omega_N)^2\tau_R^2} + \frac{3\tau_R}{1+\omega_N^2\tau_R^2}\right)$$

$$+ \frac{6\tau_R}{1+(\omega_H+\omega_N)^2\tau_R^2}\right) + \frac{2(\gamma_N B_0 \Delta\sigma)^2}{15}\left(\frac{\tau_R}{1+\omega_N^2\tau_R^2}\right)$$

(1)

where $\tau_R$ is the rotational correlation time, $\gamma_H$, $\gamma_N$, $\omega_H$ and $\omega_N$ are the gyromagnetic ratio and the angular Larmor Frequencies for the proton and the nitrogen, respectively. $B_0$ is the strength of the magnetic field, $\mu_0$ is the vacuum magnetic permeability, $\Delta\sigma$ is the chemical shift anisotropy (here we used $\Delta\sigma =-$ 160 ppm for amide nitrogens), $r_{HN}$ is the proton nitrogen distance, that in amide group is about 104 pm.

Equation (1) shows that [15]N $T_1$ directly depends on the molecular rotational correlation time considered as a rigid body tumbling in the solution. We neglect at this level eventual internal motion that can differently affect the relaxation behaviour of each amide nitrogen in the peptide.

Equation (1) can be solved for each experimental [15]N $T_1$ data in order to obtain the values of $\tau_R$. Indeed, two possible values of $\tau_R$ can satisfy equation (1), one corresponding to the "fast-motion" condition, and the other in the "slow-motion" regime. The complete distinction between these regimes can be done acquiring also other relaxation parameters, like transverse relaxation data [15]N $T_2$ or [1]H-^{15}N NOE, which would make also possible to determine NH order parameters ($S^2$) and to quantify internal motion. In the present case, fast-motion and slow-motion correlation times are also well distinct each other to easily recognize the correct correlation time, discarding the other solution without

need of acquiring $^{15}$N T2 data. In turn, the rotational correlation time can be used to estimate the hydrodynamic volume through the Stokes-Einstein relation:

$$\tau_R = \frac{4\pi\eta r^3}{3kT} = \frac{\eta V}{kT}$$

(2)

where $r$ is the hydrodynamic radius, $\eta$ is the solvent viscosity (here 0.3450 mPa s for acetonitrile at 298 K), $k$ is the Boltzmann constant and $T$ is the temperature. This radius estimates as an approximate sphere the size of the molecule, but is precise enough to distinguish between the volume of a monomeric or a dimeric structure of the molecule.

### *6.3.2    Modelling details*

Cartesian coordinates for the $\alpha_1$ and $\alpha_2$ POMs were taken from available X-ray structures. Structures were reoptimized using density functional theory at the BP86/6-31G(d)/Lanl2dz level of theory, with an implicit solvent model (IEFPCM) to account for acetonitrile solvation. The Gaussian09 software Revision D.01 was used for the quantum chemical calculations.[8]

Classical molecular dynamics simulations were performed with Amber12 Molecular Dynamic software package.[13] GAFF[14] and ff14SB[15] force field parameters were used. Point charges for the POM unit listed in Table S3 were generated following the RESP procedure,[16] and a charge redistribution of 0.1396e was used to ensure the neutrality of the system. The Amber topology input files for the POM@Gly$_x$ ($x$=3−6) species were generated with LEaP basic preparation program: the polyglycine chain was generated to be in a β-sheet conformation.

Seven tetramethylammonium ions (MTA) were added as counterions to neutralize the organo-POM charge. A parallelepiped box of acetonitrile ~150* 170* 170 A$^3$ with ~3000 atoms was used to solvate each molecule.

Each system was preliminary minimized in 5000 steps, then heated from 0K to 300K in a thermalization step of 30 ps. Each system was then equilibrated during 1 ns: during our simulations, the temperature was kept at 300K using the Langevin thermostat with a collision frequency $\gamma$*ln equal to 1ps$^{-1}$. Finally, a production run of 300 ns was run for each system.

NMR chemical shifts were estimated through DFT calculations within the GIAO (Gauge independent atomic orbitals) formalism. They were performed at the PBE0/6-311+G*(LanL2DZ) level of theory, taking the final folded structure from our molecular dynamics and using a continuum description for the solvent. The choice of the atomic basis set was justified by the fact we wanted to assign only proton $^1$H-NMR.

## 6.4 Bibliography

[1]  R. G. Finke, B. Rapko, R. J. Saxton, P. J. Domaille, *J. Am. Chem. Soc.* **1986**, *108*, 2947–2960.

[2]  C. Boglio, K. Micoine, É. Derat, R. Thouvenot, B. Hasenknopf, S. Thorimbert, E. Lacôte, M. Malacria, *J. Am. Chem. Soc.* **2008**, *130*, 4553–4561.

[3]  C. Madhavaiah, M. Parvez, S. Verma, *Bioorg. Med. Chem.* **2004**, *12*, 5973–5982.

[4]  I. V. Gorokhova, A. A. Chinarev, A. B. Tuzikov, S. V. Tsygankova, N. V. Bovin, *Russ. J. Bioorganic Chem.* **2006**, *32*, 420–428.

[5]  J. Oble, B. Riflade, A. Noël, M. Malacria, S. Thorimbert, B. Hasenknopf, E. Lacôte, *Org. Lett.* **2011**, *13*, 5990–5993.

[6]  J. Li, I. Huth, L.-M. Chamoreau, B. Hasenknopf, E. Lacôte, S. Thorimbert, M. Malacria, *Angew. Chem. Int. Ed.* **2009**, *48*, 2035–2038.

[7]  J. M. Poblet, X. López, C. Bo, *Chem. Soc. Rev.* **2003**, *32*, 297–308.

[8]  Gaussian 09, Revision A.02, M. J. Frisch, G. W. Trucks, H. B. Schlegel, G. E. Scuseria, M. A. Robb, J. R. Cheeseman, G. Scalmani, V. Barone, G. A. Petersson, H. Nakatsuji, X. Li, M. Caricato, A. Marenich, J. Bloino, B. G. Janesko, R. Gomperts, B. Mennucci, H. P. Hratchian, J. V. Ortiz, A. F. Izmaylov, J. L. Sonnenberg, D. Williams-Young, F. Ding, F. Lipparini, F. Egidi, J. Goings, B. Peng, A. Petrone, T. Henderson, D. Ranasinghe, V. G. Zakrzewski, J. Gao, N. Rega, G. Zheng, W. Liang, M. Hada, M. Ehara, K. Toyota, R. Fukuda, J. Hasegawa, M. Ishida, T. Nakajima, Y. Honda, O. Kitao, H. Nakai, T. Vreven, K. Throssell, J. A. Montgomery, Jr., J. E. Peralta, F. Ogliaro, M. Bearpark, J. J. Heyd, E. Brothers, K. N. Kudin, V. N. Staroverov, T. Keith, R. Kobayashi, J. Normand, K. Raghavachari, A. Rendell, J. C. Burant, S. S. Iyengar, J. Tomasi, M. Cossi, J. M. Millam, M. Klene, C. Adamo, R. Cammi, J. W. Ochterski, R. L. Martin, K. Morokuma, O. Farkas, J. B. Foresman, and D. J. Fox, Gaussian, Inc., Wallingford CT, 2016., **2016**.

[9] Ivano Bertini, Claudio Luchinat, Giacomo Parigi, *Solution NMR of Paramagnetic Molecules, Volume 2- 1st Edition*, **2001**.

[10] D. Lachkar, *Synthèses, Études Structurales et Applications Catalytiques d'Organo-Polyoxométallates*, Paris 11, **2014**.

[11] R. P. Herrera, V. Sgarzani, L. Bernardi, A. Ricci, *Angew. Chem. Int. Ed.* **2005**, *44*, 6576–6579.

[12] "Nuclear Spin Relaxation in Liquids: Theory, Experiments, and Applications," can be found under https://www.crcpress.com/Nuclear-Spin-Relaxation-in-Liquids-Theory-Experiments-and-Applications/Kowalewski-Maler/p/book/9780750309646, **2006**.

[13] D.A. Case, D.S. Cerutti, T.E. Cheatham, III, T.A. Darden, R.E. Duke, T.J. Giese, H. Gohlke, A.W. Goetz, D. Greene, N. Homeyer, S. Izadi, A. Kovalenko,

T.S. Lee, S. LeGrand, P. Li, C. Lin, J. Liu, T. Luchko, R. Luo, D. Mermelstein, K.M. Merz, G. Monard, H. Nguyen, I. Omelyan, A. Onufriev, F. Pan, R. Qi, D.R. Roe, A. Roitberg, C. Sagui, C.L. Simmerling, W.M. Botello-Smith, J. Swails, R.C. Walker, J. Wang, R.M. Wolf, X. Wu, L. Xiao, D.M. York and P.A. Kollman; Amber, University of California, San Francisco, **2015**.

[14] J. Wang, R. M. Wolf, J. W. Caldwell, P. A. Kollman, D. A. Case, *J. Comput. Chem.* **2004**, *25*, 1157–1174.

[15] A. Pérez, I. Marchán, D. Svozil, J. Sponer, T. E. Cheatham, C. A. Laughton, M. Orozco, *Biophys. J.* **2007**, *92*, 3817–3829.

[16] C. I. Bayly, P. Cieplak, W. Cornell, P. A. Kollman, *J. Phys. Chem.* **1993**, *97*, 10269–10280.